

Mitigation of corrosion and scale by combined inhibitors

Michal Ciolkowski

Submitted in accordance with the requirements for the degree of
Doctor of Philosophy

The University of Leeds

School of Mechanical Engineering

October, 2015

The candidate confirms that the work submitted is his own, except where work which has formed part of jointly authored publications has been included. The contribution of the candidate and the other authors to this work has been explicitly indicated below.

The candidate confirms that appropriate credit has been given within the thesis where reference has been made to the work of others.

The work in Chapter 5, 6 and 7 of the thesis has appeared in publication as follows:

A Systematic Scale-Corrosion Study of a Combined Inhibitor in Scale-Corrosion Environment Via Experimental Design; March 2014; Michal Ciolkowski and Anne Neville.

All the work in the paper mentioned above is a contribution of the candidate, under the supervision of the co-authors.

This copy has been supplied on the understanding that it is copyright material and that no quotation from the thesis may be published without proper acknowledgement.

Acknowledgements

I would like to thank my supervisors Professor Anne Neville for her enthusiasm, wise words and continuing support throughout this project. Thanks also for providing the initial idea for the project, and introducing me to a fascinating subject.

Many thanks to the technical and administrative staff of Leeds University for their involvement and contribution: Ron, Graham, Mark, Brian, Jackie and Fiona.

I would also like to thank the whole the mechanical engineering team: Rick, Laura, James, Thibaut, Michael, Yugal, Ben, Jide, Ogbemi, Wassim, Louise, Thawhid, Frederick, Akbar, Yusheng for friendship and discussion.

I would like to thank Adrian Eagles, John Harrington and Stuart Micklethwaite for their support and guidance in using the surface analysis equipment.

Specials thanks to Dr Timothy Comyn for help with Rietveld analysis and even bigger thanks to Greg de Boer for help with MATLAB programming.

Thanks also to the FAST team in Heriot Watt University for their support and involvement.

The most special thank goes to my best partner and friend, my wife. Anna, you gave me your unconditional support and love through all this long process. Thank you.

Thanks to my family back home; my parents Jozef Ciolkowski and Zuzanna Ciolkowska and my in-law mother Krzysztofa Kobiela and grandmother Cecylia Zaton and my brother Arkadiusz Ciolkowski and his wife Renata Stono-Ciolkowska with their daughter Julia Ciolkowska for their love and support.

Abstract

Corrosion and scale deposition on pipelines are two of the major flow assurance issues which have been recognized in the oilfield. Corrosion control of carbon steel pipelines requires understanding of the simultaneous occurrence of both processes. To date there have been few studies demonstrating the interactions between surface scale deposition and corrosion processes. Combined scale/corrosion inhibitors (mixture of scale and corrosion inhibitors) are gaining in popularity in the oil and gas industry as one of many methods to mitigate both those processes.

A newly developed methodology of combined bulk jar scaling/bubble cell technique (corrosion) was used to assess the corrosion rate, CaCO_3 deposition on the material surface and bulk precipitation in a CO_2 environment. In this study the effects of single components of scale and corrosion inhibitors on the corrosion processes (general and localized corrosion) and scale deposition (bulk and surface deposition) have been investigated. Surface analysis techniques (SEM, EDX and Light Interferometry) and bulk analysis (Turbidity meter and ICP-MS) enable the corrosion/scale mechanisms to be studied in detail for X65 pipeline material. An experimental design method has been used to evaluate single and/or synergistic effect of single components of combined scale/corrosion inhibitor on the corrosion and scale processes.

The methodology used in this study a newly-developed combined bulk jar scaling/bubble cell prove that is very effective tool in assessment of corrosion and scale interactions when they occurs simultaneously. Assessment of calcium carbonate precipitation on the sample showed that scale plays an important role of accelerating pitting corrosion by providing a suitable environment. XRD analysis showed that the calcium carbonate crystals which formed on the metal sample in the tests with 2-mercapthoethanol were calcite crystals only.

The simple linear regression model was developed to predict corrosion and scale when these process occur simultaneously. The model also enables the interactions between the corrosion and scale inhibitor components to be quantified.

Table of Contents

Acknowledgements	iii
Abstract	iv
Table of Contents	v
List of Tables	xii
List of Figures	xiv
Chapter 1 Introduction	1
1.1 Oil and gas: origin and exploration	1
1.2 Inorganic scaling and impact for the oil and gas industry	3
1.3 Present removal and inhibition methods	3
1.4 Corrosion and impact for the industry	3
1.5 Current prevention methods.....	4
1.6 Combined inhibitors	4
1.7 Aims and Objectives of the PhD.....	4
1.8 Scope of work	6
1.9 Outline of the thesis	6
1.10 Contribution of this Research	Error! Bookmark not defined.
Chapter 2 Theory of scale and corrosion	8
2.1 Introduction	8
2.2 Mechanisms of calcium carbonate formation	8
2.2.1 Calco-carbonic equilibrium	8
2.2.2 Saturation.....	8
2.2.3 Induction time.....	10
2.2.4 Nucleation	10
2.2.5 Growth	12
2.2.5.1 Surface energy theory.....	12
2.2.5.2 Adsorption layer theory	13
2.2.5.3 Dislocation	13
2.2.5.4 Growth mechanism	14
2.3 Aqueous corrosion	14
2.3.1 Definition of corrosion	14
2.3.2 Thermodynamics.....	15
2.3.2.1 Free energy.....	15

2.3.2.2	The Corrosion cell.....	15
2.3.2.3	Corrosion reactions.....	15
2.3.2.4	The Nernst equation and cell potential.....	17
2.3.3	The mechanism of aqueous corrosion and electrical double layer (EDL)	17
2.3.3.1	The relationship between EDL chemical composition, electric current and voltage	18
2.3.4	Electrochemical measurement techniques.....	19
2.3.4.1	Linear Polarisation Resistance (LPR) method	19
2.3.4.2	Tafel plots	20
2.4	CO ₂ corrosion mechanism	21
2.4.1	Cathodic reactions in CO ₂ environment	21
2.4.2	Anodic reactions in CO ₂ environment	22
2.5	Summary.....	23
Chapter 3	Literature reviews of calcium carbonate and CO₂ corrosion.....	24
3.1	Introduction	24
3.2	Different types of scales	24
3.3	Calcium carbonate polymorphism	25
3.3.1	Factors influencing calcium carbonate formation	26
3.3.1.1	Effect of temperature	26
3.3.1.2	Effect of pressure.....	27
3.3.1.3	Effects of hydrodynamic conditions.....	27
3.3.1.4	Effect of supersaturation	27
3.3.1.5	Effect of pH	28
3.3.1.6	Effect of divalent ions.....	29
3.3.1.6.1	Effect of calcium (Ca ²⁺)	29
3.3.1.6.2	Effect of iron.....	29
3.3.1.6.3	Effect of other divalent ions.....	29
3.3.1.6.4	Effect of magnesium	30
3.4	Methods of scale inhibition and removal	30
3.4.1	Mechanisms of inhibition and chemicals	31
3.4.1.1	Mechanism of inhibition	31
3.4.2	Scale inhibitors.....	32
3.4.2.1	Phosphonates	32
3.4.2.2	Polyphosphate	33

3.4.2.3	Polyelectrolyte.....	33
3.4.3	Removal methods	34
3.5	Different methodologies used to study calcium carbonate	35
3.5.1	Scale precipitation in the solution.....	35
3.5.2	Scale deposition on a surface	36
	<u>Non electrochemical methods</u>	36
	<u>Electrochemical methods</u>	36
3.6	Different types of internal corrosion.....	38
3.7	Types of CO ₂ corrosion damage	39
3.7.1	General corrosion.....	39
3.7.2	Pitting corrosion	39
3.8	Factors affecting CO ₂ corrosion	40
3.8.1	Water chemistry	40
3.8.2	Formation of CO ₂ corrosion product.....	40
3.8.3	Effect of pH	41
3.8.4	Partial pressure	42
3.8.5	Temperature.....	42
3.8.6	Effect of flow.....	42
3.8.7	Effect of chemical composition and microstructure	43
3.8.8	Effect of calcium on CO ₂ corrosion	43
3.9	Pitting corrosion of in CO ₂ environment	43
3.10	Corrosion mitigation	45
3.10.1	Corrosion inhibitors	45
3.10.1.1	Common corrosion inhibitors	46
3.10.1.1.1	Inhibitors structure relevant to this PhD with description. 47	
3.11	Combined inhibitors	49
3.11.1	Effect of corrosion inhibitor on scale inhibition and scale formation.....	49
3.11.2	Effect of scale inhibitor on corrosion inhibition	50
3.12	Summary.....	51
Chapter 4	Methodology	52
4.1	Introduction	52
4.2	Jar test/bubble cell	52
4.2.1	Hot plate stirrer.....	53
4.2.2	Working electrode	53

4.2.3	Combined reference and counter electrode	54
4.2.4	pH electrode and apparatus	54
4.2.5	Solution composition	54
4.2.6	Inhibitors	55
4.3	Corrosion measurements	56
4.3.1	General corrosion.....	56
4.3.2	Localized corrosion	56
4.4	Bulk and surface scale measurements	59
4.4.1	Bulk scale measurements	59
4.4.2	Surface scale measurements.....	60
4.5	Interaction of the inhibitors with scale on surface measurements	63
4.6	Experimental design.....	64
4.6.1	Design of Experiments (DOE).....	65
4.6.2	Two Level Full Factorial Experiments [224]	65
4.6.3	The analysis of variance (ANOVA).....	66
4.7	Experimental procedure summary	68
Chapter 5	Corrosion and scale results in the absence of combined inhibitor	70
5.1	Introduction	70
5.2	Corrosion results	70
5.2.1	General corrosion.....	70
5.2.2	Localized corrosion	72
5.3	Bulk and surface scaling results.....	75
5.3.1	Bulk solution scaling.....	75
5.3.1.1	Turbidity results and pH – for bulk scaling	75
5.3.2	Inductively coupled plasma mass spectrometry (ICP – MS) results from bulk solution and surface	76
5.3.3	Surface scale	77
5.3.3.1	Scanning Electron Microscopy (SEM) and X- Ray Diffraction (XRD).....	77
5.4	Summary.....	79
Chapter 6	Corrosion and scale results in the presence of single components of combined inhibitor	80
6.1	Introduction	80
6.2	Concentration of the single components	80
6.3	Corrosion results	81

6.3.1	General corrosion.....	81
6.3.2	Localized corrosion	84
6.4	Bulk and Surface scaling results	89
6.4.1	Bulk solution scaling.....	89
6.4.1.1	Turbidity results.....	89
6.4.2	Inductively coupled plasma mass spectrometry (ICP – MS) results from bulk solution and surface	92
6.4.3	Surface scale	93
6.4.3.1	Scanning Electron Microscopy (SEM) and X-ray diffraction (XRD).....	93
6.5	Systematic ranking of the single components of the combined inhibitor	98
6.6	Summary.....	100
Chapter 7	Corrosion and scale results in the presence of combined inhibitor	102
7.1	Introduction	102
7.2	Experimental matrix - 2 ⁵ full factorial design method	102
7.3	Corrosion results	103
7.3.1	General corrosion.....	103
7.3.2	Localized corrosion	104
7.4	Bulk and surface scaling results.....	105
7.4.1	Bulk solution scaling.....	105
7.4.1.1	Turbidity results.....	105
7.4.2	Inductively coupled plasma mass spectrometry (ICP – MS) results from bulk solution	106
7.4.3	Surface scale	107
7.4.3.1	Inductively coupled plasma mass spectrometry (ICP – MS) results from surface	107
7.4.3.2	Inductively coupled plasma mass spectrometry (ICP – MS) results from surface	108
7.4.4	Empirical equation.....	111
7.5	ANOVA analysis of general corrosion inhibition	112
7.6	ANOVA analysis of localized corrosion inhibition	115
7.7	ANOVA analysis of bulk scaling inhibition	116
7.8	ANOVA analysis of surface scaling inhibition.....	118
7.9	Summary.....	120

Chapter 8	FTIR and RAMAN spectroscopy analysis of single components of combined inhibitors	121
8.1	Introduction	121
8.2	FTIR analysis of single components and interaction with calcium carbonate and iron carbonate	121
8.2.1	FTIR analysis of single components and interaction with calcium carbonate	121
8.2.2	FTIR analysis of single components and interaction with iron carbonate	123
8.3	Raman analysis of single components and interaction with calcium carbonate and iron carbonate	125
8.3.1	Raman analysis of single components and interaction with calcium carbonate.....	125
8.3.2	Raman analysis of single components and interaction with iron carbonate.....	127
8.4	Summary.....	130
Chapter 9	Discussion.....	131
9.1	Introduction	131
9.2	Corrosion and scale processes in an environment where both processes occurs simultaneously.....	131
9.3	Inhibition effect of single components of combined inhibitor on corrosion and scale processes in the environment where both processes occurs simultaneously.....	134
9.3.1	Effect of 2-mercaptoethanol (souring agent) on corrosion and scale processes in the environment where both processes occurs simultaneously.....	134
9.3.2	Effect of alcohol ethoxy phosphate ester (corrosion inhibitor 1), C12-C14 alkyldimethyl-benzylammonium chloride (corrosion inhibitor 2) and ethoxylated imidazolines (corrosion inhibitor 3) on corrosion and scale processes in the environment where both processes occurs simultaneously.....	137
9.3.3	Effect of polyphosphinocarboxylic acid (PPCA – scale inhibitor) on corrosion and scale processes in the environment where both processes occurs simultaneously	141
9.4	Effect of single components and their interactions on the corrosion and scale processes.....	142
9.4.1	Effect of single components and their interactions on general corrosion inhibition	143
9.4.2	Effect of single components and their interactions on localized corrosion inhibition	144

9.4.3	Effect of single components and their interactions on bulk scaling inhibition	145
9.4.4	Effect of single components and their interactions on surface scaling inhibition	146
9.4.5	Empirical equations (prediction model)	147
Chapter 10	Conclusions.....	149
10.1	Introduction	149
10.2	Corrosion and scale process in the environment where both processes occurs simultaneously without presence of the inhibitor.....	149
10.3	Inhibition effect of single components of combined inhibitor on corrosion and scale processes in the environment where both processes occurs simultaneously.....	150
10.4	Effect of single components and their interactions on the corrosion and scale processes when their blend together as combined inhibitor	152
Chapter 11	Future work.....	153
	List of References	155
	Appendix A	169
	Appendix B	179

List of Tables

Table 2.1 Standard electrode potential E° (V) standard hydrogen electrode (SHE)[41].....	16
Table 3.1 Most common oilfield scales [56].....	25
Table 3.2: Description of the three calcium carbonate polymorphs.....	26
Table 4.1: Chemical composition (wt.%) X65 carbon steel [202]	53
Table 4.2: Brine composition	55
Table 4.3: Description of the single inhibitors.....	55
Table 4.4: 32 combination of combined inhibitors	66
Table 4.5: The average outputs of individual factors for each level	67
Table 4.6: Test conditions	69
Table 5.1: Deepest pits in the tests in the absence of combined inhibitor and for reference polished samples.....	72
Table 5.2: Pit density in the tests in the absence of combined inhibitor.....	75
Table 5.3: ICP-MS results in the tests in the absence of combined inhibitor at the end of tests	77
Table 5.4: Different polymorphs of CaCO_3 formed in the tests in the absence of combined inhibitor by Rietveld Analysis	78
Table 6.1: Corrosion potential, corrosion current and Tafel slopes	82
Table 6.2: Deepest pits in the tests in the presence of single components of combined inhibitor after 72hrs	85
Table 6.3: Pit densities in the tests in the presence of single components of combined inhibitor after 72 hrs	88
Table 6.4: Induction time in the tests with single components of combined inhibitor	92
Table 6.5: Different polymorphs of CaCO_3 formed in the tests in the presence of single components of combined inhibitor by Rietveld Analysis	98
Table 6.6: Effect of the single components of combined inhibitor effect on general corrosion and pitting corrosion	98
Table 6.7: Effect of the single components of combined inhibitor effect on induction time, amount of calcium sustained in the bulk solution and surface scaling	99
Table 6.8: Ranking of the single components of combined inhibitor.....	100

Table 7.1: Corrosion rate at the end of the tests with different combinations of single components in the combined inhibitor after 4 hours	103
Table 7.2: Deepest pits in the tests with different combination of single components in combined inhibitor after 72hrs	104
Table 7.3: The induction time results in the tests with different combination of single components in combined inhibitor in bulk solution.....	105
Table 7.4 ICP-MS results in the tests with different combinations of single components in combined inhibitor in bulk solution	106
Table 7.5 ICP-MS results in the tests with different combination of single components in combined inhibitor on metal surface.....	107
Table 7.6 Size and structure of CaCO₃ formed in the tests (Run 1 to Run 16) with different combination of single components in combined inhibitor.....	108
Table 7.7 Size and structure of CaCO₃ formed in the tests (Run 17 to Run 32) with different combination of single components in combined inhibitor.....	109
Table 7.8: Crystals formed during the test with different combination of combined inhibitor divided into in three groups.....	111
Table 7.9 The contributions of single components and their interaction to inhibition of general corrosion.....	112
Table 7.10: The contributions of single components and their interaction to inhibition of localized corrosion	115
Table 7.11: The contributions of single components and their interaction to inhibition of bulk scaling inhibition	117
Table 7.12: The contributions of single components and their interaction to inhibition of surface scaling.....	118
Table 8.1: Peaks of calcium carbonate found in this PhD work and literature.....	122
Table 8.2: Peaks of iron carbonate found in this PhD work and literature.....	125
Table 8.3: Peaks of calcium carbonate found in this PhD work and literature.....	126
Table 8.4: Peaks of iron carbonate found in this PhD work and literature.....	128

List of Figures

Figure 1.1 Alteration of sediments [5]	1
Figure 1.2 Oil and gas migration from the source rock [6].....	2
Figure 1.3 Methods for oil recovery [7]	2
Figure 2.1: A representation of crystallisation in the absence and presence of macroseeds [23].....	9
Figure 2.2: Schematic representations of processes involved in the initial stages of scale formation: (a) ion pairing, (b) prenucleation aggregate growth, (c) and (d) particle nucleation and growth [30]	11
Figure 2.3 The different types of nucleation [22].....	11
Figure 2.4: Velocities of crystal growth faces: (a) invariant crystal: (b) overlapping crystal [22]	12
Figure 2.5: Growing crystal surfaces: (A) flat surfaces, (B) steps, (C) kinks [22].....	13
Figure 2.6: Development of growth spiral starting from screw dislocation [22].....	13
Figure 2.7 An electrochemical cell [40]	15
Figure 2.8: Representing how to determine Tafel slopes [42].....	20
Figure 3.1: The crystalline polymorphs of calcium carbonate: (a) calcite, (b) aragonite and (c) vaterite [60]	26
Figure 3.2: Solubility of calcium carbonate in water as a function of temperature [63].....	27
Figure 3.3 Distribution of carbon total fraction as a function of pH	28
Figure 3.4: Three main processes of scale inhibition [100].....	31
Figure 3.5: Molecular structure of phosphonates used as scale inhibitors : a) HEDP (Hydroxyethylidene Diphosphonic acid) and b) DETPMP (Diethylenetriaminepenta-methylenephosphonic acid).....	32
Figure 3.6: Chemical structure of linear polyphosphate	33
Figure 3.7: Schematic representation of polyelectrolytes used as scale inhibitors: a) Polyphosphinocarboxylic acid (PPCA), b) Polyvinyl sulfonate and Polyacrylic acid copolymer (PVS) and c) 2-phosphono-butane-1,2,4-tricarboxylic acid (PBTC)	34
Figure 3.8: Typical chronoamperometry curve [133]	37
Figure 3.9: The different cross-sectional shapes of pits [143].....	39
Figure 3.10: Different types of protective and non-protective corrosion layers – from Crolet <i>et al.</i> [151]	41

Figure 3.11: Schematic of the critical velocity effect for erosion-corrosion [141]	42
Figure 3.12: General chemical structure phosphate ester	47
Figure 3.13: General chemical structure quaternary ammonium salts	48
Figure 3.14: The molecular structure imidazoline	48
Figure 3.15: The molecular structure thiol compound	48
Figure 4.1 A combined bulk jar test/bubble cell: 1) hot-plate/stirrer, 2) working electrode, 3) temperature probe, 4) combined reference and counter electrode, 5) pH electrode, 6) CO₂ inlet and 7) CO₂ outlet [199]	52
Figure 4.2: The microstructure of X65 steel in 50 magnification	53
Figure 4.3: Schematic figure of the multiphase equilibrium model [203]	54
Figure 4.4: Schematic layout of a White light Interferometer [206]	58
Figure 4.5: Schematic of representation of a threshold on a sample	58
Figure 4.6: Schematic of representation of tested surface area for analyses of pitting corrosion	59
Figure 4.7 Schematic representation of the turbidity-meter [209]	59
Figure 4.8 Schematic representation of the ICP-MS [210]	60
Figure 4.9 Schematic representation of the SEM [211]	61
Figure 4.10 Schematic representation of the energy-dispersive X-ray [212]	61
Figure 4.11: Schematic representation of the X-rays production [213]	62
Figure 4.12: Bragg diffraction [214]	62
Figure 4.13: Schematic representation of the FTIR [219]	64
Figure 4.14: Schematic representation of the Raman spectrometer [220]	64
Figure 5.1: Tafel plots for carbon steel in blank brine solution at 80°C after 4 hours	71
Figure 5.2: General corrosion results in the absence of combined inhibitor at 80°C over 4hours	71
Figure 5.3: Scanning electron micrographs in the test in the absence of combined inhibitor after cleaning by Clarke's solution	72
Figure 5.4: Schematic representation of a sample after test with representation of a threshold	73

Figure 5.5: Light interferometry images of deepest pit on surface in the tests in the absence of combined inhibitor: a) grooves on polished sample, b) pit after 4hrs test and c) pit1 after 72hrs	74
Figure 5.6: Turbidity results in the tests in the absence of combined inhibitor at 80°C over 4 hours	75
Figure 5.7: pH results in the tests in the absence of combined inhibitor	76
Figure 5.8: Scanning electron micrographs of CaCO ₃ formed in the tests in the absence of combined inhibitor	77
Figure 5.9: XRD spectrum of scale formed in the tests in the absence of combined inhibitor	78
Figure 6.1: Tafel plots after 4 hours in tests with 2-mercaptoethanol and alcohol ethoxy phosphate ester (anodic and cathodic curves were constructed using separate samples)	81
Figure 6.2: Tafel plots after 4 hours in tests with C12-C14alkyl dimethyl benzyl ammonium chloride, ethoxylated imidazolines and PPCA (anodic and cathodic curves were constructed using separate samples).....	83
Figure 6.3: General corrosion results in the presence of single components of combined inhibitor	84
Figure 6.4: Light interferometry images of deepest pits on surface in the tests in the presence of single components of combined inhibitor: a) 2-mercaptoethanol, b) Alcohol ethoxy phosphate ester; c) C12-C14 Alkyldimethyl-benzylammonium chloride; d) Ethoxylated imidazolines and e) PPCA	87
Figure 6.5: Turbidity results in the tests over 4hours in the presence of single components of combined inhibitor: a) 2-mercapthoethanol, b) alcohol ethoxy phosphate ester; c) C12-C14 alkyldimethyl-benzylammonium chloride; d) ethoxylated imidazoline and e) PPCA	91
Figure 6.6: Surface scaling versus bulk scaling in the tests with single components	93
Figure 6.7: Scanning electron micrographs of CaCO ₃ formed at the surface in the tests in the presence of single components of combined inhibitor: a) 2-mercaptoethanol, b) alcohol ethoxy phosphate ester; c) C12-C14 alkyldimethyl-benzylammonium chloride and d) ethoxylated imidazolines and e) PPCA.....	94
Figure 6.8: XRD spectrum of scale formed in the tests in the presence of single components of combined inhibitor: a) 2-mercaptoethanol, b) alcohol ethoxy phosphate ester; c) C12-C14 alkyldimethyl-benzylammonium chloride; d) ethoxylated imidazolines and e) PPCA	97

Figure 7.1: Examples of scale formed during the test: (a) none scale – Run 25, (b) clusters – Run2, (c) small crystals <20 μm – Run 21, (d) smaller crystals than 2 μm – Run16 and (e) crystals bigger >80 μm – Run9	110
Figure 7.2: Half-Normal Probability Plot showing the effect of the single components of combined inhibitor and their interaction on inhibition of general corrosion.....	112
Figure 7.3: 2D-countour plot of empirical relationship of general corrosion inhibition	114
Figure 7.4: Half-Normal Probability Plot showing the effect of the single components of combined inhibitor and their interaction on inhibition of localized corrosion	115
Figure 7.5: 2D-contour plot of empirical relationship of localized corrosion inhibition	116
Figure 7.6: Half-Normal Probability Plot showing the effect of the single components of combined inhibitor and their interaction on inhibition of bulk scaling	117
Figure 7.7: Linear graph of empirical relationship of bulk scaling inhibition	118
Figure 7.8: Half-Normal Probability Plot showing the effect of the single components of combined inhibitor and their interaction to inhibition of surface scaling.....	119
Figure 7.9: 2D-contour plot of empirical relationship of surface scale inhibition.....	119
Figure 8.1: Infrared spectrum for neat 2-mercaptoethanol.....	122
Figure 8.2: Infrared spectrum for: a) calcium carbonate formed with presence of 2-mercaptoethanol, b) calcium carbonate reference and c) carbon steel	123
Figure 8.3: Infrared spectrum for: a) iron carbonate formed with presence of 2-mercaptoethanol, b) iron carbonate reference and c) carbon steel	124
Figure 8.4: Raman spectrum for neat 2-mercaptoethanol	126
Figure 8.5: Raman spectrum for: a) calcium carbonate formed with presence of 2-mercaptoethanol, b) calcium carbonate reference and c) carbon steel	127
Figure 8.6: Raman spectrum for: a) iron carbonate formed with presence of 2-mercaptoethanol, b) iron carbonate reference and c) carbon steel	129
Figure 9.1: Scale and corrosion surface interaction in calco-carbonic/ CO_2 corrosion environment	132
Figure 9.2: Preferential sites of formation calcium carbonate on carbon steel X65.....	133

Figure 9.3: Results presenting effect of all single components on corrosion and scale processes.....	135
Figure 9.4: Schematic of film formed by 2-mercaptoethanol	135
Figure 9.5: Schematic of film formed by C12-C14 alkyldimethyl-benzylamonium chloride and ethoxylated imidazolines	138
Figure 9.6: Schematic of inhibitor film formation in presence of oil [241].....	139
Figure 9.7: Pit corrosion in the test with alcohol ethoxy phosphate ester	140
Figure 9.8: Schematic of inhibition of pits by a) alcohol ethoxy phosphate ester and b)2- mercapthoethanol.....	145
Figure A.0.1: Infrared spectrum for neat alcohol ethoxy phosphate ester	169
Figure A.0.2: Infrared spectrum for neat C12-C14 alkyl dimethyl benzyl- ammonium chloride.....	169
Figure A.0.3: Infrared spectrum for neat ethoxylated imidazolines....	170
Figure A.0.4: Infrared spectrum for neat polyphosphinocarboxylic acid (PPCA).....	170
Figure A.0.5: Infrared spectrum for calcium carbonate formed with presence of alcohol ethoxy phosphate ester, calcium carbonate reference and carbon steel	171
Figure A.0.6: : Infrared spectrum for calcium carbonate formed with presence of C12-C14 alkyl dimethyl benzyl- ammonium chloride, calcium carbonate reference and carbon steel	172
Figure A.0.7: Infrared spectrum for calcium carbonate formed with presence of ethoxylated imidazolines, calcium carbonate reference and carbon steel	173
Figure A.0.8: Infrared spectrum for calcium carbonate formed with presence of polyphosphinocarboxylic acid (PPCA), calcium carbonate reference and carbon steel	174
Figure A.0.9: Infrared spectrum for iron carbonate formed with presence of alcohol ethoxy phosphate ester, iron carbonate reference and carbon steel	175
Figure A.0.10: Infrared spectrum for iron carbonate formed with presence of C12-C14 alkyl dimethyl benzyl- ammonium chloride, iron carbonate reference and carbon steel.....	176
Figure A.0.11: Infrared spectrum for iron carbonate formed with presence of ethoxylated imidazolines, iron carbonate reference and carbon steel	177
Figure A.0.12: Infrared spectrum for iron carbonate formed with presence of polyphosphinocarboxylic acid (PPCA, iron carbonate reference and carbon steel	178

Figure B.0.1: Raman spectrum for neat alcohol ethoxy phosphate ester	179
Figure B.0.2: Raman spectrum for neat C12-C14 alkyl dimethyl benzyl- ammonium chloride.....	179
Figure B.0.3: Raman spectrum for neat ethoxylated imidazolines	180
Figure B.0.4: Raman spectrum for neat polyphosphinocarboxylic acid (PPCA).....	180
Figure 0.5: Raman spectrum for calcium carbonate formed with presence of alcohol ethoxy phosphate ester, calcium carbonate reference and carbon steel	181
Figure 0.6: Raman spectrum for calcium carbonate formed with presence of C12-C14 alkyl dimethyl benzyl-amonium chloride, calcium carbonate reference and carbon steel	182
Figure 0.7: Raman spectrum for calcium carbonate formed with presence of ethoxylated imidazolines, calcium carbonate reference and carbon steel	183
Figure 0.8: Raman spectrum for calcium carbonate formed with presence of polyphosphinocarboxylic acid (PPCA), calcium carbonate reference and carbon steel	184
Figure 0.9: Raman spectrum for iron carbonate formed with presence of alcohol ethoxy phosphate ester, iron carbonate reference and carbon steel	185
Figure 0.10: Raman spectrum for iron carbonate formed with presence of C12-C14 alkyl dimethyl benzyl-amonium chloride, iron carbonate reference and carbon steel.....	186
Figure 0.11: Raman spectrum for iron carbonate formed with presence of ethoxylated imidazolines, iron carbonate reference and carbon steel	187

Chapter 1 Introduction

Oil and gas remains one of the largest sources of energy in the world [1]. The natural reserves of this product are very important from a political and social point of view. However the most important factor of oil and gas is its economic potential.

World use of petroleum products continues to grow [1]. In the hunt for new lands rich in oil and gas, drilling activities have moved to more severe environments - deeper high-pressure/high-temperature wells and in deeper waters. As a consequence, scale, corrosion and biofouling are major operational problems in oil and gas production [2]. The present project focuses on calcium carbonate scale inhibition and CO₂ corrosion inhibition in the oil and gas industry.

1.1 Oil and gas: origin and exploration

Crude oil is derived mainly from the remains of plants and animals [3, 4]. Organic material falls on the sea bed buried by other materials and decays. These organic remains can become source rocks for crude oil or natural gas. As the temperature and pressure of the buried organic matter grows due sediment material overlay transformation to kerogen occurs (Figure 1.1).

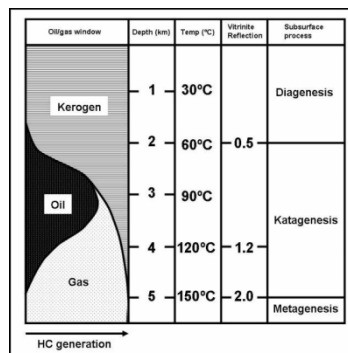


Figure 1.1 Alteration of sediments [5]

Kerogen changes into liquid state (oil) at around 90°C and into a gas at around 150°C [3]. The lighter densities of gas and oil then rise up through the water and other substances in the pore spaces of the surrounding rock formation. The oil and gas movement is stopped by impermeable rock formations. However they escape to the surface sometimes and appear as surface seeps (Figure 1.2).

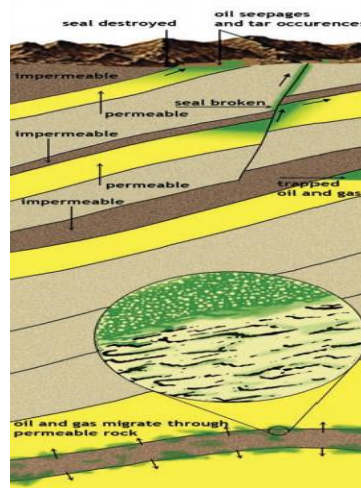


Figure 1.2 Oil and gas migration from the source rock [6]

If the presence of oil or gas is confirmed, the exploration stage is implemented. According to the Speight [7] three phases of recovering oil can be distinguished: primary, secondary and tertiary. The recovery techniques are presented in Figure 1.3.

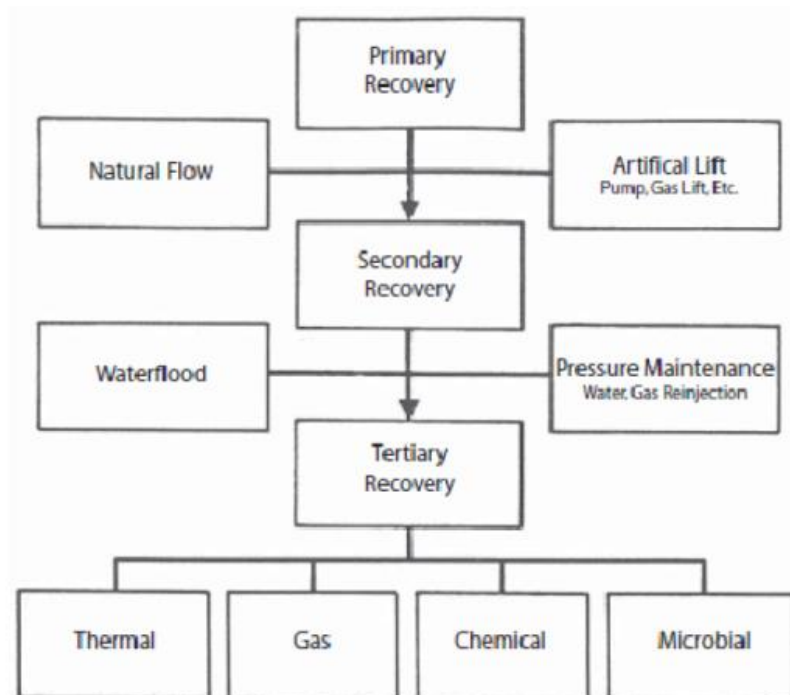


Figure 1.3 Methods for oil recovery [7]

The oil is driven through the reservoir by natural pressure caused by formation water. The pressure is usually high enough to pump oil to the surface. This type of recovery refers to the primary recovery process. As the reservoir matures the pressure inside the well starts to decrease. At this

point secondary recovery techniques need to be applied. This involves the injection of gas or water into reservoir, with the aim to lift oil or natural gas to the surface. The third method is tertiary recovery which relies on increasing liquid mobility within the reservoir. It can be achieved by injecting solvents, detergents or steam [7].

The mixture of oil, gas and saline water are typically in a state of equilibrium within the reservoir. The oil or natural gas extraction usually results in a change away from equilibrium state which causes scale deposition [8]. While CO₂ dissolved in the formation water forms weak carbonic acid and it causes the problem of corrosion (CO₂ corrosion – sweet corrosion) [9].

1.2 Inorganic scaling and impact for the oil and gas industry

Scale deposit formation is a natural consequence of handling water associated with crude oil. The formation of scales from flowing brine solutions occurs due to brine being supersaturated with scaling minerals, suitable nucleation sites and sufficient time are available. Scale deposition can cause many problems such as: blocked pores in the reservoir, reduced cross-section of pipelines and reduced efficiency of surface facilities [8]. Many different mineral scales are found in oilfields: sulphates (barium, strontium and calcium), carbonates (e.g. calcium, magnesium), iron scales (iron oxides and hydroxides). However calcium carbonate and barium sulphate are the most common due to their very low solubility.

1.3 Present removal and inhibition methods

Scaling conditions can be avoided by applying one or two known techniques: antiscalants surfaces [10], mechanical cleaning (scraping, wiping, etc.) and chemical (inhibitors) [8, 10]. However, the most popular method used in the oil and gas industry is scale inhibitors. Scale inhibitors can be quite specific in their action towards individual scaling minerals due to their different mechanisms of scale inhibition [9].

1.4 Corrosion and impact for the industry

The crude oil and natural gas from the oil reservoir typically contain some level of CO₂ or/and H₂S. CO₂ dissolves with the water forming carbonic acid and makes brines very corrosive. The corrosion of drilling, production, refinery and transportation facilities can have serious influences: lost revenue, lost production, delays in production, contaminated products,

environmental damage, safety risks, excessive maintenance and replacement costs [11]. Over 25% of these difficulties in the oil and gas industry are related to corrosion with sweet corrosion being responsible for more than half [11].

1.5 Current prevention methods

Corrosion attack in many cases can be reduced to acceptable levels. However it is impossible to totally eliminate the corrosion process. Numerous methods are applied to reduce corrosion: cathodic protection, corrosive gas removal, coatings, material selection, design and chemical inhibition (inhibitors) [12]. Different corrosion inhibitors slow the corrosion process by: reducing ion diffusion to the metal surface or changing the electrochemical potential of the metal to more cathodic or noble [12].

1.6 Combined inhibitors

Corrosion and scale deposition are routinely controlled by the use of corrosion inhibitors (CI) and scale inhibitors (SI). However, the application of combined inhibitors (ComI) is establishing itself as the preferred option [13]. The reasons for this lie in the fact that they help to minimise potential compatibility problems between corrosion and scale inhibiting chemicals also lack of umbilicals for injection as well as reducing chemical costs. The development of combined inhibitors is a logical choice and researchers have indicated that combined inhibitors are capable of adequately controlling corrosion and scale processes [14-17].

1.7 Aims and objectives of the PhD

Corrosion and scale deposition are well known flow assurance issues in the oil and gas industry. Corrosion control of carbon steel and scaling in pipelines requires an understanding of the simultaneous occurrence of both processes. There are a number of studies which have separately researched general corrosion, pitting corrosion, bulk scaling and surface scaling with and without the presence of inhibitors. However, in the oilfield engineers have to tackle two, three or four processes in the field at the same time. To date there have been few studies demonstrating the interactions between scale and corrosion processes. However, combined scale/corrosion inhibitors (mixture of single components (scale and corrosion inhibitors)) are

gaining popularity in the oil and gas industry as means of mitigating both those processes. The aims of this PhD study are as follows:

- Asses the newly-developed combined bulk jar scaling/bubble cell [18] as a method of assessing:
 1. general corrosion
 2. localised corrosion
 3. bulk precipitation
 4. surface depositionwhen all processes occurring simultaneously
- Evaluate the effect of single components of the combined inhibitors on all four processes when only single component is present in the system
- Evaluate the effects of the single components of the combined scale/corrosion inhibitor and/or synergistic effects on all four processes when all single components are blended together
- Develop empirical relation equation (model) for prediction corrosion and scale processes

Objectives of the PhD

- Run number of the test in the lab with the use a newly developed bulk jar test/bubble cell. Use electrochemical techniques to measure in-situ general corrosion and measure bulk scaling by turbidity meter and Inductively Coupled Plasma. Use surface analysis techniques such as: Scanning Electron Microscope, X-Ray Diffraction Analysis and Light Interferometry to assess the localized corrosion and surface scaling.
- Use an experimental design method to design test matrix and quantify the effects of the single components of the combined scale/corrosion inhibitor and/or synergistic effects on all four processes.

1.8 Contribution of this research

- Further understanding of effect CaCO_3 scaling on general corrosion by finding that scale forms mainly on ferrite grains microstructure leaving pearlite grains uncovered.
- 2-mercapthoethanol almost completely prevents of formation of calcium carbonate on the metal surface. Small calcium carbonate crystals which formed during the tests with 2-mercapthoethanol were composed only by calcite crystals.
- Polyphosphinocarboxylic acid showed good inhibition against the localised corrosion.
- The simple linear regression model was developed to predict corrosion and scale when these processes occurs simultaneously.

1.9 Scope of work

The scope of work was to do literature review and study methodology to produce reproducible results in a newly developed bulk jar test/bubble cell. At the same time, the work also focused on choosing the most suitable method from an experimental design to study the effect of the combined inhibitors on the general corrosion, localized corrosion, bulk scaling and surface scaling. The interaction between inhibitors and the scale (iron carbonate and calcium carbonate) has been investigated by FTIR and Raman spectroscopy analysis. Simultaneously, the work was concentrated to develop an empirical equation to predict corrosion and scale.

1.10 Outline of the thesis

Chapter 1 gives a brief introduction of the industrial background associated to mineral scale and corrosion problems in the oil and gas industry as well as the aims and the objectives of this thesis.

Chapter 2 presents overview of mechanism of calcium carbonate formation and theories of nucleation and crystal growth. It presents the background of the mechanism of aqueous corrosion and CO_2 corrosion.

Chapter 3 provides the literature review for calcium carbonate scale and CO₂ corrosion in the oil and gas field. A review the different parameters influencing calcium carbonate formation and CO₂ corrosion and the different methodologies to study them. It presents the mechanisms of inhibition of corrosion and scale, and the different inhibitors used in the industry.

Chapter 4 presents the methodology and materials used to complete the aims and objectives of this research.

Chapter 5, 6, 7 and 8 presents the results obtained in this study.

Chapter 5 provides results for the test when the corrosion and scale process occurring simultaneously in the absence of any inhibitor while Chapter 6 gives the results of the effect of the single component of combined inhibitor on the corrosion and scale processes occurring simultaneously. Chapter 7 presents results of corrosion and scale assessments in the presence of the combined inhibitor and calculation of the quantitative effect of single component inhibitor and their interactions: on general corrosion, localized corrosion, surface scaling and bulk precipitation. Chapter 8 gives the results obtained with the Fourier Transform Infrared Spectroscopy and Raman spectroscopy. The interactions between the single components and calcium carbonate or iron carbonate formed on the metal sample has been investigated.

In Chapter 9 the results are discussed also referring to the literature reviewed.

Chapter 10 presents the main findings from this thesis and Chapter 11 present some recommendations for future work.

Chapter 2 Theory of scale and corrosion

2.1 Introduction

This PhD project has focused only on calcium carbonate and CO₂ corrosion. The aim of this chapter is to present the theory of mechanism of calcium carbonate formation and the mechanism of aqueous corrosion and CO₂ corrosion.

2.2 Mechanisms of calcium carbonate formation

Calcium carbonate precipitation from a solution occurs in three steps: supersaturation, nucleation and crystal growth. The liquid needs to be supersaturated for the nuclei to form and increase in size.

2.2.1 Calco-carbonic equilibrium

The calco-carbonic system is derived from the dissolution of carbon dioxide and carbonate minerals into the water [19]. Calcium carbonate is governed by the following equilibria [20]:



The reaction in Equation (2-4) can be shifted in the direction to dissolve or precipitate scale and this depends on: supersaturation, temperature, pH and flow rate of the solution [19].

2.2.2 Saturation

The saturation ratio of the calcium carbonate formation has an important impact on the induction, growth, crystal morphology and rate of scale formation [21]. The saturation ratio (*SR*) of calcium carbonate can be calculated from the following equation:

$$SR = \frac{(a_{Ca^{2+}}) * (a_{CO_3^{2-}})}{K_{sp}} \quad (2-5)$$

where K_{sp} is the solubility product ($CaCO_3$) depending on the temperature and the pressure, and $(a_{Ca^{2+}})$ and $(a_{CO_3^{2-}})$ is the ion activity [22].

According to Mullin [22] three different levels of solution SR can be distinguished:

- $SR < 1$: the solution is undersaturated and scale formation is not thermodynamically feasible.
- $SR = 1$: The solution is saturated. The scale formation and dissolution rate in the solution is the same and no scale is formed in the solution.
- $SR > 1$: The solution is supersaturated and scale formation is thermodynamically possible.

In a solution which is undersaturated or at equilibrium homogenous spontaneous nucleation cannot occur. Crystals added to an undersaturated solution will dissolve while in a solution at equilibrium the crystals will not be dissolved (no nucleation or the growth). The supersaturated region can be divided in three parts [23]:

1. the metastable zone – no homogenous spontaneous nucleation however, crystals added will grow
2. the labile zone – spontaneous homogenous nucleation occurs
3. the precipitation zone – oversaturated in which an amorphous precipitate is formed

In calcium carbonate formation ions are the crystallizing agents and the crystals of calcium carbonate are the macromolecules.

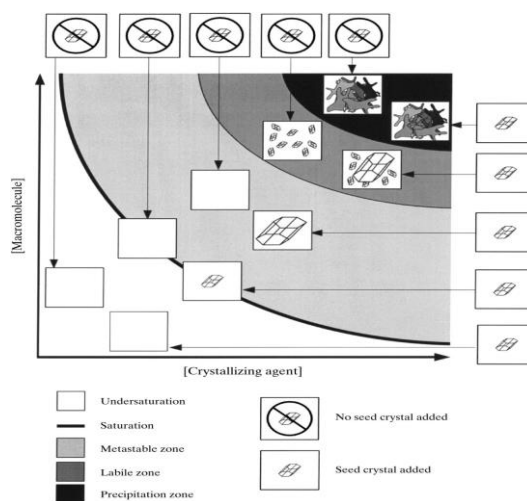


Figure 2.1: A representation of crystallisation in the absence and presence of macroseeds [23]

The change of Gibbs free energy is the driving force for calcium carbonate formation. During formation the Gibbs free energy is changing. Equation (2-6) demonstrates the differences in the Gibbs free energy during a nucleation (formation) process [24]:

$$\Delta G = -\frac{1}{2}R_g T \ln \left(\frac{IP}{K_S^0} \right) \quad (2-6)$$

with R_g as the gas constant, T the absolute temperature, IP the activity product of CaCO_3 in the solution and K_S^0 solubility at equilibrium.

After the solution reaches supersaturation and when crystals start form, the time before the solution reaches supersaturation and first nucleation starts, is called induction time.

2.2.3 Induction time

The induction time can be defined as the time before supersaturation and the first observable changes in the physical property of the precipitating system (ie. the appearance of crystals or turbidity, change of solution conductivity and change in solution composition etc.) [25, 26]. The induction time (t_{ind}) equals the nucleation time (t_n) and the time needed for a nucleus to grow until a detectable size (t_g) as seen in Equation (2-7) [27]. The precise measurement of induction time is very challenging because the detection of the nuclei depends on the accuracy of the method used.

$$t_{\text{ind}} = t_n + t_g \quad (2-7)$$

In case where the homogeneous nucleation is followed by a diffusional growth, the induction period is defined by Equation (2-8) [26]:

$$\log t_{\text{ind}} = C + \frac{\alpha_t}{(\log S_a)^2} \quad (2-8)$$

where t_{ind} is the induction time, C is a constant, α_t is the slope of $\log t_{\text{ind}}$ versus $(\log S_a)^2$ function and S_a is the supersaturation of the solution.

The relationship between the induction time and supersaturation are presented in the equation developed by Gill *et al.* [28].

$$K = T_{Ca}^{(p-1)} t \quad (2-9)$$

where K is a constant, T_{Ca} is the molar concentration of ions, p the apparent number of ions in the critical nucleus, t the induction time.

2.2.4 Nucleation

The stable nucleus is formed from several molecules. The different crystals mainly contain from 10 to several thousand molecules. The molecules

before they become stable ('insoluble') need to coagulate and have a certain orientation within a fixed lattice. The nucleation process is a 'chain reaction', starting by two molecules colliding into each other followed by further collision with other molecules until the nucleus is formed [22]. In calcium carbonate, calcium ions with carbonate ions dissolved in solution are paired and clustered by electrostatic interactions (Figure 2.2). This is followed by growth of the clusters by the addition of ions, until they reach a critical size [29].

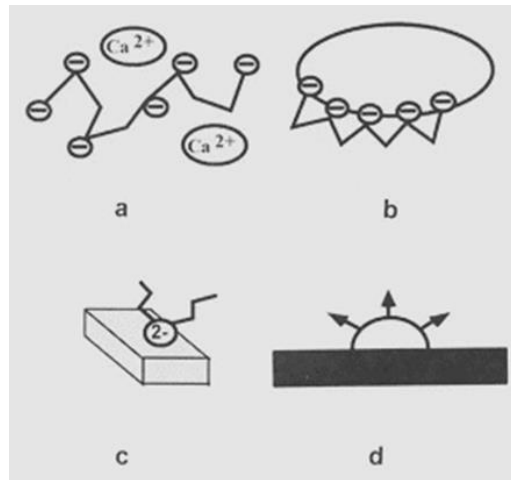


Figure 2.2: Schematic representations of processes involved in the initial stages of scale formation: (a) ion pairing, (b) prenucleation aggregate growth, (c) and (d) particle nucleation and growth [30]

Three different forms of nucleation are distinguished: primary homogenous nucleation, primary heterogeneous and secondary nucleation [22] as shown on Figure 2.3.

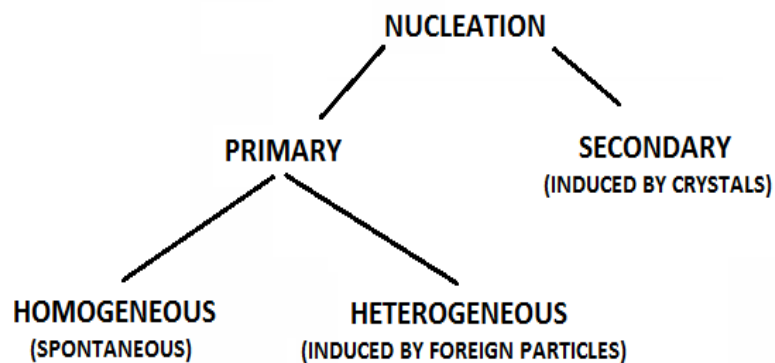


Figure 2.3 The different types of nucleation [22]

Primary homogeneous nucleation is determined by the formation of nuclei in an extremely supersaturated bulk solution free of any particles or impurities. From Equation (2-10), it can be calculated the number of crystals formed during the homogeneous nucleation following diffusional growth [14].

$$\log N = D - \frac{\alpha_N}{(\log S_a)^2} \quad (2-10)$$

where N is the number of crystals, D a constant, α_N the slope of $\log N$ versus $(\log S)^{-2}$ function and S_a the supersaturation.

Primary heterogeneous nucleation is induced by the solid surfaces which are present, impurities or ions in the solution. Primary heterogeneous nucleation is more predominant than primary homogeneous nucleation [31] and is possible in low supersaturated solutions.

Secondary nucleation is induced by parent crystals in the bulk solution.

2.2.5 Growth

After nucleation, the growth process leads to the formation of crystals of a noticeable size. There are three main theories of crystals: surface energy theory, adsorption-layer theory and dislocation theory [22].

2.2.5.1 Surface energy theory

According to Gibbs crystal growth is the entire free energy of a crystal when it is in equilibrium with its surroundings at a stable temperature and pressure would be a minimum for given volume (energy) [22]. If a crystal grows in a supersaturated solution, the development of the various faces will grow in such manner as to ensure that all crystal faces have the lowest total surface energy for a given volume [22]. In theory the surface energy and the rate of growth of faces should be inversely proportional to the reticular (lattice) density of the lattice plane. It means that crystal faces which have low reticular densities grow rapidly and eventually disappear while at the same time crystal faces with high reticular densities grow slow. Figure 2.4 presents an invariant crystal which grows and retains its shape during the growth process and the overlapping crystal which does not always maintain its shape during growth.

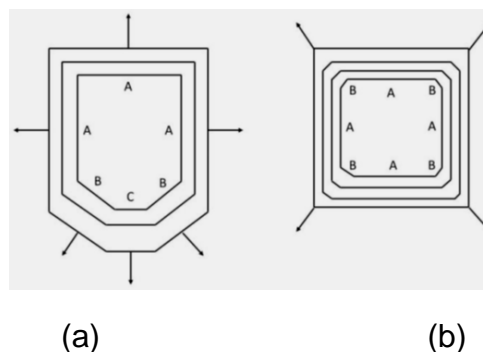


Figure 2.4: Velocities of crystal growth faces: (a) invariant crystal: (b) overlapping crystal [22]

2.2.5.2 Adsorption layer theory

Kossel, Stranski and Volmer (KSV) developed the adsorption theory [32]. This theory suggested that the crystal surface is not homogeneous, it contains smooth surfaces, steps and kink sites (Figure 2.5). Kink sites are most likely the sites where growth will occur. A kink site has three faces which can be linked to the growth unit (atoms, molecules or ions) and the binding energy. It has the highest binding energy compared to the step site and the flat surface site [33]. It has been suggested that atoms tend to bind to the crystal lattice where the binding force are the greatest; and this step will continue until the whole plane is completed. This means that no new layer can be erected till the formation of the previous has finished. Though, this last suggestion was not confirmed by experimental work [33].

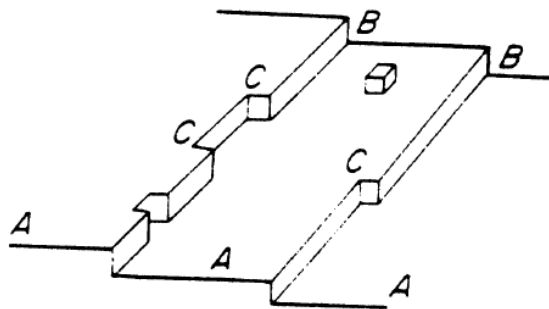


Figure 2.5: Growing crystal surfaces: (A) flat surfaces, (B) steps, (C) kinks [22]

2.2.5.3 Dislocation

A dislocation is a defect of the crystal structure. It is very common for crystals to grow in irregular shapes. The most common cause of that are impurities, foreign atoms or ions. The screw dislocation has been characterized by the Burton, Cabrera, Franck (BCF) theory [22, 32]. Throughout the process of the crystal growth occasionally some small faces can be excessively develop leading to one of the parts of the crystal to be dislocated.

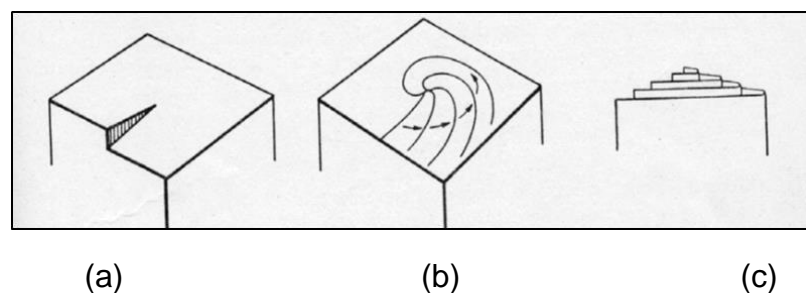


Figure 2.6: Development of growth spiral starting from screw dislocation [22]

2.2.5.4 Growth mechanism

Crystal growth occurs in three successive reaction steps [34]:

- the transport of solute to the crystal solution interface
- the adsorption of solute at the surface
- the incorporation of the crystal constituents into the lattice

According to Noyes and Whitney [35] crystallisation is the reverse dissolution. Crystallisation and dissolution rates corresponded to the change of concentration at the surface and concentration in the bulk solution. This is shown in Equation (2-11) [22]:

$$\frac{dm}{dt} = k_m A (c - c^*) \quad (2-11)$$

where m is the mass of the solid deposited with time, k_m the coefficient of mass transfer, A the surface area of the crystal, C the solute concentration in the solution and C^* the equilibrium saturation concentration.

In the case of calcium carbonate, the decrease of calcium concentration has been expressed by Nancollas and Reddy according to Equation (2-12) and is shown below [26]:

$$\frac{-d[Ca]}{dt} = k_c A(t) (C_{Ca} - C_{Ca_{eg}})^g \quad (2-12)$$

where k_c is the crystal growth constant, $A(t)$ the surface area of the crystal, C_{Ca} is the molar concentration of calcium, $C_{Ca_{eg}}$ is the molar concentration of calcium at equilibrium and g the kinetic order of crystal growth.

2.3 Aqueous corrosion

2.3.1 Definition of corrosion

Corrosion has been defined as the degradation of a material's properties or mass over time due to a chemical reaction with the environment [36, 37]. The mechanism of CO_2 corrosion is complex; and its understanding, prediction and control are important challenges [38].

The corrosion of metals in aqueous solution is an electrochemical mechanism. In this mechanism atoms at the surface of the metal depart their matrix and go in to solution as metal ions. Then, electrons migrate through the metal to a site where appropriate reaction occurs. Electrons are consumed by electrochemically active species in contact with the metal surface [37].

2.3.2 Thermodynamics

2.3.2.1 Free energy

Metals are transformed from ores (low energy level) with the use of external energy. Metals try to revert to their lower energy state by spontaneously reacting with the corrosive environment [37, 39]. The driving force for metallic corrosion is the Gibbs free energy change (ΔG), the change (ΔG) in Gibbs free energy show tendency of the corrosion reaction to occur [37]. If $\Delta G < 0$, the corrosion reaction occurs spontaneously [37]. When ΔG is positive, the metal requires energy to react with the surrounding environment. However ΔG is not indicating the rate of the reaction, the rate of reaction is influenced by other factors.

2.3.2.2 The Corrosion cell

Aqueous corrosion is an electrochemical process established by Michael Faraday. An electrochemical corrosion cell (Figure 2.7) contains four key components [37]:

- The anode, which is the corroding metal and where the anodic/oxidation reaction occurs
- The cathode, which is the metal or another electronic conductor and where the cathodic/reduction reactions occurs
- The electrolyte, which provides a conducting path between the cathode and anode
- The electrical connection, which enables electrons to move between the cathode and anode

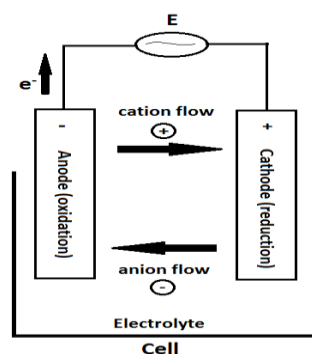


Figure 2.7 An electrochemical cell [40]

2.3.2.3 Corrosion reactions

Corrosion reactions can be divided into cathodic and anodic reactions. The anodic reaction is:



where M is the metal and n is the number of electrons (e^-) released by the metal.

The electrons produced do not go into the solution. They remain on the corroding metal and migrate through the electrical connection between the cathode [37].

The cathodic reaction consumes electrons produced by the anode. The reducible species in the electrolyte adsorb on the metal surface and remove the electrons [37]. Both reactions (the anodic and cathodic) of the corrosion processes are occurring on the same metal surface and the free energy changes for each reaction can be measured as electrical potentials and current flow [41].

An equation derived by Faraday relates potential difference and charge transported with the Gibbs free energy change of the corrosion process:

$$\Delta G = (-nF)E \quad (2-14)$$

where ΔG is the free energy change for the corrosion reaction in kJmol^{-1} ; n is the number of electrons taking part in the corrosion reaction; F is the Faraday constant (96 494 Coulombs/mole) and E is the potential difference at non-standard conditions in Volts.

By using the superscript ($^\circ$), this equation can be rewritten to represent standard conditions: temperature of 273.15 K and pressure of 1 atmosphere.

$$\Delta G^\circ = (-nF)E^\circ \quad (2-15)$$

Values of E° are provided in standard tables using the half redox reaction. Examples of standard half cell potentials are provided in Table 2.1. Metals with a positive value of E° (for example gold) are qualified as noble metals. Metals with a negative value of E° corrode readily and tend to be anodes.

Table 2.1 Standard electrode potential E° (V) standard hydrogen electrode (SHE)[41]

Electrode	Standard Electrode Potential E° (V) (SHE)
$Au^{3+} + 3e^- = Au$	+1.50
$Fe^{3+} + e^- = Fe^{2+}$	+0.771
$2H^+ + 2e^- = H_2$	0.000 (by definition)
$Fe^{2+} + 2e^- = Fe$	-0.440
$Zn^{2+} + 2e^- = Zn$	-0.763

2.3.2.4 The Nernst equation and cell potential

Corrosion is dependent upon temperature because the free energy states of the species depend upon temperature. The change in Gibbs free energy can be calculated at given activities of the reactants and products of reaction, as follows:

$$\Delta G = \Delta G^o + RT \ln \frac{[a_{\text{products}}]}{[a_{\text{reactants}}]} \quad (2-16)$$

where R is the gas constant (8.314 J/mol*K), T is the absolute temperature in Kelvins (K), and $[a_{\text{products}}]$ or $[a_{\text{reactants}}]$ are the concentrations of all the product or reactant species multiplied together in moles.

The Nernst equation was deduced by combining the thermodynamic equations and Faraday's Law. This equation determines how the cell potential varies with cell conditions:

$$\Delta E = \Delta E^o + \frac{RT}{nF} \ln \frac{[a_{\text{products}}]}{[a_{\text{reactants}}]} \quad (2-17)$$

Cell potential containing of both anodic and cathodic reaction can be combined arithmetically from electrode potentials. If the difference of cell voltage is calculated from Equation (2-18), (the galvanic potential cells which operate spontaneously) will give a positive cell voltage.

$$E_{\text{cell}} = E_{\text{cathodic}} - E_{\text{anodic}} \quad (2-18)$$

where E_{cell} is the cell potential in Volts, E_{cathodic} is the reduction potential of the cathodic reaction and E_{anodic} is the reduction potential of the anodic reaction.

If reduction in Gibbs energy occurs then a spontaneous reaction of corrosion occurs, therefore ΔG must be negative. So, E_{cell} must be positive for corrosion to occur.

2.3.3 The mechanism of aqueous corrosion and electrical double layer (EDL)

After a metal is immersed into an aqueous solution small local anodic and cathodic areas are generated rapidly at the interface between the solids and liquids. This is caused by differences in free energy states between reacting sites. As mentioned before, once metal corrodes, ions at the surface of the metal depart from their matrix leaving behind their electrons. This causes a negative charge on the metal surface and tends to attract some of the positively charged ions. Water molecules then surround the metal ions as they escape the lattice, hydrating them. The water layer around the ions

prevents them diffusing freely in the bulk solution and they are prohibited from becoming metal atoms. Simultaneously, the positive charged ions in the electrolyte are attracted toward the opposite charge surface [42].

Therefore, electrolytes which contain water molecules and ions from both the metal and bulk electrolyte are adjacent to an electrode surface; it has a different composition compared to the rest of the bulk phase. It is referred as the electrical double layer (EDL) [42].

When two opposite charged planes created by the EDL are separate physically, it causes capacitor-like behaviour. The level of capacitance can be defined by the metal and electrolyte composition. Excess electrons which are transferred to the electrochemically active ions can be resisted by metal. So, the EDL can behave as a resistor too [42].

When two opposite charged planes in an EDL are separate, this separation certainly creates an electrical potential which can be measured. Subsequently the participation of electron transfer in corrosion process suggests that, it is a relationship between the EDL chemical composition, voltage and electric current [42].

2.3.3.1 The relationship between EDL chemical composition, electric current and voltage

E_{corr} is a free corrosion potential at which the sum of the anodic and cathodic reaction rates are equal zero. The metal and the nature of the solution influences the E_{corr} . The corresponding current density is called i_{corr} (the corrosion current density) [43].

E_{corr} values can change when EDL chemical composition changes and applied voltages change the EDL chemical composition. EDL behaviour to electrical potential can be expressed by The Nernst equation:

$$\Delta E = \Delta E^o + \frac{RT}{nF} \ln \frac{[a_{products}]}{[a_{reactants}]} \quad (2-19)$$

The chemical activity components of the reaction ($[a_{products}]$ and $[a_{reactants}]$) can be replaced with the activity coefficient (γ) multiplied by the concentrations of species represented by an element symbol in brackets (e.g. $[Fe^{2+}]$). Therefore, the equation can be rewritten as:

$$\Delta E = \Delta E^o + \frac{RT}{nF} \ln \frac{\gamma_p [products]}{\gamma_r [reactants]} \quad (2-20)$$

Where γ_p and γ_r are the activity coefficients for products and reactants, respectively.

The potential which is measured, depends on the concentrations of both the metal ions and electrochemically active species in the EDL. The measured potential is dependent upon the concentrations of both the metal ions and electrochemically active species in the EDL. The magnitude of a measured potential will therefore change with EDL chemical composition. Hence, if the bulk electrolyte composition is changed in this way it will change the EDL chemical composition, E_{corr} will change too [42, 44].

The Nernst equation expresses the potential of a material to corrode, not the rate at which the material will corrode. Ohm's Law states that if the EDL has a voltage and a resistance it must have a current. The Butler-Volmer equation describes the relationship which is experimentally observed between applied current density and potential corroding electrodes; in the environment where no competing reduction-oxidation reactions occur [45]. This relationship can be applied in the presence of single anodic reactions and a single cathodic reactions:

$$i_o = i_{corr} \left[e^{\left(\frac{(1-\alpha)nF(E-E_{corr})}{RT}\right)} - e^{\left(\frac{-\alpha nF(E-E_{corr})}{RT}\right)} \right] \quad (2-21)$$

where i_o is the external current in Amps/cm² flowing to or from the electrode because of an applied potential, i_{corr} is the corrosion current density in Amps/cm² that occurs when the electrode is at E_{corr} , E_{corr} is the free corrosion potential in Volts (V), E is the applied potential in Volts (V), a is a coefficient ranging from 0 to 1 and n , F , R and T have been explained before.

This equation can be expressed in term of Tafel slopes (β_a and β_c) respectively. Which are given by the slopes of the polarisation curves in the anodic and cathodic regions for a plot of E vs $\log(i)$:

$$i_o = i_{corr} \left[e^{\left(\frac{2.303(E-E_{corr})}{\beta_a}\right)} - e^{\left(\frac{-2.303(E-E_{corr})}{\beta_c}\right)} \right] \quad (2-22)$$

This relationship offers the foundation for the electrochemical polarisation technique for a corroding electrode at its E_{corr} , [45].

2.3.4 Electrochemical measurement techniques

2.3.4.1 Linear Polarisation Resistance (LPR) method

The linear relationship between applied voltage and current inside a few millivolts of polarisation from E_{corr} , has been observed by many researchers. Stern and Geary [46] simplified (Equation (2-22)) relationship to the following form:

$$R_p = \left[\frac{\Delta E}{\Delta i} \right]_{(E-E_{corr}) \rightarrow 0} = \frac{1}{2.303} \left[\frac{\beta_a \beta_c}{\beta_a + \beta_c} \right] \quad (2-23)$$

Reordering this equation gives:

$$i_{corr} = \frac{1}{2.303 R_p} \left[\frac{\beta_a \beta_c}{\beta_a + \beta_c} \right] = \frac{B}{R_p} \quad (2-24)$$

where R_p is the polarisation resistance ($\text{Ohm} \cdot \text{cm}^2$), $R_p = \frac{\Delta E}{\Delta i}$ for a plot of E vs I . The B factor is influenced more by the smaller of the β_a and β_c Tafel slope, in situations where both are unequal.

If R_p , β_a and β_c are known, then the corrosion rate can be determined at any particular time [45]. Within the range of $\pm 5-20$ mV of E_{corr} the measured current is behaving nearly linearly. Therefore, this method is commonly called the linear polarisation technique.

2.3.4.2 Tafel plots

One of the advantages of linear polarisation curves are that there is no need to regularly replace electrodes. However, the corrosion rate is estimated because the Tafel slopes are not measured. The range of potential in which Tafel plots are measured is around 200 to 500mV from E_{corr} [42]. Tafel plots provide more information than linear polarisations tests [42].

The measured current in the different potentials are plotted on a logarithmic scale illustrating the cathodic and anodic branch as presented in Figure 2.8. Both of them can be activation controlled - controlled by the reaction rate or diffusion controlled - dictated by the rate of diffusion of species to and from the surface.

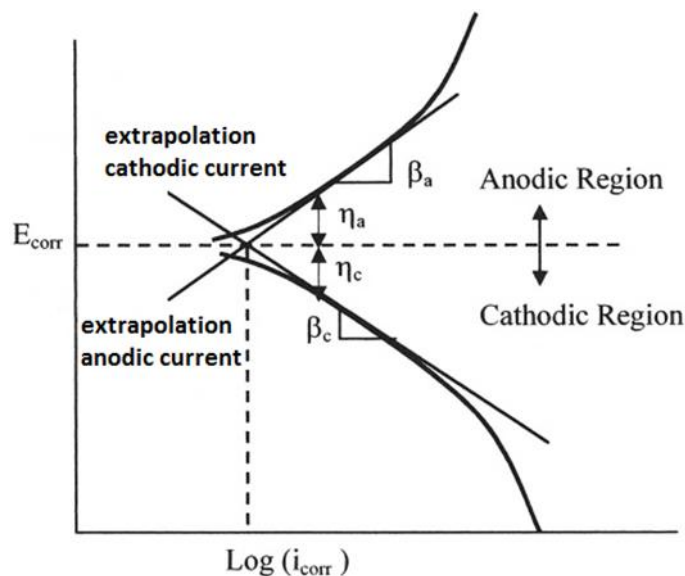


Figure 2.8: Representing how to determine Tafel slopes [42]

Tafel slopes have units of mV/decade (decade is related to the current). This can be found by determining the slope of the anodic and cathodic slopes from the linear parts of the E vs $\log(i)$ plot. By determining Tafel slopes, it is possible to calculate the corrosion rate of a metal. If this information is used in combination with linear polarisation data and the Stern-Geary equation, a value of corrosion rate can be calculated [47]. Otherwise, i_{corr} (corrosion current density) can simply be read directly from a Tafel plots.

After i_{corr} has been read, then the corrosion rate (CR) in mils per year can be calculated as showed in Equation (2-25) [42]:

$$CR = i_{corr}(K) \frac{1}{\rho} (\epsilon) \quad (2-25)$$

where K is a conversion terms equal to $1.287 \cdot 10^5$ (eq.s.mils)/(C.cm.y), ρ is the metal density (equal to 7.85 g/cm^3 for carbon steel) and ϵ is the equivalent weight which is the molecular weight/number of electrons in the metal anodic half reaction (equal to 27.9 g/eq).

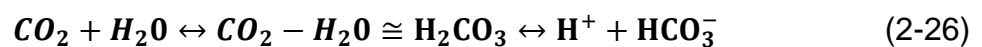
The value of the corrosion rate can be converted from mils per year (mpy) to millimetres per year (mm/y) ($1\text{mpy} = 0.0254 \text{ mm/y}$) [48].

Tafel plots can be used only to measure the general corrosion not localised corrosion. It requires extended anodic polarisations for these types of tests [42].

2.4 CO₂ corrosion mechanism

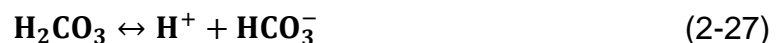
2.4.1 Cathodic reactions in CO₂ environment

CO₂ dissolves in water to give a weak carbonic acid H₂CO₃ ([38]:



Then partially dissociates in two steps [49, 50]:

a) forming bicarbonate ions



b) forming carbonate ions



Hydrogen evolution is then the next step:



The reaction of the dissociation Equation (2-27) and Equation (2-28) occurs much faster than other simultaneous reactions in the system. Reaction of

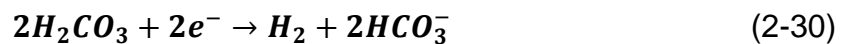
CO₂ dissolving in Equation (2-26) is much slower than the dissociation reactions.

The most important cathodic reaction is considered the hydrogen evolution reaction (Equation (2-29)). It is limited by the rate at which hydrogen ions (H⁺) can be transported from the bulk solution to the steel surface [51].

The reaction (Equation (2-29)) is easily influenced by the pH level. The fast consumption H⁺ ions can be readily replenished by the dissociation reactions of H₂CO₃. Therefore, in the environment where the pH is greater than 4; the presence of CO₂ makes a much more corrosive environment than that can be found in a solution of strong acid at the same pH [51].

The cathodic reaction (Equation (2-29)) is dominating in the CO₂ system; where the pH is lower than 4 because of the high concentration of H⁺. In the pH range from 4 to 6, another cathodic reaction becomes important in addition to the reduction of H⁺ [49].

This reaction is the direct reduction of H₂CO₃ [49]:



This reaction is controlled by the reaction of CO₂ dissolving in water (Equation (2-26)). It is related to the H₂CO₃ concentration; which depends on the partial pressure of CO₂ [51].

2.4.2 Anodic reactions in CO₂ environment

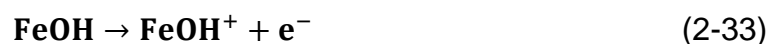
The anodic reaction is a dissolution of metal in solutions containing CO₂. The main anodic reaction for a carbon steel in solution containing CO₂ is as follows:



According to Bockris *et al.* [52], the Fe is oxidized by reaction with water (first step):



Then is followed by further oxidation of Fe²⁺ (second step):



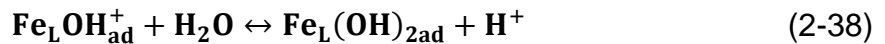
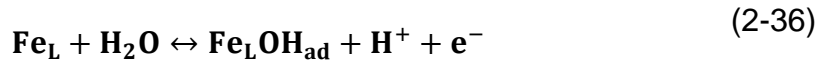
The second step is considered as the rate determining step in the overall anodic reaction [53].

In the third final step Fe²⁺ is produced:

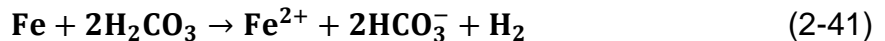


In literature, the majority of research articles appear to support the mechanism suggested by Bockris *et al.* [52].

In a recent study by Nešić *et al.* [54], it is suggested that the anodic dissolution of iron is influenced by the presence of CO₂. The different kinetics reactions of iron dissolution in solution saturated with CO₂ for strong acids are explained. The difference is to be associated with carbonic species acting as chemical ligands and stimulating the dissolution of iron. This effect was found to be independent of pH. The concentration of the carbonic species H₂CO₃ and CO₂ is pH independent. In this mechanism, the ligand Fe_L denotes the complex Fe-CO₂ which is formed and adsorbed at the electrode surface. This stimulates the dissolution of iron. Numerous sequential models have been used to explain this findings. One of them explains the experimental results for pH > 5:



The overall reaction is presented in Equation (2-41):



2.5 Summary

This chapter is presented the theory of mechanism of calcium carbonate formation and the mechanism of aqueous corrosion and CO₂ corrosion.

In the next chapter in the first part of literature review will present how different parameters affect the formation of calcium carbonate. It will present different strategies to prevent formation of calcium carbonate. The second part will present the literature review of CO₂ corrosion as a complex process. It will present the formation of iron carbonate scale and how various factors influencing it. The third part of literature review will present the effect of combined inhibitors on scale and corrosion processes and factors influencing performance of the combined inhibitor.

Chapter 3

Literature reviews of calcium carbonate and CO₂ corrosion

3.1 Introduction

This PhD project has focused only on calcium carbonate and on carbon steel corrosion in CO₂-containing environments.

The aim of the first part of this chapter is to present various form of scale, the different polymorphs of calcium carbonate and the different chemical and physical parameters influencing the formation process. In first part of chapter a review of the different methods of scale removal and inhibition used in oil and gas industry, with a main focus on scale inhibitors, will be presented. The mechanisms of inhibition will be presented as well as the common scale inhibitors in oil and gas industry. The first part of chapter will also present the different methods used to generate and to study CaCO₃ on the surface and in the bulk solution.

The aim of the second part of this chapter is to present different types of CO₂ corrosion. The second part of this chapter will outline the influence of different factors, including temperature and pH, on the CO₂ corrosion and the formation of the corrosion product (FeCO₃ - iron carbonate). The second part of chapter will also present a review of corrosion mitigation by corrosion inhibitors. Finally the mechanisms of inhibition as well as common corrosion inhibitors in the oil and gas industry will be reviewed.

The aim of third part of this chapter is to present the different methods of testing of combined inhibitors. The third part of the chapter will outline the influence of different factors on performance of combined inhibitor. Finally this third part of this chapter will also present a review of effect of corrosion inhibitors on scale processes and the effect of scale inhibitors on corrosion processes.

3.2 Different types of scales

Various types of scales can be found in oilfields. Inorganic scaling can occur in the well tubing and near wellbore formations of production, block pores in the reservoir, reduce cross-sections of pipeline, efficiency of surface facilities

and injection wells [55]. Different factors can cause formation of different scale deposits (Table 3.1 below).

Table 3.1 Most common oilfield scales [56]

Name	Chemical Formula	Primary Variables
Calcium Carbonate	CaCO_3	Temperature, Partial pressure of CO_2 , Total dissolved salts, pH
Calcium Sulphate: Gypsum Hemihydrate Anhydrite	$\text{CaSO}_4 \cdot 2\text{H}_2\text{O}$ $\text{CaSO}_4 \cdot 1/2\text{H}_2\text{O}$ CaSO_4	Temperature, Total dissolved salts, Pressure
Barium sulphate	BaSO_4	Temperature, Pressure
Strontium Sulphate	SrSO_4	Temperature, Pressure, Total dissolved salts
Iron Compounds: Ferrous Carbonate Ferrous Sulphide	FeCO_3 FeS	Corrosion, Dissolved gases, pH

3.3 Calcium carbonate polymorphism

Calcium carbonate is a substance that is capable of crystallizing into different crystal forms - known as polymorphs. It is encountered in several polymorphic crystalline phases. According to Brecevic *et al.* [57] the first polymorph that crystallizes as a “predecessor” is the amorphous calcium carbonate which evolves into a more stable state to form anhydrous polymorphs: calcite, vaterite and aragonite. Two other phases: hexa and monohydrate have been also studied [58, 59]. Examples of anhydrous polymorphs are shown in Figure 3.1 below.

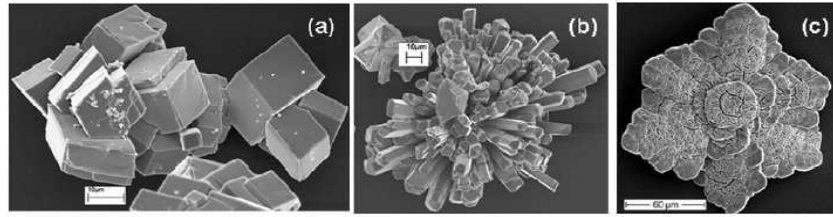
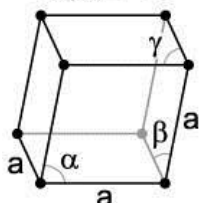
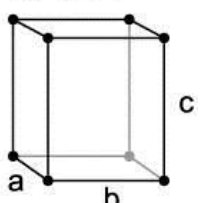
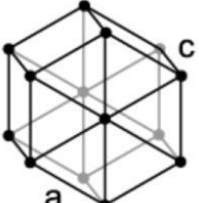


Figure 3.1: The crystalline polymorphs of calcium carbonate: (a) calcite, (b) aragonite and (c) vaterite [60]

The most stable form are aragonite and calcite, which can be found in nature. Vaterite is the unstable form of calcium carbonate, it is easily transformed into a more stable polymorph [61]. To differentiate the polymorphs, various techniques can be used such as SEM, XRD, Raman or FT-IR [58, 62].

Table 3.2 presents a summary of different information that can be found in the literature about the three polymorphs.

Table 3.2: Description of the three calcium carbonate polymorphs

Parameter	Calcite	Aragonite	Vaterite
Crystal system	Rhombohedral	Orthorhombic	Hexagonal
	$\alpha, \beta, \gamma \neq 90^\circ$ 	$a \neq b \neq c$ 	$a \neq c$ 
Crystal morphology	Cubic to rhombohedral	Needlike	Spherical or disclike
Density (g/cm^3)	2.71	2.93	2.66

3.3.1 Factors influencing calcium carbonate formation

3.3.1.1 Effect of temperature

Temperature is one of the most influencing factors to consider for a study of calcium carbonate formation. Calcite, aragonite and vaterite polymorph solubility in water decreases as temperature increases (Figure 3.2) [63].

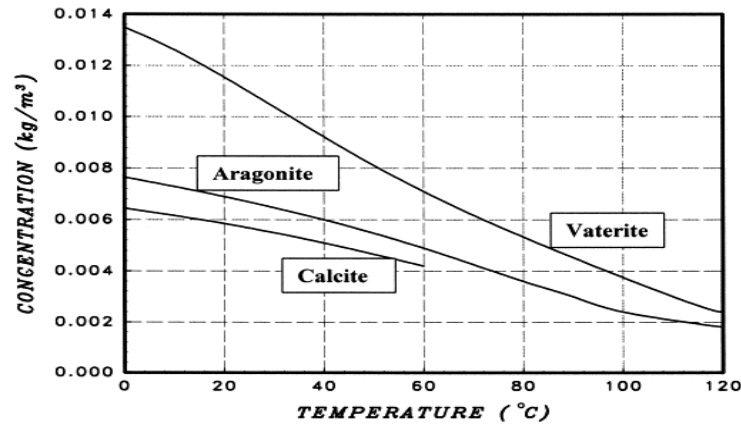


Figure 3.2: Solubility of calcium carbonate in water as a function of temperature [63]

In addition when the temperature increases the solution becomes more supersaturated and the nucleation process occurs faster which leads to a shorter induction time [64, 65].

At 25°C deposits are composed of calcite and vaterite while at higher temperatures aragonite is formed (50°C [66] and 60°C [67]).

3.3.1.2 Effect of pressure

During oil and gas production pressure in the system varies significantly and can reach 100MPa. According to researchers [68] scaling tendency marginally decreases when pressure increases. The effect of the pressure is more significant at high temperature (180°C) than at lower (50°C) [68].

3.3.1.3 Effects of hydrodynamic conditions

Hydrodynamic conditions of the system can affect scale growth rate. Deposition rate increases with Reynolds number [69, 70]. A higher flow supply provides more scaling elements onto the surface and the necessary activation energy needed for the nucleation or epitaxial growth of the crystals. Mass transport has been demonstrated to be diffusion controlled [69].

The morphology of the deposit is affected by the flow, thus in an environment where the flow rate is low, the CaCO₃ which is formed has bigger crystals and the layers are more compact [71, 72].

3.3.1.4 Effect of supersaturation

Supersaturation affects induction time [21, 73] and the growth of crystals in the bulk solution and on the metal surface [21]. In solutions with high supersaturation, with respect to calcium carbonate, the induction time is short and the growth of CaCO₃ is rapid for crystals nucleated in the bulk or

on the surface. While In solutions with low supersaturation, with respect to calcium carbonate, the induction time increases and the growth slowdown is only for the crystals nucleated in the bulk solution.

Heterogeneous nucleation occurs at low supersaturation and both heterogeneous and homogeneous nucleation occurs at higher supersaturation [73]. Increasing supersaturation results in a faster nucleation rates and in a development of 2-D nuclei [74].

The morphology of the crystals is affected by supersaturation. Decreasing supersaturation increases the aragonite fraction and results in the disappearance of the calcite polymorph in the scale that is formed [75, 76].

3.3.1.5 Effect of pH

Calcium carbonate is controlled by the calcocarbonic equilibrium presented in Equation (2-1) - (2-4). This system equilibrium is influenced by the pH. Figure 3.3 presents the distribution of the carbonic species according to pH. Calcium carbonate forms easily at a high pH.

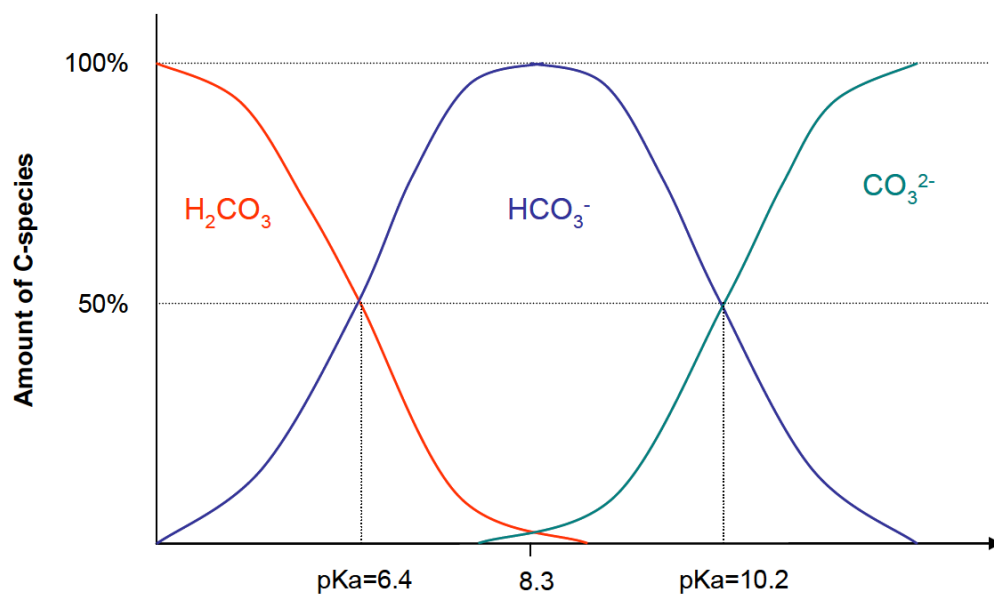


Figure 3.3 Distribution of carbon total fraction as a function of pH

pH affects crystal morphology, the higher the pH the greater the effect [77]. At a higher pH smaller average size particles formed due to higher supersaturation [78, 79]. Higher supersaturation increases the nucleation rate which leads to a change of the morphology of the crystals formed. When the pH increases the induction time decreases accordingly [21, 80].

3.3.1.6 Effect of divalent ions

Different ions are very often present in produced water. Their presence effects the crystallisation of calcium carbonate.

3.3.1.6.1 Effect of calcium (Ca^{2+})

In water with a low degree of hardness (10°F) nucleation is gradual and vaterite polymorph's are formed. Whereas in water with a higher degree of hardness (30°F and 50°F) nucleation is instant and calcite polymorph's are observed. There is a correlation between nucleation and the type of crystal which is formed [81]. The nucleation time of calcium carbonate decreases with increasing water hardness degree [73].

The number of calcium carbonate crystals and the average size of each crystal formed increases with an increase in Ca^{2+} ions [82].

3.3.1.6.2 Effect of iron

FeCO_3 precipitates on the surface of calcite inhibiting calcite growth [83]. Fe^{3+} has smaller inhibiting effect than Fe^{2+} . Fe^{2+} has an inhibition effect on calcite and a small or negligible inhibition effect on aragonite growth.

Fe^{2+} and Fe^{3+} are effective in inhibiting calcite growth and the inhibition effect increases with the presence of oxygen [84]. More effective growth inhibition is observed at larger iron concentrations, smaller supersaturations, smaller seed loadings, and higher alkalinity. Inhibition is caused by the absorption of iron into the calcite surface which reduces the growth rate and enables a higher calcium concentration to exist in solution in "equilibrium" with calcite seeds.

Iron ions delay calcium carbonate formation in tube blocking tests [85]. The iron ions are thought to have an inhibitory effect on the calcium carbonate formation and/or enable the preferential formation of iron carbonate [85].

3.3.1.6.3 Effect of other divalent ions

The kinetics and morphology of calcium carbonate formation is affected by presence of seven divalent cations [86]. The divalent cations Fe^{2+} , Mg^{2+} , Ni^{2+} , Co^{2+} , Zn^{2+} and Cu^{2+} promote aragonite formation whereas Cd^{2+} seems to have no effect. In the absence of these impurities aragonite polymorph are nucleated initially then transformed into calcite. In the presence of Fe^{2+} , Ni^{2+} , Mg^{2+} and Zn^{2+} aragonite does not to transform into calcite.

Aragonite polymorph is favoured by the presence of divalent ions such as Ag^+ , Al^{3+} and Cr^{3+} also they reduce the crystal growth rate by impurity adsorption [87].

It has been observed that in the presence of zinc ions a high number of small calcium crystals are formed [88]. Calcium carbonate formation is reduced in the presence of copper or zinc.

Recent studies have shown that trace amounts of copper and zinc can inhibit the formation of calcium carbonate by the formation of a neutral complex which inhibits the growth of the crystals. The effectiveness of copper is higher than zinc in inhibition [89]. When zinc is present in trace amounts the amount of scale is reduced [90].

3.3.1.6.4 Effect of magnesium

Magnesium ions (Mg^{2+}) do not affect aragonite crystal growth because they are not adsorbed readily on to the surface and into the aragonite crystal lattice [91, 92]. However, magnesium ions are adsorbed readily into the surface of the calcite and incorporated into the crystal structure inhibiting crystal growth [91, 92]. Free magnesium ions in seawater inhibit the formation of calcium carbonate at low temperatures [93].

The magnesium amount incorporated in calcite increases with the magnesium concentration and is affected by salt type in the solution [94].

Calcite growth is inhibited by the presence of magnesium and non-uniform magnesium incorporated into the calcite crystal surface. New crystals have higher Mg^{2+} density and lower growth rate than the original calcite [95].

Magnesium inhibits calcium carbonate precipitation in the bulk and on the metal surface [96]. The inhibition effect is greater on the bulk solution. Magnesium increases the induction time of scale forming in the bulk solution and suppresses the vaterite formation (calcite dominate). Magnesium which is absorbed into the surface of the calcite causes distorted crystals which have rough surfaces [97].

In the early stages of calcium carbonate formation magnesium incorporates into nuclei [98].

3.4 Methods of scale inhibition and removal

There are two main methods of dealing with organic scale. The first method is a strategy of inhibition which prevents the scale formation in the first place. The second method is mechanical and chemical removal of scale. This

method allows the scale to build up in downhole tubes, heat exchangers and pipes, etc. and then the scale is mechanically or chemically removed.

3.4.1 Mechanisms of inhibition and chemicals

One of the most common methods of prevention of scale formation is the use of chemical inhibitors. The inhibition mechanisms and common inhibitors are presented in the next section.

3.4.1.1 Mechanism of inhibition

There are three process involved in scale inhibition [99]:

- threshold effect
- crystal distortion
- dispersancy

Figure 3.4 illustrates these three process.

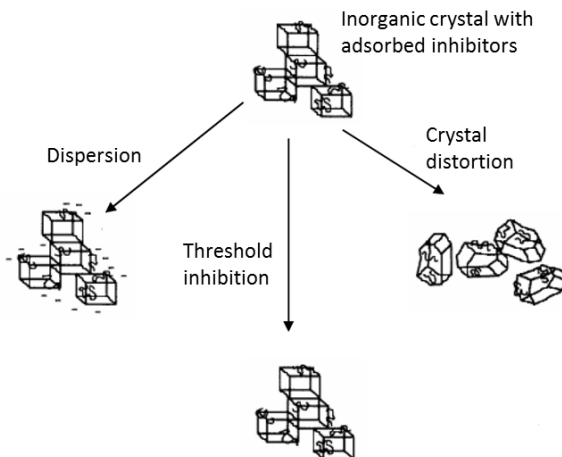


Figure 3.4: Three main processes of scale inhibition [100]

Inhibitors can act in three different ways: on the nucleation step, the crystal growth or on the agglomeration of the fine scale particles. The Minimum Inhibitor Concentration (MIC) is the concentration which prevents scale formation during the test period [101]. The larger the amount of scaling ions the inhibitor can maintain in solution, the more effective the inhibitor is.

Threshold effect - In the 1930's it was noticed that a greater amount of insoluble material can be maintained in solution by the addition of a small amount of inhibitors [102]. This is known as the threshold effect. Threshold inhibitors (organic chemical) prevent or retard the scale formation at a sub-stoichiometric levels (ppm) [99]. These inhibitors are often used to prevent scale formation [29].

Crystal distortion - Crystals are distorted by the presence of inhibitors in the solution. Distorted crystals are less adherent and have a reduced propensity to agglomerate [79, 99].

Dispersancy – Is the ability to minimize agglomeration and setting of suspended solids. The attachment of inhibitors on the surface can increase the negative charge density which causes particles to repel each other [99, 103].

3.4.2 Scale inhibitors

There are various types of inhibitors used in the oilfields: polycarboxylic acids, polyelectrolytes, phosphonates and polyphosphates.

3.4.2.1 Phosphonates

Phosphonates (organophosphorus compounds) are widely used in the water treatment industry and the oil and gas industry. Phosphonates are used as threshold scale inhibitors, chelating metal ions, crystal growth modifications and corrosion inhibitors [104]. HEDP (Hydroxyethylidene Diphosphonic acid) and DETPMP (Diethylenetriaminepenta-methylenephosphonic acid) are presented in Figure 3.5.

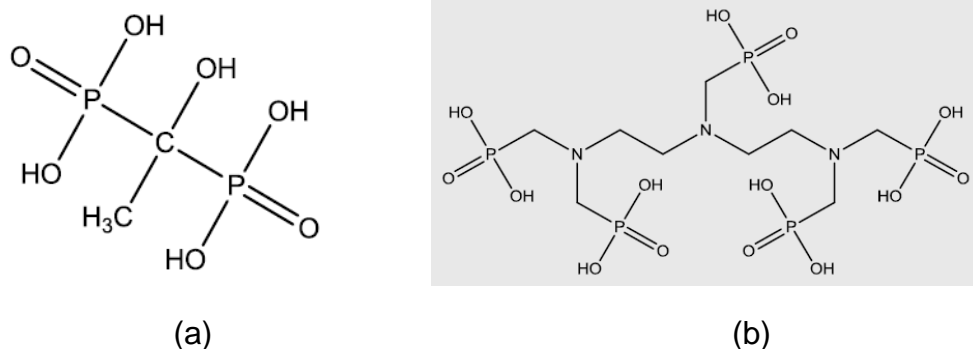


Figure 3.5: Molecular structure of phosphonates used as scale inhibitors : a) HEDP (Hydroxyethylidene Diphosphonic acid) and b) DETPMP (Diethylenetriaminepenta-methylenephosphonic acid)

The mechanism of inhibition of CaCO₃ by phosphonates involves blockage of crystal growth sites, inhibiting nucleation and inhibition by threshold effect [105-110].

Phosphonates are effective against calcium carbonate and stable in high temperature [108]. They have better adsorption with shorter chain and scaling inhibition. The phosphonate molecules are more resistant to hydrolysis and aid effectiveness in scaling inhibition [106].

Semi-empirical mathematical inhibitor models based on results obtained during tests using NaCl brine show that HEDP and NTMP are the most effective inhibitors for calcium carbonate in test conditions [105].

DETPMP effectiveness against scale is not improved by the addition of EDTA and citric acid [111].

As temperature increases from 25 to 200°C the induction time for calcium carbonate formation in the presence of DETPMP decreases significantly [112].

3.4.2.2 Polyphosphate

Polyphosphate inhibitors show good inhibition of calcium carbonate in a range of temperatures: 20 to 50°C. However, the efficiency decreases with time with increasing temperature. This is associated with the fact that the hydrolysis reaction of phosphates with water is accelerated with rising temperature [106]. The chemical structure of phosphate is presented in Figure 3.6.

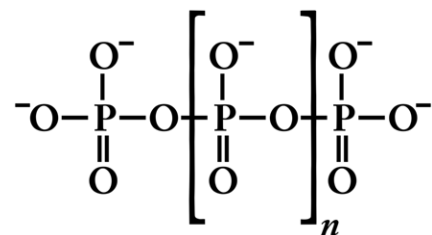


Figure 3.6: Chemical structure of linear polyphosphate

Adsorbed polyphosphate molecules inhibit the calcite crystal growth by adsorbing to the surface and blocking active crystal growth sites [113]. Tripolyphosphate has stronger inhibitory effects than pyrophosphate and hexametaphosphate. Tripolyphosphate inhibition effect is two orders of magnitude greater than the inhibition effect of orthophosphate.

The presence of inorganic orthophosphate in supersaturated solutions at levels as low as 8×10^{-8} mole dm^{-3} entirely inhibits crystal growth by adsorption of phosphate, at the active growth sites, and by the reduction of crystal growth rates [114].

3.4.2.3 Polyelectrolyte

Senogles *et al.* [115] characterize a polymeric inhibitors in three groups: polymers containing carboxylic acids, polymers containing phosphate groups and polymers containing sulfonate groups. In Figure 3.7 are presented the different types of polymers used as scale inhibitors in water treatment and the oil and gas industry .

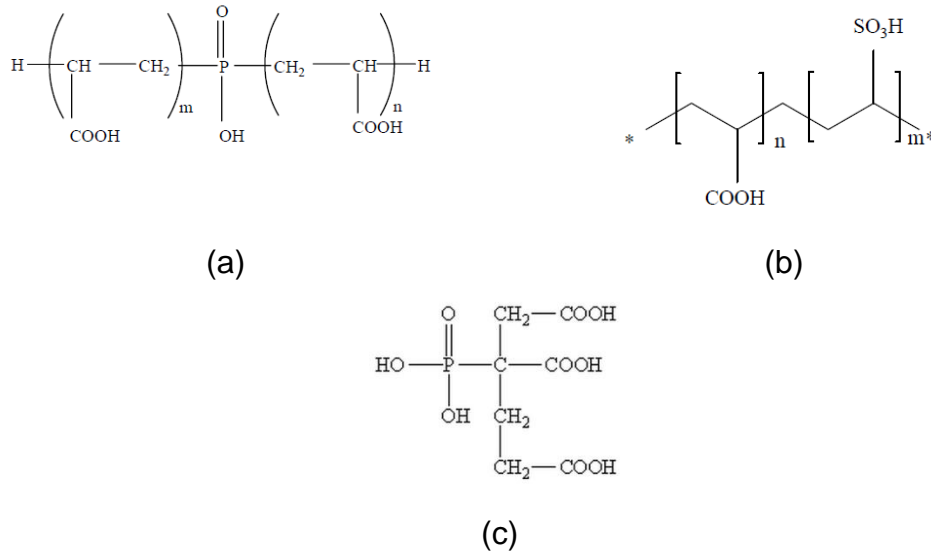


Figure 3.7: Schematic representation of polyelectrolytes used as scale inhibitors: a) Polyphosphinocarboxylic acid (PPCA), b) Polyvinyl sulfonate and Polyacrylic acid copolymer (PVS) and c) 2-phosphono-butane-1,2,4-tricarboxylic acid (PBTC)

The Phosphinopolycarboxylic acid (PPCA) is considered as a nucleation inhibitor and it has a great affinity with calcium ions.

Chen *et al.* [116] found out that PPCA inhibits surface deposition, suppress the calcite formation and resulted vaterite dominated scale. With increasing PPCA concentration in the scaling solution the induction time of surface deposition increases [109, 116]. PPCA has greater inhibition effect on calcite plane (110) than (113) plane [116].

Chen *et al.* [109] found out that increasing concentration of PPCA increases the induction time of scale formation in the bulk solution. PPCA delays nucleation where the delays are associated with complexation with Ca^{2+} ions and the growth of crystals is retarded (DETPMP better efficiency).

Smith *et al.* [117] showed that 5ppm of PPCA was able completely prevent the scale build up in the tube blocking test.

PPCA has greater affinity for calcium ions than magnesium ions at all calcium levels. When the high levels of calcium are present in the solution with PPCA, the effectiveness of the inhibitor decreases because PPCA dropped out of solution as precipitate (less in the solution) [118].

3.4.3 Removal methods

Scale deposition can be removed by chemical and mechanical methods, or sometimes a combination of both methods [8].

In the oil and gas industry many different mechanical removing techniques are in use, such as: abrasive slurries, milling, fluid mechanical jetting methods or explosives. Each of these methods have some limitations in application so proper selection depends on the type of scale deposition and the well type [8].

One of the most common techniques is dissolution of calcium carbonate by hydrochloric acid (HCl) [8, 119]. This technique is very effective against carbonates due to their high solubility in HCl. Other chemicals agents used include Ethylenediaminetetraacetic Acid (EDTA) which acts as a dissolver and chelating agent [119].

3.5 Different methodologies used to study calcium carbonate

The scale occurs as surface deposition and/or the bulk precipitation. Calcium carbonate formation and inhibition are studied by various test methods. In industry, these methods are used to select the right type of inhibitor and concentration [120].

3.5.1 Scale precipitation in the solution

Bulk jar tests – these are usually used to test the kinetics of scale formation in the bulk and/or the efficiency of inhibitors. Two brines are mixed in a jar or a beaker and the precipitation is followed. Chen *et al.* [96] studied the effects of magnesium by comparing the bulk precipitation and surface deposition. The kinetics of the scaling have been determined by using a supersaturated brine and the weighing the filtrate after the experiment.

Scale precipitation inhibition has been studied by turbidity measurements [121]. He *et al.* [105] investigated the induction time of calcium carbonate precipitation at 25 and 90°C by turbidity measurements.

The precipitation can be characterised by various bulk chemical analysis.

Calcium carbonate precipitation has been studied by observation of changes in the pH. pH measurements are usually performed using a pH meter. While no further changes in the pH value are observed, it is assumed that the precipitation has ended [67].

Changes in Ca^{2+} levels can be used to study the precipitation process. Calcium ion concentration can be followed using radioactive isotopes (^{47}Ca [122] or ^{45}Ca [123]) as well as selective ion electrode [124-127].

3.5.2 Scale deposition on a surface

Surface deposition studies can be divided in two categories: non electrochemical or electrochemical.

Non electrochemical methods

Dynamic tube blocking test – The formation of scale is evaluated by measuring, with time, the differential pressure between inlet and outlet of the pipe. During scale formation by flow of the solution which contains scaling ions, the pressure in the tube is dropping by the scale which build up on the surface of the tube [8]. Dyer and Graham [68] used this method to study effects of the temperature and the pressure on formation of calcium carbonate and barium sulphate. They found out that the temperature has greater effect on the scaling tendency. Zhang *et al.* [128] used this method to develop a kinetic model to predict the scale formation.

The quartz microbalance technique (QCMB) – A thin film which is depositing on the surface decreases the frequency in proportion to the mass of the film. Increase of 0.5ng can be measured according to the model of the QCMB [129]. Abdel-Aal *et al.* [130, 131] studied the adhesion mechanism of CaCO₃ by QCM. They found that calcium carbonate precipitates firstly as an amorphous compound and then as a stable crystalline form. At high supersaturation mainly calcite precipitated while at low at low supersaturation ratio leaf-like vaterite precipitated.

Electrochemical methods

Chronoamperometry - It was first electrochemical method proposed by Ledion *et al.* in 1985 [132]. The principle is to apply a negative potential on metal electrode immerse in solution to reduce oxygen dissolved in water (Equation (3-1)). The local increase of the pH (by the generation of hydroxide ions) in the vicinity of the electrode forcing the calcium carbonate to form on the electrode surface.



The limiting current (I_L) is proportional to the flow of oxygen moving towards the electrode. Current decreases when the active surface gets blocked by the adsorbing scale. I_L reaches the value close to zero when the surface of the electrode is totally covered by the calcium carbonate.

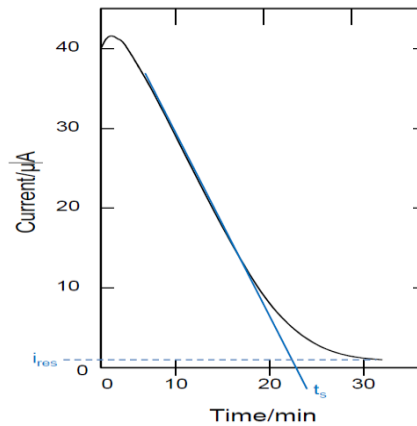


Figure 3.8: Typical chronoamperometry curve [133]

Figure 3.8 shows typical chronoamperometric curve. Scaling rate is related to the falling current. Ledion defined the scaling time, t_s , as the intersection between the time axis and the line extrapolate from step reduction of the current. It provides the rough estimation of the scaling potential of the solution.

Electrochemical impedance technique - In this method during the measurement of the electrochemical impedance two time constants are apparent: C_{HF} – a pseudo high frequency capacitance and R_{HF} - a pseudo high frequency resistance. These two are related to the coverage of the scale. C_{HF} depends on the on the surface coverage and R_{HF} on the morphology of the deposit [134].

The measurement of the impedance when the surface of electrode is covered completely by scale provides information on the morphology, the compactness and thickness of scale deposit. During the tests, the thicknesses of the deposit does not change and the porosity changes with time [135].

Chronoelectrogravimetry (EQCMB) - This is the method that is often connect to the QCM. Determination of the nucleation is possible and the total mass formed on the electrode surface as a function of time is followed by precision measurement of mass [136].

Garcia *et al.* [137] have combined this method with the a channel flow cell which allowed them to study the effect of the hydrodynamic condition on the scale formation and inhibition.

The Rotating Disc Electrode (RDE) - It has been developed by Neville *et al.* [138, 139]. It allows the study of the extent of surface coverage on scaled electrodes. The RDE method allows measurement of the exact coverage of

the surface by enabling uniform controlled hydrodynamic conditions over the surface of the electrode.

The limiting current (i_L) relation with the rotational speed allows calculate of the percentage of surface coverage in accordance with the Levich equation (Equation (3-2)).

$$i_L = 0.62nFAC^bD^{\frac{2}{3}}\nu^{-\frac{1}{6}}\omega^{\frac{1}{2}} \quad (3-2)$$

where i_L is the limiting current (mA), n is the number of electrons involved in the reaction, F is the Faraday's constant (96487 Coulombs/mole), A is the electrode area (cm^2), C^b is the bulk concentration of electroactive species (mol dm^3), D is the diffusion coefficient of the electroactive species ($\text{cm}^2 \text{s}^{-1}$), ν is the kinematic viscosity ($\text{cm}^2 \text{s}^{-1}$) and ω is the angular velocity of the RDE (rad s^{-1}).

By plotting i_L against $\omega^{\frac{1}{2}}$, the percentage of the surface covered by scale can be determined.

$$\text{surface coverage} = [(m_1 - m_2)/m_1] \times 100 \quad (3-3)$$

where m_1 and m_2 are the gradient of the i_L against $\omega^{\frac{1}{2}}$ plot for the unscaled surface before test and scaled surface after the test respectively.

Chen *et al.* [21] used RDE to measure calcium carbonate surface scaling and the ICP (Induced Coupled Plasma) to assess bulk precipitation. They found out that crystals which formed on the surface are bigger than crystals precipitated in the bulk solution. They suggested that studying both bulk precipitation and surface scaling is necessary to completely understand a real scaling system.

3.6 Different types of internal corrosion

Four different types of internal corrosion of pipelines can occur in the oil and gas industry [140]:

1. **Sour corrosion** – associated with the presence of hydrogen sulphide (H_2S) in brine.
2. **In the water injection pipelines** – associated with presence of oxygen in the water or presence of sulphate-reducing bacteria (SRB).
3. **Microbiological corrosion** – associated with activity and growth of SRB in the pipeline.
4. **CO_2 corrosion (sweet corrosion)** – related to presence of carbon dioxide dissolved in the fluids. This corrosion is typically slow.

3.7 Types of CO₂ corrosion damage

According Kermani and Morshed [38], CO₂ corrosion occurs mainly in form general corrosion and localized corrosion. Three types of localized corrosion can be distinguished:

- pitting - occurs at low flow conditions and adjacent to non-metallic inclusions
- mesa attack - occurs in low to medium flow conditions, it places where the protective iron carbonate film forms but it is remove by the flow.
- flow-induced localized corrosion - starts from pits and/or sites of mesa attack above critical flow velocities

In this thesis, the focus will be assessed on general and pitting corrosion.

3.7.1 General corrosion

General corrosion (uniform corrosion) results in a fairly uniform metal loss (or thinning) over the entire exposed metal surface [141]. General corrosion is electrochemical reactions uniformly proceed on the whole exposed surface or over a large area [142].

3.7.2 Pitting corrosion

Pitting is a highly localized form of the corrosion which results in holes in the metal. A pit is defined as a hole or a cavity with a surface diameter equal or less than the depth of the pit [142]. Pits may have various sizes and shapes which are presents on Figure 3.9.

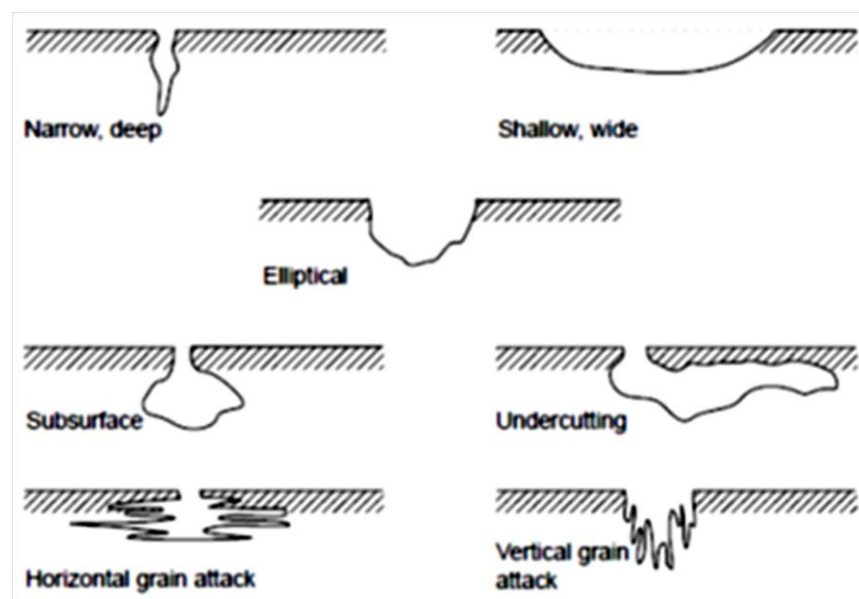


Figure 3.9: The different cross-sectional shapes of pits [143]

3.8 Factors affecting CO₂ corrosion

3.8.1 Water chemistry

The solution chemistry has the biggest effect on CO₂ corrosion. The composition of the water can vary from one brine to the other [54]. It can contain different ions such as sodium, chloride, bicarbonate, calcium, magnesium, hydrogen, hydroxide, iron, potassium, barium, strontium, acetate and sulphate, and dissolved gases such as CO₂, H₂S and Oxygen - associated with the formation of localised corrosion [144], and the presence of crude oil [54]. Organic acids can also be present in the system, for instance acetic acid, this can influence the corrosion rate [54, 144-147].

3.8.2 Formation of CO₂ corrosion product

During the carbon steel corrosion process, Fe²⁺ ions are released from the surface into the electrolyte. Iron ions together with carbonate ions can form iron carbonate FeCO₃ (Siderite) which it is commonly known as the CO₂ corrosion product (Equation (3-4)).



Iron carbonate formation can inhibit the corrosion kinetics by covering the surface of the steel or by forming a diffusion barrier for the corrosive species participating in the corrosion reactions [38, 51, 148, 149]. The corrosion product will be protective only if it is adherent and covers the whole surface. However, localised corrosion can occur on the regions of the steel where the scale has broken down and/or did not form [54].

The corrosion product protectiveness and growth depend on several parameters: the supersaturation [150], temperature, pH, CO₂ partial pressure, metal composition and microstructure [54]. However, supersaturation and temperature are considered as the most influential.

Supersaturation is the main factor influencing the formation of FeCO₃. To precipitate a protective film, supersaturation needs to be exceeded in order to obtain a precipitation [54], which can be calculated from Equation (3-5).

$$\text{SR} = \frac{(a_{\text{Fe}^{2+}})(a_{\text{CO}_3^{2-}})}{K_{\text{sp}}} \quad (3-5)$$

where K_{sp} is the solubility product (FeCO₃) , and $a_{\text{Fe}^{2+}}$ and $a_{\text{CO}_3^{2-}}$ is the ion activity.

It is important to remember that in the case of iron carbonate, SR is only high in close vicinity to the metal surface while in the case of calcium carbonate the whole bulk solution is supersaturated.

At room temperature, even at high supersaturation the precipitation of iron carbonate is slow. An unprotective film with voids will form unless the pH is very high. It has been described [54] that iron carbonate films are more protective and dense at higher temperatures: above 60°C (even at low supersaturation). The increase of temperature reduces the solubility of iron carbonate which accelerates the precipitation process of iron carbonate.

Crolet *et al.* [151] found that corrosion product layers built from the same solid components can be extremely protective, very little protective or even corrosive. Crolet *et al.* [151] studies showed that corrosion layers contain iron carbonate (insoluble) and/or cementite (Fe_3C - retaining a solid form). It was concluded that the main difference between protective and unprotective corrosion layers is the presence of unfilled space between the Fe_3C and the steel.

Crolet *et al.* [151] illustrated the different types of protective and non-protective corrosion layers:

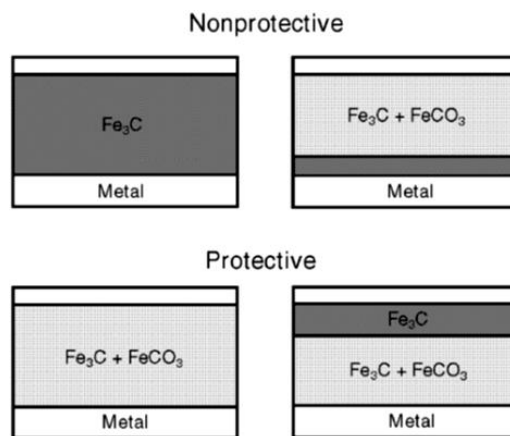


Figure 3.10: Different types of protective and non-protective corrosion layers – from Crolet *et al.* [151]

3.8.3 Effect of pH

Another important factor in FeCO_3 scale formation is pH. The pH values influence the electrochemical mechanisms and the formation of protective iron carbonate films [152]. An increasing pH decreases the FeCO_3 solubility, promotes its precipitation and causes lower corrosion rates. While a low pH; causes the dissolution of the FeCO_3 film formation [153] and a higher corrosion rate. It is considered that below the pH value of 5 is a non-film-forming condition. Above the pH of 5, it is easy for an iron carbonate film to

grow on the metal surface, after reaching FeCO_3 supersaturation, which can contribute to a lower corrosion rate [54].

3.8.4 Partial pressure

In the CO_2 environment, where the steel surface is free from corrosion products and the CO_2 partial pressure increases it results in an increased corrosion rate. The concentration of carbonic acid (H_2CO_3) is increasing with increasing P_{CO_2} , which enhances the cathodic reaction, and eventually the corrosion rate [54]. In the environment with conditions favourable for the precipitation of corrosion product (high pH), the increase of P_{CO_2} will increase the rate of the formation of the corrosion product by increasing the concentration of bicarbonate and carbonate ions [38].

3.8.5 Temperature

Temperature accelerates the corrosion reactions (Nernst equation). In the environment where the pH is low, the temperature increase is causing an increase of the corrosion rate (no formation of corrosion product) [54]. However, in the environment where the pH is high, the corrosion rate will decrease because the high temperature reduces the solubility of iron carbonate and facilitates the formation of the protective corrosion product. Depending on the water chemistry and flow behaviour, the corrosion peak tends to be expected between 60°C and 80°C . It is referred to as the 'scaling temperature' [154].

3.8.6 Effect of flow

In an environment where corrosion products do not form, the turbulent flow enhances the transport of species to the metal surface and away. This causes an increase in the corrosion rate [54, 144]. Corrosion rate can be increased even in an environment where a corrosion product or an inhibitor film is present on a surface. This is associated with the removal of the protective corrosion product or the inhibitor film by high flow velocity [54].

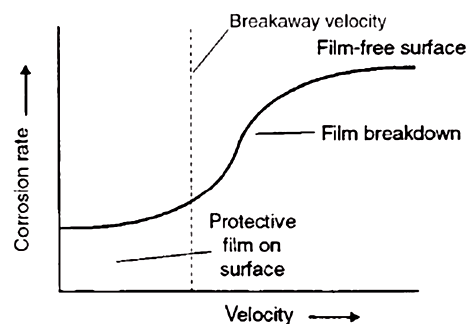


Figure 3.11: Schematic of the critical velocity effect for erosion-corrosion [141]

3.8.7 Effect of chemical composition and microstructure

Chemical composition and microstructure are two important factors and are not independent. Different chemical compositions can be used to manufacture a metal with the same microstructure and two different microstructures can be manufactured from the same chemical composition [155].

General corrosion rate is significantly reduced with increasing Cr content in low-alloy steels by the formation of a stable chromium oxide film [38]. Better resistance against corrosion is achieved by the addition of stronger carbide-forming elements such as: chromium, vanadium and molybdenum. At the same time, small quantities of silicon and nickel are added to regain the strength of low carbon steel [156].

The potential difference on a metal surface is the driving force for the corrosion in a solution. This potential difference is caused by heterogeneities (inclusions or impurities, chemically different phases, the structure) in the material [157]. Heterogeneities are predominantly controlled by the chemical composition, thermal and mechanical heat treatments [157]. Different heterogeneities of the steel microstructure provide sites for the anodic and cathodic reactions and can affect the corrosion rate [157, 158].

3.8.8 Effect of calcium on CO₂ corrosion

The presence of calcium affects the corrosion behaviour by the formation of non-protective calcium carbonate which restricts the formation of protective FeCO₃ [159]. In a solution with a low concentration of the Ca²⁺ (<100 ppm) the corrosion rate was seen not to be significantly affected. While at high concentration of Ca²⁺ (>=10000ppm) the corrosion rate measured was high [159].

It is concluded that corrosion rate decreased in a short period in the presence of Ca²⁺ and Mg²⁺, but there was no big difference at longer periods of exposure [160, 161]. However, it is claimed that the corrosion rate increased with increasing concentration of the Ca²⁺ in the solution [162].

3.9 Pitting corrosion of in CO₂ environment

Pitting corrosion is a complex process with a sequence of steps [163]:

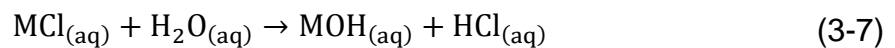
- initiation or nucleation of pits - breakdown of the passive film or corrosion product film

- pit growth - pits growth depends on the material composition, pit electrolyte concentration and its bottom potential
- metastable pitting - Metastable pits are pits that initiate and grow for a limited period before re-passivating

Pit initiation is only possible in the situation that the passive film of passivating metal will breakdown. However, pit initiation in the active materials occurs while some voids are present in the corrosion products formed on the surface. Halide anions promote the pit initiation, while the chloride (Cl^-) anion is the most aggressive [143, 164, 165].

Kvarekval [166], Nesic *et al.* [51] and Papavinasam *et al.* [167] suggested that the same mechanism of film breaking and pit initiation occurs in the carbon steel in the oil and gas industry.

After initiation, the processes within a pit produce conditions which are stimulating and necessary for further growth. Growth is an autocatalytic process [168]. The metal dissolution is increased by reaction of metal ions with halide anions (for example Cl^-) (Equation (3-6)). Then hydrolysis reaction (Equation (3-7)) occurs which produces acids and lower pH inside pit and promotes pit growth [143].



Pit growth is also related to the chemical composition and microstructure of the material, chemistry of electrolyte, local solution conditions and duration of attack [169].

Pit can stop growing or die – when corrosion product will cover the pit or cavities become dried out [170].

Pitting corrosion in the CO_2 environment is highly associated with the formation and removal of corrosion product.

Crolet *et al.* [151] suggested that if protective corrosion product is not formed at the start of corrosion, uniform corrosion will occur. It may slowly progress to localised (pitting) corrosion due to the formation of non-protective corrosion product. Different viewpoint is suggested by Papavinasam *et al.* [167]. When the corrosion product does not form, the corrosion rate will be uniform. However, if a complete and protective corrosion product forms, the corrosion rate will decrease to a negligible value.

3.10 Corrosion mitigation

Several different approaches in mitigation of corrosion have been developed [141]:

- Material selection
- Coatings
- Design
- Cathodic protection
- Inhibitors

This PhD study focus only corrosion mitigation by inhibitors.

3.10.1 Corrosion inhibitors

Corrosion inhibitors are chemical compounds specifically designed to mitigate corrosion of metals. The National Association of Corrosion Engineers (NACE) defines corrosion inhibitors as: A substance which retards corrosion when added to an environment in small concentrations [171]. Corrosion inhibitors are chemicals effective in certain environments. Corrosion inhibitor effectiveness are affected by the conditions under which they are applied and the interaction with surface. Inhibitors form adsorption layers or protective films, which influence the electrochemical reactions at the metal-electrolyte interface causing inhibition of corrosion. The corrosion inhibitor can also promote passivation or change the solution chemistry [172].

Corrosion inhibitors affect the corrosion rate, which are determined by the anodic and cathodic reactions. The four groups of corrosion inhibitor are referred to as [172]:

- anodic inhibitor - which directly affects the anodic reaction by adsorption on active anodic sites on the surface. It changes the activation energies involved in the dissolution of the metal surface, thus lowering corrosion rate.
- cathodic inhibitor - which directly affects the cathodic reactions. The corrosion potential is change by adsorption of inhibitor. This affects the point at which the Tafel polarisation curve changes from activation controlled to mass transfer control
- mixed inhibitor - which directly affects the anodic and cathodic reactions

- passivating inhibitors - which change the corrosion potential into positive range and the metal passivation occurs

Corrosion inhibitors adsorb onto the metal by: physical adsorption (physisorption) and chemical adsorption. On the level of the adsorption few factors have an effect, such as: the chemical properties of the inhibitor, the metal surface condition, the environment and the electrochemical potential at the interface [173].

Physical adsorption is due to electrostatic forces occurring between the inhibitor compounds (which are generally ionic in nature) and the metal surface. Physisorption are weak intermolecular forces - van der Waals forces. Physical adsorption is an easily reversible process by changing the environmental conditions such as the temperature or the velocity [174].

Chemical adsorption (chemisorption) occurs when the forces involved are valence forces - the forces involved in the formation of chemical compounds. The inhibitor with the surface forms covalent or ionic bond by the transfer or sharing of the inhibitor molecules charge - electrons. The chemisorption process is slower than physical adsorption, it occurs faster at elevated temperatures [174]. Chemisorption is specific for certain metals and the types of material. The inhibitor molecule, if is a positively charged (have an unshared, lone pair of electrons) in the functional group adsorb to a negatively charged surface and the electron transfer is enabled from the inhibitor to the metal [175].

The reactions are reduced by inhibitor which not always occupied whole surface but sites which are electrochemically active. The corrosion rate it is reduced proportionally with the number of sites inhibited by the inhibitor [152].

3.10.1.1 Common corrosion inhibitors

CO₂ corrosion inhibitors are amphiphilic, surface-active molecules (charged polar head) with hydrocarbon chains typically in the range C12-C18 [176]. Surface-active molecules of the inhibitor adsorb into the metal surface to anodic or cathodic sites. The hydrophobic stick out from surface into solution and attract the oil particles. This forms a hydrophobic film which gives protection against corrosion. The charged polar head which adsorb into metal surface contains heteroatoms: nitrogen, phosphorous, sulphur and oxygen [177, 178].

3.10.1.1.1 Inhibitors structure relevant to this PhD with description.

Phosphate ester is generally considered as the inhibitor which protects the anode [179, 180]. The general chemical structure of phosphate ester is presented in Figure 3.12.

Phosphate esters form fairly insoluble salts/complexes with Fe^{2+} and Ca^{2+} [179]. Phosphates esters which contain a hydrophobic nonylphenol group have better inhibition effects than linear or branched aliphatic phosphate esters [179].

When phosphate ester is adsorbed to the surface and Fe^{2+} ions are added to the solution, the growth of FeCO_3 scale is prevented [181]. However, Wong *et al.* [181] suggested that the added Fe^{2+} and phosphate ester interact to form a more protective film on the surface.

Polyhydric alcohol phosphate esters (PAPE) retard both the dissolution of metal and hydrogen evolution in sea water (an anodic and cathodic inhibitor) [182]. It adsorbs immediately and compactly on the steel surface and with time the thickness of inhibitor film increases. It adsorbs to the metal surface by complexation with metal ions accumulated on the steel surface, i.e. Fe^{2+} , Ca^{2+} , etc [182].

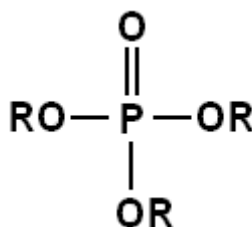


Figure 3.12: General chemical structure phosphate ester

Quaternary ammonium salts (Figure 3.13) have high solubility in the oil faze and the nitrogen atoms carry a positive charge [178].

Benzyl dimethyl-n-hexadecylammonium chloride (BHDC) in solutions saturated with CO_2 inhibit the anodic process and are absorbed by charge sharing the positively charged nitrogen atoms and electrons in the benzene ring [183].

The rate of growth of the iron carbonate scale increases with the presence of quaternary amine [184]. Iron carbonate crystals are smaller and the layer is thinner compared with a scale formed without the presence of quaternary amine [184]. At 50 ppm concentration of quaternary amine the iron carbonate is not entirely prevented [184].

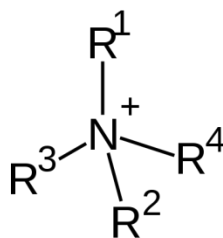


Figure 3.13: General chemical structure quaternary ammonium salts

Imidazolines and their salts are very common inhibitors in the oil and gas industry and their structure is presented in Figure 3.14. The head group is very important in the adsorption process [185]. While the hydrocarbon chain in an imidazoline film provide a barrier to water and chloride ingress [185].

Imidazoline inhibitors have been seen to interact with Fe^{2+} ions, creating an adsorbing film that decreases the corrosion rate [181]. The imidazoline inhibitor stopped the growth of $FeCO_3$ at concentrations above 25 ppm. However, imidazoline at concentrations of 10 ppm or less promoted tightly packed $FeCO_3$ scale with higher impedance of the film compared to $FeCO_3$ scale formed when no inhibitor was present [181].

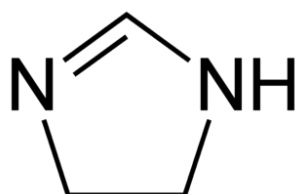


Figure 3.14: The molecular structure imidazoline

Thiols compounds are generally considered as anodic inhibitors and electron acceptors [186] however, in some studies mercaptoethanol (thiols compound) has not been considered as anodic or cathodic inhibitor [187].

Mercaptoethanol is predominantly cathodic inhibitor and has good inhibition effect on general and pitting corrosion [188].

Mercapto compounds due to oxidation of the mercapto group (-SH) to disulphide groups (-S-S-) adsorbed to the metal surface by formation complexes with iron ions [188].

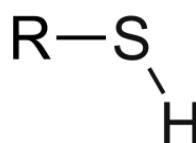


Figure 3.15: The molecular structure thiol compound

3.11 Combined inhibitors

In many oil and gas fields during production operations, different chemicals are added to control both corrosion and inorganic scale issues. During the design stage of well or subsea systems in the oil and gas industry, fewer injection lines was predicted which was the reason for development of the combined inhibitors [13]. Very often a scale inhibitors and corrosion inhibitors are incompatible when mixed. This problem can be overcome by development of multifunctional molecules which works as the corrosion inhibitor and the scale inhibitor or an active component have to be chosen with care to avoid any negative effect on the performance of one of the active components [13, 189, 190]. Performance of the scale inhibitors and the corrosion inhibitors blend can be reduce beside physical incompatibilities by [191, 192]:

- competitive adsorption – of one species would limit adsorption of the other species and overall reduce its performance
- the scale inhibitor and the corrosion inhibitor complexation – in solution would effectively reduce their performance
- surface adhesion – of the corrosion inhibitors have impact on the adherence and the growth of the scale crystals on the surface and bulk scale inhibition performance

Other factors such as brine composition – different concentrations of scaling ions, pH and organic acid were investigated [189, 193]. So, laboratory tests methods used to investigate the combined inhibitors performance have to be chosen with care.

3.11.1 Effect of corrosion inhibitor on scale inhibition and scale formation

The effect of corrosion inhibitors on the bulk scaling and surface scaling was investigated.

It was presented that the two commercial corrosion inhibitors A and B are ineffective at preventing bulk inhibition while the scale inhibitor is absent. However, the corrosion inhibitor A and B by presence on the metal coupons surfaces minimises the amount of heterogeneous nucleation and growth that adheres to the metal coupons [191, 192]. It could be observed that the corrosion inhibitors have an effect on the morphology of scale which have formed on the metal coupons [191, 192].

It is observed that four different inhibitors introduced to the test brine (Forties and Heron brine systems) results in a reduction in performance of the scale inhibitors against (DETPMP, PPCA and PVS - poly vinyl sulphonate) [191].

Electrochemical impedance spectroscopy (EIS) was used to study scale and corrosion processes [194]. The corrosion and the scale processes are closely linked and occur simultaneously at different sites of the metallic surface. Hydroxyphosphonoacetic acid (HPA) corrosion inhibitor chelates with Ca^{2+} ions and formed a compact layer which provides respectable protection against corrosion [194].

3.11.2 Effect of scale inhibitor on corrosion inhibition

Different researchers have investigated how scale inhibitors affect the corrosion processes.

The effect of two different types of inhibitor (polycarboxylic acid type inhibitor and polymeric phosphate based inhibitor) on general corrosion rate and formation of iron carbonate was investigated [15]. Both inhibitors presented some reduction of corrosion rate, however scale inhibitors did not lower the corrosion rate below 0.1 mm/year. The scale inhibitors interfered with the iron carbonate growth and formation of dense film [15].

Scale inhibitor (1-hydroxy-ethane-1,1-diphosphonic acid (HEDP)) reduces scale formation on surface by modifying the structure of calcium carbonate on being incorporated into the crystals, furthermore shows a corrosion inhibition effect [194].

Polyamino Polyether Methylene Phosphonate (PAPEMP) is an effective calcium carbonate inhibitor at low and moderate saturations compared to HEDP (1-Hydroxyethylidene-1,1-Diphosphonic Acid). It is far more efficient at high saturation ratio values. PAPEMP has excellent inhibition properties against corrosion in supersaturated brines with respect to calcium carbonate than HEDP [195].

Three different phosphonates (LPA – laurylphosphonic acid, ELP – ethyllarylphosphonate and DELP – diethylaurylphosphonate) effect on the formation a corrosion protective film was investigated [196]. ELP provides corrosion inhibition by formation of protective film on the carbon steel surface with the optimum protection after 24h immersion in the solution [196]. However, phosphonobutanetricarboxylic acid scale inhibitor added to solution has no substantial effect on the corrosion rates [197].

Polyacrylamide was tested as corrosion and scale inhibitor in the cooling systems [198]. Polyacrylamide reduced the corrosion rate by more than 68.2% and inhibited the anodic reaction. It was very efficient (90%) against calcium carbonate scale [198].

3.12 Summary

The first part literature review presented that the formation of calcium carbonate are affected by many different parameters. There are different strategies to prevent formation of calcium carbonate with main focus of this literature on scale inhibitors. Various techniques were reviewed which are employed to study calcium carbonate formation and inhibition.

The second part of literature review presented that CO₂ corrosion is a complex process. The electrochemistry of the carbon steel dissolution is well understood and influence of different parameters have been investigated. The formation of iron carbonate scale has been studied with various factors influencing it. There are different strategies to prevent CO₂ corrosion with main focus of this literature on corrosion inhibitors.

The third part of literature review presented that effect of combined inhibitors on scale and corrosion processes and factors influencing performance of the combined inhibitor. The effect the combined inhibitors, scale inhibitor and corrosion inhibitors on corrosion and scale process were presented.

However, most of the studies done in past has focused on general corrosion, pitting corrosion, surface scaling or bulk scaling. None of them has asses all these processes at the same time which could help to fully understand the whole system.

Chapter 4 Methodology

4.1 Introduction

This chapter discusses methodology that is used in this study. The first section describes the Jar test/bubble cell. The next two sections describe methods used to measure general, localized corrosion, surface scaling and bulk precipitation. The fourth part describes different technique used to study interaction of inhibitors with scale. In the last part experimental design used in this study is explained.

4.2 Jar test/bubble cell

The experiments for this PhD have been conducted under CO₂ saturated conditions using a newly developed combined bulk jar test/bubble cell methodology [18] as shown on Figure 4.1. In this set up, 4 key parameters are measured:

- general corrosion (continuously during test),
- localised corrosion (after test),
- bulk scale (continuously during test),
- surface scale deposition (after test).

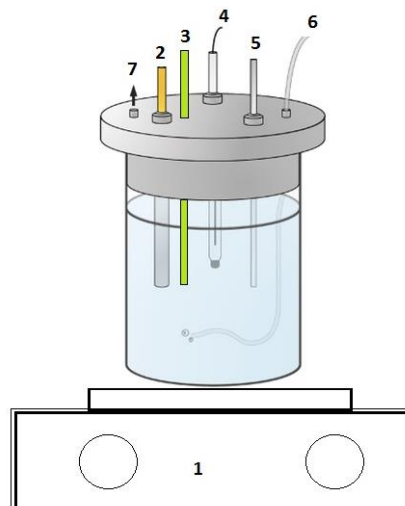


Figure 4.1 A combined bulk jar test/bubble cell: 1) hot-plate/stirrer, 2) working electrode, 3) temperature probe, 4) combined reference and counter electrode, 5) pH electrode, 6) CO₂ inlet and 7) CO₂ outlet [199]

4.2.1 Hot plate stirrer

A Multi-Hotplate Stirrer with 3 places manufactured by Witeg was used. The hotplate stirrer has an accuracy of maintaining temperature $\pm 0.3^{\circ}\text{C}$ at a set temperature with exact speed control.

4.2.2 Working electrode

The working electrodes were made up of X65 carbon steel with a chemical composition as presented in Table 4.1. The oil and gas industry frequently uses carbon and low alloy steel materials. These materials have limited CO_2 corrosion performance [200]. Their popularity could be explained by the low cost of carbon steel and protection gained from the use of inhibitors. Carbon steel used with inhibitors very often outperform corrosion resistance alloys (CRA) on field efficiency and cost [201].

Table 4.1: Chemical composition (wt.%) X65 carbon steel [202]

C	Si	Mn	P	S	Cr	Mo	Ni
0.12	0.18	1.27	0.008	0.002	0.11	0.17	0.07
Cu	Sn	Al	B	Nb	Ti	V	
0.12	0.008	0.022	0.0005	0.054	0.001	0.057	

The microstructure of X65 steel is composed of ferrite (white) and pearlite colonies as presented in Figure 4.2.

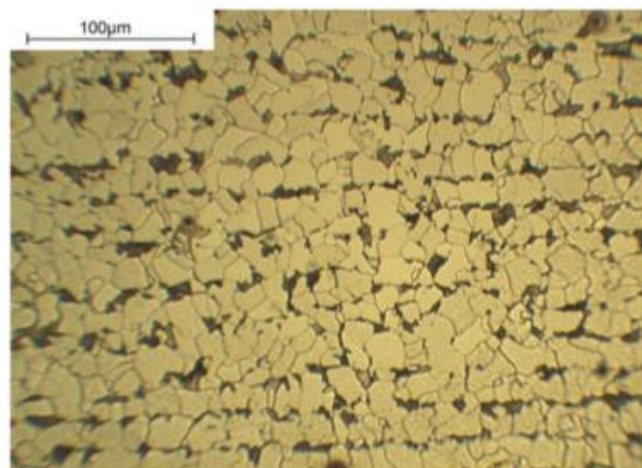


Figure 4.2: The microstructure of X65 steel in 50 magnification

The diameter of the working electrodes were 25mm. Copper wire was soldered to the back of the working electrodes and then the working electrodes were mounted into a non-conductive resin - Varidur BUEHLER. The working electrodes were then wet-ground up to 1000 grit using SiC paper on a Buehler - Beta Grinder-polisher. They were then degreased with

acetone, washed with distilled water, and dried using compressed air before being submerged into the test brine.

4.2.3 Combined reference and counter electrode

The combined electrodes were InLab® Redox-L electrodes each with a platinum ring indicator and were manufactured by METTLER TOLEDO. The manufactured specification temperature range for the combined electrodes was 0-100°C. The combined electrodes were filled with 3mol/L KCl electrolyte and the test temperature was 80°C.

4.2.4 pH electrode and apparatus

pH electrode HI1296D and pH apparatus HI 991001 were used manufactured by Hanna Instruments. The pH electrode HI1296D was filled with Ag/AgCl solution. The pH apparatus HI 991001 measured a pH range from -2.00 to 16.00 pH with an accuracy of ± 0.2 pH. The pH solution across this study was between 6.5 to 5.5.

4.2.5 Solution composition

The MultiScale software version 7.1 was used to calculate the desired brine composition with a saturation ratio (SR) with respect to the calcium carbonate. This MultiScale software is based on the multiphase equilibrium model as shown schematically in Figure 4.3 and was developed by Baard Kaasa [203] and Kristian Sandengen [204]. Three main systems can be distinguished in the model:

1. the hydrocarbon phase
2. the aqueous phase
3. the solid phases

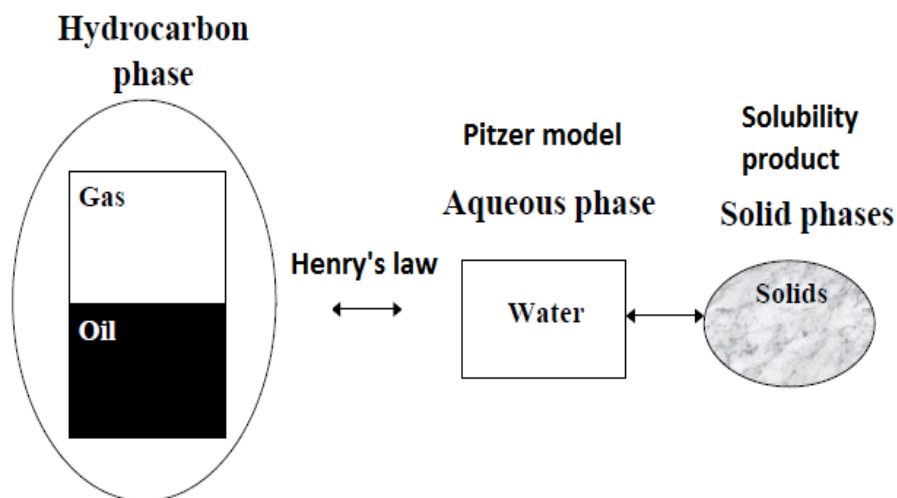


Figure 4.3: Schematic figure of the multiphase equilibrium model [203]

The exact brine composition used are presented in Table 4.2 below.

Table 4.2: Brine composition

Supersaturation of CaCO ₃ (SR)	Brine 1		Brine 2	
	≈40	CaCl ₂ •6H ₂ O g/l	NaCl g/l	NaHCO ₃ g/l
	11.39	77.7	4.36	80.24

To prepare the supersaturated solutions calcium chloride (CaCl₂•6H₂O), sodium chloride (NaCl), and sodium bicarbonate (NaHCO₃) of analytical grade were used.

4.2.6 Inhibitors

The details of the single inhibitors used to blend the combined inhibitors are presented in Table 4.3.

Table 4.3: Description of the single inhibitors

Inhibitor description	Abbreviation	Active components	Supplier
Libraphos 1082	CI1	Alcohol ethoxy phosphate ester	Baker Hughes
Pentonium 24	CI2	C12-C14 Alkyldimethylbenzyl ammonium chloride	Baker Hughes
MK216K	CI3	Ethoxylated imidazolines	Baker Hughes
Bellasol S40	SI	Phosphinocarboxylic acid	Baker Hughes
2-mercaptoethanol	SA	2-mercaptoethanol	Baker Hughes

The concentration (v/v%) of the single components in the combined inhibitors was set accordingly:

- corrosion inhibitor : 0.5% low (L) or 10% high (H)
- scale inhibitor: 1% low (L) or 20% high (H)
- souring agent: 0.25% low (L) or 5% high (H)
- rest of solvent

25ppm of combined inhibitor was present in 1 litre of solution. This concentration was advised by the sponsors of this PhD. Hence, the concentrations of single components used in the tests with single components were:

- 2-mercaptoethanol – 1.25 ppm
- alcohol ethoxy phosphate ester – 2.5 ppm,
- C12-C14 alkyldimethyl-benzylammonium chloride – 2.5 ppm
- ethoxylated imidazolines – 2.5 ppm
- polyphosphinocarboxylic acid (PPCA) – 5 ppm

All single components were treated as pure chemicals (only active component see Table 4.3) - which was advised by the sponsors of this PhD. Every time before the tests 2000 μ l of fresh combined inhibitor was prepared to avoid micelle formation.

The concentrations were calculated using the dilution equation:

$$C_1V_1 = C_2V_2 \quad (4-1)$$

where: C_1 is initial concentration, V_1 is initial volume, C_2 is final concentration and V_2 is final volume.

The Table 4.4 presents the variation of concentration of the single component concentration in 32 combinations of combined inhibitors.

4.3 Corrosion measurements

4.3.1 General corrosion

General corrosion was measured using Ivium-n-Stat: multi-channel Potentiostat/Galvanostat. The Ivium-n-Stat: multi-channel potentiostat was used to control the potential of the working electrodes to a selected value with respect to the reference electrodes. Potential was measured by a voltmeter. The Ivium-n-Stat: multi-channel galvanostat supplied a constant current to the working electrode independent of the voltage and the impedance fluctuations at the electrode surface.

4.3.2 Localized corrosion

Pitting corrosion damage evaluation is associated with pit identification and characterisation. Pits can be identified by a number of methods. This includes a visual examination, metallographic examination and non-destructive inspections [169, 205]. Pitting corrosion damage evaluation in laboratories and in field applications is very challenging. The pit shape,

general morphology of pits, surface dimensions and density need to be evaluated [169]. The most important factor in localized corrosion evaluation is finding the deepest pits on an exposed surface as it is usually the first to perforate [169]. Hoepfner [169] describes pitting as;

- * negligible when at a depth of 0.025 mm (25 μm) maximum and
- * moderate pitting is viewed as potentially 0.25 mm (250 μm)

According to the ASTM standard [205] the most useful methods of evaluating pitting corrosion damage are:

- Metal penetration which is expressed in terms of maximum pit depth or average of the 10 deepest pits and most preferably both
- Metal penetration can also be expressed in terms of pitting factor defined as the ratio of the deepest metal penetration to the average metal penetration, determined by weight loss. Pitting factor of one represent uniform corrosion and the larger the number the deeper the penetration

However, pitting factor is not useful where pitting or general corrosion is very small as values of zero can be obtained when dealing with a ratio [205].

In this PhD project white light interferometry was used to evaluate the pit depth and evaluation of the deepest pits was used to characterise the extent of pitting corrosion.

NPFLEX 3D Surface Metrology made by Bruker was used to measure the pitting corrosion. NPFLEX is designed specifically for investigating different sample sizes and shapes without damaging the sample. White Light Interferometry (WLI) is not sensitive to material type. It is effective in imaging deep trenches, holes and samples with a high topographic relief.

White light interferometers scan the morphology of the test surface. The white light beam is split by a beam splitter to two beams: the reference beam which is reflected from the reference plane and the measurement beam which is placed on the sample surface (Figure 4.4). When the distance is changed between the sample and the white light interferometer, the same change is observed between the reference plane and white light interferometer. The returning beams are relayed by the beam splitter into camera. The software builds the topography of the object based on the returning beams.

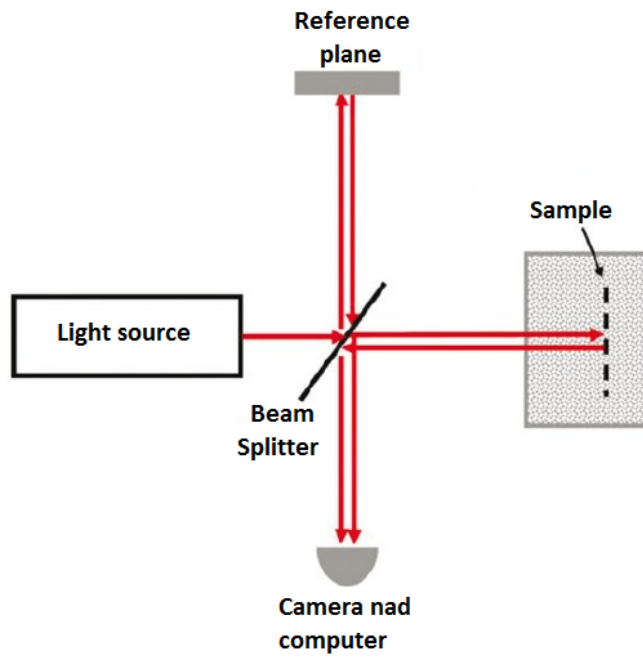


Figure 4.4: Schematic layout of a White light Interferometer [206]

For the assessment of depth of pits in this PhD, a certain threshold accordingly to the damage of sample by general corrosion was applied (Figure 4.5). Any significant hole below of this threshold was classified as a pit.

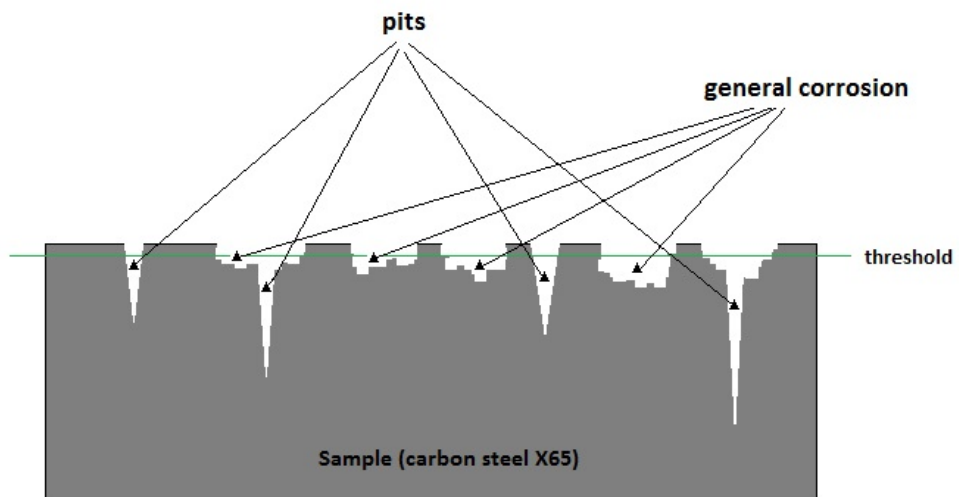
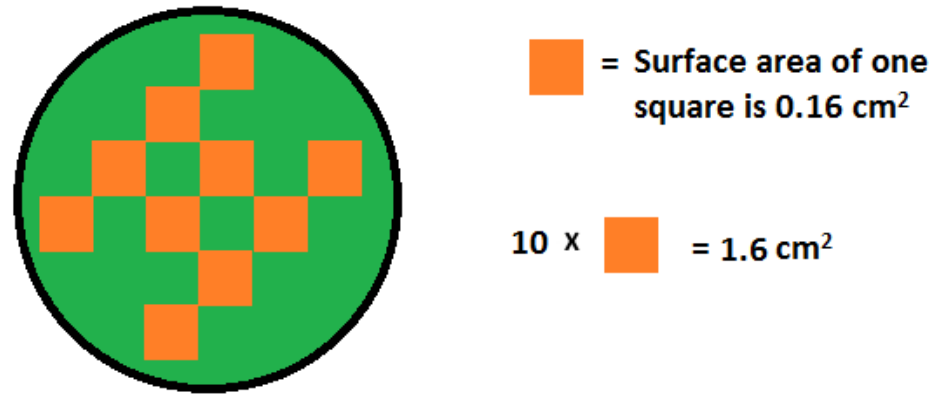


Figure 4.5: Schematic of representation of a threshold on a sample

The surface for each sample was 4.9 cm^2 . Avoiding sides of the sample, ten small squares were chosen for scanning for pits as shown on Figure 4.6. The surface area for the 10 squares was equal to 1.6 cm^2 which represents 32.65% of the tested sample surface. It represented approximately one-third of the sample surface area.



Whole surface of sample is 4.9 cm²

Figure 4.6: Schematic of representation of tested surface area for analyses of pitting corrosion

4.4 Bulk and surface scale measurements

4.4.1 Bulk scale measurements

During the combined bulk jar test/bubble cell testing, Hach DR 890 colorimeter was used to measure the turbidity of the brine. Turbidity is the optical measurement of scattered light resulting from the interaction of incident light with particulate material in a liquid sample. A higher level of scattered light reaching the detector results in a higher turbidity value. The turbidity unit is the Formazin Attenuation Unit (FAU) and is calibrated by use of the formazin polymer. FAU is specified by ISO 7027 for water treatment standards for turbidity measurements at 0° [207]. The Hach DR 890 colorimeter allowed detection up to 1000 FAU with a precision of ± 2 FAU [208].

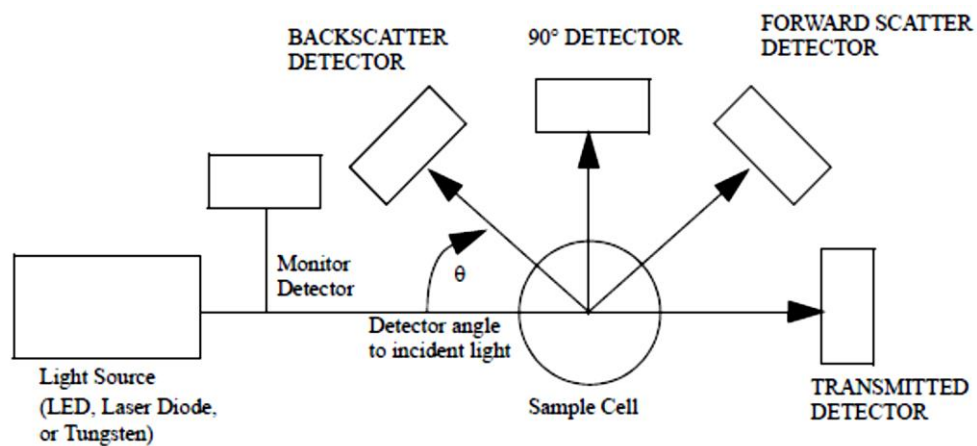


Figure 4.7 Schematic representation of the turbidity-meter [209]

An inductively coupled plasma mass spectrometry (ICP-MS) was used to measure the difference of calcium concentration before and after tests in the bulk solution and the amount of scale deposited on the sample (Figure 4.8). To measure the surface scale after the test, the sample was immersed for 48 hours into a 25 ml of 10% v/v of acetic acid to allow the surface scale to dissolve. Then 10 ml of the solution was analysed for the presence of the calcium ions. The dilution factor is accounted into results and after conversion results are expressed in mg/cm^2 . The heat energy of the plasma, strips the electrons from the elements to create ions. The ion stream from the plasma is focused and filtered. Only ions with a certain range of ratio mass-to-charge can reach the detector. The ion stream hits the detector, which produces an electrical signal which is used to determine the quantity of ions it has received. The computer software then converts the saved signal to a number of ion concentration.

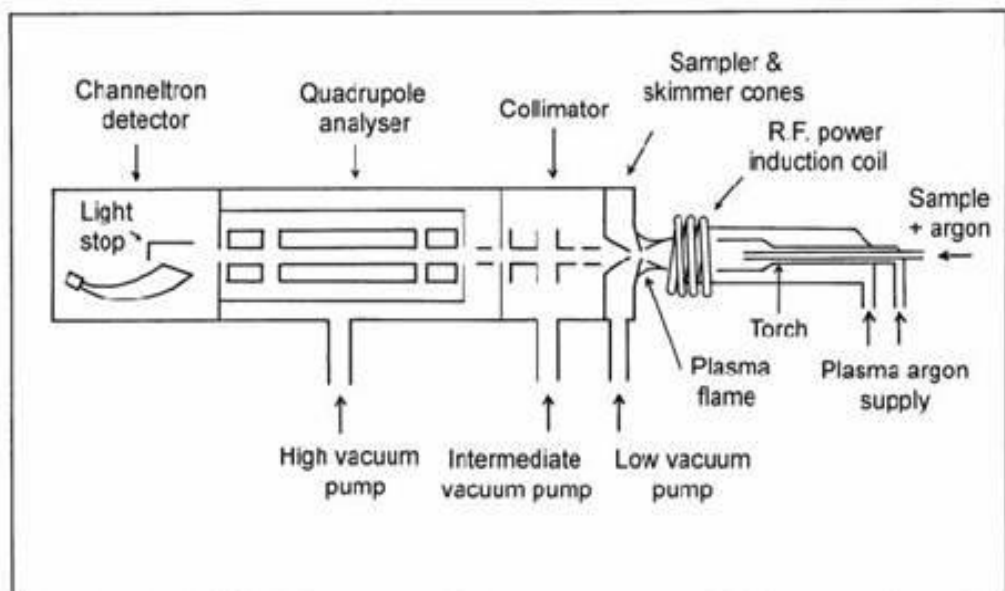


Figure 4.8 Schematic representation of the ICP-MS [210]

4.4.2 Surface scale measurements

Scanning Electron Microscopy (SEM) (Carl Zeiss EVO MA 15) was used to examine the polymorphs of the scale which formed on the samples (Figure 4.9). The SEM contains a metallic filament which is heated and produces an electron beam. The electron beam makes its way through electromagnetic lenses which focus and direct the beam on to the sample. Once it hits the sample, electrons backscattered and secondary electrons are ejected from the sample. Detectors collect the electrons and convert them to a signal which is used to produce an image on a TV screen.

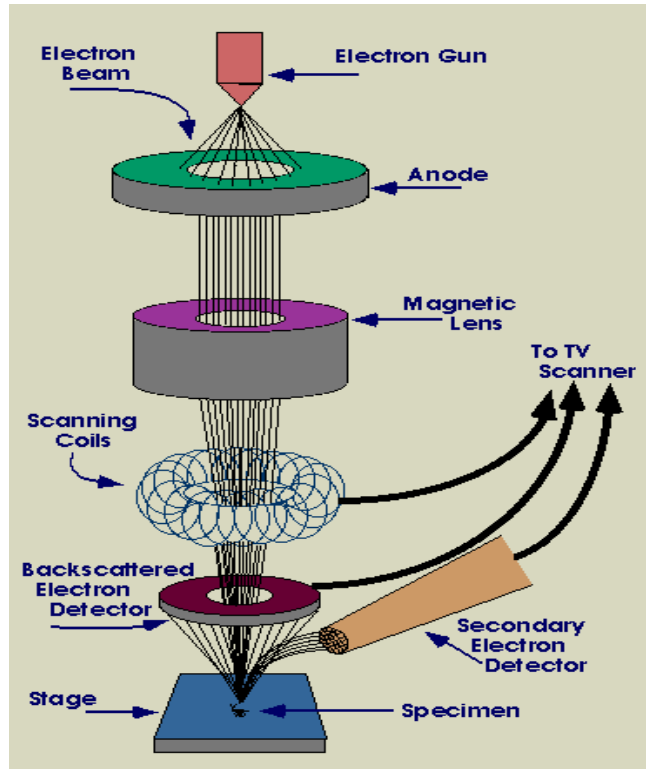


Figure 4.9 Schematic representation of the SEM [211]

Energy dispersive X-ray (EDX) is an analysis technique in which an electron beam hits a sample target and the transition from a high-energy state to a lower energy state of the chemical components results in the emission of an X-ray of equal magnitude to the energy associated with the change in state. A detector (the most common are made of Si(Li) crystals) is used to separate the characteristic emission x-rays of different elements into an energy spectrum. Software is then used to analyse the energy spectrum in order to define the abundance of the specific elements.

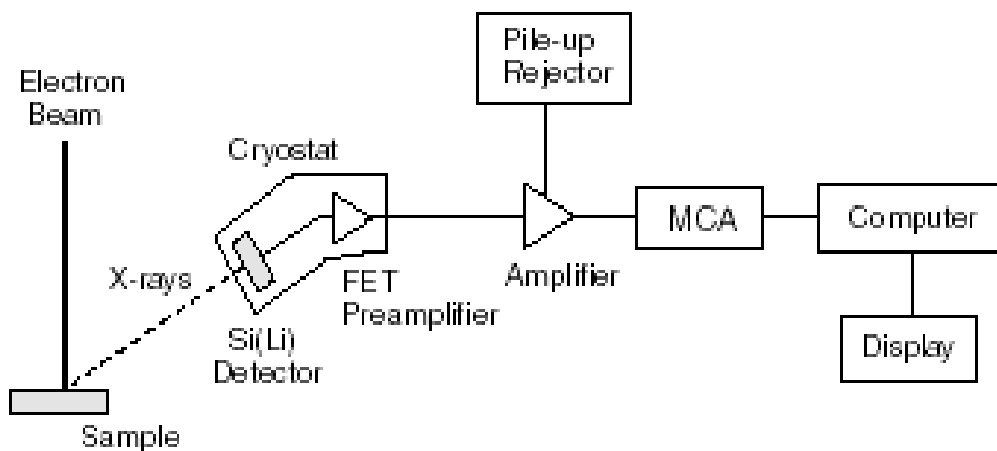


Figure 4.10 Schematic representation of the energy-dispersive X-ray [212]

X-ray diffraction (XRD) (The Philips X'Pert 1 X-ray diffractometer) was used. X-rays are produced by blasting a metal target with a beam of electrons emitted from a hot filament (Co tube). The beam will ionize electrons from the K-shell (1s) of atoms and the X-rays which are produced as vacancies are filled by electrons moving down from L (2P) or M (3p) levels (Figure 4.11).

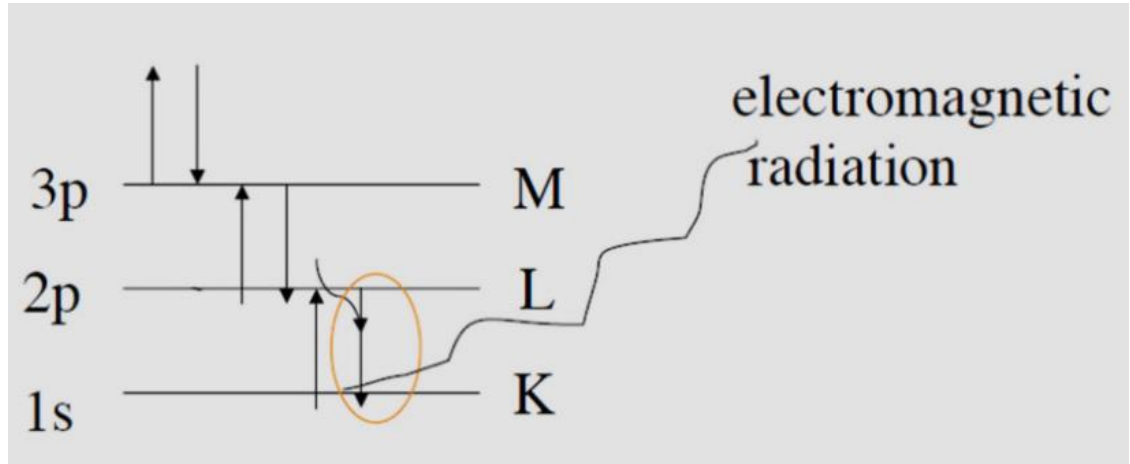


Figure 4.11: Schematic representation of the X-rays production [213]

Diffraction (interference of waves) of X-rays by crystals is described by Bragg's Law (Equation (4-2)),

$$n\lambda = 2d \sin\theta \quad (4-2)$$

where n is the integer, λ is the wavelength of the x-ray, d is the spacing of the crystal layers and θ is the incident angle.

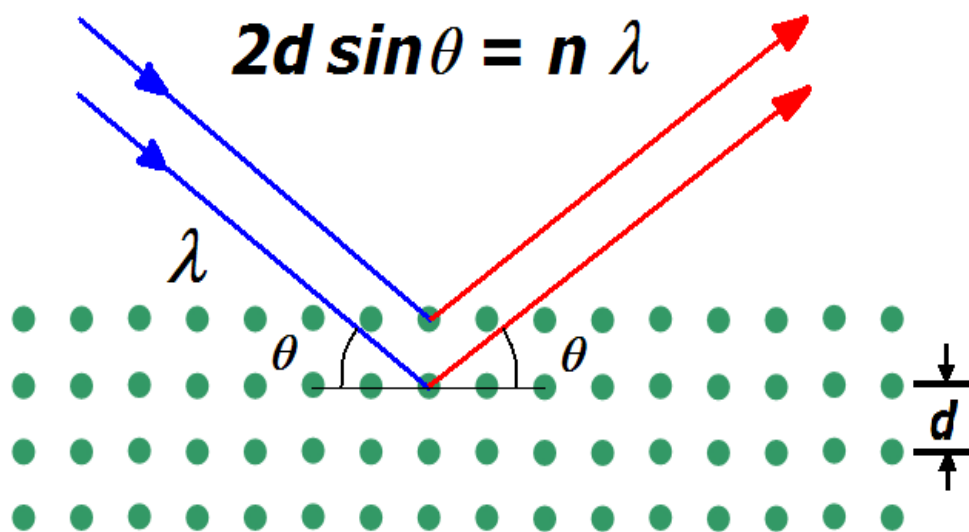


Figure 4.12: Bragg diffraction [214]

The direction of the diffraction of an X-ray depends on the size and shape of the unit cell of the material crystal. The scale formed on the surface of a metal sample has a specific X-ray diffraction pattern for each crystal. The position of the diffraction peaks and their intensities are specific for a crystalline phase.

A Hugo Rietveld [215] written computer programme which took into account the overall isotropic temperature factors, atomic coordinates, scale factors, scattering factors, background and instrumental factors to obtain a model based on a least squares fit between the calculated and observed integrated intensities, measured at regular angular intervals from powder diffraction for alkaline earth metal uranates. It was developed to get the maximum amount of information from overlapping peaks and is termed "Rietveld Refinement" [216]. The Rietveld Refinement is quite complex, it is built on several key areas that are considered for the least-squares operation. These key parameters are: peak width based on CW parameters U, V, W by Caglioti [217], orientation correction, peak profile (pseudo-Voigt, Lorentzian, Gaussian), structure factors and least square parameters (scale factor, lattice parameters, asymmetry, space group, background and temperature factors) [216].

X'Pert HiScore [218] is software based on the Rietveld Refinement and was used in this PhD project which allows quantitative phase analysis.

4.5 Interaction of the inhibitors with scale on surface measurements

Fourier Transform Infrared Spectrometry (FTIR) (Perkin Elmer® Spectrum SpotLight TM) was used. This FTIR spectroscopy machine can create a spectrum range from 650 to 4000 cm^{-1} . Infra-red intensity adsorbed by the sample is measured accordingly to the wavelength of the light emitted. The signal is digitized and sent to the computer where the Fourier transformation is measured and the infrared spectrum is presented to the operator of FTIR machine for further analysis.

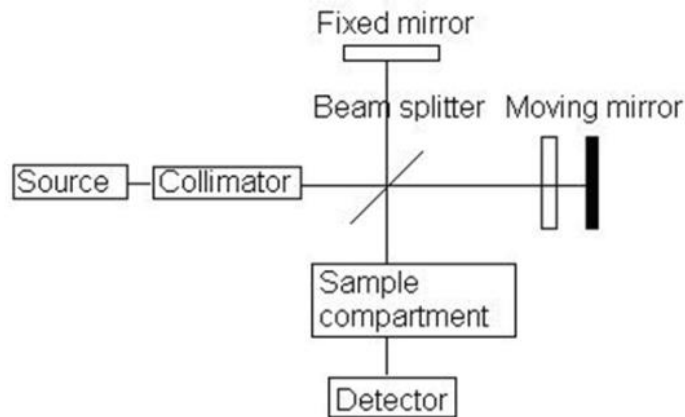


Figure 4.13: Schematic representation of the FTIR [219]

A Renishaw in Via confocal Raman microscope was used. The microscope uses a laser as a source of light which is focused by lenses onto the sample to collect scattered light. Filters then purify the reflected and scattered light which is detected by sensors. A computer is then used to display the spectrum and analyse the information. The Raman microscope measures a very tiny fraction of the scattered light which has a different colour. The light has a different colour than the source because during the scattering process it has lost some energy to the material, which is causing some of the atoms to vibrate.

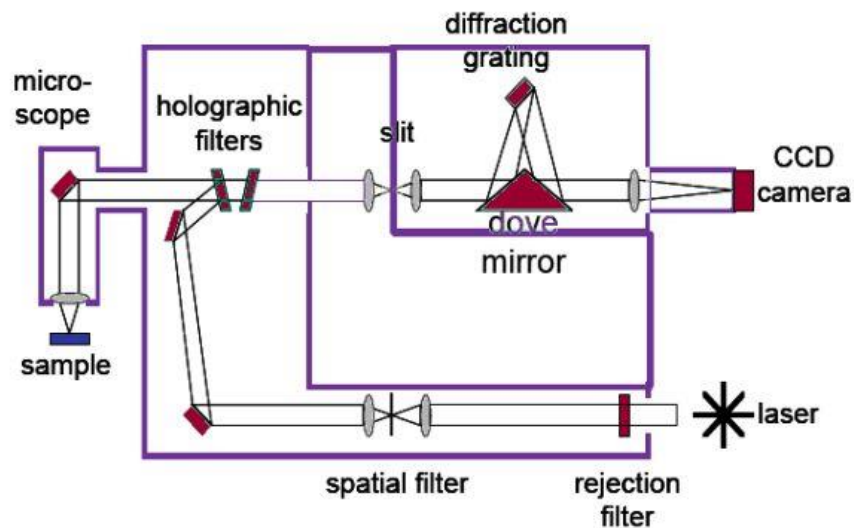


Figure 4.14: Schematic representation of the Raman spectrometer [220]

4.6 Experimental design

There are wide variety of methods and analysis techniques, known as experimental design [221]. One of the main goals of experimental design is to evaluate how changes in input factors affect the results (responses) of the

experiment [222]. Design of experiments (DOE) is a tool which can be used in a variety of experimental situations [223, 224].

4.6.1 Design of Experiments (DOE)

DOE is commonly used in research as well as in industry but for very different purposes. The main goal in scientific research is usually to demonstrate the statistical significance of the effect that a particular factor exerts on the dependent variable of interests. The DOE is a systematic approach to study a process or a system. It is used to investigate a phenomenon in order to gain an understanding or improve performance [224]. The DOE gives a well-defined framework for:

- data collection
- analysis
- interpretation.

This approach can help to answer queries linked to an assumption and understand how different factors influence interesting variables.

Several models for the DOE are available, including Full Factorial, Fractional Factorial and Taguchi approach. In this PhD study a Two Level Full Factorial Experiments was used.

4.6.2 Two Level Full Factorial Experiments [224]

A full factorial experiment is an experiment in which one or more input factors are set at two levels each. In full factorial experiments all possible combinations of these levels across all such factors are investigated. It can be investigate the effect of each factor on the response (variable), as well as the effects of the interactions between factors on the response (variable).

In this PhD study a 2^5 full factorial design method was applied to study the individual effects of each component of combined scale/corrosion inhibitor as well as their interactive effects on:

- General corrosion
- Localised corrosion
- Bulk scale
- Surface scale

The experimental tests in this study focused on 5 single components of a combined inhibitor. Each parameter (single components) was set at two levels, thus there were $2 \times 2 \times 2 \times 2 \times 2 = 32$ trials for the combined inhibitor (see Table 4.4).

Table 4.4: 32 combination of combined inhibitors

Std	Run	CI 1	CI 2	CI 3	SI	SA
23	1	L	H	H	L	H
21	2	L	L	H	L	H
5	3	L	L	H	L	L
13	4	L	L	H	H	L
11	5	L	H	L	H	L
14	6	H	L	H	H	L
6	7	H	L	H	L	L
8	8	H	H	H	L	L
4	9	H	H	L	L	L
32	10	H	H	H	H	H
1	11	L	L	L	L	L
3	12	L	H	L	L	L
12	13	H	H	L	H	L
22	14	H	L	H	L	H
31	15	L	H	H	H	H
10	16	H	L	L	H	L
25	17	L	L	L	H	H
29	18	L	L	H	H	H
28	19	H	H	L	H	H
7	20	L	H	H	L	L
17	21	L	L	L	L	H
2	22	H	L	L	L	L
20	23	H	H	L	L	H
26	24	H	L	L	H	H
30	25	H	L	H	H	H
27	26	L	H	L	H	H
24	27	H	H	H	L	H
15	28	L	H	H	H	L
18	29	H	L	L	L	H
16	30	H	H	H	H	L
19	31	L	H	L	L	H
9	32	L	L	L	H	L

A factorial experiment can be analysed using the analysis of variance (ANOVA).

4.6.3 The analysis of variance (ANOVA)

ANOVA is a collection of statistical models which are applied to analyse the differences between group means and their associated procedures. The experimental design method combined with factorial ANOVA can then be used to assess the effect that a particular factor has on the dependent variable of interest. In this PhD study the effect of 5 single components (factors) on general corrosion, localized corrosion, surface scaling and bulk precipitation (variable of interests) was assessed.

In order to obtain a systematic analysis on how the single components and their interactions effect general corrosion, localized corrosion, surface scaling and bulk precipitation a routine statistical calculation method was applied. The calculations were computed with the use of Design-Expert® Software Version 6.0.8 [225]. The design matrix for the five-parameters with two levels each was shown in Table 4.4. This table presented the thirty two different combinations which were set for the combined inhibitor (5 single components).

The contribution percentage of the 5 single components of combined inhibitor and their interactions on general corrosion, localized corrosion, surface scale and bulk scaling was calculated. Contribution percentage calculation are presented on general corrosion as example; exactly the same way contribution percentage of the 5 single components of combined inhibitor and their interactions was calculated on localised corrosion, surface scale and bulk scaling. From the Table 4.4, the trial conditions for low level of corrosion inhibitor 1 (CI1) - 1, 2, 3, 4, 5, 11, 12, 15, 17, 18, 20, 21, 26, 28, 31 and 32 were used. Hence the calculation for the average output at the CI1 at low level on general corrosion can be calculated:

$$CR_{CI1_{Lc}} = \frac{1}{16} (CR1 + CR2 + \dots + CR32) \quad (4-3)$$

where: CR1 ... and CR32 is the corrosion rate in Table 7.1 corresponding to experiment conditions 1,2,...and 32, respectively in Table 4.4.

The output at high level of CI1 on general corrosion can be calculated in the same manner. In the Table 4.5 are presented outputs of single components (factors) at each level.

Table 4.5: The average outputs of individual factors for each level

Factors	Level	
	Low	High
Corrosion inhibitor 1 (CI1)	CI1 _{Lc}	CI1 _{Hc}
Corrosion inhibitor 2 (CI2)	CI2 _{Lc}	CI2 _{Hc}
Corrosion inhibitor 3 (CI3)	CI3 _{Lc}	CI3 _{Hc}
Scale inhibitor (SI)	SI _{Lc}	SI _{Hc}
Souring agent (SA)	SA _{Lc}	SA _{Hc}

Sum of squares is the sum of the squared deviations. In this PhD study, the sum of squares of outputs due to corrosion inhibitor1 (CI1) can be obtained by using the following formula:

$$SSCR_{CI_1} = 2^2(CRCI_{1Lc} - CRG) + 2^2(CRCI_{1Hc} - CRG) \quad (4-4)$$

where $CRLC_{CI_1}$ and $CRHC_{CI_1}$ refer to the average effects analogous to the CI1 factor for low and high levels (concentration) while CRG is the average corrosion rate for 32 experiment conditions.

The sums of squares for other factors and interactions were calculated in the same way. The final part of statistical calculation of ANOVA was finished easily to obtain the percentage contribution, for example the percentage effect of corrosion inhibitor 1 (CI1) on general corrosion was be calculated by the following equation:

$$CI1(\%) = \frac{SSCR_{CI_1}}{SSCR_{CI_1} + SSCR_{CI_2} + \dots + SSCR_{CI_1SISA} + SSCR_{CI_1CI_2CI_3SISA}} * 100\% \quad (4-5)$$

where: $SSCR_{CI_1}$ and $SSCR_{CI_1SISA}$ are the sum of squares of the single components of combined inhibitor an their interactions.

4.7 Experimental procedure summary

Experiments were conducted using a newly developed combined bulk jar test/bubble cell methodology, under CO₂ saturated conditions . This setup uses a 1 litre test solution with test specimens being made from API X65 carbon steel with 4.9 cm² exposed area. Each of the samples were polished up to to 1000 grit using SiC paper, degreased with acetone, rinsed with distilled water, and dried before immersing into the test brines.

The test solution used in the experiment was saturated with respect to CaCO₃ by mixing two solutions (500 ml brine 1 containing calcium ions and 500 ml brine 2 containing bicarbonate ions). The solution compositions have been calculated by MultiScale software version 7.1 and are shown in Table 4.2. Prior to transferring the test solutions into combined bulk jar test/bubble cell, they were fully de-aerated using CO₂ overnight.

The temperature was set at 80°C and CO₂ gas was purged during whole test. The solution pH after two brines were mixed was 6.5. 25ppm of combined inhibitor was injected to the test solution (see composition of the combined inhibitor in Table 4.4), before the two brines were mixed and the specimen immersed. Test conditions are outlined in Table 4.6.

Table 4.6: Test conditions

Parameters	Conditions
Temperature	80°C / 176 °F
pH	6.5
Steel	API 5L X65
Flow condition	Static
Total Pressure	1 Bar
pCO ₂	0.5 Bar
Test duration	4hrs, 72hrs (pitting tests)

The three-electrode setup connected to Ivium n-stat potentiostat was used to monitor corrosion behaviour. A colorimeter was used to measure the turbidity of the brine; scale inhibition was then evaluated by the incubation time of precipitation in bulk. Scanning Electron Microscopy (SEM) and X-Ray Diffraction (XRD) were used for the post-test surface analysis to determine polymorphs of calcium carbonate and detection of iron carbonate; to identify that localized corrosion is present white light Interferometer profiler have been used. The Ca²⁺ ions concentrations were measured in solutions on the end of test by Inductively Coupled Plasma Mass Spectrometry (ICP-MS). This method was used to quantify Ca²⁺ ions in the scale on metal surface, which have been dissolved in 10% acetic acid to compare with bulk solutions results.

Chapter 5

Corrosion and scale results in the absence of combined inhibitor

5.1 Introduction

In this chapter, corrosion and scale occurring simultaneously in the absence of any inhibitor were studied using a new bubble cell/jar test. The objective was to better understand interactions between corrosion and scale processes. In order to measure and assess the general corrosion and pitting corrosion LPR, Tafel plots and light interferometry were used. The scale was observed under SEM and calcium carbonate polymorphs were assessed by XRD.

5.2 Corrosion results

5.2.1 General corrosion

Tafel measurements from separate tests (anodic and cathodic) in the blank solution are shown in Figure 5.1 to indicate the reproducibility of the tests. From Tafel plots presented in Figure 5.1 it is clear that β_c is equal to 148 mV/decade and β_a is equal 42 mV/decade. It is clear that corrosion rate in the system without inhibitor is controlled by the cathodic reaction ($\beta_c > \beta_a$). In the tests without inhibitor the anodic reaction is an activation-controlled reaction (controlled by charge transfer reactions), while the cathodic reaction is a mixture of activation- and mass-transfer controlled reactions (controlled by the concentration of the reagent in the vicinity of the sample and diffusion in the bulk solution to the surface). The charge transfer reactions are influenced by formation of scale on the metal surface which affects mass transfer in the bulk solution.

Figure 5.2 shows the average corrosion measurements in the tests in the absence of combined inhibitor. The repeatability is presented using error bars. Six tests have been run and the blue line in Figure 5.2 represents the average corrosion rate where the error bars represent the minimum and maximum corrosion values measured in six tests. At the beginning of the tests the corrosion rate measured was around 3.67 mm/year. After 8 minutes of tests it reached the highest level observed during tests at 4.76 mm/year; the corrosion rate then started decreasing quickly and

continuously up to the 60-minute mark. For the next 60 minutes it decreased slightly to reach a plateau of 0.20 mm/year. The corrosion rate remained steady for the rest of the tests to reach a final value of around 0.21 mm/year after 4 hours of testing.

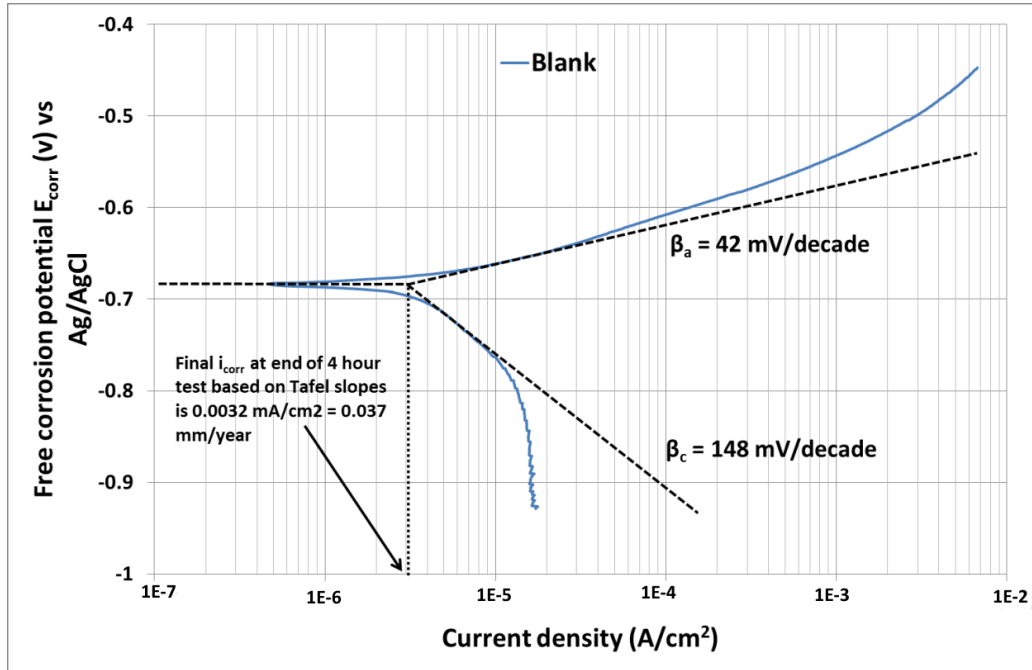


Figure 5.1: Tafel plots for carbon steel in blank brine solution at 80°C after 4 hours

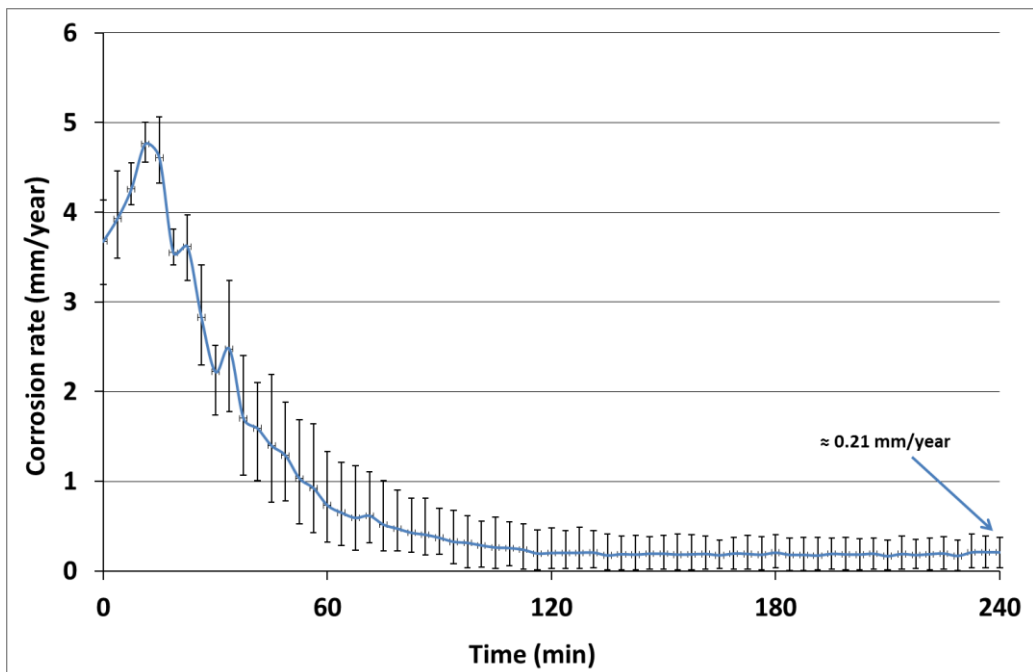


Figure 5.2: General corrosion results in the absence of combined inhibitor at 80°C over 4 hours

Figure 5.3 shows how the metal surface looks after scale has been removed by Clarke's solution at the end of the tests, in the absence of combined

inhibitor. It could be observed on the sample that there were some regions of the metal damaged by general corrosion processes. The structure of Fe_3C which remained unattacked can be seen in the areas that were corroded.

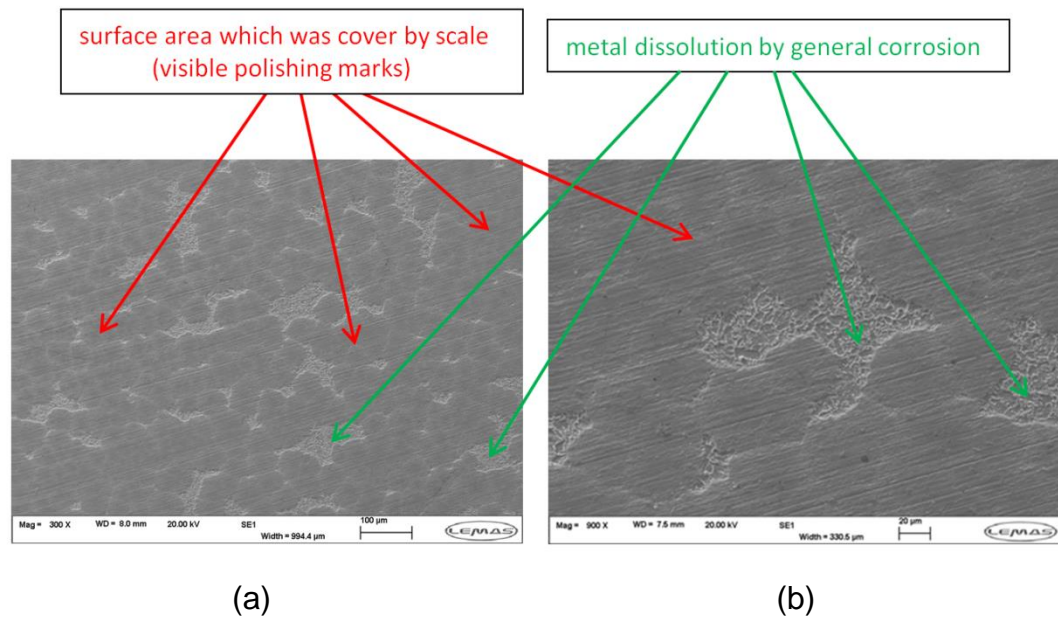


Figure 5.3: Scanning electron micrographs in the test in the absence of combined inhibitor after cleaning by Clarke's solution

5.2.2 Localized corrosion

In Table 5.1 the deepest pit depths from light interferometry analysis in tests after 4hrs, 72hrs and only polishing treatment are presented. Figure 5.4 presents a schematic representation of a surface after tests which have been then analysed. A pit is defined in this work as a cavity which is significantly deeper than threshold (more than $3\mu m$). The threshold is set at a level of the surface profile of the uniform corrosion attack.

Table 5.1: Deepest pits in the tests in the absence of combined inhibitor and for reference polished samples

Time of test	Deepest pit in the absence of combined inhibitor	Pit depth (μm)
-	Polished sample	grooves up to 0.7
4hrs	sample	3
72hrs	sample 1	24
72hrs	sample 2	23
72hrs	sample 3	23

After polishing, the grooves on the surfaces reached a depth up to $0.7\mu\text{m}$. After 4hrs of tests the deepest pit reached a depth up to $3\mu\text{m}$; because the pits were quite shallow in tests in the absence of inhibitor, tests were run for 72hrs to be able to correctly assess pitting corrosion. It could be observed that the depth of the deepest pits is repeatable in tests after 72hrs (Table 5.1 sample 1, sample 2 and sample 3). In the images acquired by light interferometry and presented in Figure 5.5. is clear that some damage has been done by general corrosion on the samples. However, in some of the cavities pitting corrosion occurred and some pits penetrated the samples and reached depths of around $24\mu\text{m}$ (Figure 5.5 c).

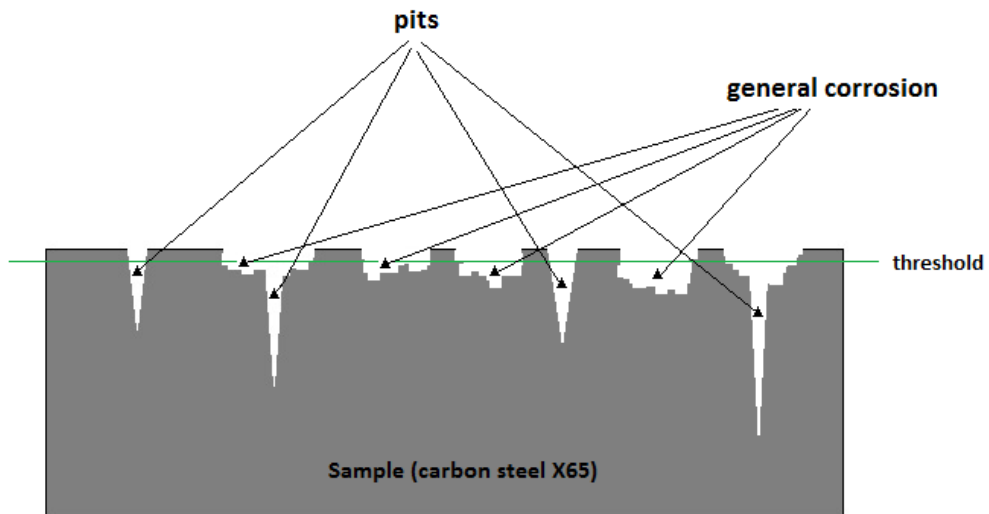
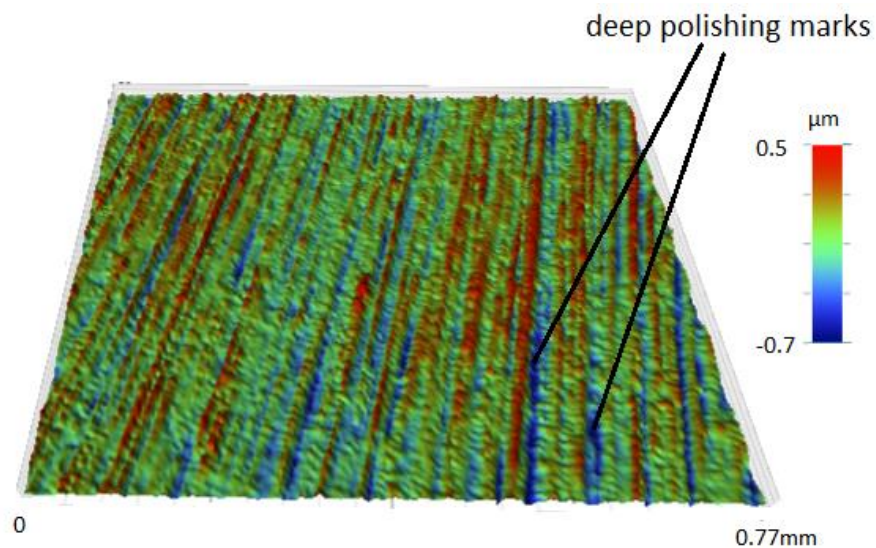
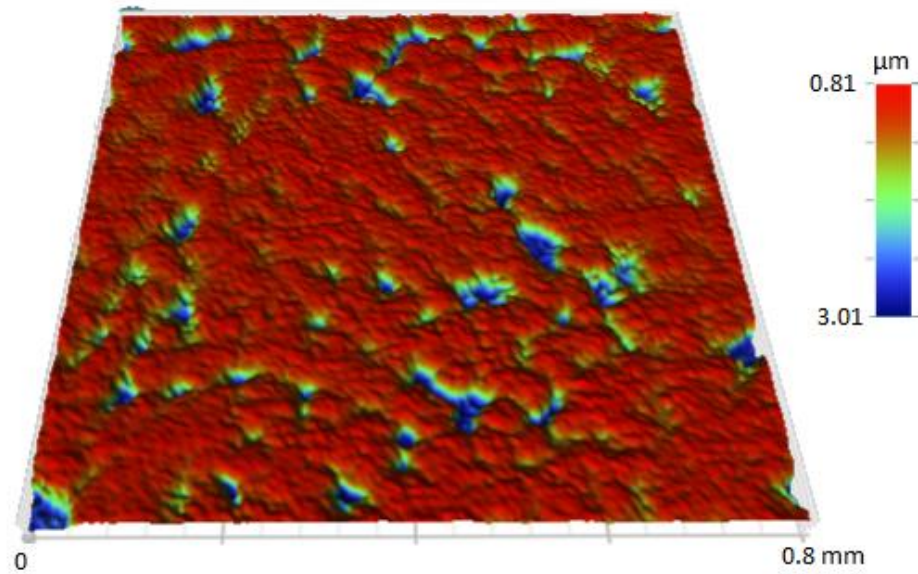


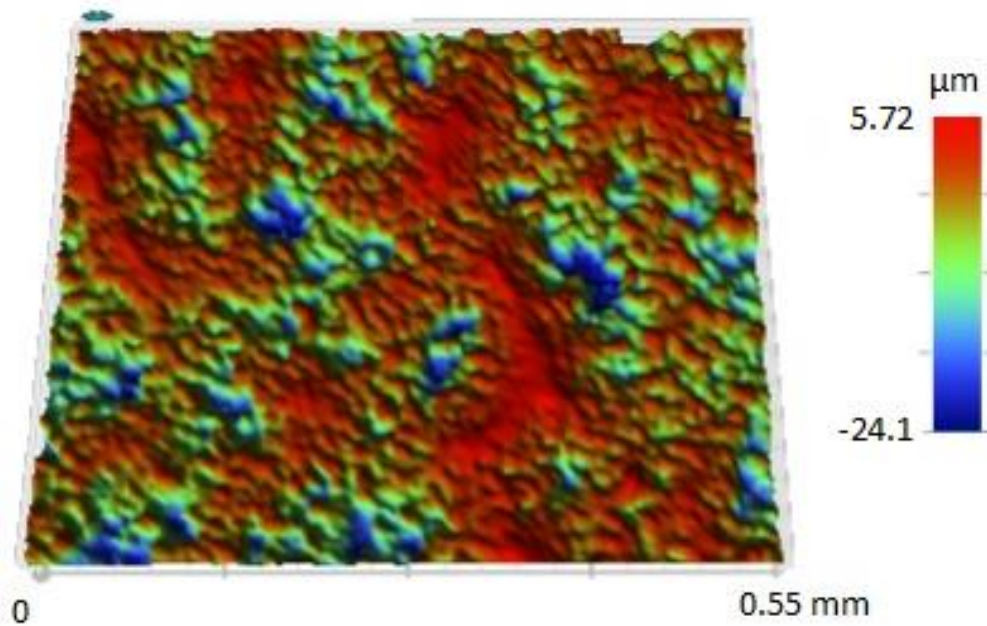
Figure 5.4: Schematic representation of a sample after test with representation of a threshold



(a)



(b)



(c)

Figure 5.5: Light interferometry images of deepest pit on surface in the tests in the absence of combined inhibitor: a) grooves on polished sample, b) pit after 4hrs test and c) pit1 after 72hrs

In Table 5.2 the pit density from light interferometry analysis in tests after 72hrs are presented. It could be observed that there are more pits in the -17.5 to -20 μm depth range than in others.

Table 5.2: Pit density in the tests in the absence of combined inhibitor

Pit depth (μm) in tests in the absence of combined inhibitor	Number of pits (per cm^2)
pit depth (μm) > 22.5	1
20 < pit depth (μm) > 22.5	5
17.5 < pit depth (μm) > 20	42

5.3 Bulk and surface scaling results

5.3.1 Bulk solution scaling

5.3.1.1 Turbidity results and pH – for bulk scaling

Turbidity trends in the test in the absence of inhibitor are shown in Figure 5.6. It can be observed that the first crystals in bulk solution have been recorded after 5 minutes (≈ 1.3 FTU). The solution is highly supersaturated with respect to calcium carbonate (Table 4.2); because of that the induction time is very short before first crystals in bulk solution can be detected. After 10 minutes the maximum value of turbidity measured was ≈ 15 FTU. Until 10 minutes the number of crystals and size of particles is constantly increasing. After 10 minutes the number of crystals and size of particles is constantly decreasing.

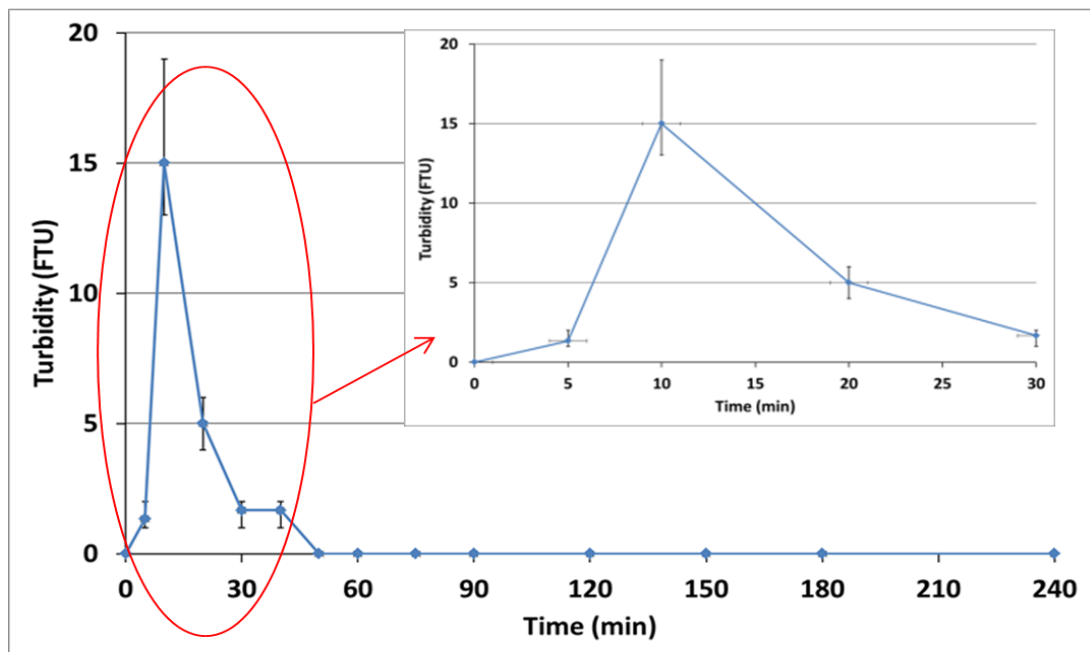


Figure 5.6: Turbidity results in the tests in the absence of combined inhibitor at 80°C over 4 hours

Then the number of scale crystals which can be detected in the bulk solution started decreasing sharply to reach 0 FTU value in 50 minutes of tests. Most of the crystals have settled on the bottom of the cell test due to their size.

The smaller particles were present in the solution. However due to their size the turbidity meter could not detect them. The crystals did not get bigger because of a drop of supersaturation ratio of the tested solution as time progressed.

The measured variations of pH in the test in the absence of inhibitor are presented in Figure 5.7. At the beginning of the test, when the two brines were initially mixed, the pH was 6.53. After mixing, the pH decreased quickly over the first few minutes until it reached a value ≈ 6.11 after 50 minutes. This drop of the pH was caused by rapid precipitation from the solution of calcium carbonate (Equation (2-4)) crystals in the bulk solution as well as on the sample surface. Next the pH continued to decrease slightly for the rest of the tests to reach a final value ≈ 5.91 . A further decrease of pH is caused by continuous formation of tiny crystals in the bulk solution (which cannot be detected by turbidity meter) and their growth as well as continuous growth of scale formed on the metal sample. The pH decrease was caused by an increase of H^+ ions due to the dissociation reaction of carbonic acid (Equation (2-2) and bicarbonate (Equation (2-3)).

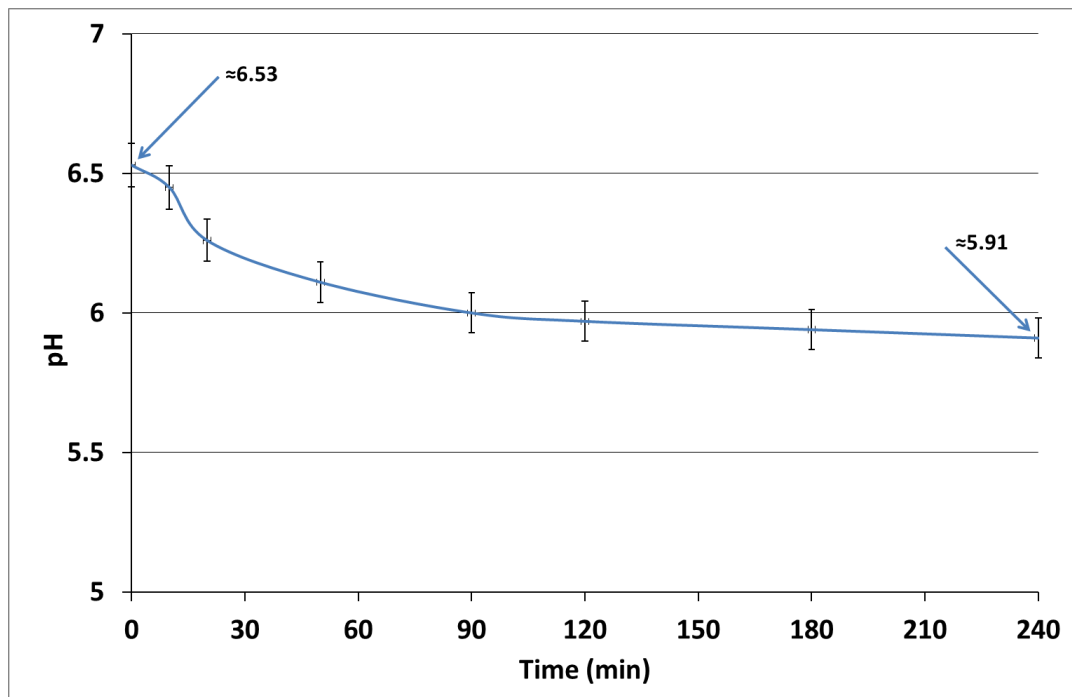


Figure 5.7: pH results in the tests in the absence of combined inhibitor

5.3.2 Inductively coupled plasma mass spectrometry (ICP – MS) results from bulk solution and surface

In Table 5.3 results from ICP-MS analysis are presented at the end of the tests from the bulk solution and from the dissolution of the deposit on the metal surface in the absence of combined inhibitor. Ca^{2+} ion concentration

has been measured to be at 694 ppm concentration in bulk solution. It could be observed that there was a substantial decrease compared to the initial concentration of Ca^{2+} of 917 ± 12 ppm (this is measured concentration after the brines have been mixed). This means that the total amount of calcium carbonate which precipitated from solution is equal to 556 mg. The amount of calcium found on the metal surface tests in the absence of combined inhibitor was 2.14 mg/cm^2 . The amount of calcium carbonate formed on the metal surface is 5.3 mg respectively which is an almost 1% of the whole scale precipitated from the bulk solution.

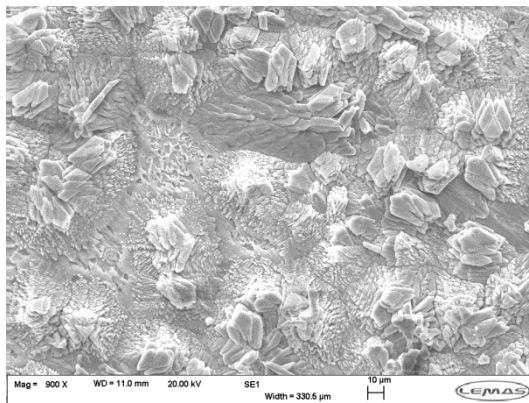
Table 5.3: ICP-MS results in the tests in the absence of combined inhibitor at the end of tests

Test	Amount of calcium in bulk on end of tests (ppm)	Amount of calcium on metal surface (mg/cm^2)
Blank	694 ± 10	2.14 ± 0.11

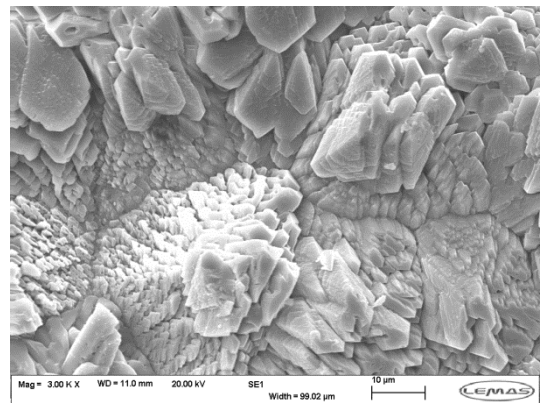
5.3.3 Surface scale

5.3.3.1 Scanning Electron Microscopy (SEM) and X-Ray Diffraction (XRD)

Figure 5.8 shows scale formed in the test in the absence of combined inhibitor. It could be observed that the scale which formed was very dense. However, there were some regions where scale did not form on the metal sample surface (Figure 5.8 a). The scale crystals which deposited on the metal samples had very irregular shapes. It can be observed that crystals had many different crystal growth sites (Figure 5.8 b).



(a)



(b)

Figure 5.8: Scanning electron micrographs of CaCO_3 formed in the tests in the absence of combined inhibitor

Figure 5.9 shows the acquired XRD spectrum of samples in the tests in the absence of combined inhibitor. It can be observed that the scale formed on the samples was only calcium carbonate. There are two peaks associated with iron carbonate in Figure 5.9. However, according to the International Centre for Diffraction Data (ICDD) [226] guidance, it needs to be at least three or more peaks to confirm presence of material (in this case is FeCO_3). Calcium carbonate which formed on the metal surface, was composed of two polymorphs: calcite and aragonite. Table 6.5 shows results from Rietveld refinement. It is clear, that the main compound of scale formed on the metal samples in the tests in the absence of combined inhibitor, was calcite (92%). The remaining 8% of scale formed was calcium carbonate polymorph - aragonite.

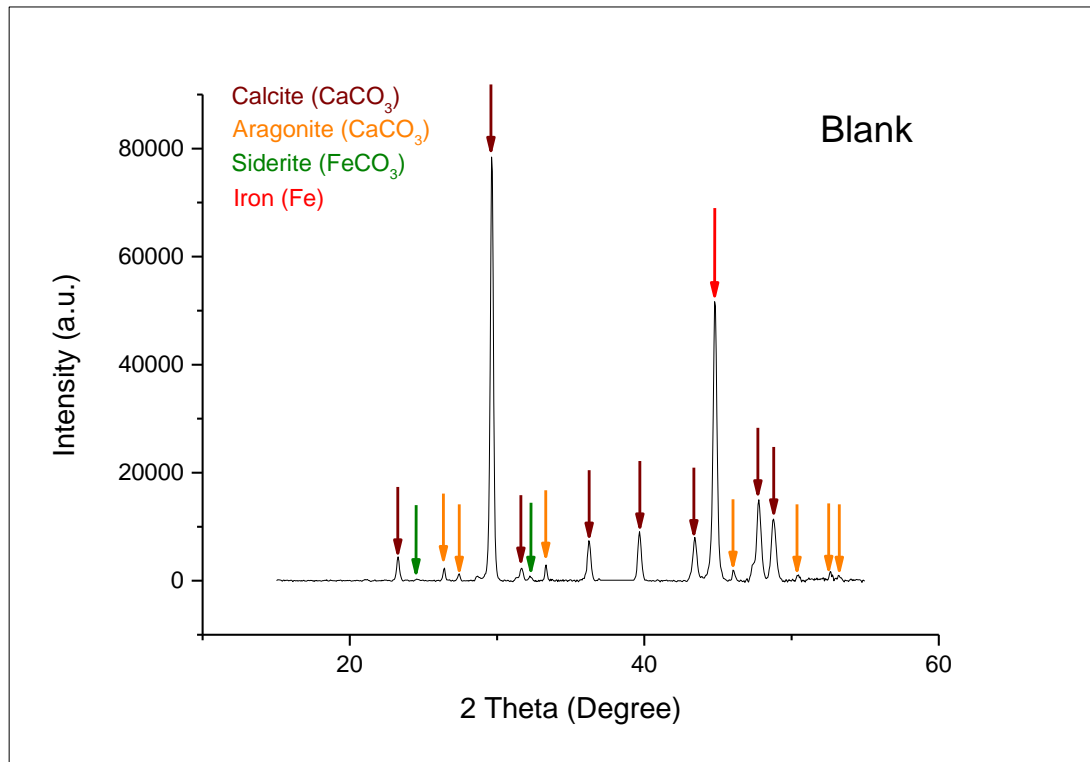


Figure 5.9: XRD spectrum of scale formed in the tests in the absence of combined inhibitor

Table 5.4: Different polymorphs of CaCO_3 formed in the tests in the absence of combined inhibitor by Rietveld Analysis

Test	% Calcite	% Aragonite
Blank	92±1	8±0.17

5.4 Summary

The corrosion and scale results in the absence of inhibitor when all processes occurring simultaneously were presented. The following conclusions could be reached.

- General corrosion at the end of the 4hr test was 0.21 mm/year
- Cathodic reaction controlled corrosion process – $\beta_c=148$ mV/decade and $\beta_a=42$ mV/decade ($\beta_c > \beta_a$)
- The cathodic reaction is a mixture of activation control and mass transfer control reaction
- The anodic reaction is activation control reaction
- Deepest pit measured on surface was 24 μm depth
- Pit density - 1 pit deeper than 22.5 $\mu\text{m}/\text{cm}^2$
- Induction time was equal 5 minutes
- Amount of scale formed during the test was 2.14 mg/cm^2
- The scale formed on surface was composed by 92% of calcite and 8% of aragonite

In the next chapter general corrosion, pitting corrosion bulk scaling and surface scaling were assessed the same way as in this chapter. However in the next chapter the single inhibitor components was presented in the test solution.

Chapter 6

Corrosion and scale results in the presence of single components of combined inhibitor

6.1 Introduction

In this chapter, corrosion and scale occurring simultaneously were studied using a new bubble cell/jar test in the presence of the single inhibitor components which would ultimately be used to make combined inhibitors. The objective was to better understand the interaction between corrosion and scale processes in the presence of the single components of combined inhibitor. In order to measure and assess the general corrosion and pitting LPR, Tafel plots and light interferometry were used. The scale was observed using SEM and calcium carbonate polymorphs were assessed by XRD.

6.2 Concentration of the single components

The combined inhibitor used for this study is composed of: 1 scale inhibitor, 3 corrosion inhibitors and 1 souring agent formulated in a solvent. This is a formulation of combined inhibitor (v/v%):

- 10v/v% corrosion inhibitor 1
- 10v/v% corrosion inhibitor 2
- 10v/v% corrosion inhibitor 3
- 20v/v% scale inhibitor base
- 5v/v% souring agent
- the rest – solvent.

25ppm concentration of blended combined inhibitor was used in the tests with combined inhibitor. Hence, the concentrations of single components used in the test were:

- 2-mercaptoethanol (souring agent) – 1.25 ppm concentration was added to the test solution,
- alcohol ethoxy phosphate ester (corrosion inhibitor 1) – 2.5 ppm concentration was added to the test solution,
- C12-C14 alkyldimethyl-benzylammonium chloride (corrosion inhibitor 2) – 2.5 ppm concentration was added to the test solution
- ethoxylated imidazolines (corrosion inhibitor 3) – 2.5 ppm concentration was added to the test solution

- polyphosphinocarboxylic acid ((PPCA) – scale inhibitor) – 5 ppm concentration was added to the test solution

6.3 Corrosion results

6.3.1 General corrosion

From Figure 6.1, it is clear that the values of i_{corr} at the end of the tests with 2-mercapthoethanol and without inhibitor were quite similar ($i_{\text{corr}} = 0.0041$, $i_{\text{corr}} = 0.0032 \text{ mA/cm}^2$). However, it could be observed that in the tests with 2-mercapthoethanol the cathodic and the anodic reactions were affected (Table 6.1). The corrosion rate was controlled by the cathodic reaction because $\beta_c = 107 \text{ mV/decade}$ is greater than $\beta_a = 52 \text{ mV/decade}$. Which indicates that the cathodic reaction occurred slower than the anodic reaction in the tests with 2-mercapthoethanol. In the tests with alcohol ethoxy phosphate ester it could be observed that corrosion current ($i_{\text{corr}} = 0.083 \text{ mA/cm}^2$) is bigger than in the tests without inhibitors and both reactions have been affected (Table 6.1). $\beta_c = 126 \text{ mV/decade}$ being larger than $\beta_a = 73 \text{ mV/decade}$ indicates that the corrosion rate is controlled by the cathodic reaction.

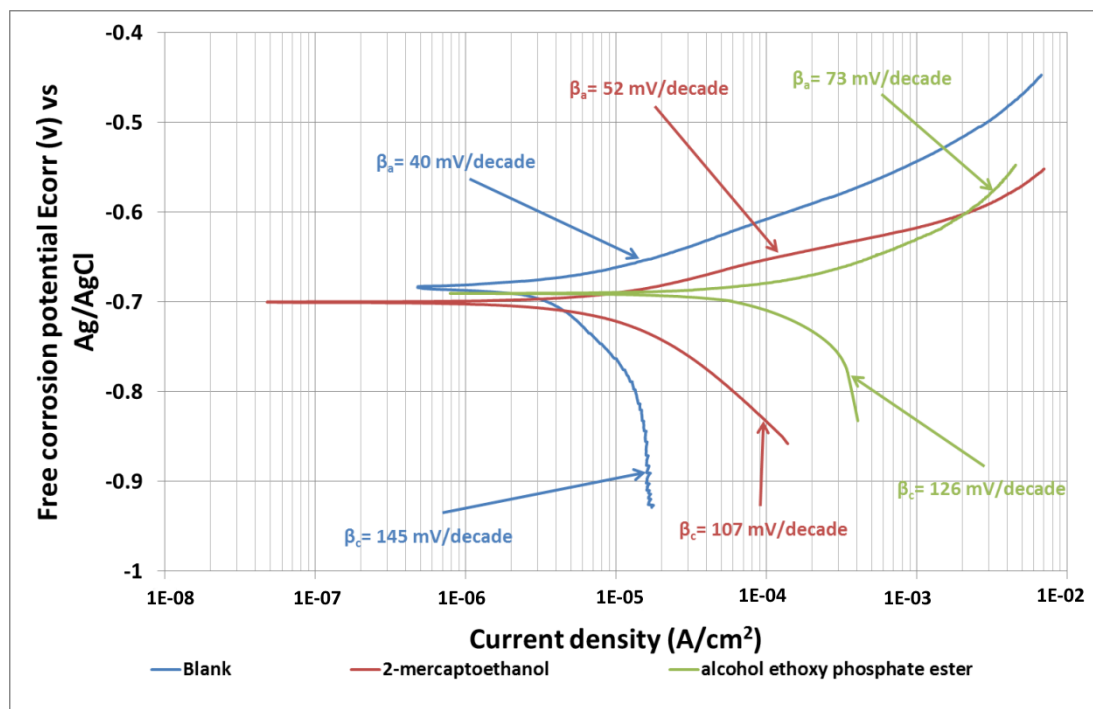


Figure 6.1: Tafel plots after 4 hours in tests with 2-mercaptoethanol and alcohol ethoxy phosphate ester (anodic and cathodic curves were constructed using separate samples)

In Figure 6.1 it is observed that the cathodic reaction in the test with alcohol ethoxy phosphate ester at the beginning of polarisation is a mixture of

activation control and mass transfer control. However, with continuous polarisation to a more negative potential, the cathodic reaction becoming more controlled by the mass transfer reactions which means that the cathodic reaction (Equation (2-29)) start reducing faster the reagent (H^+) at the surface corrosion site and its concentration become smaller than in the bulk solution. This is happening because of slow diffusion of hydrogen ions (H^+) reagent from bulk solution to the vicinity of the sample.

Table 6.1: Corrosion potential, corrosion current and Tafel slopes

Test	E_{corr} (mV)	i_{corr} (mA/cm ²)	β_a	β_c
			(mV/decade)	
Blank	-684	0.0032	40	145
2-mercapthoethanol	-700	0.0041	52	107
alcohol ethoxy phosphate ester	-690	0.083	73	126
C12-C14alkyl dimethyl benzyl ammonium chloride	-700	0.0015	80	92
ethoxylated imidazolines	-698	0.0015	67	105
Polyphosphinocarboxylic acid	-680	0.039	73	82

The biggest effect on Stern – Geary coefficient (β) (Equation (6-1)) has biggest from Tafels slope β_a and β_c which means that reaction (anodic or cathodic) control the corrosion processes (slowest reaction controls how fast corrosion process occurs).

$$\beta = \frac{1}{2.303} \left(\frac{\beta_a \beta_c}{\beta_a + \beta_c} \right) \quad (6-1)$$

Which means that the smallest parameter of β_a and β_c has largest effect on corrosion rate calculated from Linear Polarisation Resistance measurements. The smaller the value of the β_a and β_c then the corrosion rate is smaller. When the β_a and β_c is increasing and as does the corrosion rate.

In Figure 6.2 it is observed that in the tests with C12-C14 alkyl dimethyl benzyl ammonium chloride $i_{corr} = 0.0015 \text{ mA/cm}^2$ is smaller than in the test without (Table 6.1). $\beta_c = 92 \text{ mV/decade}$ controlled the corrosion rate ($\beta_a = 80 \text{ mV/decade}$). The cathodic reaction in the tests with C12-C14alkyl dimethyl

benzyl ammonium chloride is a mixture of activation - control and mass transfer control. However, with continuous polarisation to a more negative potential, the cathodic reaction becoming more controlled by the mass transfer reactions. In the test with the ethoxylated imidazolines i_{corr} is equal 0.0015 mA/cm^2 and β_c is much larger than β_a (105 to 67 mV/decade) which indicates that corrosion rate is controlled by the cathodic reaction. In the tests with ethoxylated imidazolines the anodic reaction is activation controlled while the cathodic reaction have the same trend as cathodic reaction in the tests with C12-C14alkyl dimethyl benzyl ammonium chloride. i_{corr} in the tests with the PPCA is equal 0.039 mA/cm^2 ; cathodic and anodic Tafel constants are almost equal ($\beta_c = 73$ and $\beta_a = 82 \text{ mV/decade}$). In Figure 6.2 it is observed that the anodic reaction were activation control reactions while cathodic is a mixture of activation control and mass transfer control.

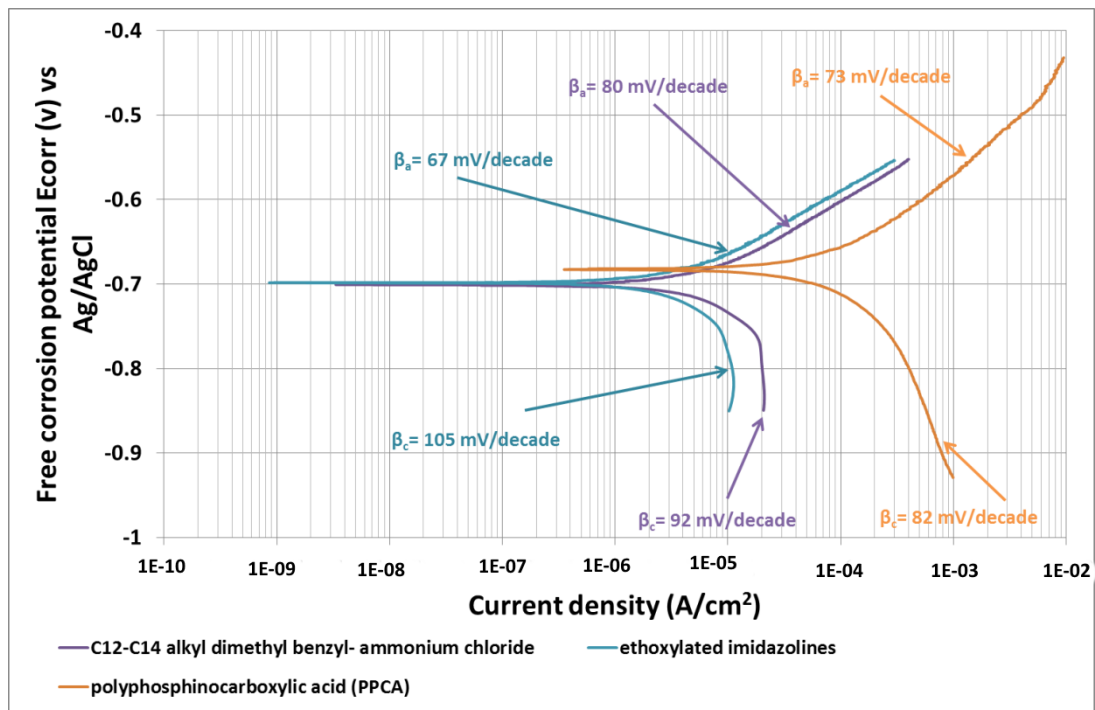


Figure 6.2: Tafel plots after 4 hours in tests with C12-C14alkyl dimethyl benzyl ammonium chloride, ethoxylated imidazolines and PPCA (anodic and cathodic curves were constructed using separate samples)

Figure 6.3 shows the average corrosion rate in the tests in the presence of single components of a combined inhibitor. The repeatability is represented using error bars. In the tests with 2-mercaptoethanol corrosion rate at the beginning of test was $\approx 0.72 \text{ mm/year}$. Then, it started decreasing continuously to reach 0.1 mm/year at 110 minutes of the tests and remain steady to the end of the tests ($\approx 0.1 \text{ mm/year}$). The corrosion rate in the tests with alcohol ethoxy phosphate ester at the start of the tests was ≈ 1.77

mm/year. After 25 minutes it increased to ≈ 2.25 mm/year and remained steady for the rest of the tests. At the end of the test with alcohol ethoxy phosphate ester the corrosion rate was ≈ 2.23 mm/year. In the tests with C12-C14 alkyl dimethyl benzyl-amonium chloride and ethoxylated imidazolines, the corrosion rate at the start of the tests was respectively ≈ 4.5 and ≈ 3.8 mm/year. Then after 8 minutes of the tests with C12-C14 alkyl dimethyl benzyl-amonium chloride the highest corrosion rate of ≈ 5 mm/year was reached while in the tests with ethoxylated imidazolines the highest corrosion rate ≈ 5.2 mm/year was reached at 4 minutes. In both tests corrosion started decreasing continuously to reach the plateau at 100 minutes with the corrosion rate ≈ 0.12 mm/year. At the end of the tests with C12-C14 alkyl dimethyl benzyl-amonium chloride and ethoxylated imidazolines the corrosion rates were accordingly 0.06 and 0.09 mm/year. The corrosion rate in the tests with PPCA at the start of the tests was ≈ 1.51 mm/year. After 33 minutes of tests it decreased to ≈ 1 mm/year and remained steady for the rest of the tests. At the end of the test with PPCA, the corrosion rate was ≈ 0.9 mm/year.

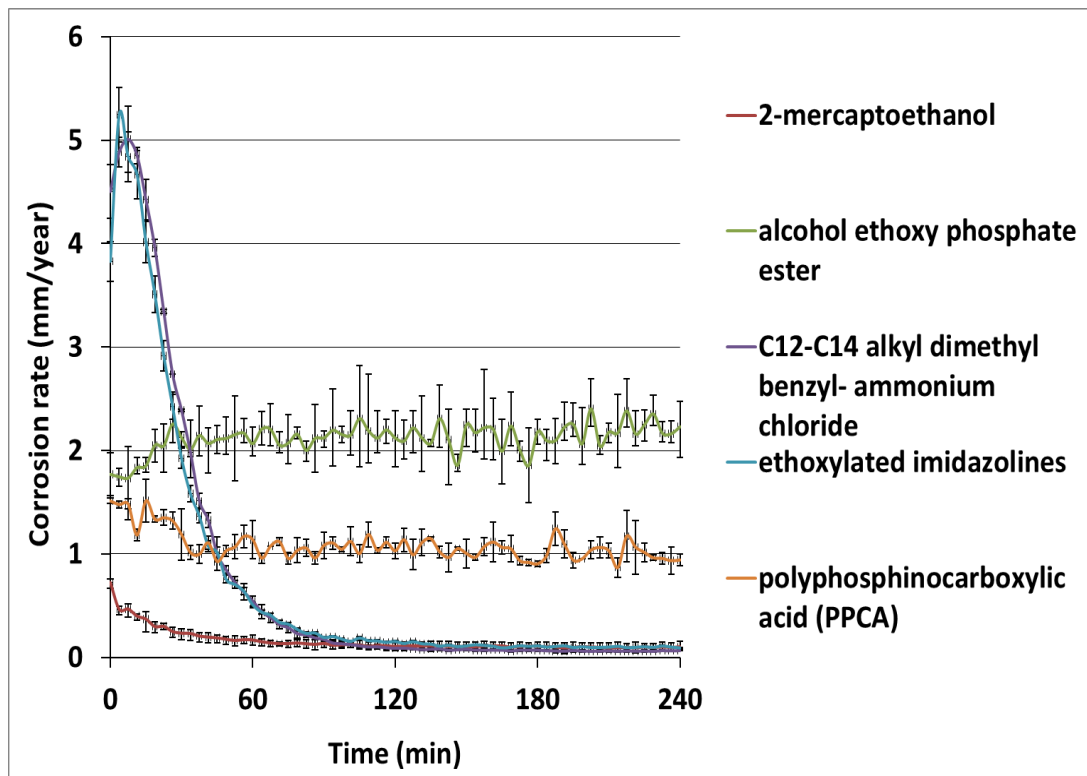


Figure 6.3: General corrosion results in the presence of single components of combined inhibitor

6.3.2 Localized corrosion

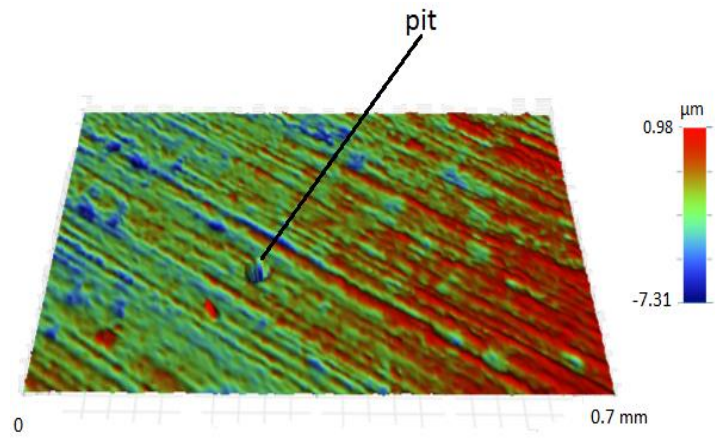
In Table 6.2 the deepest pits from light interferometry analysis in the tests in the presence of single components of combined inhibitor after 72hrs are

presented. The deepest pit was measured in the tests with single components of combined inhibitor, in the tests with C12-C14 alkyl dimethyl benzyl-amonium chloride was 32.1 μm (Figure 6.4c). Second deepest pit was measured in the tests with ethoxylated imidazolines 29.6 μm (Figure 6.4 d). In the tests alcohol ethoxy phosphate ester deepest pit detected on sample had 19.6 μm depth (Figure 6.4b). Deepest pits in the tests with PPCA and 2-mercaptoethanol were 11.6 and 7.3 μm accordingly (Figure 6.4a and d).

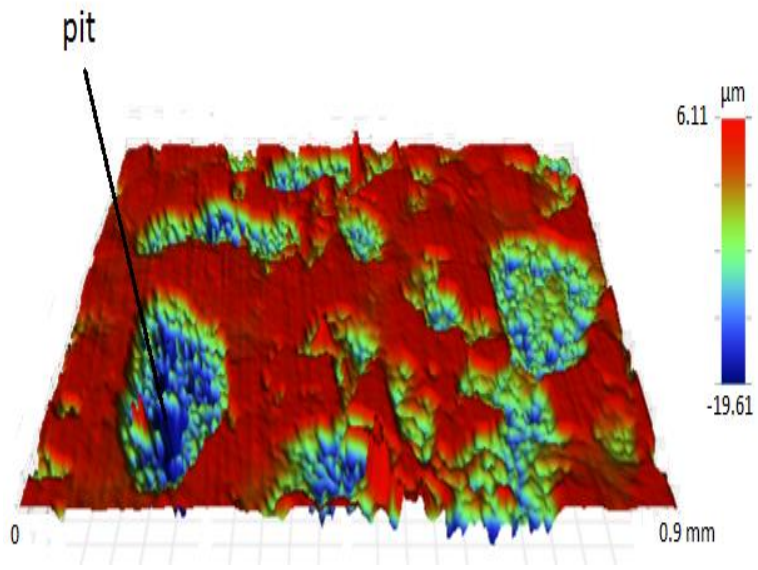
Table 6.2: Deepest pits in the tests in the presence of single components of combined inhibitor after 72hrs

Tests	Pit depth (μm)
2-mercapthoethanol	7.3 \pm 0.4
Alcohol ethoxy phosphate ester	19.6 \pm 1
C12-C14 Alkyldimethyl-benzylamonium chloride	32.1 \pm 2
Ethoxylated imidazolines	29.6 \pm 2
PPCA	11.6 \pm 0.6

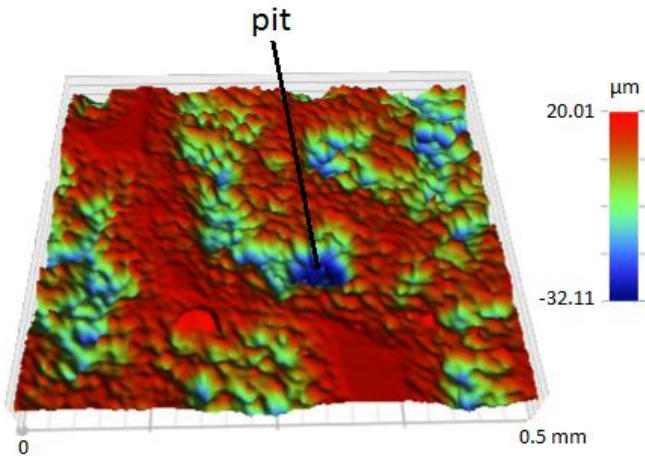
In Figure 6.4 different shapes of deepest pits can be observed in the tests in the presence of single components of combined inhibitor. In the tests with alcohol ethoxy phosphate ester, C12-C14 alkyldimethyl-benzylamonium chloride and ethoxylated imidazolines (Figure 6.4b, c and d) it is clear that some damage has been done by general corrosion to the samples. However, in some of this cavities pitting corrosion occurred and some pits penetrated the sample further. In the Figure 6.4a in the tests with 2-mercapthoethanol all the surface is quite well preserved and pit growth in random places on the sample can be observed. In the tests with PPCA (Figure 6.4d), it could be observed that most of sample area was destroyed by general corrosion and in some of these cavities pitting corrosion occurred (pit penetrated sample).



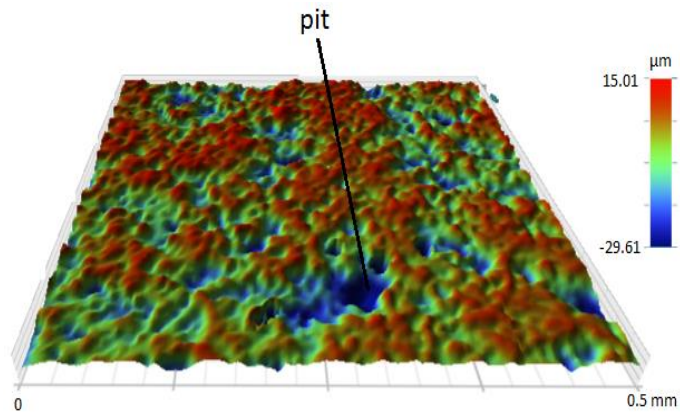
(a)



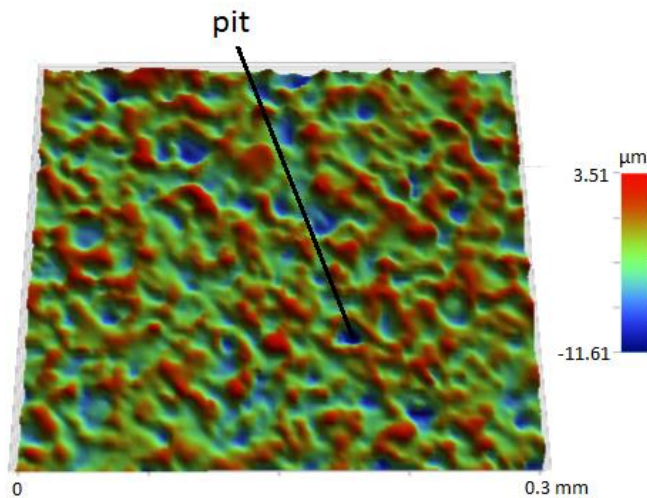
(b)



(c)



(d)



(e)

Figure 6.4: Light interferometry images of deepest pits on surface in the tests in the presence of single components of combined inhibitor: a) 2-mercaptoethanol, b) Alcohol ethoxy phosphate ester; c) C12-C14 Alkyldimethyl-benzylamonium chloride; d) Ethoxylated imidazolines and e) PPCA

In Table 6.3 pit density values from light interferometry analysis in the tests in the presence of single components of combined inhibitor after 72hrs are presented. The largest densities of deepest pits were measured in the tests with 2-mercaptoethanol and C12-C14 alkyldimethyl-benzylamonium chloride and were equal to 1 pit per cm^2 were observed. While in the tests with alcohol ethoxy phosphate ester, ethoxylated imidazolines and PPCA pit densities of deepest pits were equal to 0.6 pit per cm^2 . This is 40% less than in two previous tests. Overall the smallest pit density was observed in the test with 2-mercaptoethanol (2 pits per cm^2), while the biggest density was observed in the test with C12-C14 alkyldimethyl-benzylamonium chloride (85 pits per cm^2). Pit density in the tests with the alcohol ethoxy phosphate ester and ethoxylated imidazolines were very similar at 24 and 21 pits per cm^2

respectively. In the tests with the PPCA the pit density values were around 8 pits per cm².

Table 6.3: Pit densities in the tests in the presence of single components of combined inhibitor after 72 hrs

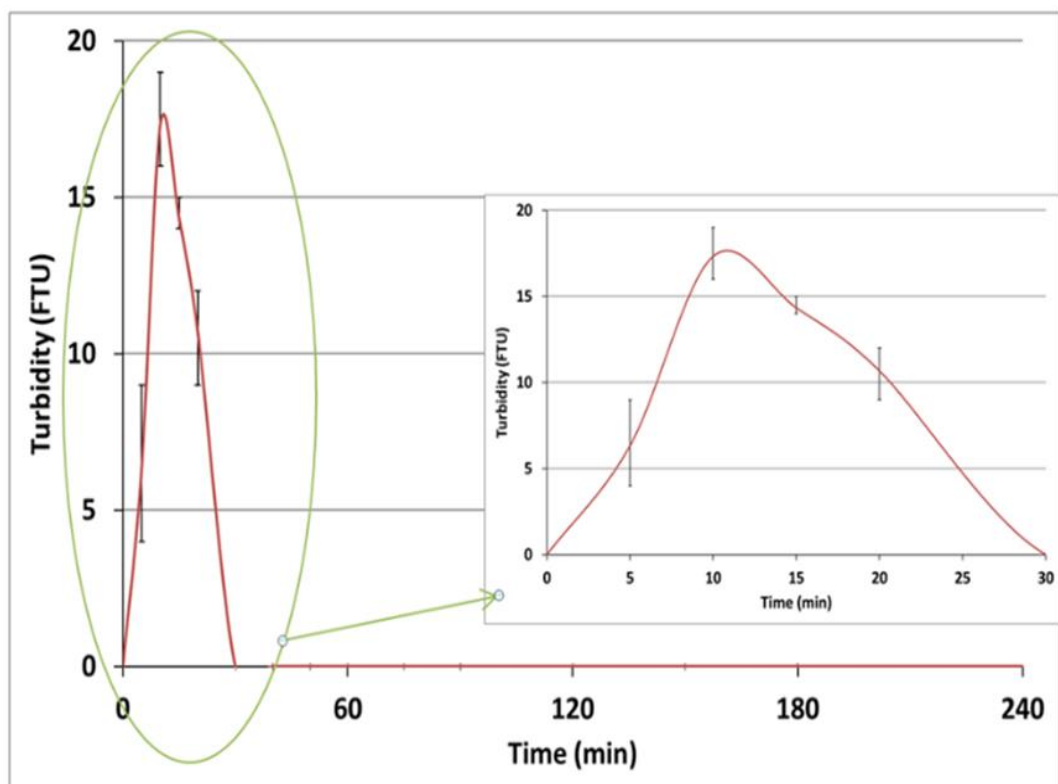
Pit depth (µm) in tests with 2-mercapthoethanol	Number of pits (per cm²)
pit depth (µm) > 5	1
4 < pit depth (µm) > 5	1
Pit depth (µm) in tests with alcohol ethoxy phosphate ester	Number of pits (per cm²)
pit depth (µm) > 15	0.6
10 < pit depth (µm) > 15	4
7.5 < pit depth (µm) > 10	20
Pit depth (µm) in tests with C12-C14 alkyldimethylbenzylamonium chloride	Number of pits (per cm²)
pit depth (µm) > 30	1
25 < pit depth (µm) > 30	32
20 < pit depth (µm) > 25	52
Pit depth (µm) in tests with ethoxylated imidazolines	Number of pits (per cm²)
pit depth (µm) > 25	0.6
22.5 < pit depth (µm) > 25	4
20 < pit depth (µm) > 22.5	17
Pit depth (µm) in tests with PPCA	Number of pits (per cm²)
pit depth (µm) > 10	0.6
8 < pit depth (µm) > 10	2
6.5 < pit depth (µm) > 8	6

6.4 Bulk and Surface scaling results

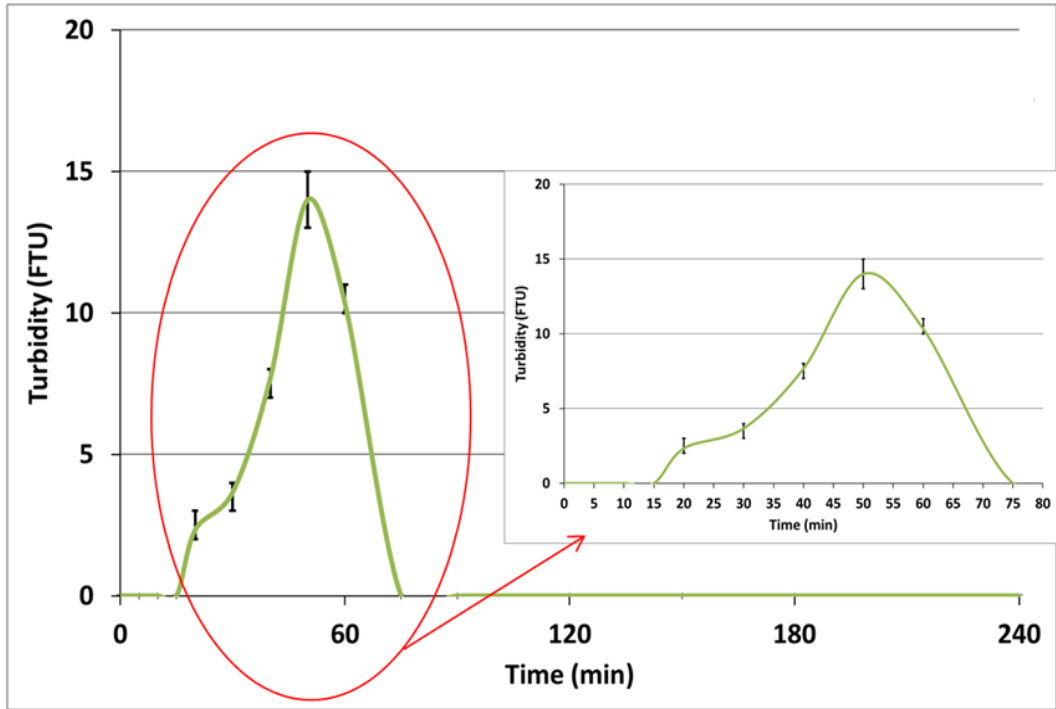
6.4.1 Bulk solution scaling

6.4.1.1 Turbidity results

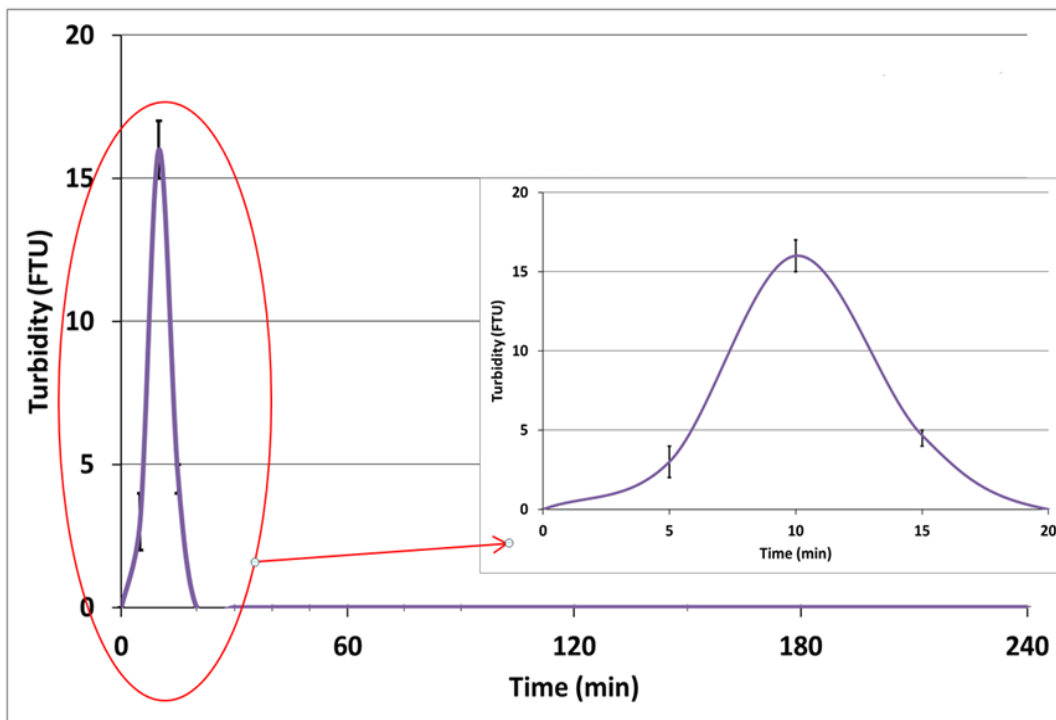
The turbidity trend in the tests in the presence of single components of combined inhibitor are shown in Figure 6.5. It could be observed that in the tests with 1.25 ppm of 2-mercaptoethanol, 2.5 ppm of C12-C14 alkyldimethyl-benzylammonium chloride and 2.5 ppm of ethoxylated imidazolines, the first crystals were detected after 5 minutes of tests and the highest amount of scale in the bulk solution was measured at 10 minutes (17, 16 and 13 FTU accordingly). The solution is highly supersaturated with respect to calcium carbonate (Table 4.2) because of that the induction time is very short before first crystals in bulk solution can be detected. None of the inhibitors have any effect on bulk scaling and their trends are similar to the tests without inhibitor (Figure 5.6). After 20 minutes of tests with 2-mercaptoethanol and C12-C14 alkyldimethyl-benzylammonium chloride no bulk scale crystals have been detected, while in the tests with ethoxylated imidazolines took 30 minutes of tests to reached 0 FTU. Crystals could not get bigger because of a drop of supersaturation ratio of the tested solution as time progressed.



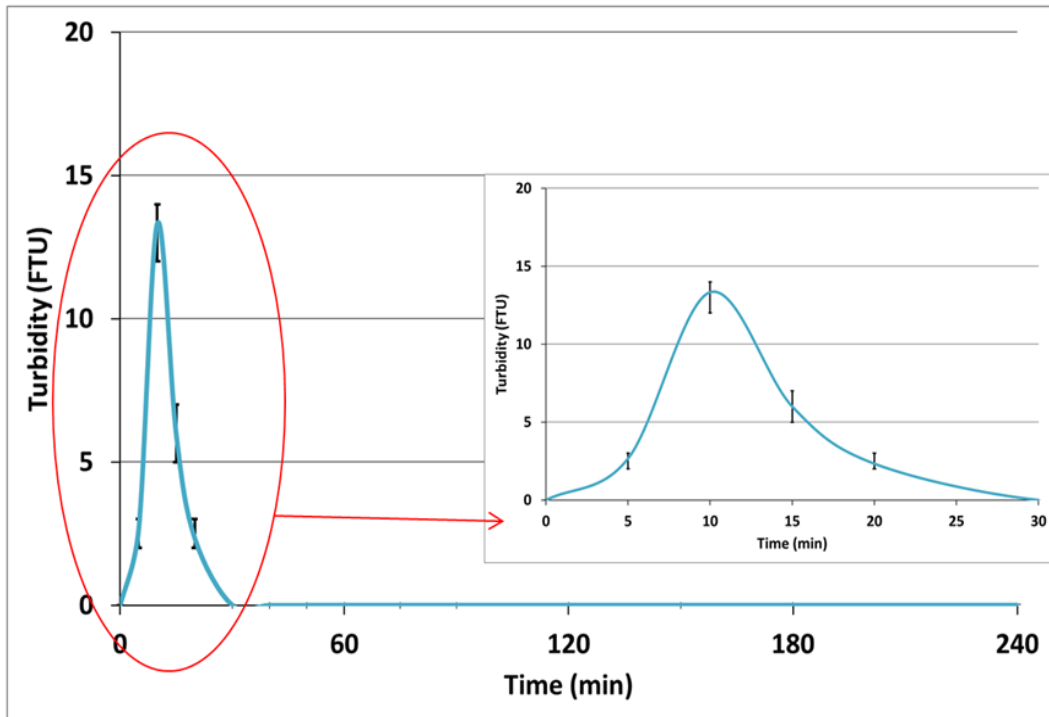
(a)



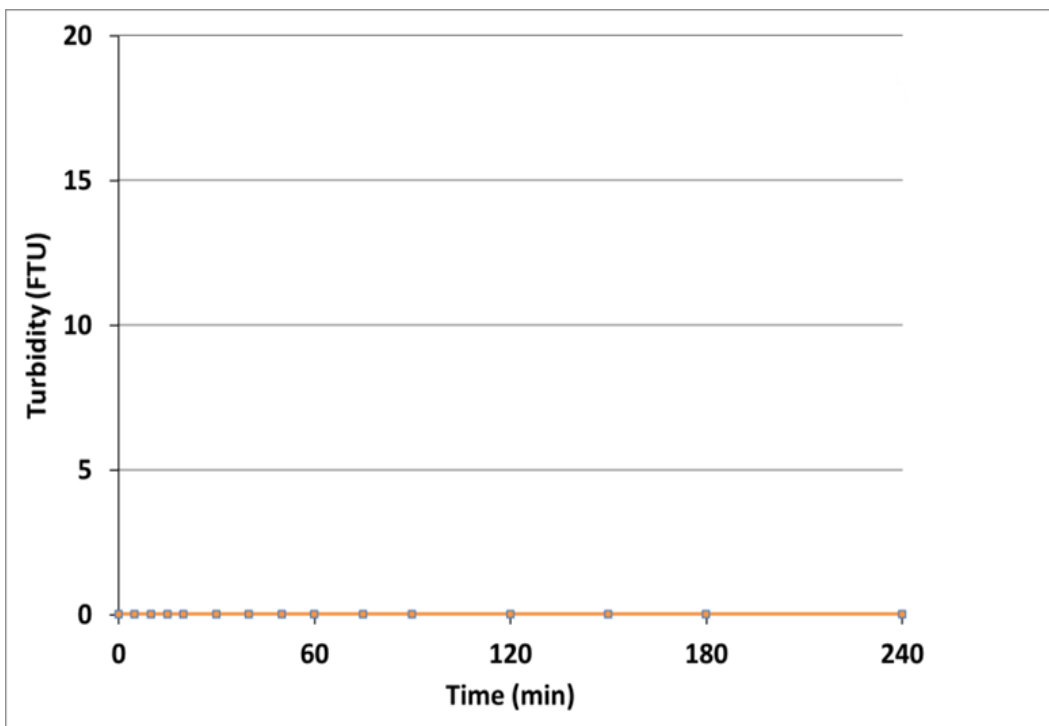
(b)



(c)



(d)



(e)

Figure 6.5: Turbidity results in the tests over 4 hours in the presence of single components of combined inhibitor: a) 2-mercapthoethanol, b) alcohol ethoxy phosphate ester; c) C12-C14 alkyldimethylbenzylamonium chloride; d) ethoxylated imidazoline and e) PPCA

In Figure 6.5b it is shown that 2.5 ppm of alcohol ethoxy phosphate ester extended the induction time to 20 minutes and the maximum scale was

recorded at 50 minutes. After 75 minutes of the test with alcohol ethoxy phosphate ester no bulk scale crystals were detected. During the tests with 5 ppm of PPCA no bulk scaling was measured for the whole duration of the tests (Figure 6.5e). Only PPCA prevented any bulk scaling during whole test duration. The induction time of single components of combined inhibitor is presented in Table 6.4.

Table 6.4: Induction time in the tests with single components of combined inhibitor

Test	Induction time (minutes)
2-mercapthoethanol	5±0.5
alcohol ethoxy phosphate ester	20±1
C12-C14 alkyldimethyl-benzylamonium chloride	5±0.5
ethoxylated imidazolines	5±0.5
PPCA	>240

6.4.2 Inductively coupled plasma mass spectrometry (ICP – MS) results from bulk solution and surface

In Figure 6.6 surface scaling versus bulk scaling in the tests with single components results from ICP-MS analysis of the bulk solution and by dissolving the scale from the metal surface in the presence of single components of combined inhibitor are presented. There is a general trend that as bulk scaling increases that surface deposition increases also. It could be observed that PPCA retained the biggest amount of Ca²⁺ ions in the testing solution at the end of the tests (904 ppm) from all single components compared to initial concentration in the test solution (917 ppm). PPCA works as nucleation and crystals growth inhibitor as well adsorb to the metal surface to prevent surface scale deposition. In the test with ethoxylated imidazolines and C12-C14 alkyldimethyl-benzylamonium chloride (corrosion inhibitors) surface scale and bulk scaling increases; this could suggests that any of this inhibitor works as nucleation or crystal growth inhibitor. However, alcohol ethoxy phosphate ester (corrosion inhibitor) has some effect on surface, bulk scaling and induction time, this could suggests that it effects the crystal growth but not nucleation process as well as it adsorbs to the metal surface to prevent surface scale deposition. 2-mercaptoethanol has small effect on bulk scaling compare to the effect which has on surface scale

deposition. It suggests that it absorbs to the metal surface and form dense film which prevents surface scale deposition.

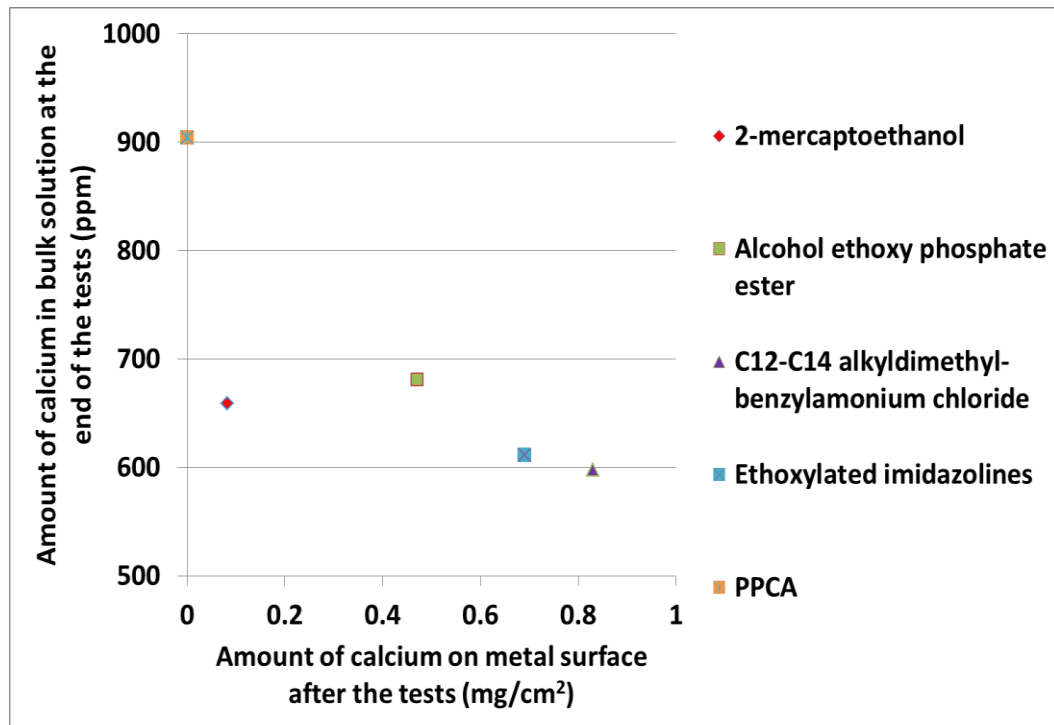


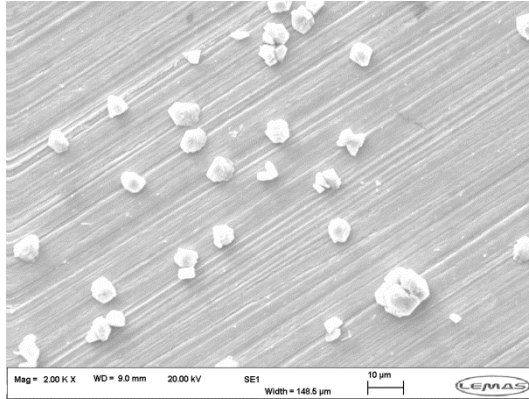
Figure 6.6: Surface scaling versus bulk scaling in the tests with single components

6.4.3 Surface scale

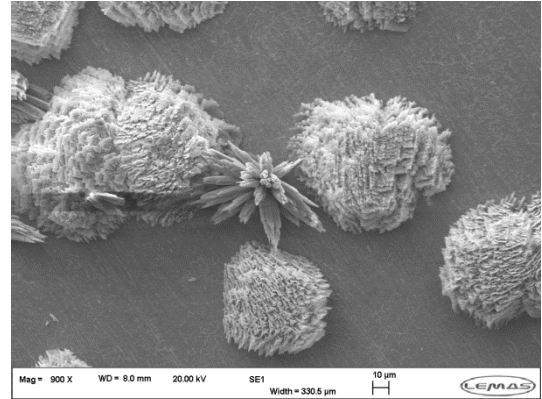
6.4.3.1 Scanning Electron Microscopy (SEM) and X-ray diffraction (XRD)

Figure 6.7 shows the effect of calcium carbonate scale formed during the tests in the presence of single components of combined inhibitor on the metal surface (not filtered from the bulk solution). In the tests with 2-mercaptoethanol most crystals of calcium carbonate were smaller than 5 μ m (Figure 6.7a). Crystals of CaCO₃ had irregular cubic shape and were spread all over the sample surface. Crystals of calcium carbonate in the tests with alcohol ethoxy phosphate ester had more than 60 μ m diameter (Figure 6.7b). The shape is an irregular half sphere. It could be observed that there are a lot of small steps which are crystals growth sites. There were needle like crystals on the sample too. Crystals have spread quite evenly all over the sample but some agglomeration of crystals have been present too. Figure 6.7c presents the CaCO₃ crystals on metal surface in the presents C12-C14 alkyldimethyl-benzylamonium chloride. In that tests calcium carbonate cover all most whole surface of the sampler. Average crystal size was around 20 μ m with very irregular rhombus shapes. Similar situations

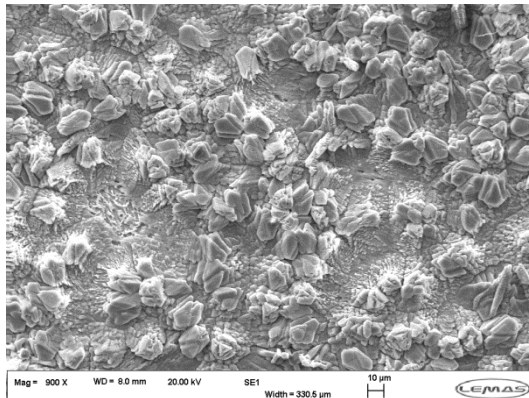
could be observed in the tests with ethoxylated imidazolines in Figure 6.7d. The difference was that crystals have been slightly bigger around $30\mu\text{m}$ and cubic irregular shapes with more sharp edges. In the tests with PPCA no scale was observed on the metal sample (Figure 6.7e)



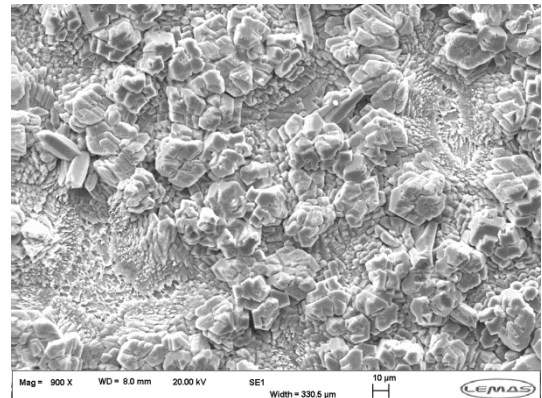
(a)



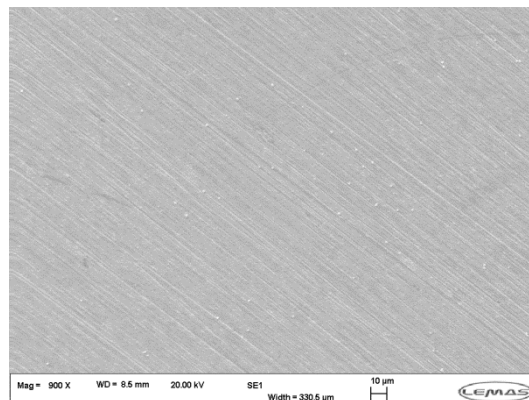
(b)



(c)



(d)

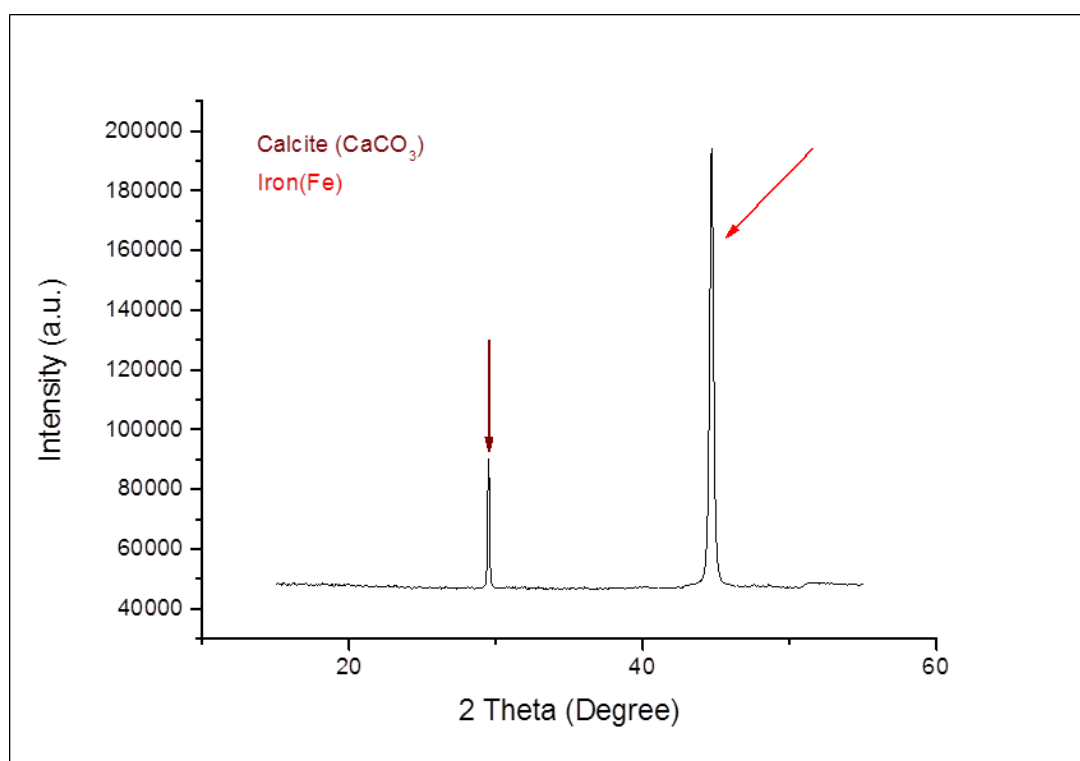


(e)

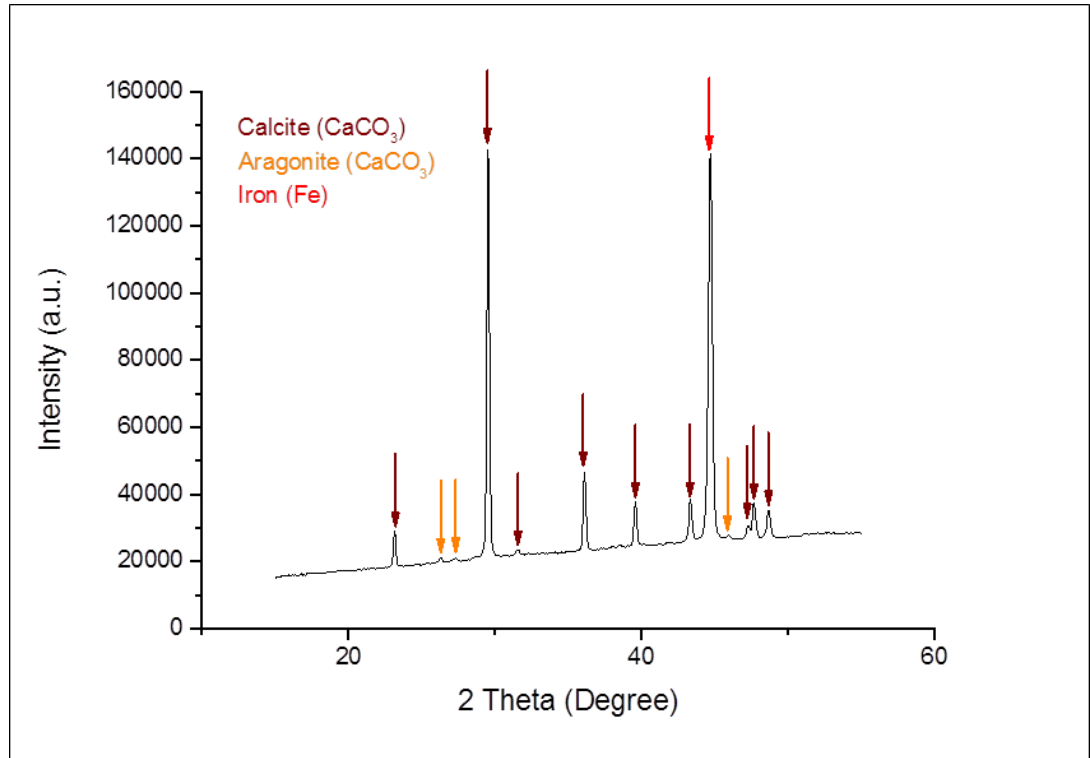
Figure 6.7: Scanning electron micrographs of CaCO_3 formed at the surface in the tests in the presence of single components of combined inhibitor: a) 2-mercaptoethanol, b) alcohol ethoxy phosphate ester; c) C12-C14 alkyldimethyl-benzylammonium chloride and d) ethoxylated imidazolines and e) PPCA

In Figure 6.8 XRD spectra of the scales formed in the tests in the presence of single components of combined inhibitor are presented. In Figure 6.8a the XRD spectra of tests with 2-mercaptoethanol are presented and only calcite peaks can be observed. In the tests with alcohol ethoxy phosphate ester, C12-C14 alkyldimethyl-benzylammonium chloride and ethoxylated imidazolines (Figure 6.8b, c and d) peaks for calcite and aragonite are detected, while in the tests with PPCA no calcium carbonate peaks can be observed (Figure 6.8e).

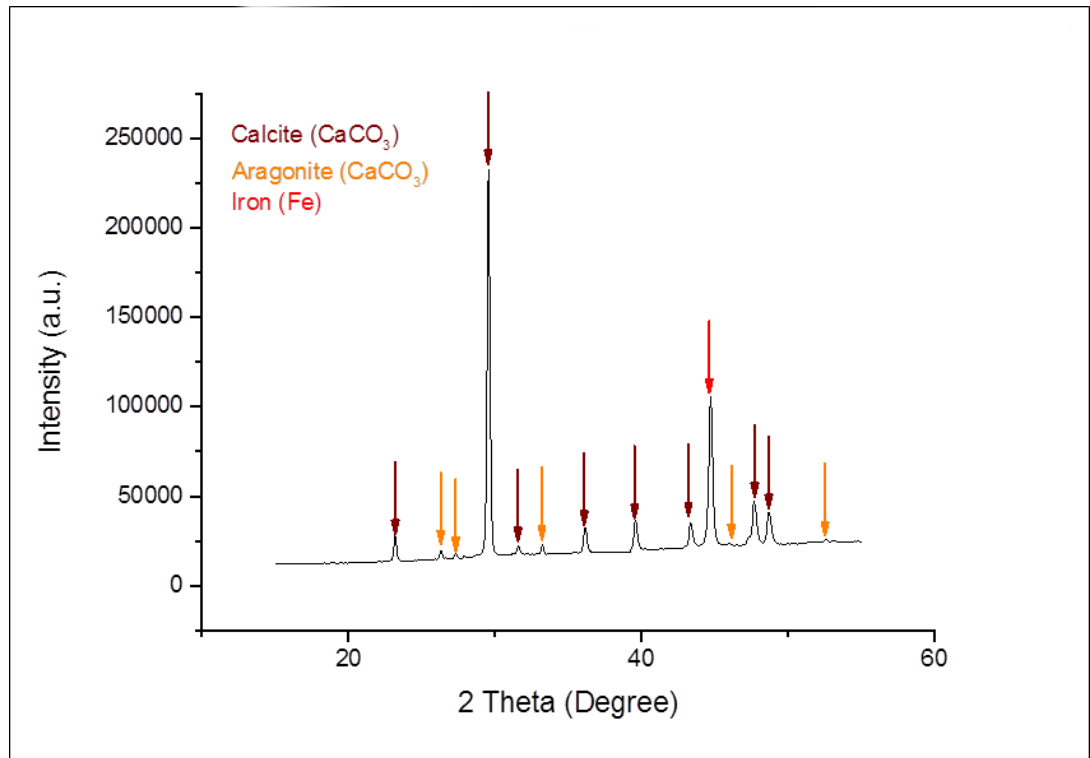
Table 6.5 shows results from Rietveld analysis in the tests in the presence of single components of combined inhibitor. The calcite is the only polymorph formed in the tests with 2-mercaptoethanol. In the tests with alcohol ethoxy phosphate ester and ethoxylated imidazolines two polymorphs of calcium carbonate have precipitated on the metal surface: calcite and aragonite. Accordingly 99.8% of calcite and 0.2% of aragonite in the tests with alcohol ethoxy phosphate ester, while in the test with ethoxylated imidazolines 99% of calcite and 1% of aragonite. In the tests with C12-C14 alkyldimethyl-benzylammonium chloride scale formed on metal surface contained 93% of calcite and 7% of aragonite (Table 6.5).



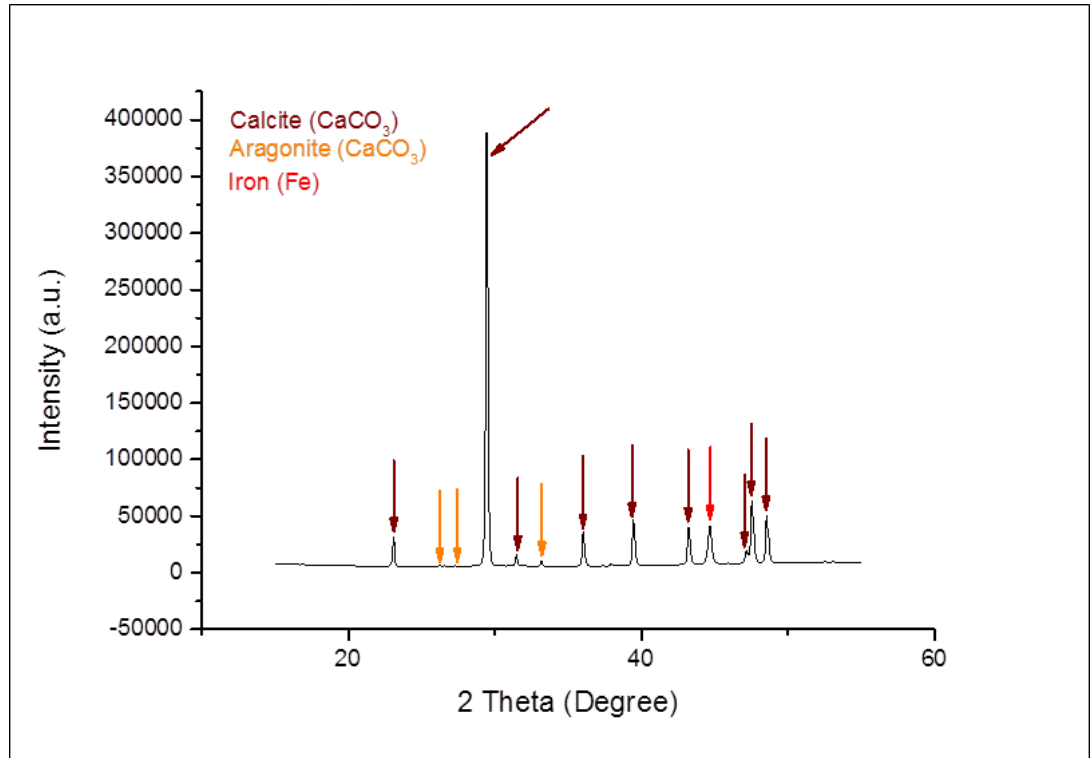
(a)



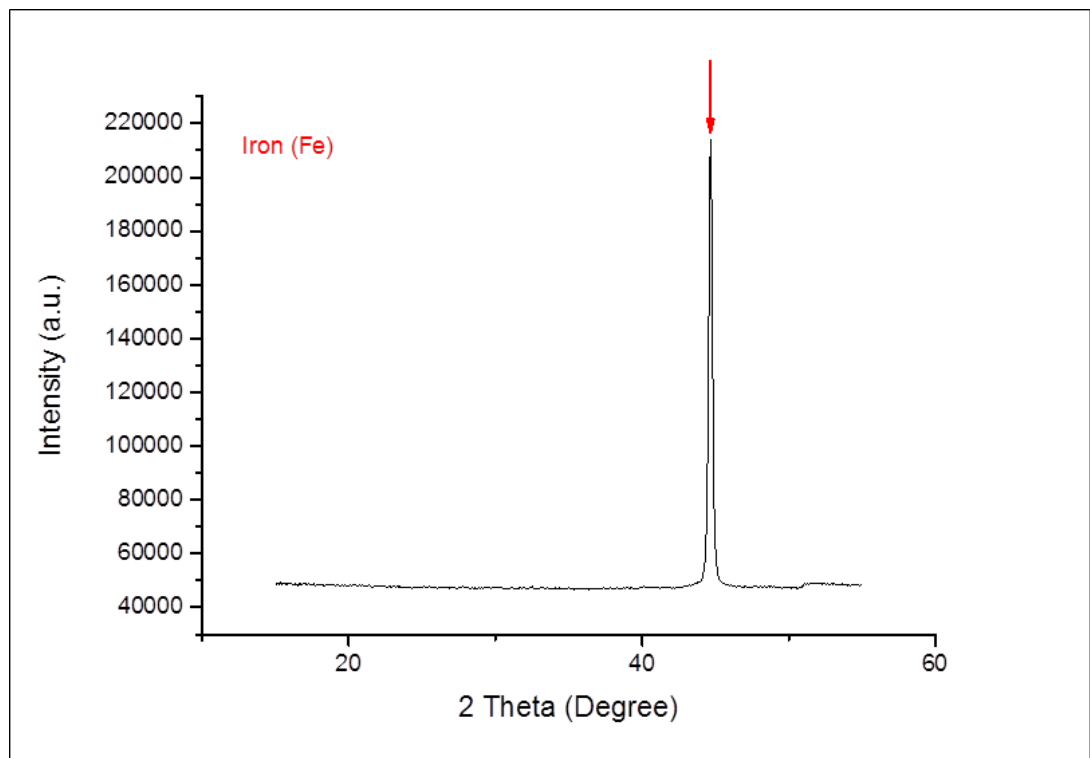
(b)



(c)



(d)



(e)

Figure 6.8: XRD spectrum of scale formed in the tests in the presence of single components of combined inhibitor: a) 2-mercaptoethanol, b) alcohol ethoxy phosphate ester; c) C12-C14 alkyldimethyl-benzylammonium chloride; d) ethoxylated imidazolines and e) PPCA

Table 6.5: Different polymorphs of CaCO₃ formed in the tests in the presence of single components of combined inhibitor by Rietveld Analysis

Test	% Calcite	% Aragonite
2-mercaptoethanol	100	-
alcohol ethoxy phosphate ester	99.8	0.2
C12-C14 alkyldimethylbenzylamonium chloride	93	7
ethoxylated imidazolines	99	1

6.5 Systematic ranking of the single components of the combined inhibitor

The single components of combined inhibitors were systematically ranked according to their effect on the 4 key parameters: general corrosion, pitting corrosion, bulk scaling (induction time and amount of calcium sustained in the bulk solution) and surface scaling. In Table 6.6 the effect on general corrosion and pitting corrosion are ranked according to the values of corrosion rate and pit depth.

Table 6.6: Effect of the single components of combined inhibitor effect on general corrosion and pitting corrosion

General corrosion – (CR) mm/year	Effect	Pitting corrosion – (pit depth) μm	Effect
CR ≤ 0.1	1	pit depth < -10	1
0.1 < CR < 0.5	2	-10 < pit depth < -15	2
0.5 < CR < 2	3	-15 < pit depth < -25	3
CR > 2	4	pit depth > -25	4

In Table 6.7 how the inhibitor has an effect on induction time and the amount

amount of calcium sustained in the bulk solution and surface scaling are ranked.

Table 6.7: Effect of the single components of combined inhibitor effect on induction time, amount of calcium sustained in the bulk solution and surface scaling

Induction time – (IT) min	Effect	Amount of calcium sustained in the bulk solution on the end of the tests – (AC) ppm	Effect
IT > 240	1	AC > 900	1
240 > IT > 120	2	900 > AC > 750	2
120 > IT > 15	3	750 > AC > 600	3
IT < 15	4	AC < 600	4
Amount of calcium on metal surface after the tests – surface scale (SS) mg/cm²		Effect	
SS < 0.1		1	
0.1 < SS < 0.25		2	
0.25 < SS < 0.5		3	
SS > 0.5		4	

The aim of systematically ranking the single components is primarily to establish a pragmatic assessment of the inhibitor effects. Each parameter is assigned a number and it is considered with the same importance. So each parameter coefficient was equal 1, all numbers multiplied with each other to give a total number. The single component with the smaller total number is considered as the more efficient component. Each parameter coefficient could be changed to represent the difference in importance (2, 3, etc.) according to the application of the single components. So, for a system requiring better inhibition against general corrosion, a higher coefficient could be applied. This is not done in the thesis and a simple assessment is made onto 4 aspects of scaling and corrosion.

In Table 6.8 the systematic ranking of the single components of the combined inhibitor is presented.

Table 6.8: Ranking of the single components of combined inhibitor

Name of the single components	CR	Pit depth	IT	AC	SS	Total number effect
	corrosion		scaling			
2-mercaptoethanol	1	1	4	3	1	12
alcohol ethoxy phosphate ester	4	3	3	3	3	324
C12-C14 alkyldimethyl-benzylamonium chloride	1	4	4	4	4	256
ethoxylated imidazolines	1	4	4	3	4	192
PPCA	3	2	1	1	1	6

The Polyphosphinocarboxylic acid (PPCA) has the best inhibition effect (6) on the whole system where corrosion (general and pitting) and scaling (induction time, amount of calcium sustained in the bulk solution and surface scaling) are assessed. While the 2-mercaptoethanol effect (12) was slightly higher than PPCA. PPCA is less effective against corrosion than 2-mercaptoethanol while PPCA is outperforming 2-mercaptoethanol in of scale prevention. The least inhibition effect on the whole system of the singles components is alcohol ethoxy phosphate ester (324).

6.6 Summary

Corrosion and scale results in the presence of single components of combined inhibitor when all processes were occurring simultaneously were presented. The following conclusions could be reached:

- The smallest corrosion rate was measured in the tests with C12-C14 alkyldimethyl-benzylamonium (0.06 mm/year) chloride and ethoxylated imidazolines (0.09 mm/year)
- The highest corrosion rate was measured in the test with alcohol ethoxy phosphate ester – 2.23 mm/year

- The smallest pit was measured in the test with 2-mercaptoethanol – 7.3 μm while the deepest in the tests with C12-C14 alkyldimethyl-benzylamonium 32.1 μm
- The shortest induction time was measured in the tests with 2-mercaptoethanol, C12-C14 alkyldimethyl-benzylamonium chloride and ethoxylated imidazolines – 5 minutes
- Polyphosphinocarboxylic acid prevent any bulk precipitation for whole duration of tests (>240 minutes)
- No surface scaling was measured in the tests with polyphosphinocarboxylic acid while the biggest amount of calcium was detected in the tests with C12-C14 alkyldimethyl-benzylamonium chloride
- 100% calcite precipitated on surface in the tests with 2-mercaptoethanol
- The single components of combined inhibitor was ranked systematically
- Polyphosphinocarboxylic acid (PPCA) has the best inhibition effect on the whole system from all single components
- The smallest inhibition effect on the whole system was seen for alcohol ethoxy phosphate ester

Chapter 7

Corrosion and scale results in the presence of combined inhibitor

7.1 Introduction

In the previous chapter an evaluation of the single components of the inhibitor was made. In this chapter the formation of an optimum inhibitor is assessed. In this chapter, a Design of Experiments (DOE) methodology was used: 2^5 full factorial design method. DOE gives a well-defined framework for data collection, analysis and interpretation. This approach can help to answer how different factors (single components) influence an interesting variable of interest have for: general corrosion, localised corrosion, bulk scaling and surface scaling. A factorial experiment was analysed using the analysis of variance (ANOVA). To calculate the quantitative effects of single component inhibitor and their interactions: on general corrosion, localized corrosion, surface scaling and bulk precipitation. The corrosion and scale occurring simultaneously was studied using a new bubble cell/jar test in the presence of the individually composed (blended) combined inhibitor. In order to measure and assess the general corrosion and pitting corrosion, LPR, Tafel plots and light interferometry were used. The scale was observed using SEM.

7.2 Experimental matrix - 2^5 full factorial design method

The experimental tests in this study focused on 5 single components of combined inhibitor (2^5 full factorial design method). Each parameter was set at two levels, thus there were $2 \times 2 \times 2 \times 2 \times 2 = 32$ trials for one combined inhibitor (Table 4.4). The experimental design was explained in details in Chapter Chapter 4 in section 4.6.

25ppm of blended combined inhibitor was present in 1 litre solution. The concentration (v/v%) of single components in combined inhibitor blend was set accordingly:

- corrosion inhibitor : 0.5v/v% low (L) and 10v/v% high (H)
- scale inhibitor: 1v/v% low (L) and 20v/v% high (H)
- souring agent: 0.25v/v% low (L) and 5 v/v% high (H)
- rest of solvent

The assessment of the inhibitor component effects was done via consideration of the 4 measurements considered to represent a full evaluation of corrosion/scale: a) general corrosion rate, b) pitting corrosion, c) bulk scale and d) surface scale.

7.3 Corrosion results

7.3.1 General corrosion

Table 7.1 shows the corrosion rate at the end of the 4 hour tests in all 32 test runs (composition of combined inhibitor blend can be found in Table 4.4).

Table 7.1: Corrosion rate at the end of the tests with different combinations of single components in the combined inhibitor after 4 hours

Number of run	Corrosion rate (mm/year)	Number of run	Corrosion rate (mm/year)
Run 1	0.03 ±0.005	Run 17	0.13 ±0.02
Run 2	0.04 ±0.02	Run 18	0.08 ±0.05
Run 3	0.67 ±0.2	Run 19	0.05 ±0.01
Run 4	0.13 ±0.03	Run 20	2.11 ±0.3
Run 5	0.05 ±0.02	Run 21	0.11 ±0.06
Run 6	0.04 ±0.01	Run 22	0.18 ±0.05
Run 7	0.06 ±0.02	Run 23	0.10 ±0.05
Run 8	0.03 ±0.01	Run 24	0.17 ±0.02
Run 9	0.03 ±0.01	Run 25	0.05 ±0.01
Run 10	0.05 ±0.02	Run 26	0.06 ±0.02
Run 11	0.18 ±0.2	Run 27	0.03 ±0.01
Run 12	1.37 ±0.2	Run 28	0.20 ±0.2
Run 13	0.10 ±0.2	Run 29	0.09 ±0.5
Run 14	0.03 ±0.01	Run 30	0.09 ±0.03
Run 15	0.09 ±0.02	Run 31	0.04 ±0.02
Run 16	0.09 ±0.01	Run 32	0.09 ±0.06

7.3.2 Localized corrosion

Table 7.2 shows the deepest pits in all 32 tests runs (composition of combined inhibitor blend can be found in Table 4.4). The tests results can be divided in to three groups: pits below 5 μm , between 5 and 15 μm and pits deeper than 15 μm .

Table 7.2: Deepest pits in the tests with different combination of single components in combined inhibitor after 72hrs

Number of run	Pit depth (μm)	Number of run	Pit depth (μm)
Run 1	5.9	Run 17	8.0
Run 2	6.7	Run 18	2.4
Run 3	11.1	Run 19	2.7
Run 4	15.0	Run 20	29.3
Run 5	7.3	Run 21	12.8
Run 6	10.8	Run 22	6.9
Run 7	10.5	Run 23	7.2
Run 8	10.0	Run 24	4.5
Run 9	9.1	Run 25	3.7
Run 10	4.2	Run 26	4.5
Run 11	25.9	Run 27	2.8
Run 12	29.3	Run 28	20.2
Run 13	7.2	Run 29	10.0
Run 14	6.0	Run 30	6.2
Run 15	3.4	Run 31	9.9
Run 16	11.4	Run 32	26.5

7.4 Bulk and surface scaling results

7.4.1 Bulk solution scaling

7.4.1.1 Turbidity results

The induction time results in the tests with different combinations of single components in combined inhibitor in bulk solution are presented in Table 7.3. The.

Table 7.3: The induction time results in the tests with different combination of single components in combined inhibitor in bulk solution

Number of run	Induction time (minutes)	Number of run	Induction time (minutes)
Run 1	10	Run 17	>240
Run 2	10	Run 18	>240
Run 3	20	Run 19	>240
Run 4	>240	Run 20	20
Run 5	>240	Run 21	10
Run 6	>240	Run 22	75
Run 7	20	Run 23	40
Run 8	10	Run 24	>240
Run 9	60	Run 25	>240
Run 10	>240	Run 26	>240
Run 11	20	Run 27	5
Run 12	15	Run 28	>240
Run 13	>240	Run 29	50
Run 14	120	Run 30	>240
Run 15	>240	Run 31	15
Run 16	>240	Run 32	>240

7.4.2 Inductively coupled plasma mass spectrometry (ICP – MS) results from bulk solution

Table 7.4 shows the amount of calcium sustained in the bulk solution by the combined inhibitor blend in all 32 tests runs (composition of combined inhibitor blend can be found in Table 4.4).

Table 7.4 ICP-MS results in the tests with different combinations of single components in combined inhibitor in bulk solution

Number of run	Amount of calcium in bulk on the end of tests (ppm)	Number of run	Amount of calcium in bulk on the end of tests (ppm)
Run 1	697	Run 17	904
Run 2	720	Run 18	909
Run 3	701	Run 19	910
Run 4	910	Run 20	652
Run 5	913	Run 21	674
Run 6	908	Run 22	696
Run 7	792	Run 23	744
Run 8	817	Run 24	915
Run 9	912	Run 25	902
Run 10	915	Run 26	908
Run 11	701	Run 27	698
Run 12	608	Run 28	909
Run 13	913	Run 29	724
Run 14	683	Run 30	911
Run 15	915	Run 31	643
Run 16	911	Run 32	906

7.4.3 Surface scale

7.4.3.1 Inductively coupled plasma mass spectrometry (ICP – MS) results from surface

Table 7.5 shows the amount of calcium deposited on the metal surface in the presence of combine inhibitor blend in all 32 tests runs (composition of combined inhibitor blend can be found in Table 4.4).

Table 7.5 ICP-MS results in the tests with different combination of single components in combined inhibitor on metal surface

Number of run	Amount of calcium on metal surface (mg/cm ²)	Number of run	Amount of calcium on metal surface (mg/cm ²)
Run 1	0.61	Run 17	0
Run 2	0.41	Run 18	0
Run 3	0.41	Run 19	0
Run 4	0	Run 20	0.41
Run 5	0	Run 21	0.82
Run 6	0	Run 22	1.02
Run 7	2.04	Run 23	2.65
Run 8	0.82	Run 24	0
Run 9	0	Run 25	0
Run 10	0	Run 26	0
Run 11	0.82	Run 27	1.84
Run 12	0.20	Run 28	0
Run 13	0	Run 29	2.65
Run 14	0.41	Run 30	0
Run 15	0	Run 31	0.82
Run 16	0	Run 32	0

7.4.3.2 Inductively coupled plasma mass spectrometry (ICP – MS) results from surface

In Table 7.6 and Table 7.7 a description of size and structure of CaCO₃ formed in the tests with different combinations of single components in all 32 tests runs are presented (composition of combined inhibitor blends can be found in Table 4.4).

Table 7.6 Size and structure of CaCO₃ formed in the tests (Run 1 to Run 16) with different combination of single components in combined inhibitor

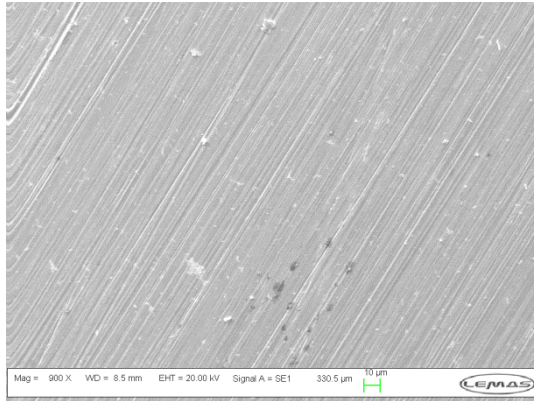
Test	No Scale	Structure	Size
Run 1		clusters, crystal	small < 20 µm
Run 2		clusters, crystal	small < 10 µm
Run 3		clusters, crystal	small < 20 µm
Run 4		crystal	small < 2 µm
Run 5		crystal	small < 2 µm
Run 6	none		
Run 7		crystals clusters, crystal	big > 100 µm small < 30 µm
Run 8		crystal clusters	big > 100 µm small < 20 µm
Run 9		crystal, clusters	big > 80 µm
Run 10	none		
Run 11		clusters, crystal	small < 30 µm
Run 12		clusters, crystal	small < 30 µm
Run 13	none		
Run 14		clusters crystal	big > 80 µm small < 2 µm
Run 15	none		
Run 16		crystal	small < 2 µm

Table 7.7 Size and structure of CaCO₃ formed in the tests (Run 17 to Run 32) with different combination of single components in combined inhibitor

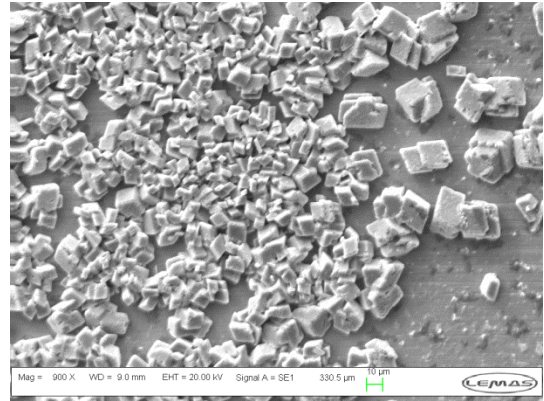
Run 17		crystal	small < 2 μm
Run 18		crystal	small < 2 μm
Run 19	none		
Run 20		crystal clusters	small < 20 μm
Run 21		crystal clusters	small < 20 μm
Run 22		crystal clusters	big > 100 μm
Run 23		crystal clusters	small < 30 μm
Run 24		crystal	small < 2 μm
Run 25	none		
Run 26	none		
Run 27		crystal clusters	small < 20 μm
Run 28		crystal	small < 2 μm
Run 29		crystal clusters, crystal	big > 80 μm small < 30 μm
Run 30		crystal	small < 2 μm
Run 31		crystal clusters	small < 20 μm
Run 32		crystal	small < 2 μm

In Figure 7.1 the different forms of scale formed during the tests with presence of combine inhibitor blend in all 32 tests runs (composition of combined inhibitor blend can be found in Table 4.4) are presented. In Figure 7.1a a representation of the surface where no scale is formed is presented – Run 25. Figure 7.1b represents a surface where clusters were found – Run2.

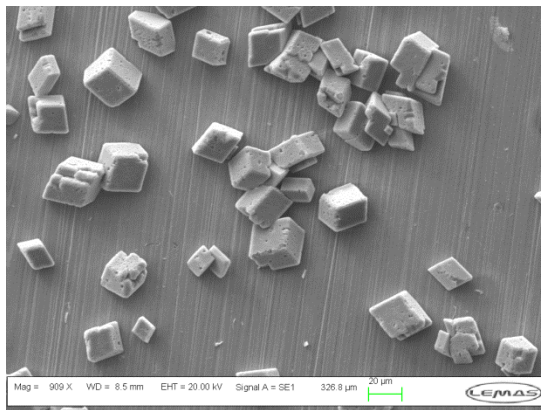
Figure 7.1 represents a surface where single crystals $<20\ \mu\text{m}$ which were present on surface – Run21. In Figure 7.1d the surface it is an example (Run16) where crystals were found smaller than $2\ \mu\text{m}$. An example of crystals bigger than $80\ \mu\text{m}$ found on surface during the test is shown in Run9 (Figure 7.1e).



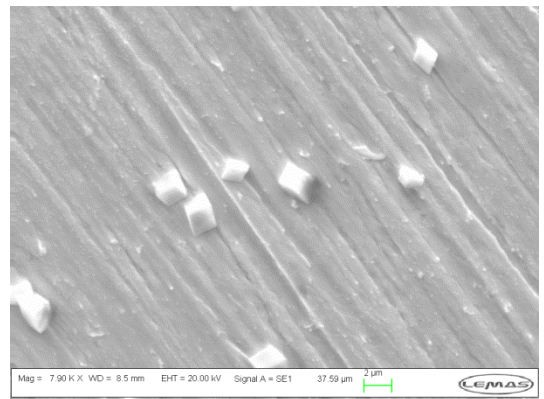
(a)



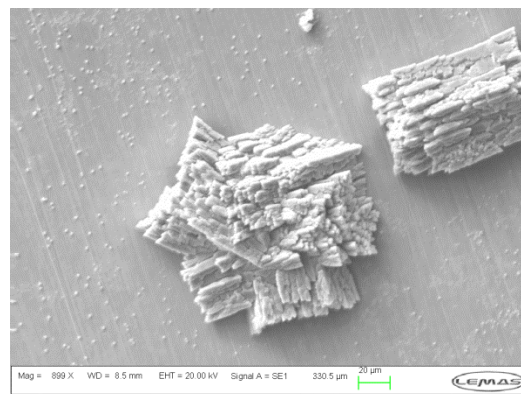
(b)



(c)



(d)



(e)

Figure 7.1: Examples of scale formed during the test: (a) none scale – Run 25, (b) clusters – Run2, (c) small crystals $<20\ \mu\text{m}$ – Run 21, (d) smaller crystals than $2\ \mu\text{m}$ – Run16 and (e) crystals bigger $>80\ \mu\text{m}$ – Run9

The test results can be divided into 3 groups: first group – none and scale crystals on surface smaller than 2µm, group two – the crystal size on the surface from 2µm to 80µm and group three – the crystal size on surface larger than 80µm. In the Table 7.8 the amount of calcium on the metal surface is presented in two groups.

Table 7.8: Crystals formed during the test with different combination of combined inhibitor divided into in three groups

Crystal size on surface (µm)	Number of run
>2µm	4, 5, 6, 10, 13, 15, 16, 17, 18, 19, 24, 25, 26, 28, 30, 32
2 > µm >80	1, 2, 3, 11, 12, 20, 21, 23, 27, 31
>80µm	7, 8, 9, 14, 22, 29

In the group with crystals on surface smaller than 2µm all runs had high concentration of scale inhibitor (PPCA). The tests runs with crystals larger than 80µm had high concentration of CI1 (alcohol ethoxy phosphate ester) added to combined inhibitor blend.

7.4.4 Empirical equation

An empirical equation can be generated from the DoE results to link the inputs (inhibitor concentration values) to the outputs (general corrosion, localised corrosion, surface scale and bulk scale). First with help of Half-Normal Probability plot, the factors (the single components of combined inhibitor or interaction between them) which had the biggest effect on the response (general corrosion, localized corrosion, surface scaling and bulk precipitation) were identified. Then with the help of Design-Expert [225] the empirical equation was calculated. The letters A, B, C, D and E are coded factors by Design-Expert accordingly to CI1, CI2, CI3, SI and SA which are actual inputs to the software.

The half-normal probability plot (Figure 7.2) is a graphical tool that helps assess which factors are important and which are unimportant. A half-normal probability plot is formed by horizontal axis from which factors (interactions) having the greatest effect on response are read and the vertical axis are given by the idealized expected values for this number of effects and ranked by increasing value.

Figure 7.2 should be read as follow. All factors and their interactions highlighted on blue (E, A, EA, DE, ADE, AD and D) have greatest effect on general corrosion. These factors and interactions have greatest effect as there are place in graph very close to the highest effect value (5) on x axis named Effect. In the similar way, Figure 7.4, Figure 7.6 and Figure 7.8 should be read.

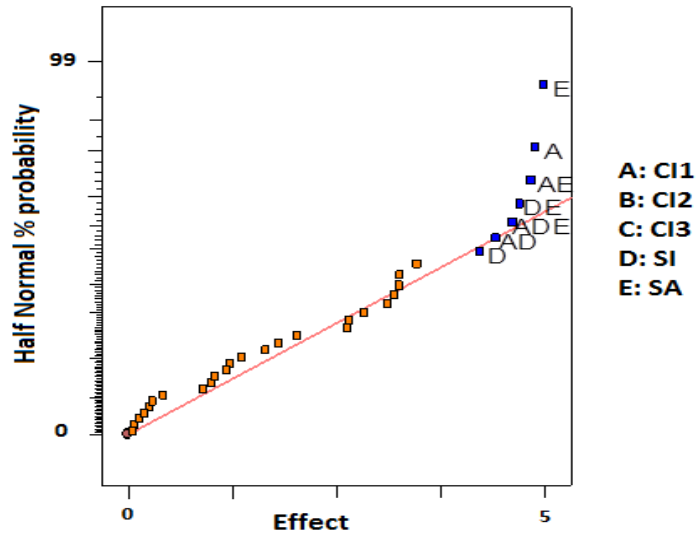


Figure 7.2: Half-Normal Probability Plot showing the effect of the single components of combined inhibitor and their interaction on inhibition of general corrosion

7.5 ANOVA analysis of general corrosion inhibition

Table 7.9 shows the quantitative effects of the single component of inhibitors and their interactions on the general corrosion calculated by the analysis of variance (ANOVA) approach. Final values of general corrosion rate from all 32 tests runs (Table 7.1) were used to calculate the percentages shown in Table 7.9; these are the values of the sum of squares for that variable relative to the total sum of squares for all variables. A higher percentage correlates to that parameter having a greater effect.

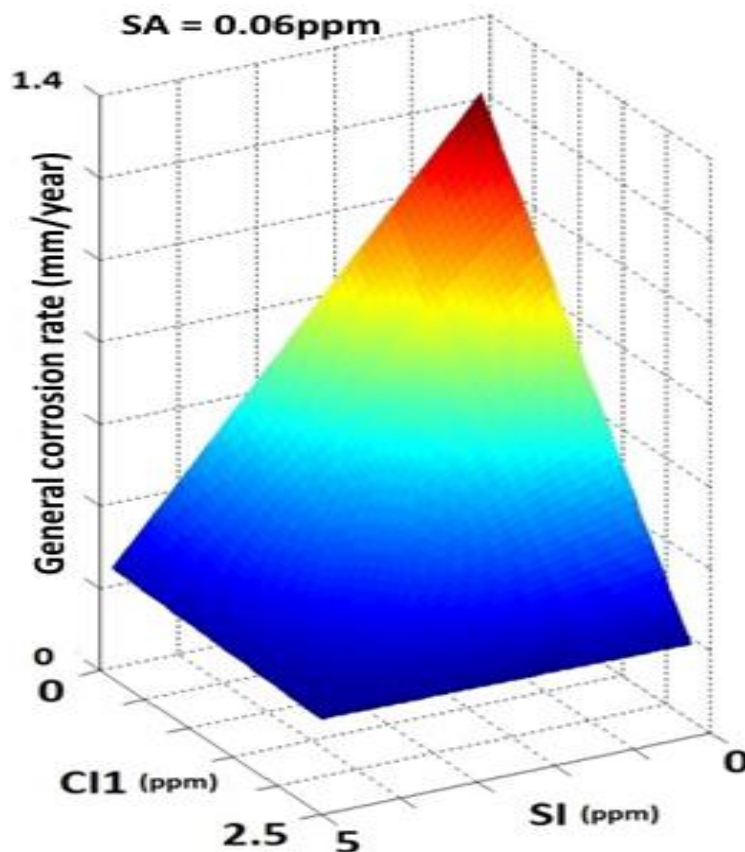
Table 7.9 The contributions of single components and their interaction to inhibition of general corrosion

SA	CI1	SI	CI2	CI3
10%	9.7%	7.2%	2.8%	0.4%
CI1,SA	SI,SA	CI1,SI	CI1,SI,SA	-
9.5%	9%	7.9%	8.6%	-

In the table results are presented for all single components as well as their interactions. However, interactions are only presented in the table if they contributed more than 7%. In this study all parameters which contributed less than 7% are considered insignificant because in the Half-Normal Probability Plot (Figure 7.2) the single components of combined inhibitor and interaction which has significant effect were identified. Using the contributions of single components and their interaction results the following empirical relationship (Equation (7-1)) was developed for general corrosion inhibition. Figure 7.3 presents a 2D-countour plot of the empirical relationship is presented based on the experiments results.

$$\begin{aligned} GCI = & - 0.47 * CI_1 & (7-1) \\ & - 0.23 * SI \\ & - 0.96 * SA \\ & + 0.09 * CI_1 * SI \\ & + 0.38 * CI_1 * SA \\ & + 0.19 * SI * SA \\ & - 0.07 * CI_1 * SI * SA \end{aligned}$$

where: **GCI** – general corrosion inhibition, **CI1** – corrosion inhibitor 1, **SI** – scale inhibitor and **SA** – souring agent



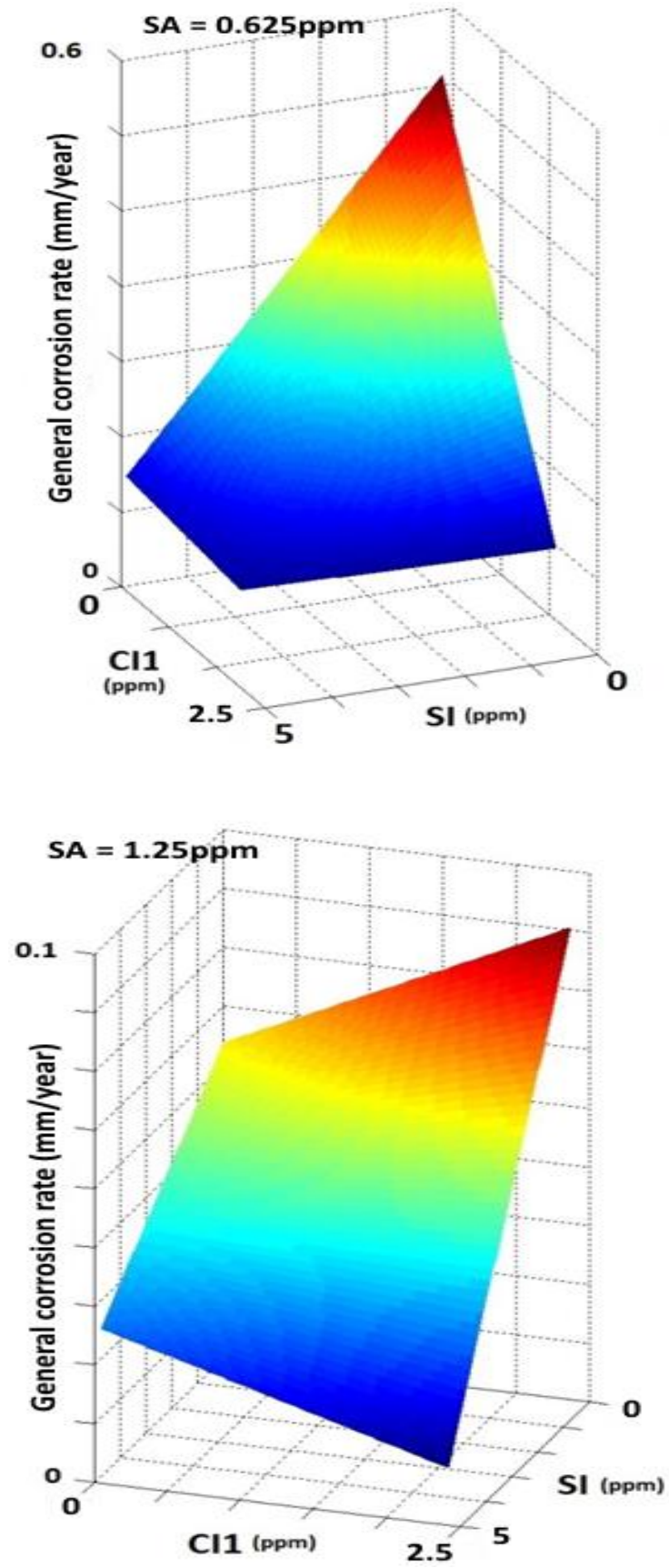


Figure 7.3: 2D-countour plot of empirical relationship of general corrosion inhibition

7.6 ANOVA analysis of localized corrosion inhibition

In Table 7.10 results are presented of the quantitative effects of single components inhibition and their interactions on the localized corrosion calculated by the analysis of variance (ANOVA) approach.

Table 7.10: The contributions of single components and their interaction to inhibition of localized corrosion

SA	CI1	SI	CI3	CI2	CI1,SA
34.2%	18.7%	5.1%	2.1%	0.3%	10.9%

The deepest pit values from all 32 tests runs (Table 7.2) were used to calculate the percentages shown in Table 7.10; these are the values of the sum of squares for that variable relative to the total sum of squares for all variables. Higher percentage values correlate to inhibitor (or interaction) having a greater effect. In the table results for all single components as well as their interactions are presented. However, interactions are only presented in the table if it contributed more than 7%. In this study all parameters which contributed less than 7% are considered insignificant because in the Half-Normal Probability Plot (Figure 7.4) the single components of combined inhibitor and interaction which has significant effect were identify. Using contributions of single components and their interaction results the following empirical relationship (Equation (7-2)) was developed for localized corrosion inhibition. In Figure 7.5 is presented a 2D-countour plot of empirical relationship based on results from 32 tests runs and empirical relationship.

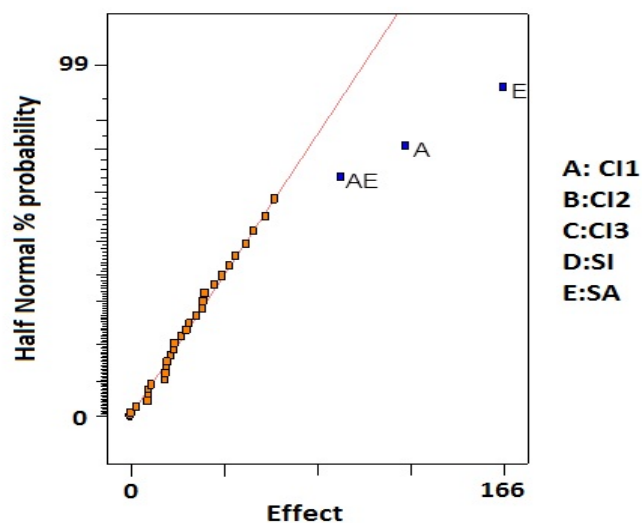


Figure 7.4: Half-Normal Probability Plot showing the effect of the single components of combined inhibitor and their interaction on inhibition of localized corrosion

$$\begin{aligned} LCI &= 21.9 && (7-2) \\ &- 5.1 * CI_1 \\ &- 12.1 * SA \\ &+ 3.6 * CI_1 * SA \end{aligned}$$

where: **LCi** – localized corrosion inhibition, **CI1** – corrosion inhibitor 1 and **SA** – souring agent

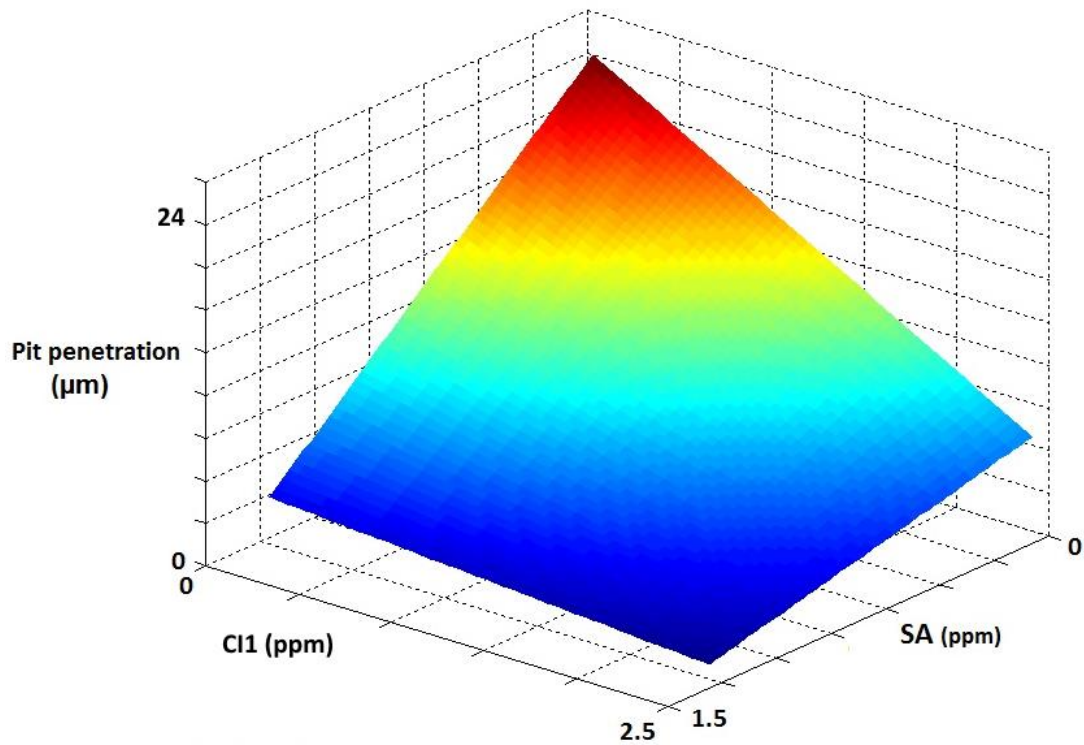


Figure 7.5: 2D-contour plot of empirical relationship of localized corrosion inhibition

7.7 ANOVA analysis of bulk scaling inhibition

Table 7.11 show the quantitative effects of single components and their interactions on the bulk scaling calculated by the analysis of variance (ANOVA) approach. Maximum values of the turbidity from all 32 tests runs (Figure) were used to calculate the percentages shown in Table 7.11; these are the values of the sum of squares for that variable relative to the total sum of squares for all variables. Higher percentage values correlate to that parameter having a larger effect. In the table results for all single components as well as their interactions are presented. However, interactions are only presented in the table if they contributed more than 7%. In this study all parameters which contributed less than 7% are considered insignificant because in the Half-Normal Probability Plot (Figure 7.6) the

single components of combined inhibitor and interaction which has significant effect were identify.

Table 7.11: The contributions of single components and their interaction to inhibition of bulk scaling inhibition

SI	CI1	SA	CI2	CI3	CI1,SI
81.6%	0.24%	0.24%	0.07%	0.04%	4.2%

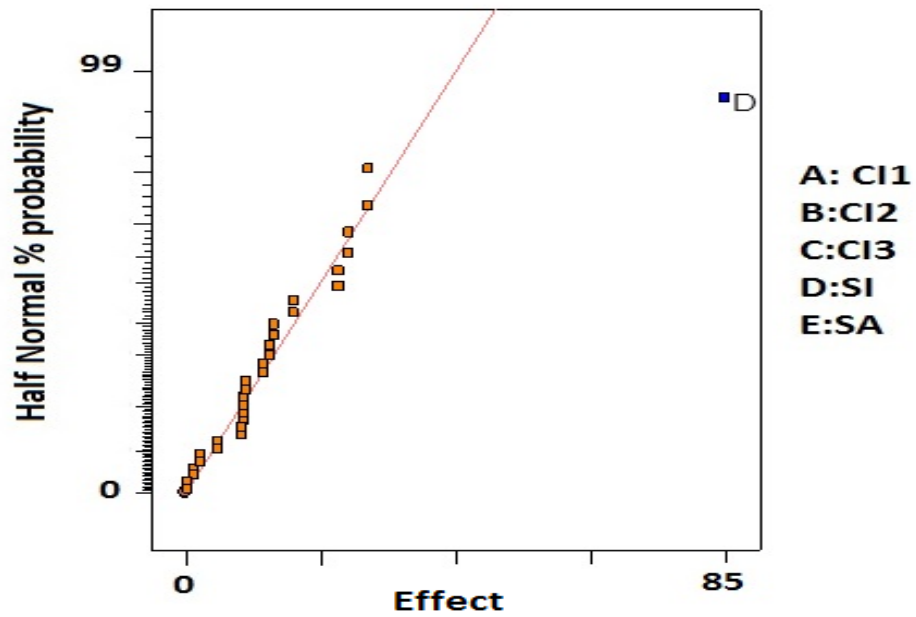


Figure 7.6: Half-Normal Probability Plot showing the effect of the single components of combined inhibitor and their interaction on inhibition of bulk scaling

Using contributions of single components and their interaction results the following empirical relationship (Equation (7-3)) was developed for bulk scaling inhibition. In Figure 7.7 is presented a 2D-countour plot of empirical relationship based on results from 32 tests runs and empirical relationship .

$$BSi = 67 * SI \tag{7-3}$$

where: **BSi** – bulk scaling inhibition and **SI** – scale inhibitor

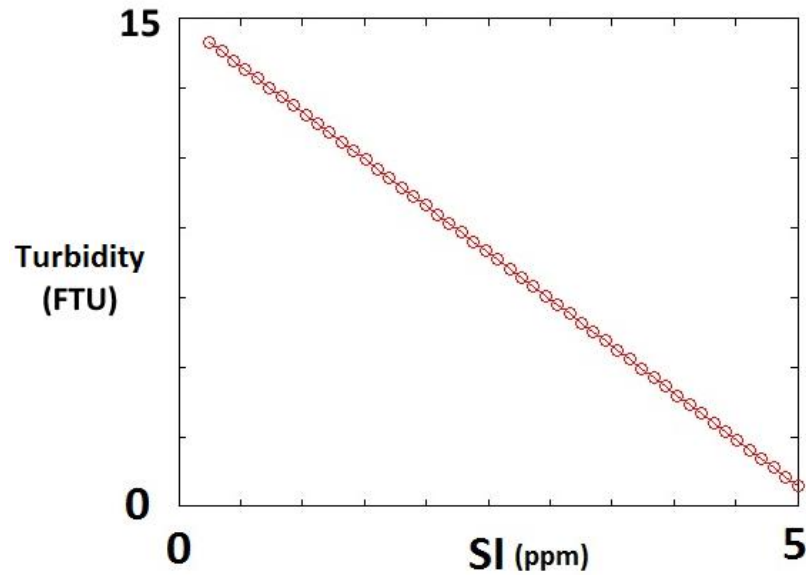


Figure 7.7: Linear graph of empirical relationship of bulk scaling inhibition

7.8 ANOVA analysis of surface scaling inhibition

In Table 7.12 results of the quantitative effects of single components and their interactions inhibition on the surface scale calculated by the analysis of variance (ANOVA) approach are presented. The amount of calcium ions dissolved at the end of the end all 32 tests runs (Table 7.5) were used to calculate the percentages shown in Table 7.12; these are the values of the sum of squares for that variable relative to the total sum of squares for all variables. Higher percentage values correlate to inhibitor (or interaction) having a greater effect. In the table are presented results for all single components as well as their interactions. However, interaction is only presented in the table if it contributed more than 7%. In this study all parameters which contributed less than 7% are considered insignificant because in the Half-Normal Probability Plot (Figure 7.8) the single components of combined inhibitor and interaction which has significant effect were identify.

Table 7.12: The contributions of single components and their interaction to inhibition of surface scaling

SI	CI1	SA	CI3	CI2	CI,SI
43.5%	8.1%	3.8%	0.8%	0.3%	7.9%

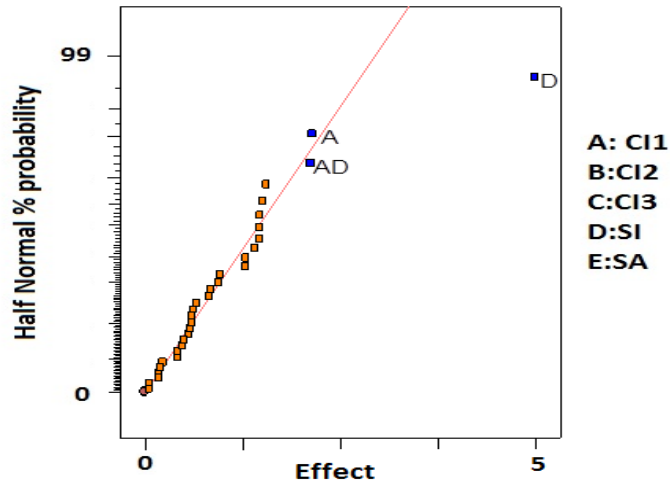


Figure 7.8: Half-Normal Probability Plot showing the effect of the single components of combined inhibitor and their interaction to inhibition of surface scaling

Using contributions of single components and their interaction results the following empirical relationship (Equation (7-4)) was developed for surface scale inhibition. In Figure 9.1 is presented a 2D-countour plot of empirical relationship based on results from 32 tests runs and empirical relationship.

$$\begin{aligned}
 SSi &= 1.8 * CI_1 & (7-4) \\
 &- 0.5 * SI \\
 &- 0.4 * CI_1 * SI
 \end{aligned}$$

where: **SSi** – surface scale inhibition, **CI₁** – corrosion inhibitor 1 and **SI** – scale inhibitor

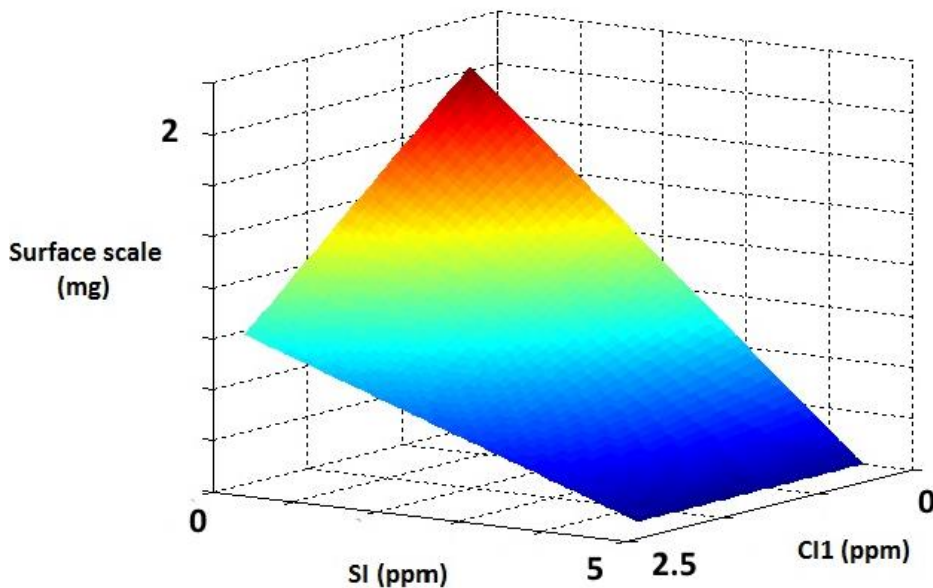


Figure 7.9: 2D-countour plot of empirical relationship of surface scale inhibition

Validation is the task of determining that the model is a reasonable representation of the real system: that it imitate system behaviour with enough fidelity to satisfy analysis objectives. There are three approaches to model validation and any combination of them may be applied as suitable to the different aspects of a particular model.

These approaches are:

- real system measurements,
- expert intuition,
- theoretical results/analysis.

In this case Real System Measurements comparison with a real system would be the most reliable and preferred way to validate a simulation model. In this PhD project, the validation of the empirical equations (model) could not be done due to time restrictions.

7.9 Summary

- 2-mercaptoethanol has the greatest effect on general corrosion inhibition as single component (10%) of combined inhibitor although alcohol ethoxy phosphate ester effect was slightly lower 9.7%
- 2-mercaptoethanol has the greatest effect on pitting corrosion inhibition as single component (34.2%) of combined inhibitor although alcohol ethoxy phosphate ester effect was also significant (18.7%)
- Polyphosphinocarboxylic acid have the greatest on bulk scale inhibition – 81.6%
- Polyphosphinocarboxylic acid has the greatest effect on surface scale inhibition as single component (43.5%) of combined inhibitor although alcohol ethoxy phosphate ester effect was lower - 8.1%

Chapter 8

FTIR and RAMAN spectroscopy analysis of single components of combined inhibitors

8.1 Introduction

Scanning electron microscope images showed that the presence of inhibitors can lead to the formation of different shapes and sizes of calcium carbonate scale during the tests with single components and combined inhibitor. Some further analyses were carried out (Fourier Transform Infrared Spectroscopy and Raman spectroscopy) to characterise the interactions between the single components and calcium carbonate or iron carbonate formed on the metal sample.

8.2 FTIR analysis of single components and interaction with calcium carbonate and iron carbonate

8.2.1 FTIR analysis of single components and interaction with calcium carbonate

In Figure 8.1 the IR-spectrum of neat liquid 2-mercaptoethanol is presented. The rest of the single component IR-spectra are presented in Appendix A. Figure 8.2 presents IR-spectra calcium carbonate formed with presence of 2-mercaptoethanol in solution, reference IR-spectrum of calcium carbonate and carbon steel. Scanning electron microscope images (Figure 6.7) showed some interactions between the inhibitors and scale formed on the metal sample. During the first stage, calcium carbonate was formed on the sample then 1.25ppm of 2-mercaptoethanol was added to the test solution and the test continued for another 4 hours. From comparison of the spectrum in Figure 8.2 it is clear that no residual inhibitor part of 2-mercaptoethanol adsorbed to calcium carbonate precipitated on the metal surface. Two spectra are almost the same. However a small shift of calcium carbonate could be observed. A similar situation was observed with the remaining single components of combined inhibitor. In Table 8.1 peaks of calcium carbonate found in this PhD work and literature are presented. For further reference of IR-spectrum of calcium carbonate formed with the rest of single components, results have been presented in Appendix A.

The small difference in peaks values are caused by various shapes and size of crystals calcium carbonate formed on sample surface as well as different thickness of scale precipitated on sample surface. In literature is pointed that PPCA can incorporate into calcium carbonate lattice [109] and phosphate esters inhibitor form insoluble salt with Ca^{2+} ions on metal surface [182]. However, in this study no residual inhibitor part in all single components test was observed in FTIR analysis. This could be caused by low concentration of the single components used during the tests.

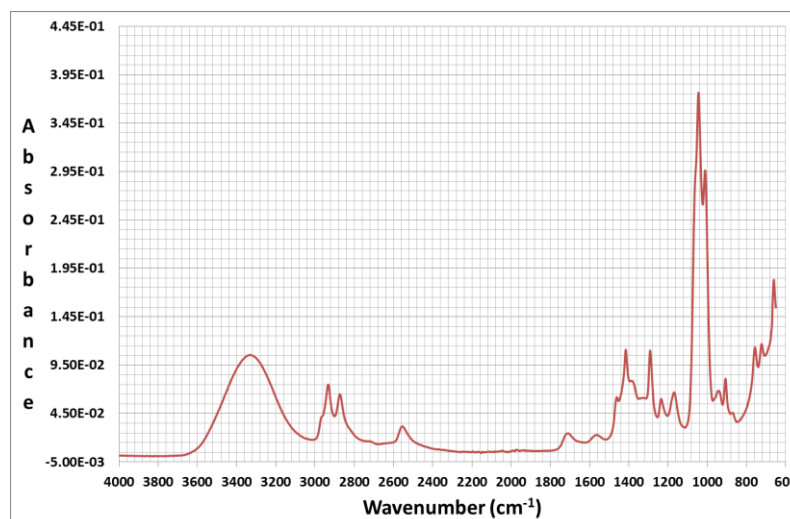


Figure 8.1: Infrared spectrum for neat 2-mercaptoethanol

Table 8.1: Peaks of calcium carbonate found in this PhD work and literature

IR-spectrum of calcium carbonate with:	Wavenumber (cm^{-1})	Reference
Blank	2536 ¹ , 1802 ² , 1403 ³ , 1101 ⁴ , 869 ⁵ , 713 ⁶ 2530, 1785, 1430, 1080, 877, 715	This work [227, 228]
2-mercapthoethanol	2533, 1803, 1406, 1100, 870, 714	This work
alcohol ethoxy phosphate ester	2529, 1801, 1402, 1102, 869, 713	This work
C12-C14alkyl dimethyl benzyl ammonium chloride	2537, 1801, 1397, 1101, 870, 714	This work
ethoxylated imidazolines	2531, 1799, 1405, 1086, 870, 712	This work
Polyphosphinocarboxylic acid	2529, 1803, 1404, 1102, 870, 713	This work

¹- $\nu_1+\nu_3$, ²- $\nu_1+\nu_4$, ³- ν_3 asymmetric CO_3 stretching, ⁴- ν_1 symmetric CO_3 stretching, ⁵- ν_2 CO_3 out of plane bending, ⁶- ν_4 CO_3 in plane bending

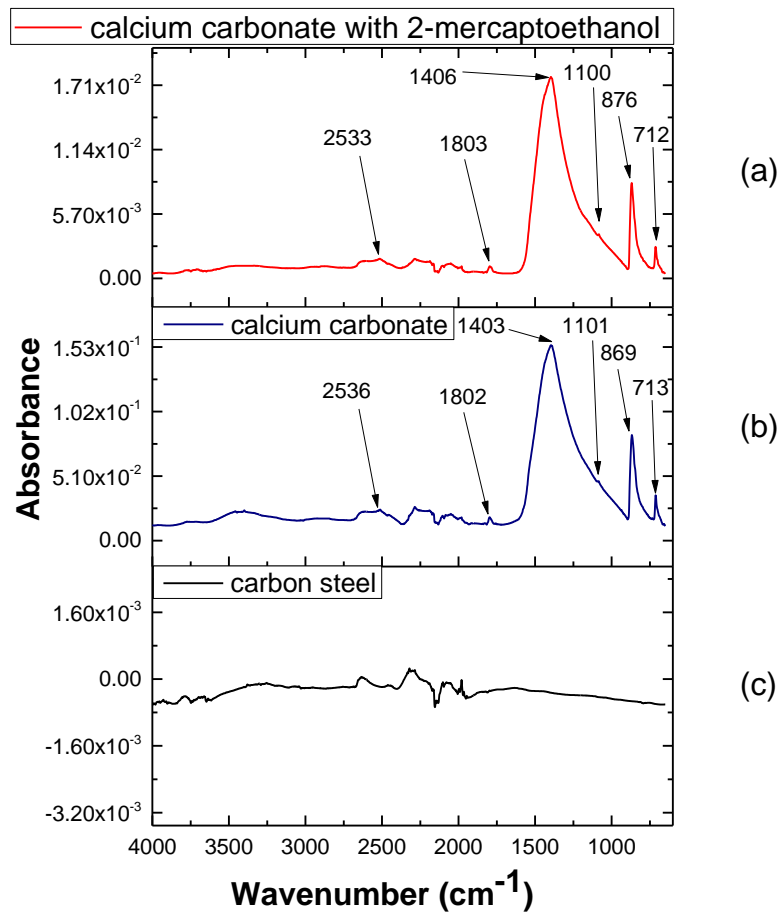


Figure 8.2: Infrared spectrum for: a) calcium carbonate formed with presence of 2-mercaptoethanol, b) calcium carbonate reference and c) carbon steel

8.2.2 FTIR analysis of single components and interaction with iron carbonate

Figure 8.3 presents the IR-spectra for iron carbonate formed with presence of 2-mercaptoethanol in solution, the reference IR-spectrum of iron carbonate and carbon steel. During the first stage, iron carbonate was formed on the sample then 1.25ppm of 2-mercaptoethanol was added to the test solution and test continued for another 4hours. From comparison of the spectrum in Figure 8.3 it is clear that no residual inhibitor part of 2-mercaptoethanol adsorbed to iron carbonate precipitated on the metal surface. The two spectra are almost the same. However a small shift of iron carbonate could be observed. A similar situation was observed with the remaining single components of combined inhibitor. In Table 8.2 peaks of

iron carbonate found in this PhD work and literature are presented. For further reference of IR-spectrum of calcium carbonate formed with the rest of single components, results have been presented in Appendix A.

The small difference in peak values are caused by various shapes and size of crystals iron carbonate formed on sample surface as well as different thickness of scale precipitated on sample surface. In the literature it is shown that PPCA was not effective at preventing iron carbonate [229] and imidazoline at low concentration and promoted tightly packed FeCO_3 scale [181]. However, in this study no residual inhibitor part in all single components test was observed in FTIR analysis. This could be caused by low concentration of the single components used during the tests.

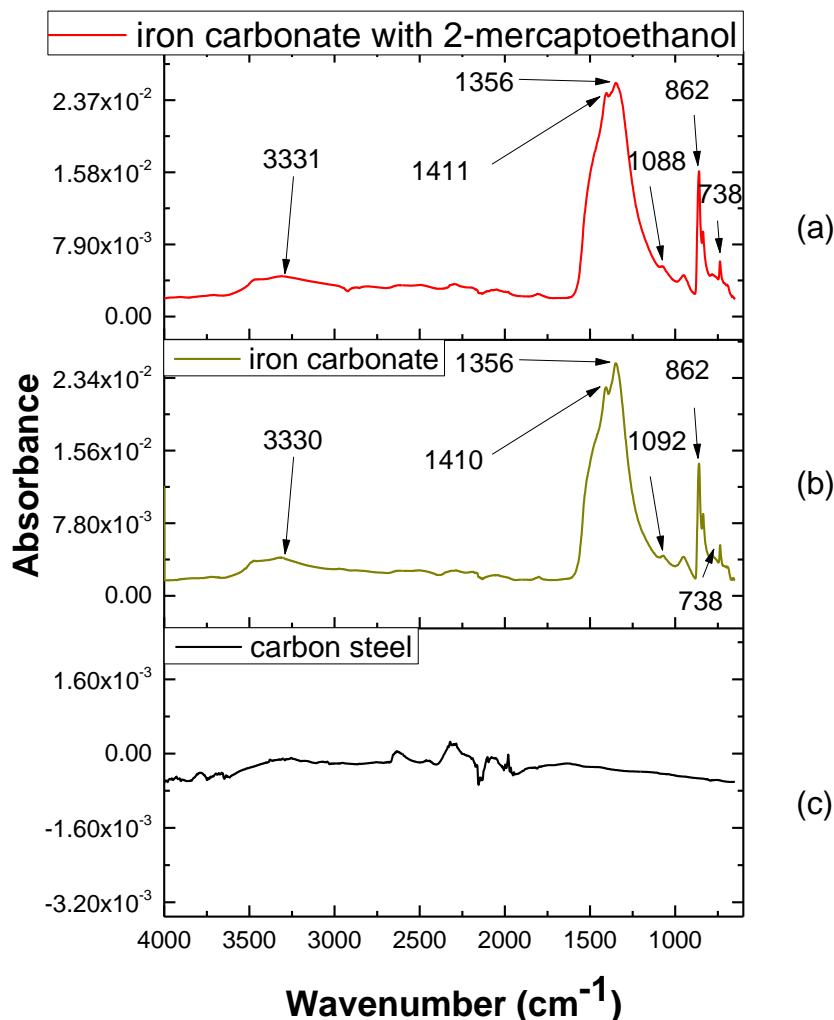


Figure 8.3: Infrared spectrum for: a) iron carbonate formed with presence of 2-mercaptoethanol, b) iron carbonate reference and c) carbon steel

Table 8.2: Peaks of iron carbonate found in this PhD work and literature

IR-spectrum of iron carbonate with:	Wavenumber (cm ⁻¹)	Reference
Blank	3330 ¹ , 1410 ² , 1356 ³ , 1092 ⁴ , 862 ⁵ , 738 ⁶ 3300, 1420, 1345, 1068, 860, 735	This work [230, 231]
2-mercapthoethanol	3331, 1411, 1356, 1088, 862, 738	This work
alcohol ethoxy phosphate ester	3340, 1414, 1356, 1090, 864, 739	This work
C12-C14alkyl dimethyl benzyl ammonium chloride	3322, 1407, 1345, 1086, 863, 739	This work
ethoxylated imidazolines	3330, 1411, 1357, 1090, 862, 738	This work
Polyphosphinocarboxylic acid	3335, 1414, 1356, 1087, 864, 739	This work

¹- -OH, ^{2, 3}- ν_3 asymmetric CO₃ stretching, ⁴- ν_1 symmetric CO₃ stretching, ⁵- ν_2 CO₃ out of plane bending, ⁶- ν_4 CO₃ in plane bending

8.3 Raman analysis of single components and interaction with calcium carbonate and iron carbonate

8.3.1 Raman analysis of single components and interaction with calcium carbonate

In Figure 8.4 the Raman spectrum of neat liquid 2-mercaptoethanol is presented. The spectra for the rest of the single components are presented in Appendix B. In Figure 8.5 calcium carbonate the Raman spectrum formed in the absence of inhibitors, the Raman spectrum of carbon steel and the Raman spectrum of interaction of 2-mercaptoethanol with calcium carbonate. During the first stage, calcium carbonate was precipitated on the metal sample in tests for 4hrs, then 1.25ppm of 2-mercaptoethanol was added to the test solution and test continued for another 4hours. From Figure 8.5, it is clear that no residual inhibitor part of 2-mercaptoethanol adsorbed to calcium carbonate precipitated on the metal surface. In Table 8.3 are presented peaks of calcium carbonate found in this PhD work and literature. Similar situation was observed with the remaining single components of combined inhibitor. Further results are presented in Appendix B.

The small difference in peaks values are caused by various shapes and size of crystals calcium carbonate formed on sample surface as well as different

thickness of scale precipitated on sample surface. In literature is pointed that PPCA can incorporate into calcium carbonate lattice [109] and phosphate esters inhibitor form insoluble salt with Ca^{2+} ions on metal surface [182]. However, in this study no residual inhibitor part in all single components test was observed in Raman analysis. This could be caused by low concentration of the single components used during the tests.

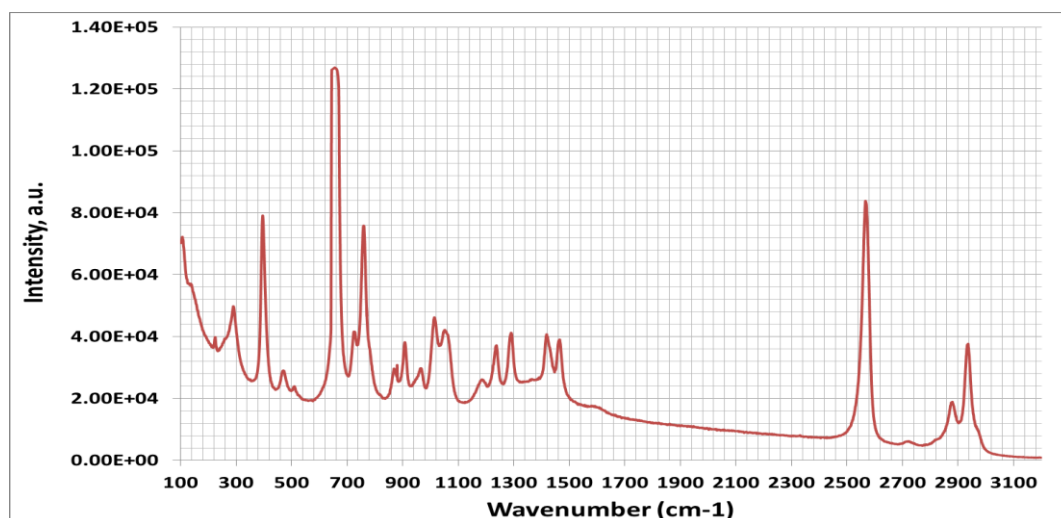


Figure 8.4: Raman spectrum for neat 2-mercaptoethanol

Table 8.3: Peaks of calcium carbonate found in this PhD work and literature

Raman spectrum of calcium carbonate with:	Wavenumber (cm ⁻¹)	Reference
Blank	156 ¹ , 282 ² , 712 ³ , 1087 ⁴ , 1438 ⁵ , 1751 ⁶ 156, 283, 713, 1086, 1436, 1749	This work [232]
2-mercapthoethanol	156, 282, 713, 1089, 1438, 1750	This work
alcohol ethoxy phosphate ester	156, 282, 713, 1089, 1438, 1748	This work
C12-C14alkyl dimethyl benzyl ammonium chloride	157, 283, 713, 1087, 1441, 1751	This work
ethoxylated imidazolines	156, 282, 712, 1087, 1436, 1750	This work
Polyphosphinocarboxylic acid	156, 282, 713, 1087, 1439, 1750	This work

^{1,2}- T – transitional lattice mode (Ca, CO₃), ³- ν_4 CO₃ in plane bending, ⁴- ν_1 symmetric CO₃ stretching, ⁵- ν_3 asymmetric CO₃ stretching, ⁶- $\nu_1+\nu_4$

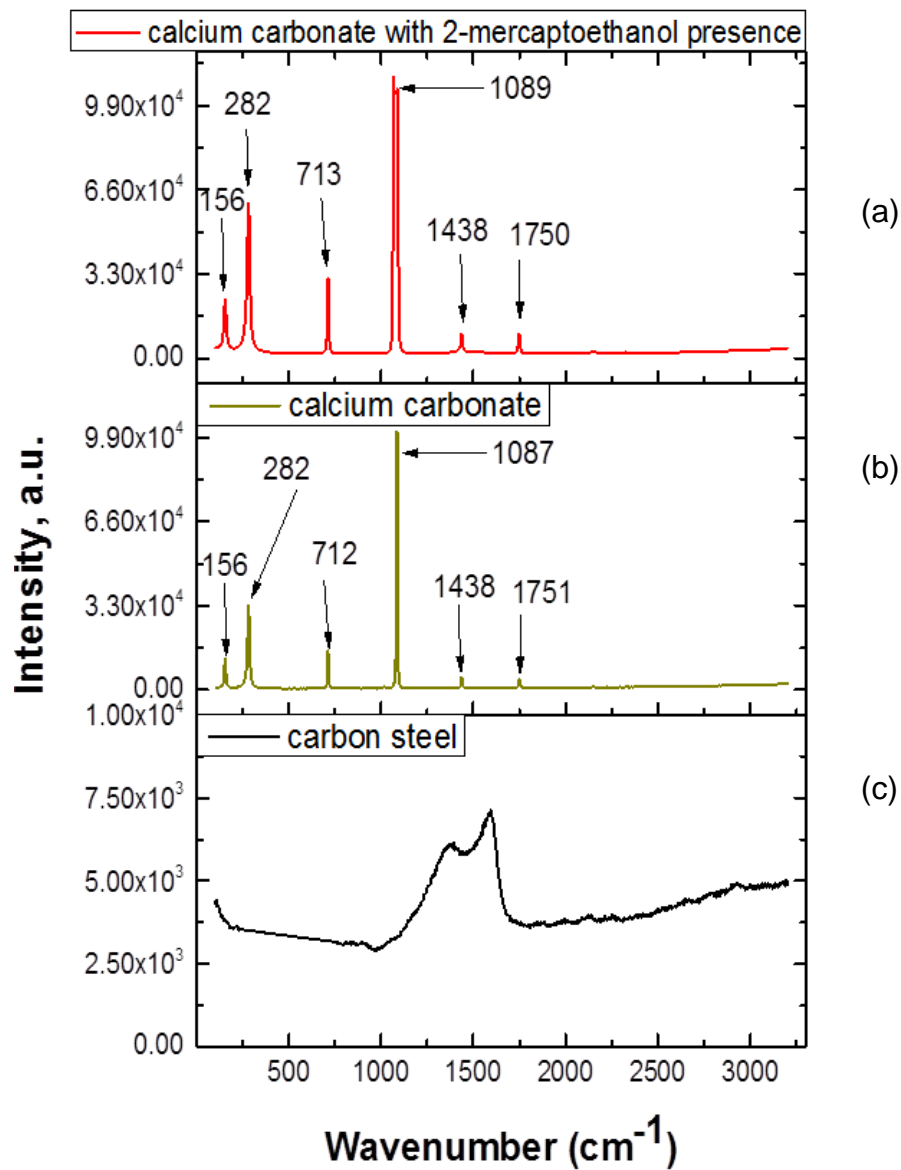


Figure 8.5: Raman spectrum for: a) calcium carbonate formed with presence of 2-mercaptoethanol, b) calcium carbonate reference and c) carbon steel

8.3.2 Raman analysis of single components and interaction with iron carbonate

In Figure 8.6 iron carbonate Raman spectrum formed in the absence of inhibitors, Raman spectrum of carbon steel and Raman spectrum of interaction of 2-mercaptoethanol with iron carbonate. As in calcium carbonate scale tests, iron carbonate was precipitated on the metal sample in tests for 5hrs, then 1.25ppm of 2-mercaptoethanol (5ppm of PPCA) was

added to the test solution and test continued for another 4hours. In Table 8.4 are presented peaks of iron carbonate found in this PhD work and literature. In Figure 8.6 could be observed characteristic peaks of iron carbonate at: 215, 271, and 1087 cm^{-1} . Similar situation is observed in the tests with alcohol ethoxy phosphate ester (212, 282, 1086 cm^{-1} - Table 8.4).

Table 8.4: Peaks of iron carbonate found in this PhD work and literature

Raman spectrum of iron carbonate with:	Wavenumber (cm^{-1})	Reference
Blank	215, 285, 1087 194 ¹ , 275 ² , 734 ³ , 745 ⁴ , 1082 ⁵ , 1729 ⁶ , 1738 ⁷	This work [233-236]
2-mercapthoethanol	215, 271, 1087	This work
alcohol ethoxy phosphate ester	212, 282, 1086	This work
C12-C14alkyl dimethyl benzyl ammonium chloride	214, 276	This work
ethoxylated imidazolines	181, 277, 732, 1081, 1718	This work
Polyphosphinocarboxylic acid	186, 284, 746, 1084, 1727	This work

^{1, 2}- T – transitional lattice mode (Ca, CO_3), ^{3, 4}- ν_4 CO_3 in plane bending, ⁴- ν_1 symmetric CO_3 stretching, ⁵- ν_3 asymmetric CO_3 stretching, ^{6, 7}- $\nu_1+\nu_4$

In the tests with C12-C14alkyl dimethyl benzyl ammonium chloride only two peaks 214, 276 cm^{-1} for iron carbonate could be observed. In the test with polyphosphinocarboxylic acid and ethoxylated imidazolines (Table 8.4) two other peaks which are associated with iron carbonate are present: 746 and 1727 cm^{-1} for PPCA and 732 and 1718 cm^{-1} for ethoxylated imidazolines. The intensity of peak 1081 cm^{-1} for PPCA and 1084 cm^{-1} ethoxylated imidazolines is bigger by one magnitude of order compare to the rest of Raman spectrums. no residual inhibitor part of 2-mercaptoethanol adsorbed to iron carbonate precipitated on the metal surface. Similar situation was observed with the reaming single components of combined inhibitor. A Raman spectrum shows peaks in region 389-399 cm^{-1} in all spectrums which is associated with goethite. For further reference results have been presented in Appendix B.

The small difference in peaks values are caused by various shapes and size of crystals iron carbonate formed on sample surface as well as different thickness of scale precipitated on sample surface. In literature is pointed that PPCA was not effective at preventing iron carbonate [229] and imidazoline at low concentration promoted tightly packed FeCO_3 scale [181]. This explain why in the tests with PPCA and ethoxylated imidazolines more peaks and higher intensity of peaks (specially peak 1081,1084 accordingly) were observed. However, in this study no residual inhibitor part in all single components test was observed in Raman analysis. This could be caused by low concentration of the single components used during the tests.

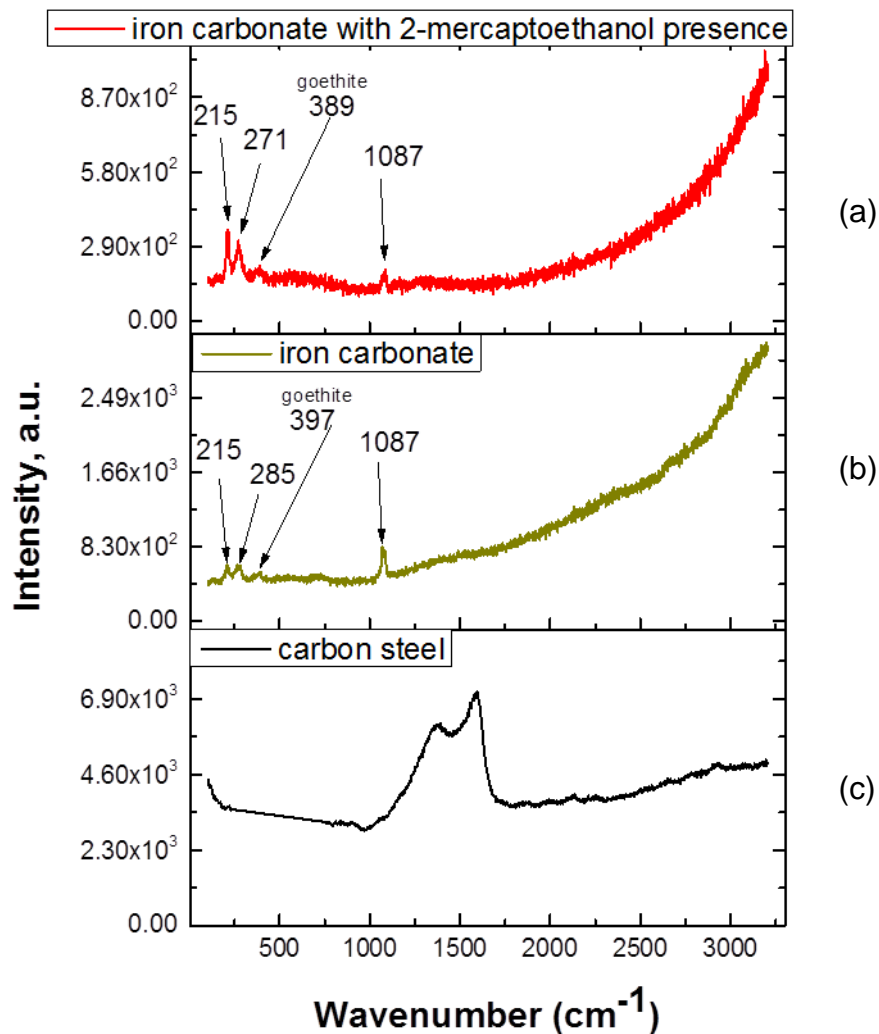


Figure 8.6: Raman spectrum for: a) iron carbonate formed with presence of 2-mercaptoethanol, b) iron carbonate reference and c) carbon steel

8.4 Summary

- No residual part of single components inhibitors incorporated with the calcium carbonate, iron carbonate was observed in the FTIR analysis
- No residual part of single components inhibitors (2-mercapthoethanol, alcohol ethoxy phosphate ester and C12-C14alkyl dimethyl benzyl ammonium chloride) incorporated with the calcium carbonate, iron carbonate was observed in the Raman analysis
- Raman analysis revealed that, in the tests with Polyphosphinocarboxylic acid an extra peak and higher intensity of peaks was measured. This is in good agreement with the findings in the literature that PPCA was not effective at preventing iron carbonate formation
- Raman analysis revealed that, in the tests with ethoxylated imidazolines an extra peak and higher intensity of peaks was measured. This is also in good agreement with the findings in the literature that imidazoline at low concentration promoted iron carbonate formation

Chapter 9 Discussion

9.1 Introduction

In this chapter, three key points are discussed, new understanding of the interactions between corrosion and scale processes in the environment where no inhibitor is present; understand the effect of single components of the combined inhibitors on general corrosion, localized corrosion, bulk scaling and surface scale deposition. Use an experimental design method to quantify the effects of the single components of the combined scale/corrosion inhibitor and/or synergistic effects on all four processes mention above.

9.2 Corrosion and scale processes in an environment where both processes occurs simultaneously

In this section, there are four main parts to discuss with respect to the behaviour of the scale-corrosion system:

- X65 microstructure influences on formation of calcium carbonate
- CO₂ corrosion mechanism in calco-carbonic environment
- Calcium carbonate role in localized pitting
- A combined jar test/bubble cell as new method of assessment corrosion and scale interaction

The carbon steel X65 used in this project has microstructure consisted of ferrite matrix with pearlite colonies (Figure 4.2). In CO₂ corrosion due to the anodic reaction preferential dissolution of iron (Fe²⁺) from pearlite colonies occurs, leaving behind the uncorroded Fe₃C phase (cementite) [237]. Simultaneously, calcium carbonate precipitation occurs in bulk and surface. At the same time the cathodic reactions occur (the most significant is considered the hydrogen-evolution reaction (Equation (2-29)) [51]. This reaction is influenced by the pH. As calcium carbonate forms on the surface (Figure 5.8), due to this formation (Equation (2-2 and (2-3)) it is providing an excess of hydrogen ions (H⁺) in the close vicinity to the sample which lowers the pH in this area (not whole bulk solution pH ≈6). In the systems where the high concentration of H⁺ is present the cathodic reaction is dominating (pH lower than 4). From Tafel measurements (Figure 5.1) it could be

observed that in calco-carbonic/ CO_2 corrosion environment, general corrosion is government by the cathodic reaction [51]. The values of Tafel slopes measured were as expected.

Figure 9.1 explains the early stages of interaction of calcium carbonate formation with carbon steel in CO_2 corrosion environment at 80°C . The metal sample as soon as is immersed in solution starts corroding and losing iron ions (Fe^{2+}) from the surface. The test solution is supersaturated with respect to calcium carbonate ($\text{SR} \approx 40$ Table 4.2), so nuclei start forming immediately at the beginning of the test. After 5 minutes of test the first crystals of calcium carbonate are forming in the bulk solution (Figure 5.6). It could be assumed that calcium carbonate crystals are forming on surface too (Figure 9.1 a), as the formation of crystals on the surface is government by primary heterogeneous nucleation. Primary heterogeneous nucleation is more predominant than primary homogeneous nucleation (which is associated with the formation of nuclei in the bulk solution (free of any particles or impurities) [31].

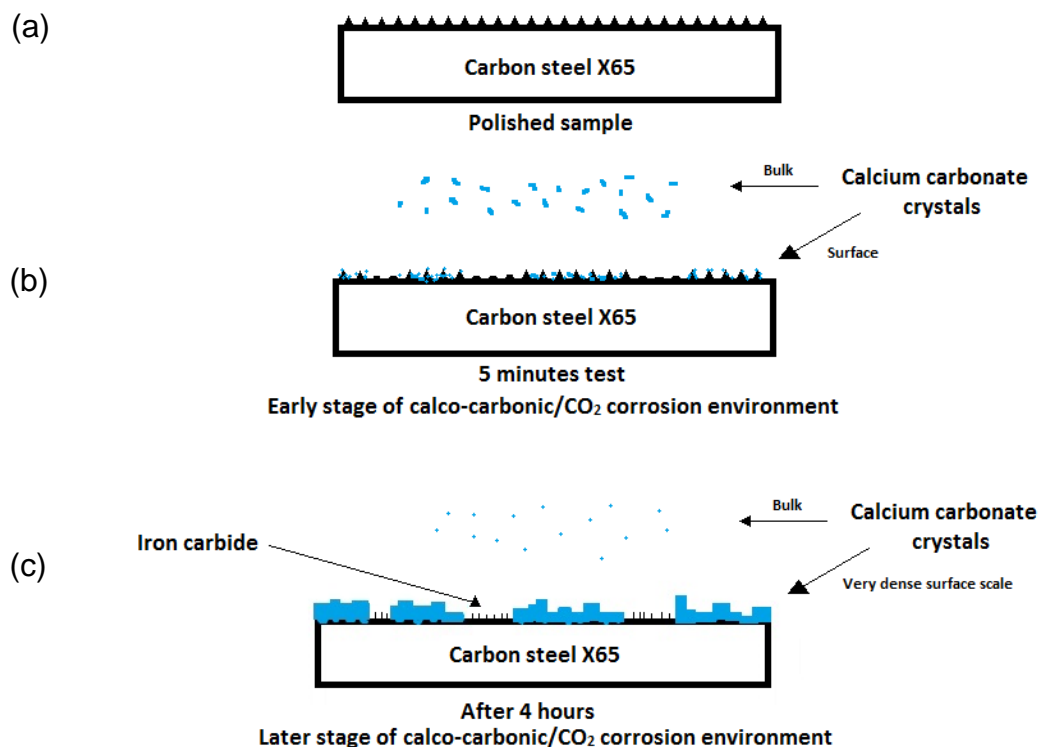


Figure 9.1: Scale and corrosion surface interaction in calco-carbonic/ CO_2 corrosion environment

For the remaining 4 hour tests calcium carbonate scale continues to precipitate on new sites on the sample and grows (Figure 9.1 c). This is supported by SEM images (Figure 5.8) which show that after 4 hours of the test most of the surface is covered with a dense calcium carbonate scale with some regions where the structure of uncorroded Fe_3C remains which looks like as uniform corrosion attack.

In Figure 9.2 explains that calcium carbonates favours precipitation on ferrite grains microstructure over pearlite grain. Ferrite (constituent part of pearlite) easily dissolves from pearlite grains due to anodic reaction in sweet corrosion. This reaction with cathodic reaction on cementite causes internal acidification, which will change the local pH and local water chemistry and create an environment in which there is a smaller probability of formation of calcium carbonate on the surface (calcium carbonate forms easily at a high pH – pH test solution are presented in Figure 5.7). This is supported by SEM image Figure 5.3 and light microscope image of microstructure Figure 4.2. In Figure 5.3 it could be observed that scale which precipitated on ferrite grains is was dense and protective as polishing marks are clearly visible. The metal dissolution sites are in good agreement with the pearlite microstructure on image in Figure 4.2.

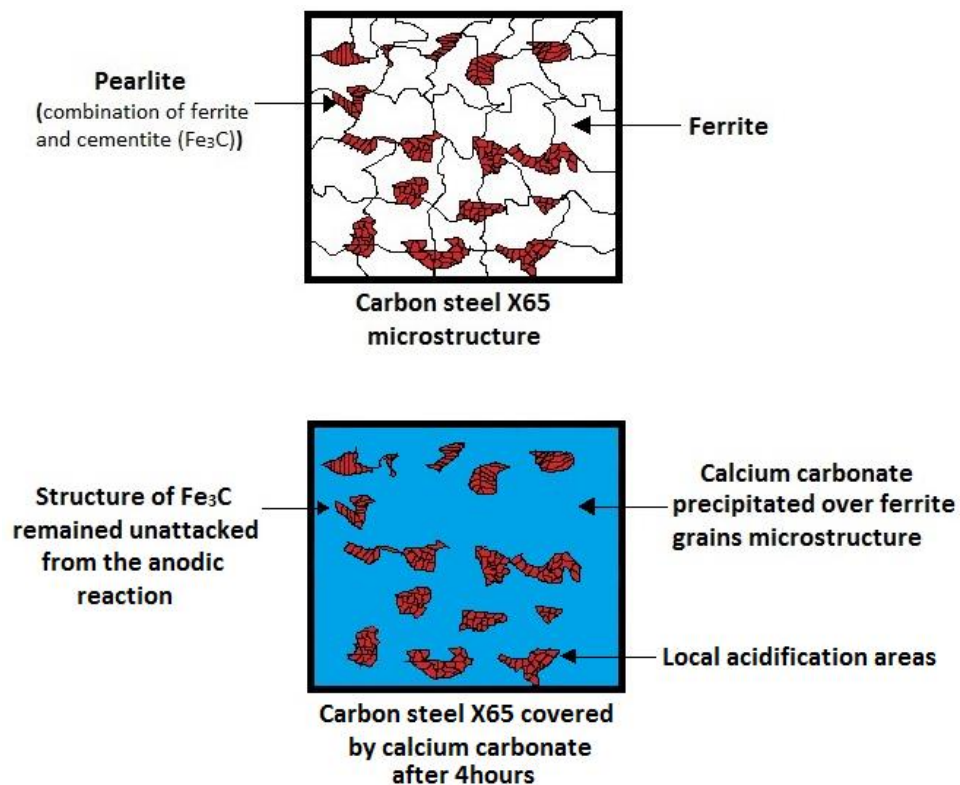


Figure 9.2: Preferential sites of formation calcium carbonate on carbon steel X65

Pearlite forms the preferential sites where the pitting corrosion initiates [237]. Calcium carbonate formation around perlite areas provide source of extra H^+ ions (not only from cathodic reaction in CO_2 corrosion). Calcium carbonate around pearlite make more difficult for solution from that recession/cavitation (pearlite areas) to mix with the rest of bulk solution and balance pH solution which cause internal acidification.

At the test condition (Table 4.6) which tests were run in the absence of the combined inhibitor, calcite (92% - Table 5.4) was main component of scale presented on the surface. The remaining 8 % of scale was aragonite.

9.3 Inhibition effect of single components of combined inhibitor on corrosion and scale processes in the environment where both processes occurs simultaneously

In this section, there are four main parts to discuss with respect to the of inhibition of the corrosion and scale in scale-corrosion system:

- CO_2 corrosion mechanism and inhibition by the single component in calco-carbonic environment
- Effect of the single component on formation of calcium carbonate
- The single component effect on localized corrosion
- A combined jar test/bubble cell as new method of assessment of inhibitors in corrosion and scale system

In order to assess the effect of the single component of combined inhibitor, the following parameters were assessed: general corrosion rate, pit depth, induction time of formation calcium carbonate crystals in bulk solution, maximum turbidity, amount of scale formed on the surface and amount of calcite in surface scale.

9.3.1 Effect of 2-mercaptoethanol (souring agent) on corrosion and scale processes in the environment where both processes occurs simultaneously

In Figure 9.3 results are presented which shows the effect of 2-mercaptoethanol on the corrosion and scale processes and results from uninhibited tests. In Figure 9.3 it could be observed that in the tests with 2-mercaptoethanol final corrosion rate was 0.1 mm/year. It was 2 times smaller than in the test without the single components. In the test without the single components the corrosion rate was lowered by the dense calcium carbonate formed on the sample surface (Figure 5.8) while in the tests with

2-mercapthoethanol the inhibition of general corrosion is caused by the adsorption of 2-mercapthoethanol to the metal surface. 2-mercapthoethanol reacted with the metals sample surface seconds after immersion in the test solution. This is evident after comparison of the initial general corrosion rate of tests with 2-mercapthoethanol - 0.72 mm/year (Figure 6.3) and uninhibited tests - 3.6 mm/year (Figure 5.2). The sample surface was covered by a dense film of 2-mercapthoethanol (Figure 9.4) with some small voids in the film formed where tiny crystals of calcium carbonate formed.

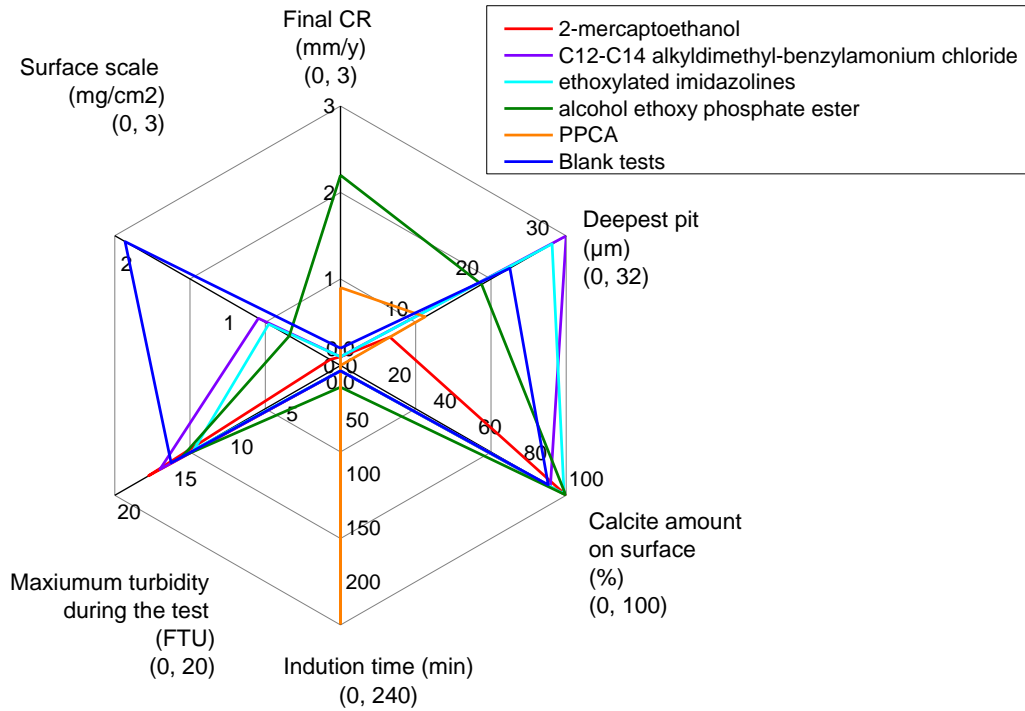


Figure 9.3: Results presenting effect of all single components on corrosion and scale processes

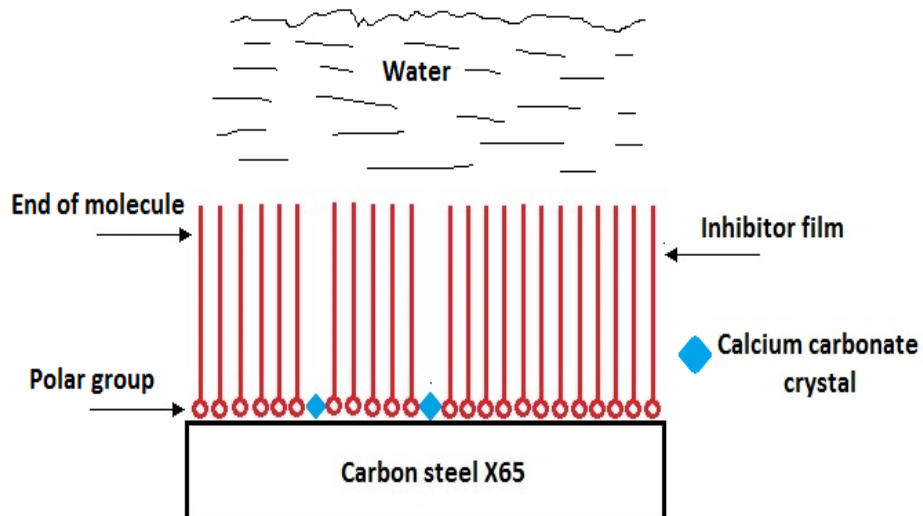


Figure 9.4: Schematic of film formed by 2-mercapthoethanol

Confirmation of that observation can be observed on SEM image presented in Figure 6.7a. In that figure it could be observed that the surface of the metal surface was well protected by film of 2-mercapthoethanol formed on the surface as the polishing marks are still visible on the surface. This is in good agreement with findings in the literature [238, 239].

From Tafel measurements (Figure 6.1) it could be observed that in calco-carbonic/CO₂ corrosion environment, general corrosion in the presence of the 2-mercapthoethanol is governed by the cathodic reaction. 2-mercapthoethanol affected both an anodic and cathodic reaction compared to the tests without the single components. However, 2-mercapthoethanol had greater effect on the anodic reaction than cathodic reaction. It also shifts E_{corr} to more cathodic potential -700 mV compared to blank test -684 mV (Table 6.1).

In Figure 6.7a it could be observed that scale crystals which precipitated on samples in the test with 2-mercapthoethanol are really small with the biggest crystal diameter around 10 µm. The crystals are spread all over the sample. Even though 2-mercapthoethanol did not completely prevent surface scale deposition (0.082 mg/cm² - Figure 6.6), it significantly reduced the amount of scale compared to the blank test (2.14 mg/cm² - Table 5.3). This confirms that 2-mercapthoethanol adsorbed quickly on the metal surface and formed a dense film which gave some protection against surface scaling.

2-mercapthoethanol has a great effect on the depth of the pit. It was able to reduce the depth of the pit more than 3 times; in the blank test pits were 24 µm of deep (Table 5.1) compared to only 7 µm in the tests with 2-mercapthoethanol (Table 6.2). In the literature was reported two different effects of 2-mercapthoethanol on pitting corrosion. Baker *et al.* [238] reported that 2-merapthoethanol caused pitting, while Jovancicevic *et al.* [188] reported good inhibition of pitting corrosion. In the blank tests, scale has played important role in localised corrosion. In the tests with 2-mercapthoethanol, which formed dense film on surface during the tests and reduced significantly amount of scale formed on the surface; 2-mercapthoethanol decreased the pit depth.

Dense film of 2-mercapthoethanol which formed on the surface has affected polymorph of calcium carbonate which precipitated on the sample. Calcite was only polymorph which precipitated on sample in the tests with 2-mercapthoethanol and this is a finding made for the first time.

The crystals which formed on the metal surface have rounded surfaces which could suggest that 2-mercapthoethanol interferes with crystal growth sites (crystal distortion effect). However, the results from FTIR and Raman analysis showed that no residual inhibitor part of 2-mercapthoethanol adsorbed to calcium carbonate crystals (Figure 8.2 and Figure 8.5). 2-mercapthoethanol did not affect induction time as well as amount of scale formed in the bulk solution which would suggest that has no effect on nucleation process.

9.3.2 Effect of alcohol ethoxy phosphate ester (corrosion inhibitor 1), C12-C14 alkyldimethyl-benzylamonium chloride (corrosion inhibitor 2) and ethoxylated imidazolines (corrosion inhibitor 3) on corrosion and scale processes in the environment where both processes occurs simultaneously

In Figure 9.3 results are presented of effect of corrosion inhibitor 1, 2 and 3 on corrosion and scale processes and results from uninhibited tests. In Figure 9.3 it could be observed that in the tests with alcohol ethoxy phosphate ester the final corrosion rate was 2.23 mm/year (It was 10 times higher than in the test without the single components). While in the test with C12-C14 alkyldimethyl-benzylamonium chloride and ethoxylated imidazolines was 0.06 and 0.09 mm/year.

In the test without the single components the corrosion rate was lowered by the dense calcium carbonate formed on the sample surface (Figure 5.3). In Figure 6.3 could be observed that general corrosion trend in the tests with C12-C14 alkyldimethyl-benzylamonium chloride and ethoxylated imidazolines are very similar to general corrosion trend in the blank tests presented in Figure 5.2. Which suggested that the mainly inhibition in the tests with C12-C14 alkyldimethyl-benzylamonium chloride and ethoxylated imidazolines are caused by the formation of calcium carbonate scale on the metal surface followed by some adsorption of the single component to reduce the general corrosion (Figure 9.5) below corrosion measured in the uninhibited tests – 0.2 mm/year (Figure 5.2). Dense film of calcium carbonate is presented in the Figure 6.7c and d.

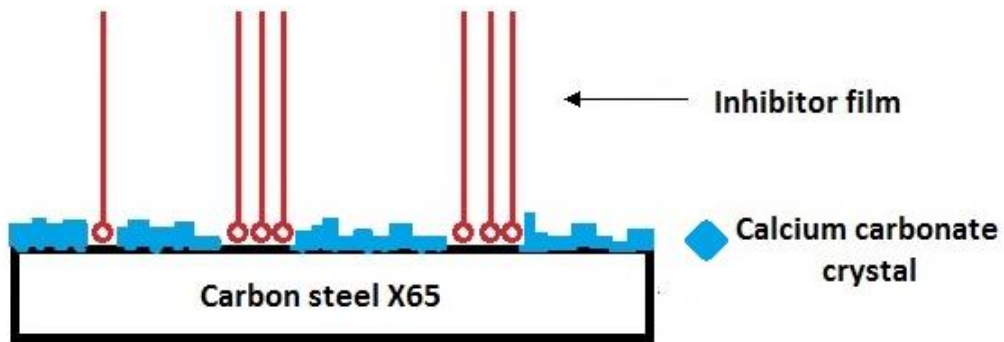


Figure 9.5: Schematic of film formed by C12-C14 alkyldimethylbenzylammonium chloride and ethoxylated imidazolines

Different situation was observed in the tests with alcohol ethoxy phosphate ester the inhibition of general corrosion is caused first by the adsorption of alcohol ethoxy phosphate ester to the metal surface and followed by formation of calcium carbonate scale. Alcohol ethoxy phosphate ester reacted with the metals sample surface seconds after immersion in it to tests solution [182]. This is evident after comparison of the initial general corrosion rate of tests with alcohol ethoxy phosphate ester - 1.77 mm/year (Figure 6.3) and uninhibited tests - 3.6 mm/year (Figure 5.2). The sample surface was cover by film of alcohol ethoxy phosphate ester with some voids in the film formed where crystals of calcium carbonate formed. Confirmation of that observation can be made from SEM image presented in Figure 6.7b. In that figure it could be observed that the surface of the metal surface was not protected by film of alcohol ethoxy phosphate ester formed on the surface as some deterioration of the metal surface could be observed. In the literature was reported that imidazoline [240] and phosphate ester [239] are very effective inhibitors against general corrosion.

Alcohol ethoxy phosphate ester and ethoxylated imidazolines are considered as oil soluble inhibitor [237, 241]. While C12-C14 alkyldimethylbenzylammonium chloride is considered as water soluble inhibitor [241]. Oil phase would form with long chain hydrocarbons barrier which would better protection against corrosion and scale (Figure 9.6). Even though alcohol ethoxy phosphate ester adsorbed immediately to the surface, it could not offer good protection against general corrosion.

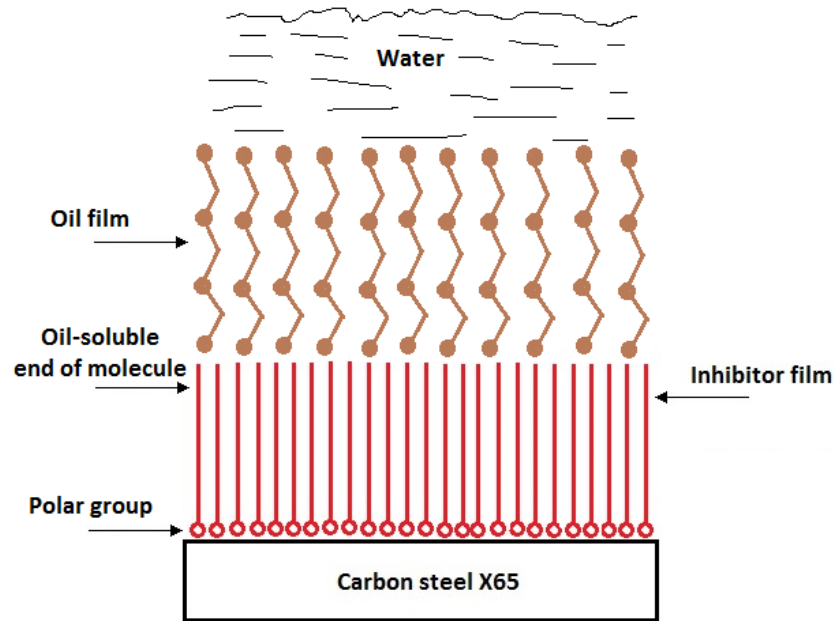


Figure 9.6: Schematic of inhibitor film formation in presence of oil [241]

From Tafel measurements (Figure 6.1 and Figure 6.2) it could be observed that in calco-carbonic/CO₂ corrosion environment, general corrosion in the presence of corrosion inhibitor 1, 2 and 3 is government by the cathodic reaction. Alcohol ethoxy phosphate ester, C12-C14 alkyldimethylbenzylamonium chloride and ethoxylated imidazolines affected both an anodic and cathodic reaction compare to the tests without the single components. However, all corrosion inhibitors had slightly bigger effect on the cathodic reaction than anodic reaction. C12-C14 alkyldimethylbenzylamonium chloride shifted E_{corr} to the most cathodic potential -700 mV than ethoxylated imidazolines -698 mV and alcohol ethoxy phosphate ester -690 mV compare to blank test -684 mV (Table 6.1).

In Figure 6.7b, c and d it could be observed that scale crystals which precipitated on samples in the test with all corrosion inhibitors. In the test with alcohol ethoxy phosphate ester, crystals were big with the average crystal diameter around 100 μm and were spread all over the sample. Different situation was observed in the test with C12-C14 alkyldimethylbenzylamonium chloride and ethoxylated imidazolines; in these tests small crystals with the average diameter around 20 μm and 30 μm accordingly formed on the surface and which covered almost whole the sample. Even though alcohol ethoxy phosphate ester, C12-C14 alkyldimethylbenzylamonium chloride and ethoxylated imidazolines did not prevent of the surface scale deposition it reduced amount of scale formed (0.47 mg/cm^2 , 0.83 mg/cm^2 , 0.69 mg/cm^2 - Figure 6.6 accordingly) compare to the blank test

(2.14 mg/cm²). As Alcohol ethoxy phosphate ester adsorbed really fast to the metal surface offered the best protection against surface scale deposition and confirms that did not form dense film on metal surface.

From alcohol ethoxy phosphate ester, C12-C14 alkyldimethyl-benzylammonium chloride and ethoxylated imidazolines only the first corrosion inhibitor reduced slightly the pit depth 19 μm , 32 μm and 30 μm accordingly (Table 6.2) compare to the test blank test 24 μm (Table 5.1). In the literature was reported that phosphate ester and imidazoline showed good inhibition of pit propagation [240], where in this thesis only phosphate ester showed small pitting corrosion inhibition. As was predominantly observed that scale has played an important role in localised corrosion in the blank tests, a similar situation was observed here with alcohol ethoxy phosphate ester. When big crystals formed close to each other, crystals form an environment between them where the solution pH was low due to formation of scale and corrosion processes and release H^+ ions. Scale crystals which surround that area make it difficult for the solution to mix with the rest of the bulk solution and balance pH solution which causes internal acidification. It would appear that this is an environment conducive for pit initiation (Figure 9.7).

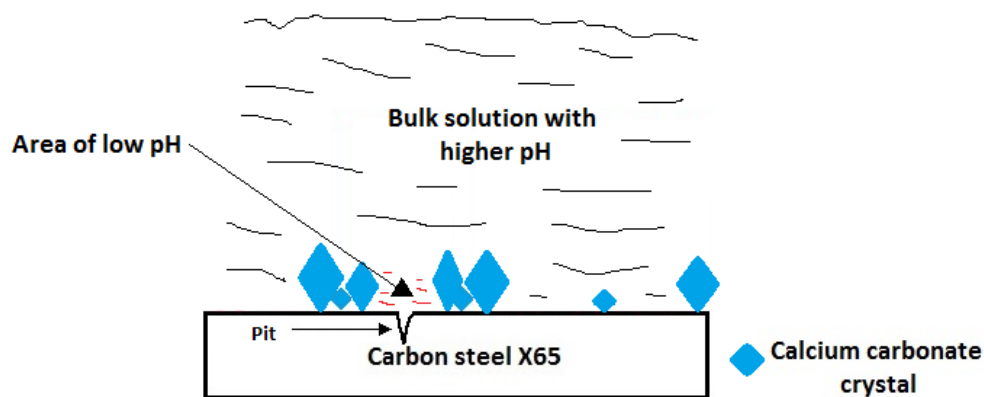


Figure 9.7: Pit corrosion in the test with alcohol ethoxy phosphate ester

Scale in the tests with C12-C14 alkyldimethyl-benzylammonium chloride and ethoxylated imidazolines precipitated in similar fashion as in the blank tests. Dense scale precipitated on ferrite grains leaving pearlite unprotected. Pearlite is preferential site in which the pitting corrosion initiates [237]. Calcium carbonate around perlite make more difficult for solution from that recession (pearlite areas) to mix with the rest of bulk solution and balance pH solution which cause internal acidification. Chlorides are compounds (C12-C14 alkyldimethyl-benzylammonium chloride) containing the element chlorine which, when it gains an electron and thus a negative charge, forms

the chloride ion. Chlorides ions play very important role of inducing pitting corrosion so this could explain deeper pit depth than in ethoxylated imidazolines and the blank tests.

From all corrosion inhibitors, the alcohol ethoxy phosphate ester affects the polymorph of calcium carbonate which precipitated on the sample the most. Calcite (99.8%) was almost the only polymorph which precipitated on the sample in the tests with alcohol ethoxy phosphate ester (0.2% aragonite) compare to blank test surface scale composition - calcite 92% and aragonite 8%. The ethoxylated imidazolines has a slightly smaller effect on the polymorph formed on the metal surface - 99% calcite and 1% aragonite. Scale composition in the tests with C12-C14 alkyldimethyl-benzylamonium chloride - 93% calcite and 7% aragonite is very similar to the blank test.

The crystals which formed on the metal surface in the test with alcohol ethoxy phosphate ester have rounded surfaces and have a lot of step-like edges which suggest that alcohol ethoxy phosphate ester interferes with crystal growth sites (crystal distortion effect). The crystals which formed on the metal surface in the tests with C12-C14 alkyldimethyl-benzylamonium chloride and ethoxylated imidazolines have similar size and shape more cubic than in the blank tests.

However, the results from FTIR and Raman analysis showed that no residual inhibitor part of alcohol ethoxy phosphate ester, C12-C14 alkyldimethyl-benzylamonium chloride and ethoxylated imidazolines adsorbed to calcium carbonate crystals (Figure A.0.5, Figure A.0.6, Figure A.0.7, Figure 0.5, Figure 0.6 and Figure 0.7).

9.3.3 Effect of polyphosphinocarboxylic acid (PPCA – scale inhibitor) on corrosion and scale processes in the environment where both processes occurs simultaneously

In Figure 9.3 results are presented of effect of PPCA on corrosion and scale processes and results from uninhibited tests. In Figure 9.3 it could be observed that in the tests with PPCA final corrosion rate was 0.9 mm/year. It was more than 4 times higher than in the test without the single components (Figure 5.2). In the test without the single components the corrosion rate was lower by the dense calcium carbonate formed on the sample surface (Figure 5.3) while in the tests with PPCA the inhibition of general corrosion is caused only by the adsorption of PPCA to the metal surface (Figure 6.7e). PPCA reacted with the metals sample surface seconds after immersion in it to tests solution. This is evident after comparison of the initial general corrosion rate

of tests with PPCA - 1.51 mm/year (Figure 6.3) and uninhibited tests - 3.6 mm/year (Figure 5.2). PPCA film formation on metal surface is enhanced by electrochemical activity (cathodic sides) of sample surface and Ca^{2+} ions play important role by facilitating the transport and adsorption of the inhibitor [242]. In Figure 6.7d it could be observed that the surface of the metal surface was protected by film of PPCA formed on the surface as the polishing marks are still visible on the surface.

From Tafel measurements (Figure 6.2) it could be observed that in calcocarbonic/ CO_2 corrosion environment, general corrosion in the presence of the PPCA is governed by the cathodic reaction. PPCA affected both an anodic and cathodic reaction compare to the tests without the single components. However, PPCA had greater effect on the cathodic reaction than anodic reaction. And it shift E_{corr} to slightly more anodic potential -680 mv compare to blank test -684 mv (Table 6.1).

In Figure 6.7d it could be observed that scale did not precipitated on samples in the test with PPCA. As PPCA is nucleation inhibitor, it prevent completely of the surface scale deposition (0 mg/cm^2 - Figure 6.6) compare to the blank test (2.14 mg/cm^2).

As no scale formed on the metal surface it was impossible to determine what polymorphs would precipitate in the tests condition present in the Error! eference source not found. and presence of PPCA.

The results from FTIR and Raman analysis showed that no residual inhibitor part of PPCA adsorbed to calcium carbonate crystals (Figure A.0.8 and Figure 0.8). PPCA had great effect on induction time (more than 240 minutes) as well as amount of scale formed in the bulk solution (no scale detected) which confirms that is working as nucleation inhibitor.

PPCA has great effect on the depth of the pit. It was able reduce reduced depth of the pit 2 times, in the blank test pit has 24 μm of depth compare to only 12 μm pit depth in the tests with PPCA. As it was observed that scale has played important role in localised corrosion in the blank tests but PPCA by preventing of scale formed on the sample and by forming film on surface with facilitation of calcium ions during the tests decreased the pit depth.

9.4 Effect of single components and their interactions on the corrosion and scale processes

In the following section the contribution of the single components – when all are blended as a combined inhibitor and their interactions to inhibition of

general corrosion, pitting corrosion, bulk scaling and surface scaling is discussed. With the help the ANOVA analysis method the individual effects and interactions were studied.

The final part of this section will discuss the empirical equations (model) developed to predict the corrosion and scale damage when the single components are present in the system.

9.4.1 Effect of single components and their interactions on general corrosion inhibition

Variable have higher effect when the sum of square is high. Higher effects are more significant, for example 10% contribution by a two-level factor means that factor is responsible for 1/10 of the total information in the data generated.

The results of ANOVA analysis in Table 7.9 shown that 2-mercaptoethanol – SA (10%) has the highest effect on the inhibition of general corrosion from all the single components when all together are blended as combined inhibitor. Then alcohol ethoxy phosphate ester - CI1 (9.7%) and polyphosphino carboxylic acid (PPCA) – SI (7.2%) has great effect on inhibition. The interaction between SA and CI1 (9.5%) has the greatest effect on inhibition from all interactions. The greatest effect between 3 single components CI1, SI and SA has contributed 8.6% to inhibition. All parameters which contributed significantly (above 7% in this study) to the inhibition of the general corrosion has contribution sum equal almost 62%. Which means that 3 factors and 4 of their interactions between them are responsible for more than 60% information generated in this a two-level factor system. The rest of factors and their interactions (25 together) are only responsible for 38% of generated data.

The explanation why these components (SA, CI1 and SI) have such a big effect is in their reactivity with the surface of the sample. They reacted immediately with the sample surface offering protection against general corrosion which could be observed on Figure 6.3. 2-mercapthoethanol (SA) and alcohol ethoxy phosphate ester (CI1) shifted E_{corr} to more cathodic potential would suggest that are anodic inhibitors which is in agreement with the literature [179, 188]. On the other side PPCA shifted slightly E_{corr} to more anodic potential would suggest that is cathodic inhibitor which is in agreement with the literature in which was suggested that is film formation on metal surface is enhanced by electrochemical activity (cathodic sides) of sample surface and Ca^{2+} ions play important role by facilitating the transport

and adsorption of the inhibitor [242]. In the literature was pointed that mercapthoethanol has synergistic effect with imidazoline on the general corrosion [188], however in this study no significant interaction between SA and CI3 (ethoxylated imidazoline) and effect on general corrosion was observed.

Combined inhibitors are most effective when they contain anodic and cathodic inhibitors because they are effecting both corrosion reactions.

As these three single components reacted really fast with metal surface covering with dense film, they did not leave to much free sites (anodic and cathodic) on the metal for the remain components to adsorb to the surface and have some effect on the general corrosion rate.

9.4.2 Effect of single components and their interactions on localized corrosion inhibition

The results of ANOVA analysis in Table 7.10 shown that 2-mercaptoethanol – SA (34.2%) has the highest effect on the inhibition of localized corrosion from all the single components when all together are blended as combined inhibitor, this is a finding made for the first time. Then alcohol ethoxy phosphate ester - CI1 (18.1%) has great effect on inhibition of localized. The interaction between SA and CI1 (10.9%) has the greatest effect on inhibition effect on localized corrosion from all interactions. All parameters which contributed significantly (above 7% in this study) to the inhibition of the localized corrosion has contribution sum equal almost 64%. Which means that 2 factors and interactions between them are responsible for more than 60% information generated in this a two-level factor system. The rest of factors and their interactions (29 together) are only responsible for 36% of generated data.

It is suggested that mercapthoethanol is inhibiting corrosion by formation not very soluble salt complex with iron [188]. While it is suggested that the phosphate ester is transported to the metal surface to perform complexes with Fe^{2+} and form iron phosphate and absorbed at the pitting site, which reduces the iron dissolution and stops further pitting propagation. Better effectiveness of the 2-mercapthoethanol against localized corrosion than alcohol ethoxy phosphate ester could explain by the difference of the chemical structure of the single components as these two single components inhibits anodic reaction.

2-mercapthoethanol is much smaller molecule than alcohol ethoxy phosphate ester which contain long chain of hydrocarbon, so it easier for 2-

mercapthoethanol to penetrate the pit and inhibit anodic reaction inside the pit (Figure 9.8).

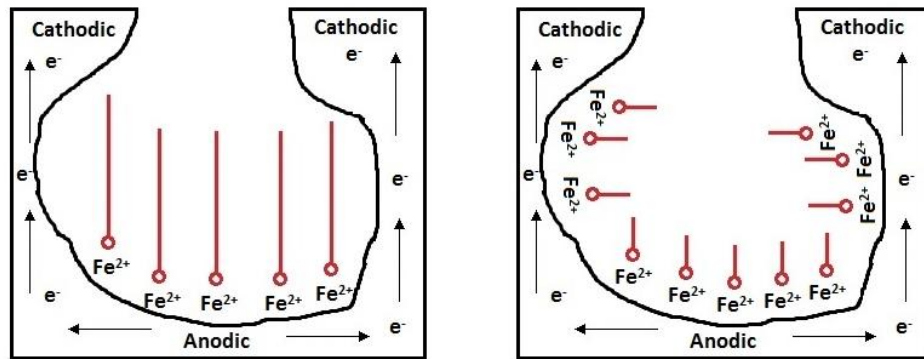


Figure 9.8: Schematic of inhibition of pits by a) alcohol ethoxy phosphate ester and b) 2-mercapthoethanol

2-mercapthoethanol was very effective against pitting corrosion in the tests with only single components while alcohol ethoxy phosphate ester did not reduce pitting significantly in that test. However it should be pointed out that in the test with ethoxy phosphate ester a significant role in pitting corrosion was played by surface scale.

9.4.3 Effect of single components and their interactions on bulk scaling inhibition

The results of ANOVA analysis in Table 7.11 shown that polyphosphino carboxylic acid (PPCA) – SI (81.6%) has the highest effect on the inhibition of bulk scale from all the single components when all together are blended as combined inhibitor. Only SI contributed significantly - above 7% in this study - to the inhibition of the bulk scale. Which means that 1 factor (SI) is responsible for more than 81% information (inhibition) generated in this a two-level factor system. The rest of factors and their interactions (31 together) are only responsible for 18% of generated data (inhibition).

PPCA mechanisms of calcium carbonate inhibition are by delays nucleation by complexation with Ca²⁺ ions and retard the crystals growth. In this study, results showed that PPCA is very effective against bulk scaling and this is in good agreement with the result found in the literature [109] where is pointed that PPCA increases the induction time of scale formation in the bulk solution.

In this study could be observed that PPCA prevent bulk scaling efficiently when it was present in the test solution as single components and when it was mixed with other single components and added as combined inhibitor to the test solution.

The results suggest that PPCA performance against bulk scaling is not affected by the present of other single components (alcohol ethoxy phosphate ester, 2-mercapthoethanol, alkyl dimethyl benzyl-amonium chloride and ethoxylated imidazolines) used in this study.

9.4.4 Effect of single components and their interactions on surface scaling inhibition

The results of ANOVA analysis in Table 7.12 shown that polyphosphino carboxylic acid (PPCA) – SI (43.5%) has the highest effect on the inhibition of surface scale from all the single components when all together are blended as combined inhibitor. Then alcohol ethoxy phosphate ester - CI1 (8.1%) has great effect on inhibition of localized. The interaction between SI and CI1 (7.9%) has the greatest effect on inhibition effect on surface scale from all interactions. All parameters which contributed significantly (above 7% in this study) to the inhibition of the localized corrosion has contribution sum equal almost 60%. Which means that 2 factors and interactions between them are responsible for 60% information generated in this a two-level factor system. The rest of factors and their interactions (29 together) are only responsible for 40% of generated data.

PPCA is effective against surface deposition as was showed in the literature [116, 117]. It was pointed that 5ppm of PPCA was able completely prevent the scale build up in the tube blocking test [117]. In this study 92% of scale which formed on surface was calcite (no inhibited test - Table 5.4) and PPCA suppress the calcite formation [116] so this could explain why PPCA has good surface scale inhibition in this study.

Alcohol ethoxy phosphate ester showed significant contribution to the inhibition of the surface scale in the test when all single components were blended together. However, from the results presented in the Table 7.5 could be observed that in the most of the test (run 7, 8, 22, 23, 27 and 29) where the higher concentration of the alcohol phosphate ester is added (PPCA is present in low concentration – Table 4.4) to the combined inhibitor; amount of scale formed on the surface is higher than in the same blend but with low concentration of alcohol ethoxy phosphate ester (accordingly to run mentioned above – run 3, 20, 11, 31, 1 and 21). This is visually presented on Figure 7.9 where could be observed that with increasing amount of the alcohol ethoxy phosphate ester in the test solution the amount of scale precipitated increase too.

9.4.5 Empirical equations (prediction model)

One of the most commonly used statistical techniques to predict unknown values between the known variable levels is linear regression. It is applied in this study to develop empirical corrosion and scale equations (prediction mode) based on the outputs collected under 32 testing conditions for tests condition presented in Table 4.4. Initial framework is done and improved prediction can be made by further experimental work by future studies. Example of linear regression model can be presented as the following empirical equation (Equation 6.4).

$$X = Y + Y*A + Y*B + Y*C + Y*D + Y*E + Y*AB + \dots \quad (9-1) \\ + Y*A*B*C*D*E$$

In which corrosion inhibitor 1, corrosion inhibitor 2, corrosion inhibitor 3, scale inhibitor and souring agent are set as A, B, C, D and E respectively. Based on the results (general corrosion) at 32 test conditions [X] (Table 4.4), the coefficients of the empirical equation [Y] can be calculated by the matrix algorithm (32x32 matrix).

The laboratory testing contribute built up a huge database to develop the empirical equation (prediction model) for future corrosion and scale prediction. The methodology for modelling was a linear regression method. This is the first attempt to build the skeleton of empirical equation which more and more experimental points can be added so the accuracy of the empirical equation (model) could be enhanced.

One function of this empirical equations (prediction model) are to show general corrosion, localised corrosion, bulk scaling and surface scale deposition over a range of different concentration inhibitors in tests. This will improve prediction for example scale condition on measured general corrosion in varied conditions.

The empirical equations (Equation (7-1) to Equation (7-4)) were developed and based on the coefficient calculated from ANOVA analysis and presented in the tables (Table 7.9 to Table 7.12).

The empirical equations and data were put to MatLab which is a technical computing environment for high performance numeric computation and visualization.

The visualization of this empirical equations developed in Matlab is presented in figures (Figure 7.3, Figure 7.5, Figure 7.7 and Figure 7.9).

Another function of these empirical equations (prediction modelling) could be tracking of the condition present in the pipelines transporting of oil when the different levels of inhibitors were measured in different point of time. These could be useful investigation tool for failure analysis.

Chapter 10 Conclusions

10.1 Introduction

In this chapter it will be presented the different findings arising from this work on corrosion and scale interaction in the system when this process occurs simultaneously and on the performance of different single components and combined inhibitor regarding corrosion and scale inhibition. Four main objectives were achieved:

- Evaluating the new developed a newly-developed combined bulk jar scaling/bubble cell as a method of assessing corrosion and scale interaction
- Evaluating the performance of single components of combined inhibitor on corrosion and scale process occurring simultaneously
- Evaluating the effects of the single components of the combined scale/corrosion inhibitor and/or synergistic effects on all four processes by experimental design method
- Developed empirical relation equation (model) for prediction corrosion and scale processes

10.2 Corrosion and scale process in the environment where both processes occurs simultaneously without presence of the inhibitor

- SEM analysis of specimens observed that the calcium carbonate film is dense and it is covering almost whole surface. Scale form mainly on ferrite grains microstructure leaving pearlite grains uncover and as favourite side for corrosion.
- General corrosion environment is government by the cathodic reaction and level of general corrosion was highly affected by formation of calcium carbonate scale on the surface.

- Calcium carbonate precipitation on the sample play important role of accelerating of pitting corrosion by providing suitable environment.
- XRD analysis observed that the calcium carbonate was mainly composed by calcite with small amount of aragonite.
- The methodology used in this study a newly-developed combined bulk jar scaling/bubble cell prove that is very effective tool in assessment of corrosion and scale interactions when they occurs simultaneously.

10.3 Inhibition effect of single components of combined inhibitor on corrosion and scale processes in the environment where both processes occurs simultaneously

- 2-mercapthoethanol showed excellent inhibition effect against the general corrosion and the localised corrosion by forming dense film on sample surface.
- 2-mercapthoethanol prevented almost completely of formation of calcium carbonate on the metal surface.
- XRD analysis observed that the calcium carbonate crystals which formed on the metal sample in the tests with 2-mercapthoethanol were calcite crystals only.
- Alcohol ethoxy phosphate ester had small effect of inhibition on general and localised corrosion.
- SEM analysis observed big crystals of calcium carbonate on the metal surface in the tests with alcohol ethoxy phosphate ester which play important role of accelerating of pitting corrosion by providing suitable environment.

- XRD analysis observed that the calcium carbonate crystals which formed on the metal sample in the tests with alcohol ethoxy phosphate ester were mainly calcite 99.8% crystals with small amount of aragonite.
- In the tests C12-C14 alkyldimethyl-benzylamonium chloride main inhibition of general corrosion is coming from formation of dense calcium carbonate scale.
- Calcium carbonate precipitation on the sample in the tests with C12-C14 alkyldimethyl-benzylamonium chloride play important role of accelerating of pitting corrosion by providing suitable environment.
- XRD observed that scale composition in the tests with C12-C14 alkyldimethyl-benzylamonium chloride was very similar to the test without inhibitor 93% calcite and 7% aragonite.
- In the tests ethoxylated imidazolines main inhibition of general corrosion is coming from formation of dense calcium carbonate scale.
- Calcium carbonate precipitation on the sample in the tests with ethoxylated imidazolines play important role of accelerating of pitting corrosion by providing suitable environment.
- XRD analysis observed that the calcium carbonate crystals which formed on the metal sample in the tests with ethoxylated imidazolines were mainly calcite 99% crystals with small amount of aragonite.

- Polyphosphinocarboxylic acid showed small inhibition effect against the general corrosion but good inhibition against the localised corrosion.
- Polyphosphinocarboxylic acid showed excellent inhibition effect against the surface scale and the bulk scale.

10.4 Effect of single components and their interactions on the corrosion and scale processes when their blend together as combined inhibitor

- 2-mercaptoethanol , alcohol ethoxy phosphate ester and polyphosphino carboxylic acid (PPCA) their interactions between them contributed more than 60% to general corrosion inhibition.
- 2-mercaptoethanol has the greatest effect on pitting corrosion inhibition (34.2%), as single component of combined inhibitor although alcohol ethoxy phosphate ester effect was also significant (18.7%).
- 2-mecaptoethonal and alcohol ethoxy phosphate ester showed great synergistic effect on inhibition on pitting corrosion (10.9%).
- Polyphosphino carboxylic acid contributed more than 80% to bulk scale inhibition.
- Polyphosphino carboxylic acid (43.5%) has the highest effect on the inhibition of surface scale from all the single components when all together are blended as combined inhibitor although alcohol ethoxy phosphate ester effect was also significant (8.1%). PPCA and alcohol ethoxy phosphate ester showed great synergistic effect on inhibition on pitting corrosion (7.9%).
- The simple linear regression model was developed to predict corrosion and scale when these processes occurs simultaneously.

Chapter 11

Future work

- It has been shown in this thesis that inhibitors which form dense film on the surface can prevent successfully scale deposition. This aspect of this study is important as the down-hole and pipe surfaces can be very hard to clear from any scale deposition. The next step should be investigation of formation of film of inhibitor onto a surface covered by scale deposit to reduce further scale agglomeration.
- The effect of calcium carbonate on pitting and inhibition of both these process are an interesting area and very important issue in field service. Further investigation needs to be done relating to gain a better understanding of the mechanism of failure due to these problems and inhibition.
- Improving newly-developed combined bulk jar scaling/bubble cell but addition of continuous monitoring of the bulk scaling and develop of sampling method of bulk scale crystals for further analysis. It would also be useful to create an system with a constant super saturation (SR).
- Modify the existing tube-blocking apparatus by build an electrochemical cell, turbidity meter and filter for bulk scale particles for a further evaluation of combined scale/corrosion inhibitors in flow system. This would provide much needed equipment for data collection on the effect of flow on the corrosion and scale process occurring simultaneously.
- The validation and the further development by adding different temperature range, use bigger variety of inhibitor concentration and addition of different inhibitors to the corrosion scale prediction tool.
- This model could be used to develop commercial software, which can provide general information of scale and corrosion process in different environments.

- It has been shown in this thesis that scale inhibitor provide good inhibition of localized corrosion and some inhibition of general corrosion. The next step should be investigation of different scale inhibitors chemistries effect on two processes mentioned above.
- Further research should consider testing different type of scale such as barium sulfate which is the second most common scale in oil and gas industry in the jar test/bubble cell.

List of References

1. EIA, U.S.E.I.A. *INTERNATIONAL ENERGY OUTLOOK 2011*. 2011 September 19, 2011.
2. Demadis, K.D., et al., *Industrial water systems: problems, challenges and solutions for the process industries*. Desalination, 2007. **213**(1–3): p. 38-46.
3. Hsu, C.S. and P.R. Robinson, *Practical advances in petroleum processing*2006, New York: Springer.
4. Tiab, D. and E. Donaldson, *Petrophysics*. Chemical, Petrochemical & Process2004: Elsevier Gulf. 1-880.
5. Pedersen, J.H. *Oil and gas geology*. 29/07/2012]; Available from: http://www.oilandgasgeology.com/oil_gas_window.jpg.
6. IQTeam. *United States Department of Energy*. 29/07/2012]; Available from: <http://energy.gov/>.
7. Speight, J.G., *Enhanced Recovery Methods for Heavy Oil and Tar Sands*, Gulf Publishing Company.
8. Frenier, W.W. and M. Ziauddin, *Formation, removal, and inhibition of inorganic scale in the oilfield environment*2008: Society of Petroleum Engineers.
9. Sorbie, K.S. and N. Laing, *How Scale Inhibitors Work: Mechanisms of Selected Barium Sulphate Scale inhibitors Across a Wide Temperature Range*, in *SPE International Symposium on Oilfield Scale*2004, Society of Petroleum Engineers Aberdeen, United Kingdom.
10. Parsons, S.A. and J. MacAdam, *Scaling On Heat Transfer Surfaces: Chemical Versus Non-chemical Control*, in *CORROSION 2004*2004, NACE International: New Orleans, La.
11. Kermani, M.B. and D. Harrop, *The Impact of Corrosion on Oil and Gas Industry*. SPE Production & Facilities, 1996.
12. Chilingar, G.V., R. Mourhatch, and G.D. Al-Qahtani, *Fundamentals of Corrosion and Scaling - For Petroleum and Environmental Engineers*, Gulf Publishing Company.
13. Feasey, N.D., et al., *Development and Deployment of Improved Performance "Green" Combined Scale/Corrosion Inhibitor for Subsea and Topside Application, North Sea Basin*, NACE International.
14. Sallis, J.D., Juckes W., and Anderson M.E., *"Phosphocitrate - Potential to influence Deposition of Scaling ions and Corrosion"*, in *Mineral Scale and Inhibition*, Z. Amjad, Editor 1995, Plenum Press: New York.
15. Foss, M., Seiersten M., and Nisancioglu K., *Interaction Between Scale Inhibitors and FeCO₃ Precipitation on Carbon Steel*, in *SPE International Oilfield Corrosion Symposium 2006*, Society of Petroleum Engineers Aberdeen, UK.
16. Collins, I.R., et al., *The Development of a Novel Environmentally Friendly Dual Function Corrosion and Scale Inhibitor*, in *SPE International Symposium on Oilfield Chemistry*2001, Society of Petroleum Engineers Houston, Texas.

17. Patel S., *An Investigation of Sulphonated Polymers for Deposit and Corrosion Control*, in *NACE Conference 1998*, NACE International: San Diego Ca.
18. Sanders, L., et al., *Assessment of combined scale/corrosion inhibitors – A combined jar test/bubble cell*. *Journal of Petroleum Science and Engineering*, 2014. **118**(0): p. 126-139.
19. Hamrouni, B. and M. Dhahbi, *Calco-carbonic equilibrium calculation*. *Desalination*, 2003. **152**(1–3): p. 167-174.
20. Devos, O., et al., *Nucleation-Growth Process of Scale Electrodeposition Influence of the Supersaturation*. *Journal of The Electrochemical Society*, 2003.
21. Chen, T., A. Neville, and M. Yuan, *Calcium carbonate scale formation—assessing the initial stages of precipitation and deposition*. *Journal of Petroleum Science and Engineering*, 2005. **46**(3): p. 185-194.
22. Mullin, J.W., *Crystallization*. 4th ed 2001: Butterworth-Heinemann.
23. Luft, J.R. and G.T. DeTitta, *A method to produce microseed stock for use in the crystallization of biological macromolecules*. *Acta crystallographica*, 1999. **55**: p. 988-993.
24. Dalas, E. and P.G. Koutsoukos, *The effect of magnetic fields on calcium carbonate scale formation*. *Journal of Crystal Growth*, 1989. **96**(4): p. 802-806.
25. Jones, A.G., *Crystallization Process Systems* 2002: Elsevier.
26. Söhnel, O. and J.W. Mullin, *Precipitation of calcium carbonate*. *Journal of Crystal Growth*, 1982. **60**(2): p. 239-250.
27. Söhnel, O. and J.W. Mullin, *Interpretation of crystallization induction periods*. *Journal of Colloid and Interface Science*, 1988. **123**(1): p. 43-50.
28. Gill, J.S. and G.H. Nancollas, *Kinetics of growth of calcium sulfate crystals at heated metal surfaces*. *Journal of Crystal Growth*, 1980. **48**(1): p. 34-40.
29. Tomson, M.B., *Effect of precipitation inhibitors on calcium carbonate scale formation*. *Journal of Crystal Growth*, 1983. **62**(1): p. 106-112.
30. Davis, R.V., et al., *The Use of Modern Methods in the Development of Calcium Carbonate Inhibitors for Cooling Water Systems*, in *Mineral Scale Formation and Inhibition*, Z. Amjad, Editor 1995, Springer US. p. 33-46.
31. Chen, T., et al., *Influence of PPCA inhibitor on CaCO₃ scale surface deposition and bulk precipitation at elevated temperature*. *Progress in Natural Science*, 2005. **15**(Green chemistry and future energy).
32. Vere, A.W., *Crystal growth : principles and progress*, New York: Plenum Press.
33. Nancollas, G.H., *The growth of crystals in solution*. *Advances in Colloid and Interface Science*, 1979. **10**(1): p. 215-252.
34. Kaeding, J., *W. Stumm und J. J. Morgan: Aquatic Chemistry An Introduction Emphasizing Chemical Equilibria in Natural Waters*. New York, London, Sydney, Toronto, Wiley-Interscience, 1970, 583 S., *zahlr. Abb. und Tab. Acta hydrochimica et hydrobiologica*, 1973. **1**(1): p. 117-117.

35. Noyes, A.A. and W.R. Whitney, *THE RATE OF SOLUTION OF SOLID SUBSTANCES IN THEIR OWN SOLUTIONS*. Journal of the American Chemical Society, 1897. **19**(12): p. 930-934.
36. Dieter, L., *Introduction*, in *Corrosion and Surface Chemistry of Metals*2007, EFPL Press. p. 1-13.
37. Stansbury, E.E.B.R.A., *Fundamentals of electrochemical corrosion*2000, Materials Park, OH: ASM International.
38. Kermani, M.B. and A. Morshed, *Carbon Dioxide Corrosion in Oil and Gas Production A Compendium*. Corrosion, 2003.
39. Hu, X., *The Corrosion and Erosion-Corrosion Behaviour of High Alloy Stainless Steels*, in *School of Mechanical Engineering*2003, University of Leeds.
40. Lytron. *Avoiding Galvanic Corrosion*. 2014 [2014/12/10]; Available from: <http://www.lytron.com/Tools-and-Technical-Reference/Application-Notes/Avoiding-Galvanic-Corrosion>.
41. Bradford, S.A., *Corrosion control*2001, Edmonton: CASTI Pub.
42. Tait, W.S., *An introduction to electrochemical corrosion testing for practicing engineers and scientists*1994, Racine, Wis.: PairODocs Publications.
43. Wang, C., *Erosion-corrosion mitigation using chemicals*, 2007, University of Leeds: Leeds.
44. Crow, D.R., *Principles and applications of electrochemistry*1998, Cheltenham: Stanley Thornes.
45. Scully, J.R., *Polarization Resistance Method for Determination of Instantaneous Corrosion Rates*. Corrosion, 2000.
46. Stern, M., *A Method for Determining Corrosion Rates from Linear Polarization Data*. Corrosion, 1958. **14**.
47. ASTM, *Calculation of Corrosion Rates and Related Information for Electrochemical Measurements*, in *ASTM-G1022*2010, ASTM: West Conshohocken, PA.
48. *Corrosion.Doctors*. [10/10/2014]; Available from: <http://www.corrosion-doctors.org/index.htm>.
49. de Waard, C. and D.E. Milliams, *Carbonic Acid Corrosion of Steel*. Corrosion Science, 1975. **31**(5): p. 131-135.
50. Linter, B.R. and G.T. Burstein, *Reactions of pipeline steels in carbon dioxide solutions*. Corrosion Science, 1999. **41**(1): p. 117-139.
51. Nescic, S., et al., *An Open Source Mechanistic Model For CO₂ / H₂S Corrosion Of Carbon Steel*, NACE International.
52. Bockris, J.O.M., D. Drazic, and A.R. Despic, *The electrode kinetics of the deposition and dissolution of iron*. Electrochimica Acta, 1961. **4**(2-4): p. 325-361.
53. Nescic, S., et al., *Electrochemical Properties of Iron Dissolution in the Presence of CO₂ - Basics Revisited*, NACE International.
54. Nešić, S., *Key issues related to modelling of internal corrosion of oil and gas pipelines – A review*. Corrosion Science, 2007. **49**(12): p. 4308-4338.
55. Bader, M.S.H., *Sulfate removal technologies for oil fields seawater injection operations*. Journal of Petroleum Science and Engineering, 2007. **55**(1-2): p. 93-110.
56. Moghadasi, J., et al., *Scale formation in Iranian oil reservoir and production equipment during water injection*, in *International*

- Symposium on Oilfield Scale*2003, Society of Petroleum Engineers: Aberdeen.
57. Ljerka, B. and K. Damir, *ChemInform Abstract: On Calcium Carbonates: From Fundamental Research to Application*. ChemInform, 2008. **39**(5).
 58. Tlili, M.M., et al., *Characterization of CaCO₃ hydrates by micro-Raman spectroscopy*. Journal of Raman Spectroscopy, 2002. **33**(1): p. 10-16.
 59. Brooks, R., *Calcium carbonate and its hydrates*1950: Royal Soc.
 60. Mukkamala, S.B., C.E. Anson, and A.K. Powell, *Modelling calcium carbonate biomineralisation processes*. Journal of Inorganic Biochemistry, 2006. **100**(5–6): p. 1128-1138.
 61. Brecevic, L. and D. Kralj, *On Calcium Carbonates: from Fundamental Research to Application*. Croatica Chemica Acta, 2007(80(3-4)): p. 467-484.
 62. Ni, M. and B.D. Ratner, *Differentiating calcium carbonate polymorphs by surface analysis techniques—an XPS and TOF-SIMS study*. Surface and Interface Analysis, 2008. **40**(10): p. 1356-1361.
 63. Helalizadeh, A., H. Müller-Steinhagen, and M. Jamialahmadi, *Mixed salt crystallisation fouling*. Chemical Engineering and Processing: Process Intensification, 2000. **39**(1): p. 29-43.
 64. Østvold, T. and P. Randhol, *Kinetics of CaCO₃ Scale Formation. The Influence of Temperature, Supersaturation and Ionic Composition*, Society of Petroleum Engineers.
 65. Alahmad, M., *Factors Affecting Scale Formation in Sea Water Environments – An Experimental Approach*. Chemical Engineering & Technology, 2008. **31**(1): p. 149-156.
 66. Kitamura, M., *Controlling factor of polymorphism in crystallization process*. Journal of Crystal Growth, 2002. **237–239**, Part 3(0): p. 2205-2214.
 67. Han, Y.S., et al., *Factors affecting the phase and morphology of CaCO₃ prepared by a bubbling method*. Journal of the European Ceramic Society, 2006. **26**(4–5): p. 843-847.
 68. Dyer, S.J. and G.M. Graham, *The effect of temperature and pressure on oilfield scale formation*. Journal of Petroleum Science and Engineering, 2002. **35**(1–2): p. 95-107.
 69. Hasson, D., et al., *Mechanism of Calcium Carbonate Scale Deposition on Heat-Transfer Surfaces*. Industrial & Engineering Chemistry Fundamentals, 1968. **7**(1): p. 59-65.
 70. Yang, Q., et al., *Investigation of induction period and morphology of CaCO₃ fouling on heated surface*. Chemical Engineering Science, 2002. **57**(6): p. 921-931.
 71. Gryta, M., *Alkaline scaling in the membrane distillation process*. Desalination, 2008. **228**(1–3): p. 128-134.
 72. Martinod, A.C., *An Integrated Study of CaCO₃ Formation and Inhibition*2008: University of Leeds (School of Mechanical Engineering).
 73. Amor, M.B., et al., *Influence of water hardness, substrate nature and temperature on heterogeneous calcium carbonate nucleation*. Desalination, 2004. **166**(0): p. 79-84.

74. Teng, H.H., P.M. Dove, and J.J. De Yoreo, *Kinetics of calcite growth: surface processes and relationships to macroscopic rate laws*. *Geochimica et Cosmochimica Acta*, 2000. **64**(13): p. 2255-2266.
75. Hu, Z. and Y. Deng, *Supersaturation control in aragonite synthesis using sparingly soluble calcium sulfate as reactants*. *Journal of Colloid and Interface Science*, 2003. **266**(2): p. 359-365.
76. Hu, Z. and Y. Deng, *Synthesis of needle-like aragonite from calcium chloride and sparingly soluble magnesium carbonate*. *Powder Technology*, 2004. **140**(1–2): p. 10-16.
77. Cheng, B., et al., *Preparation of monodispersed cubic calcium carbonate particles via precipitation reaction*. *Materials Letters*, 2004. **58**(10): p. 1565-1570.
78. Feng, B., A.K. Yong, and H. An, *Effect of various factors on the particle size of calcium carbonate formed in a precipitation process*. *Materials Science and Engineering: A*, 2007. **445–446**(0): p. 170-179.
79. Yu, J., et al., *Effects of PAA additive and temperature on morphology of calcium carbonate particles*. *Journal of Solid State Chemistry*, 2004. **177**(3): p. 681-689.
80. Cölfen, H. and L. Qi, *A Systematic Examination of the Morphogenesis of Calcium Carbonate in the Presence of a Double-Hydrophilic Block Copolymer*. *Chemistry – A European Journal*, 2001. **7**(1): p. 106-116.
81. Euvrard, M., C. Filiatre, and E. Crausaz, *A cell to study in situ electrocrystallization of calcium carbonate*. *Journal of Crystal Growth*, 2000. **216**(1–4): p. 466-474.
82. Dickinson, S.R., G.E. Henderson, and K.M. McGrath, *Controlling the kinetic versus thermodynamic crystallisation of calcium carbonate*. *Journal of Crystal Growth*, 2002. **244**(3–4): p. 369-378.
83. Herzog, R.E., et al., *Magnetic water treatment: the effect of iron on calcium carbonate nucleation and growth*. *Langmuir*, 1989. **5**(3): p. 861-867.
84. Katz, J.L., et al., *Calcite growth inhibition by iron*. *Langmuir*, 1993. **9**(5): p. 1423-1430.
85. Graham, G.M., R. Stalker, and R. McIntosh, *The Impact of Dissolved Iron on the Performance of Scale Inhibitors Under Carbonate Scaling Conditions*, Society of Petroleum Engineers.
86. Wada, N., K. Yamashita, and T. Umegaki, *Effects of divalent cations upon nucleation, growth and transformation of calcium carbonate polymorphs under conditions of double diffusion*. *Journal of Crystal Growth*, 1995. **148**(3): p. 297-304.
87. Wada, N., K. Yamashita, and T. Umegaki, *Effects of Silver, Aluminum, and Chrome Ions on the Polymorphic Formation of Calcium Carbonate under Conditions of Double Diffusion*. *Journal of Colloid and Interface Science*, 1998. **201**(1): p. 1-6.
88. Ghizellaoui, S., et al., *Inhibition of scaling in the presence of copper and zinc by various chemical processes*. *Desalination*, 2007. **206**(1–3): p. 185-197.
89. Zeppenfeld, K., *Prevention of CaCO₃ scale formation by trace amounts of copper (II) in comparison to zinc (II)*. *Desalination*, 2010. **252**(1–3): p. 60-65.
90. Lisitsin, D., et al., *Inhibition of CaCO₃ scaling on RO membranes by trace amounts of zinc ions*. *Desalination*, 2005. **183**(1–3): p. 289-300.

91. Berner, R.A., *The role of magnesium in the crystal growth of calcite and aragonite from sea water*. *Geochimica et Cosmochimica Acta*, 1975. **39**(4): p. 489-504.
92. Deleuze, M. and S.L. Brantley, *Inhibition of calcite crystal growth by Mg²⁺ at 100°C and 100 bars: Influence of growth regime*. *Geochimica et Cosmochimica Acta*, 1997. **61**(7): p. 1475-1485.
93. Lin, S.H. and S.C. Dexter, *Effects of Temperature and Magnesium Ions on Calcareous Deposition*. *Corrosion*, 1988. **44**(9): p. 615-622.
94. Kralj, D., et al., *Effect of Inorganic Anions on the Morphology and Structure of Magnesium Calcite*. *Chemistry-a European Journal*, 2004. **10**(7): p. 1647-1656.
95. Zhang, Y. and R.A. Dawe, *Influence of Mg²⁺ on the kinetics of calcite precipitation and calcite crystal morphology*. *Chemical Geology*, 2000. **163**(1-4): p. 129-138.
96. Chen, T., A. Neville, and M. Yuan, *Influence of Mg²⁺ on CaCO₃ formation—bulk precipitation and surface deposition*. *Chemical Engineering Science*, 2006. **61**(16): p. 5318-5327.
97. Chen, T., A. Neville, and M. Yuan, *Assessing the effect of Mg²⁺ on CaCO₃ on scale formation—bulk precipitation and surface deposition*. *Journal of Crystal Growth*, 2005. **275**(1-2): p. e1341-e1347.
98. Chen, T., A. Neville, and M. Yuan, *Influence of Mg²⁺ on initial stages of CaCO₃ scale formed on metal surface*. *Journal Name: MACROMOLECULES*; *Journal Volume: 38*; *Journal Issue: 1*, 2004: p. Medium: X; Size: Pages: 61 - 68.
99. Freedman, A., *Cooling water technology in the eighties*, in *NACE International Conference 1983*: Houston.
100. Chen, T., *New insights into the mechanisms of calcium carbonate mineral scale formation and inhibition*, in *School of Engineering and Physical Sciences 2005*, Heriot-Watt University: Edinburgh.
101. Jordan, M.M., et al., *The Use of Scale Inhibitor Squeeze Placement Software to Extend Squeeze Life and Reduce Operating Costs in Mature High Temperature Oilfields*, NACE International.
102. Cooper, K.G., et al., *The threshold scale inhibition phenomenon*. *Desalination*, 1979. **31**(1-3): p. 257-266.
103. Darton, E.G., *Scale inhibition techniques used in membrane systems*. *Desalination*, 1997. **113**(2-3): p. 227-229.
104. Tomson, M., et al., *Solution and Precipitation Chemistry of Phosphonate Scale Inhibitors*, in *Mineral Scale Formation and Inhibition*, Z. Amjad, Editor 1995, Springer US. p. 307-322.
105. He, S., A.T. Kan, and M.B. Tomson, *Inhibition of calcium carbonate precipitation in NaCl brines from 25 to 90°C*. *Applied Geochemistry*, 1999. **14**(1): p. 17-25.
106. Ketrane, R., et al., *Efficiency of five scale inhibitors on calcium carbonate precipitation from hard water: Effect of temperature and concentration*. *Desalination*, 2009. **249**(3): p. 1397-1404.
107. Tang, Y., et al., *Investigation of CaCO₃ scale inhibition by PAA, ATMP and PAPEMP*. *Desalination*, 2008. **228**(1-3): p. 55-60.
108. Reddy, M.M. and G.H. Nancollas, *Calcite crystal growth inhibition by phosphonates*. *Desalination*, 1973. **12**(1): p. 61-73.

109. Chen, T., A. Neville, and M. Yuan, *Effect of PPCA and DETPMP Inhibitor Blends on CaCO₃ Scale Formation*, Society of Petroleum Engineers.
110. Graham, G.M., L.S. Boak, and K.S. Sorbie, *The Influence of Formation Calcium and Magnesium on the Effectiveness of Generically Different Barium Sulphate Oilfield Scale Inhibitors*.
111. Yuan, M.D., E. Jamieson, and P. Hammonds, *Investigation of Scaling and Inhibition Mechanisms and the Influencing Factors in Static and Dynamic Inhibition Tests*, NACE International.
112. Jonasson, R.G., et al., *Effect of phosphonate inhibitors on calcite nucleation kinetics as a function of temperature using light scattering in an autoclave*. *Chemical Geology*, 1996. **132**(1–4): p. 215-225.
113. Lin, Y.-P. and P.C. Singer, *Inhibition of calcite crystal growth by polyphosphates*. *Water Research*, 2005. **39**(19): p. 4835-4843.
114. Giannimaras, E.K. and P.G. Koutsoukos, *The crystallization of calcite in the presence of orthophosphate*. *Journal of Colloid and Interface Science*, 1987. **116**(2): p. 423-430.
115. Senogles, E., W.O.S. Doherty, and O.L. Crees, *Scale inhibitors, polymeric*. *Encyclopedia of Polymer Science and Technology*, ed. J. Kroschwitz 1996, Boca Raton: Wiley-Interscience.
116. Chen, T., et al., *In-situ monitoring the inhibiting effect of polyphosphinocarboxylic acid on CaCO₃ scale formation by synchrotron X-ray diffraction*. *Chemical Engineering Science*, 2009. **64**(5): p. 912-918.
117. Smith, J.K., et al., *Performance of Scale Inhibitors under Carbonate and Sulfide Scaling Conditions*, Society of Petroleum Engineers.
118. Boak, L.S., *FACTORS THAT IMPACT SCALE INHIBITOR MECHANISMS*, in *Institute of Petroleum Engineering 2012*, Heriot-Watt University: Edinburgh.
119. Crabtree, M., et al., *Fighting Scale: Removal and Prevention*. *Oilfield Review*, 1999. **11**(3).
120. Graham, G.M., et al., *The Importance of Appropriate Laboratory Procedures for the Determination of Scale Inhibitor Performance*, in *International Symposium on Oilfield Scale 2002*, Society of Petroleum Engineers: Aberdeen, United Kingdom.
121. Tantayakom, V., et al., *Scale inhibition study by turbidity measurement*. *Journal of Colloid and Interface Science*, 2005. **284**(1): p. 57-65.
122. Turner, C.W. and D.W. Smith, *Calcium Carbonate Scaling Kinetics Determined from Radiotracer Experiments with Calcium-47*. *Industrial & Engineering Chemistry Research*, 1998. **37**(2): p. 439-448.
123. Reddy, M.M. and G.H. Nancollas, *The crystallization of calcium carbonate: I. Isotopic exchange and kinetics*. *Journal of Colloid and Interface Science*, 1971. **36**(2): p. 166-172.
124. Clarkson, J.R., T.J. Price, and C.J. Adams, *Role of metastable phases in the spontaneous precipitation of calcium carbonate*. *Journal of the Chemical Society, Faraday Transactions*, 1992. **88**(2): p. 243-249.
125. Grases, F. and J.G. March, *Determination of phosphate based on inhibition of crystal growth of calcite*. *Analytica Chimica Acta*, 1990. **229**(0): p. 249-254.

126. Verraest, D., et al., *Carboxymethyl inulin: A new inhibitor for calcium carbonate precipitation*. Journal of the American Oil Chemists' Society, 1996. **73**(1): p. 55-62.
127. Abdel-Aal, N. and K. Sawada, *Inhibition of adhesion and precipitation of CaCO₃ by aminopolyphosphonate*. Journal of Crystal Growth, 2003. **256**(1–2): p. 188-200.
128. Zhang, Y., et al., *The kinetics of carbonate scaling—application for the prediction of downhole carbonate scaling*. Journal of Petroleum Science and Engineering, 2001. **29**(2): p. 85-95.
129. O'Sullivan, C.K. and G.G. Guilbault, *Commercial quartz crystal microbalances – theory and applications*. Biosensors and Bioelectronics, 1999. **14**(8–9): p. 663-670.
130. Abdel-Aal, N., K. Satoh, and K. Sawada, *Study of Adhesion Mechanism of Calcareous Scaling by Using Quartz Crystal Microbalance Technique*. Analytical Sciences/Supplements, 2002. **17icas**: p. i825-i828.
131. Abdel-Aal, N., K. Satoh, and K. Sawada, *Study of the adhesion mechanism of CaCO₃ using a combined bulk chemistry/QCM technique*. Journal of Crystal Growth, 2002. **245**(1–2): p. 87-100.
132. Lédion, J., J.P. Leroy, and J.P. Labbé, *Détermination du caractère incrustant d'une eau par un essai d'entartrage accéléré*. TSM. L'eau, 1985. **80**: p. pp. 323–328.
133. Gabrielli, C., et al., *Characterization of the efficiency of antiscalant treatments of water Part I: Chemical processes*. Journal of Applied Electrochemistry, 1996. **26**(11): p. 1125-1132.
134. Deslouis, C., et al., *Impedance techniques at partially blocked electrodes by scale deposition*. Electrochimica Acta, 1997. **42**(8): p. 1219-1233.
135. Gabrielli, C., et al., *Study of calcium carbonate scales by electrochemical impedance spectroscopy*. Electrochimica Acta, 1997. **42**(8): p. 1207-1218.
136. Gabrielli, C., et al., *Nucleation and growth of calcium carbonate by an electrochemical scaling process*. Journal of Crystal Growth, 1999. **200**(1–2): p. 236-250.
137. Garcia, C., et al., *Study of the scale inhibition by HEDP in a channel flow cell using a quartz crystal microbalance*. Electrochimica Acta, 2001. **46**(7): p. 973-985.
138. Neville, A., T. Hodgkiess, and A.P. Morizot, *Electrochemical assessment of calcium carbonate deposition using a rotating disc electrode (RDE)*. Journal of Applied Electrochemistry, 1999. **29**(4): p. 455-462.
139. Morizot, A., A. Neville, and T. Hodgkiess, *Studies of the deposition of CaCO₃ on a stainless steel surface by a novel electrochemical technique*. Journal of Crystal Growth, 1999. **198–199, Part 1**(0): p. 738-743.
140. Palmer, A.C. and R.A. King, *Subsea pipeline engineering*2004, Tulsa: PennWell Corporation.
141. Davies, J.R., *Corrosion: Understanding the Basics*2000: Asm International.
142. Fontana, M.G., *Corrosion Engineering*2005: Tata McGraw-Hill.

143. *ASM Handbook - Formerly Ninth Edition, Metals Handbook -: Volume 13 : Corrosion*1987: ASM.
144. Schmitt, G. and M. Horstemeier, *Fundamental Aspects of CO₂ Metal Loss Corrosion - Part II: Influence of Different Parameters on CO₂ Corrosion Mechanisms*, NACE International.
145. Bretherton, N., et al., *Impact Of Acetic Acid On Weld Corrosion And Its Mitigation*, NACE International.
146. Harrop, D. and W.H. Durnie, *Our Water Chemistry Contains Organic Acids - So What Does it Mean?*, Society of Petroleum Engineers.
147. Gulbrandsen, E. and K. Bilkova, *Solution Chemistry Effects on Corrosion of Carbon Steels in Presence of CO₂ and Acetic Acid*, NACE International.
148. Dugstad, A., *Mechanism of Protective Film Formation During CO₂ Corrosion of Carbon Steel*, NACE International.
149. Dugstad, A., H. Hemmer, and M. Seiersten, *Effect of Steel Microstructure Upon Corrosion Rate and Protective Iron Carbonate Film Formation*, NACE International.
150. Tomson, M.B. and M.L. Johnson, *How Ferrous Carbonate Kinetics Impacts Oilfield Corrosion*, Society of Petroleum Engineers.
151. Crolet, J.L., N. Thevenot, and S. Netic, *Role of Conductive Corrosion Products on the Protectiveness of Corrosion Layers*, NACE International.
152. Schmitt, G. and M. Kriek-Defrain, *pH-Static Experiments in High Pressure CO₂ Corrosion of Steel. Effect on Scale Morphology and Chemical Composition, Corrosion Rate, Pitting Susceptibility and Inhibitor Performance*, in *11th International Corrosion Congress*1990: Florence, Italy. p. 529.
153. Netic, S., J. Lee, and V. Ruzic, *A Mechanistic Model of Iron Carbonate Film Growth and the Effect on CO₂ Corrosion of Mild Steel*, in *NACE conference*, NACE International: Denver, Co.
154. de Waard, C., U. Lotz, and D.E. Milliams, *Predictive Model for CO₂ Corrosion Engineering in Wet Natural Gas Pipelines*. *Corrosion*, 1991. **47**(12): p. 976-985.
155. López, D.A., T. Pérez, and S.N. Simison, *The influence of microstructure and chemical composition of carbon and low alloy steels in CO₂ corrosion. A state-of-the-art appraisal*. *Materials & Design*, 2003. **24**(8): p. 561-575.
156. Kermani, B., et al., *Development of Superior Corrosion Resistance 3%Cr Steels for Downhole Applications*, NACE International.
157. Clover, D., et al., *The influence of microstructure on the corrosion rate of various carbon steels*. *Journal of Applied Electrochemistry*, 2005. **35**(2): p. 139-149.
158. Al-Hassan, S., et al., *Effect of Microstructure on Corrosion of Steels in Aqueous Solutions Containing Carbon Dioxide*.
159. Esmaeely, S.N., et al., *Effect of Calcium on the Formation and Protectiveness of Iron Carbonate Layer in CO₂ Corrosion*, NACE International.
160. Zhao, G.-x., et al., *Formation Characteristic of CO₂ Corrosion Product Layer of P110 Steel Investigated by SEM and Electrochemical Techniques*. *Journal of Iron and Steel Research, International*, 2009. **16**(4): p. 89-94.

161. Xian, Z., et al., *Effect of Ca²⁺ and Mg²⁺ on CO₂ corrosion behavior of tube steel*. J. Iron. Steel Res. Int., 2005. **12**: p. 38-42.
162. Ding, C., K.-w. Gao, and C.-f. Chen, *Effect of Ca²⁺ on CO₂ corrosion properties of X65 pipeline steel*. International Journal of Minerals, Metallurgy and Materials, 2009. **16**(6): p. 661-666.
163. Frankel, G., *Pitting corrosion of metals a review of the critical factors*. Journal of The Electrochemical Society, 1998. **145**(6): p. 2186-2198.
164. Scully, J.C., *The fundamentals of corrosion* 1990, Oxford, Angleterre: Pergamon Press.
165. Schütze, M., *Corrosion and environmental degradation* 2000, Weinheim; New York: Wiley-VCH.
166. Kvarekvål, J., *Corrosion Layer Breakdown And Localized Corrosion In CO₂/H₂S Environments*, NACE International.
167. Papavinasam, S., A. Doiron, and R.W. Revie, *Model to Predict Internal Pitting Corrosion of Oil and Gas Pipelines*. Corrosion, 2010. **66**(3): p. 035006-035006-11.
168. Ghali, E. and V.S. Sastri, *Corrosion Prevention and Protection: Practical Solutions* 2007: Wiley.
169. Hoepfner, D.W., *Pitting Corrosion: Morphology and Characterization*, in *Corrosion Fatigue and Environmentally Assisted Cracking in Aging Military Vehicles* 2011.
170. Roberge, P., *Corrosion Engineering: Principles and Practice* 2008: McGraw-Hill Education.
171. *NACE Glossary of Corrosion Terms* 1965.
172. Magnussen, O.M., *Corrosion Protection by Inhibition*, in *Encyclopedia of Electrochemistry* 2007, Wiley-VCH Verlag GmbH & Co. KGaA.
173. Sanyal, B., *Organic compounds as corrosion inhibitors in different environments — A review*. Progress in Organic Coatings, 1981. **9**(2): p. 165-236.
174. Ahmad, Z., *Principles of Corrosion Engineering and Corrosion Control* 2006: Elsevier Science.
175. Sastri, V.S., *Corrosion inhibitors : principles and applications* 1998, Chichester ; New York: Wiley.
176. Durnie, W., et al., *Development of a Structure-Activity Relationship for Oil Field Corrosion Inhibitors*. Journal of The Electrochemical Society, 1999. **146**(5): p. 1751-1756.
177. Ai, J. and X. Guo, *AFM and FTIR studies of organic cation adsorption on carbon steel coupled with stainless steel*. Surface and Interface Analysis, 2006. **38**(8): p. 1218-1222.
178. Ai, J.Z., et al., *Adsorption behavior and synergistic mechanism of a cationic inhibitor and KI on the galvanic electrode*. Colloids and Surfaces A: Physicochemical and Engineering Aspects, 2006. **281**(1–3): p. 147-155.
179. Alink, B.A., et al., *Mechanism of CO₂ Corrosion Inhibition by Phosphate Esters*, NACE International.
180. McGregor, W.M., *Novel Synergistic Water Soluble Corrosion Inhibitors*, Society of Petroleum Engineers.
181. Wong, J.E. and N. Park, *Further Investigation On The Effect Of Corrosion Inhibitor Actives On The Formation Of Iron Carbonate On Carbon Steel*, 2009, NACE International.

182. Yu, H., et al., *Corrosion inhibition of mild steel by polyhydric alcohol phosphate ester (PAPE) in natural sea water*. Corrosion Engineering, Science and Technology, 2006. **41**(3): p. 259-262.
183. Zvauya, R. and J.L. Dawson, *Inhibition studies in sweet corrosion systems by a quaternary ammonium compound*. Journal of Applied Electrochemistry, 1994. **24**(9): p. 943-947.
184. Wong, J.E. and N. Park, *Effect Of Corrosion Inhibitor Active Components On The Growth Of Iron Carbonate Scale Under CO2 Conditions*, 2008, NACE International.
185. Jovancicevic, V., S. Ramachandran, and P. Prince, *Inhibition of CO2 Corrosion of Mild Steel by Imidazolines and Their Precursors*, NACE International.
186. Rostami, A., *Review and Evaluation of Corrosion Inhibitors Used in Well Stimulation*, Society of Petroleum Engineers.
187. Reid, M., et al., *Determining Optimal Dose Rate of Oilfield Corrosion Inhibitors by Step-wise Incremental Dosing*, NACE International.
188. Jovancicevic, V., et al., *CO2 Corrosion Inhibition by Sulfur-Containing Organic Compounds*, NACE International.
189. Stalker, R., G.M. Graham, and C. Simpson, *The Impact of Inorganic Scale Deposits and Their Removal on General CO2 Corrosion Rates and Corrosion Inhibitor Performance*, Society of Petroleum Engineers.
190. Al Hashem, A., J.A. Carew, and A. Al Borno, *The Synergistic Effect of Corrosion, Scale and Biocide Inhibitors on the Corrosion Rate of L- 80 Steel in Seawater*, NACE International.
191. Graham, G.M. and C.P. McMahon, *The Effect of Scale Inhibitor Performance Against Bulk (Homogeneous) and Surface (Heterogeneous) Scale Nucleation and Growth by the Addition of Film Forming Corrosion Inhibitors*, NACE International.
192. Labille, S., et al., *An Assessment of Adhesion of Scale and Electrochemical Pre-treatment for the Prevention of Scale Deposition on Metal Surfaces*, Society of Petroleum Engineers.
193. Spicka, K., et al., *The Impact of Organic Acid on Scale Inhibitor/Corrosion Inhibitor Interaction, a Case Study from West Africa*, Society of Petroleum Engineers.
194. Marín-Cruz, J., et al., *EIS study on corrosion and scale processes and their inhibition in cooling system media*. Electrochimica Acta, 2006. **51**(8–9): p. 1847-1854.
195. Cognetti, A., et al., *Operation of Cooling Towers at High Cycles of Concentration: Corrosion and Scale Control*, NACE International.
196. To, X.H., et al., *A corrosion-protective film formed on a carbon steel by an organic phosphonate*. Corrosion Science, 1997. **39**(10–11): p. 1925-1934.
197. Andijani, I. and S. Turgoose, *Studies on corrosion of carbon steel in deaerated saline solutions in presence of scale inhibitor*. Desalination, 1999. **123**(2–3): p. 223-231.
198. Soror, T.Y., *Scale and Corrosion Prevention in Cooling Water Systems Part I: Calcium Carbonate*. The Open Corrosion Journal, 2009. **2**: p. 45-50.
199. Ma, W., et al., *Investigating electron-transfer processes using a biomimetic hybrid bilayer membrane system*. Nat. Protocols, 2013. **8**(3): p. 439-450.

200. Kermani, B., *Depiction of Metallurgical Parameters as Governing CO₂ Corrosion*, NACE International.
201. Palmer, J.W., W. Hedges, and J.L. Dawson, *Use of Corrosion Inhibitors in Oil and Gas Production: (EFC 39)*, Maney Publishing.
202. LTD, I.F.A., *Certificate of conformity*, 2008.
203. Kaasa, B., *Prediction of pH, mineral precipitation and multiphase equilibria during oil recovery*, 1998, Institutt for unorganisk kjemi, Norges teknisk-naturvitenskapelige universitet (NTNU): Trondheim.
204. Sandengen, K., *Prediction of mineral scale formation in wet gas condensate pipelines and in meg (mono ethylene glycol) regeneration plants*, in *Department of Materials Technology 2006*, Norwegian University of Science and Technology: Trondheim.
205. ASTM, *Standard Guide for Examination and Evaluation of Pitting Corrosion*, in *ASTM G46 - 942013*, ASTM: West Conshohocken, PA.
206. Chen, Y., et al., *Review of advanced imaging techniques*. *Jornal of Pathology Informatics*, 2012. **3**(22).
207. ISO, *ISO 7027 Water quality—Determination of turbidity*, 1994, International Standards Organization: Geneva.
208. Hach, *Turbidity*, in *DR/820 COLORIMETER PROCEDURES MANUAL*, 2004, H. Company. p. 225-228.
209. (U.S.), G.S., *National Field Manual for the Collection of Water-Quality Data*, Geological Survey (U.S.).
210. Dickin, A. *On a Faraway Day Contents...* 2008 [cited 2012 06/12/2012]; Available from: <http://www.onafarawayday.com/Radiogenic/Ch2/Ch2-2.htm>.
211. Technology, I.S.U.o.S.a. *How the SEM Works*. [cited 2012 06/12/2012]; Available from: <http://www-archive.mse.iastate.edu/microscopy/path2.html>.
212. Martinez, M.V. *Forensic Science*. 2008 [cited 2012 06/12/2012]; Available from: <http://www.forensicevidence.net/iama/sem-edxtheory.html>.
213. *The University of South Carolina, Department of Chemistry & Biochemistry*. 2015 02/02/2015]; Available from: http://www.chem.sc.edu/faculty/zurloye/xrdtutorial_2013.pdf.
214. Aboalbiss. *Bragg's law*. 2009 02/02/2015]; Available from: http://commons.wikimedia.org/wiki/File:Bragg's_Law.PNG.
215. Rietveld, H.M., *The crystal structure of some alkaline earth metal uranates of the type M₃UO₆*. *Acta crystallographica*, 1966. **20**(4): p. 508-513.
216. Rietveld, H.M., *A Profile Refinement Method for Nuclear and Magnetic Structures*. *Journal of Applied Crystallography*, 1969. **2**: p. 65-71.
217. Caglioti, G., A. Paoletti, and F.P. Ricci, *Choice of collimators for a crystal spectrometer for neutron diffraction*. *Nuclear Instruments*, 1958. **3**(4): p. 223-228.
218. B.V., P., *X'Pert HiScore Plus*, 2014.
219. ChemWiki, U.D. *How an FTIR Spectrometer Operates*. Available from: http://chemwiki.ucdavis.edu/Physical_Chemistry/Spectroscopy/Vibrational_Spectroscopy/Infrared_Spectroscopy/How_an_FTIR_Spectrometer_Operates#Contributors.

220. Begum, N., et al. *Phonon Confinement Effect in III-V Nanowires*. Nanowires 2010; Available from: <http://www.intechopen.com/books/nanowires/phonon-confinement-effect-in-iii-v-nanowires>.
221. Box, G.E.P., W.G. Hunter, and J.S. Hunter, *Statistics for experimenters: an introduction to design, data analysis, and model building* 1978: Wiley.
222. Kelton, W.D., *Experimental design for simulation*, in *Winter Simulation Conference* 2000.
223. Hinkelmann, K. and O. Kempthorne, *Design and Analysis of Experiments, Advanced Experimental Design* 2005: Wiley.
224. Rasch, D., et al., *Optimal experimental design with R*, ed. D. Rasch 2011, Boca Raton, FL :: CRC Press.
225. Stat-Ease, *Design-Expert*, 2002.
226. Faber, J., T. Fawcett, and R. Goehner, *The Powder Diffraction File (PDF): A Relational Database For Electron Diffraction*. Microscopy and Microanalysis, 2005. **11**(Supplement S02): p. 778-779.
227. Miller, F.A. and C.H. Wilkins, *Infrared Spectra and Characteristic Frequencies of Inorganic Ions*. Analytical Chemistry, 1952. **24**(8): p. 1253-1294.
228. Cai, G.-B., et al., *1,3-Diamino-2-hydroxypropane-N,N,N[prime or minute],N[prime or minute]-tetraacetic acid stabilized amorphous calcium carbonate: nucleation, transformation and crystal growth*. CrystEngComm, 2010. **12**(1): p. 234-241.
229. Yean, S., et al., *Ferrous Carbonate Nucleation and Inhibition*, Society of Petroleum Engineers.
230. Legrand, L., et al., *Study of oxidation products formed on iron in solutions containing bicarbonate/carbonate*. Electrochimica Acta, 2000. **46**(1): p. 111-117.
231. Blengino, J.M., et al., *Physico-chemical characterization of corrosion layers formed on iron in a sodium carbonate-bicarbonate containing environment*. Corrosion Science, 1995. **37**(4): p. 621-643.
232. Edwards, H.G.M., et al., *FT-Raman spectroscopic study of calcium-rich and magnesium-rich carbonate minerals*. Spectrochimica Acta Part A: Molecular and Biomolecular Spectroscopy, 2005. **61**(10): p. 2273-2280.
233. Boulard, E., F. Guyot, and G. Fiquet, *The influence on Fe content on Raman spectra and unit cell parameters of magnesite-siderite solid solutions*. Physics and Chemistry of Minerals, 2012. **39**(3): p. 239-246.
234. Savoye, S., et al., *Experimental investigations on iron corrosion products formed in bicarbonate/carbonate-containing solutions at 90°C*. Corrosion Science, 2001. **43**(11): p. 2049-2064.
235. BUZGAR, N. and A.I. APOPEI, *THE RAMAN STUDY OF CERTAIN CARBONATES*. ANALELE ȘTIINȚIFICE ALE UNIVERSITĂȚII, 2009.
236. Rutt, H.N. and J.H. Nicola, *Raman spectra of carbonates of calcite structure*. Journal of Physics C: Solid State Physics, 1974. **7**(24): p. 4522.
237. Kvarekval, J., *Morphology Of Localised Corrosion Attacks In Sour Environments*, NACE International.

238. Barker, R., et al., *Determining the Behavior of Sulfur Compounds in Controlling Preferential Weld Corrosion in CO₂- saturated Brine*, NACE International.
239. Barker, R., B. Pickles, and A. Nevill, *General Corrosion of X65 Steel under Silica Sand Deposits in CO₂-Saturated Environments in the Presence of Corrosion Inhibitor Components*, NACE International.
240. Neville, A., X. Hu, and I.M. Ismail, *Investigation of Pitting Corrosion and Inhibition in Sweet Conditions*, NACE International.
241. Lyons, W.C. and G.J. Plisga, *Standard Handbook of Petroleum and Natural Gas Engineering (2nd Edition)*, Elsevier.
242. Morizot, A.P. and A. Neville, *Insights into Electrodeposition of an Inhibitor Film and Its Inhibitive Effects on Calcium Carbonate Deposition*. Journal of Colloid and Interface Science, 2002. **245**(1): p. 40-49.

Appendix A

Infrared spectrum for neat single components.

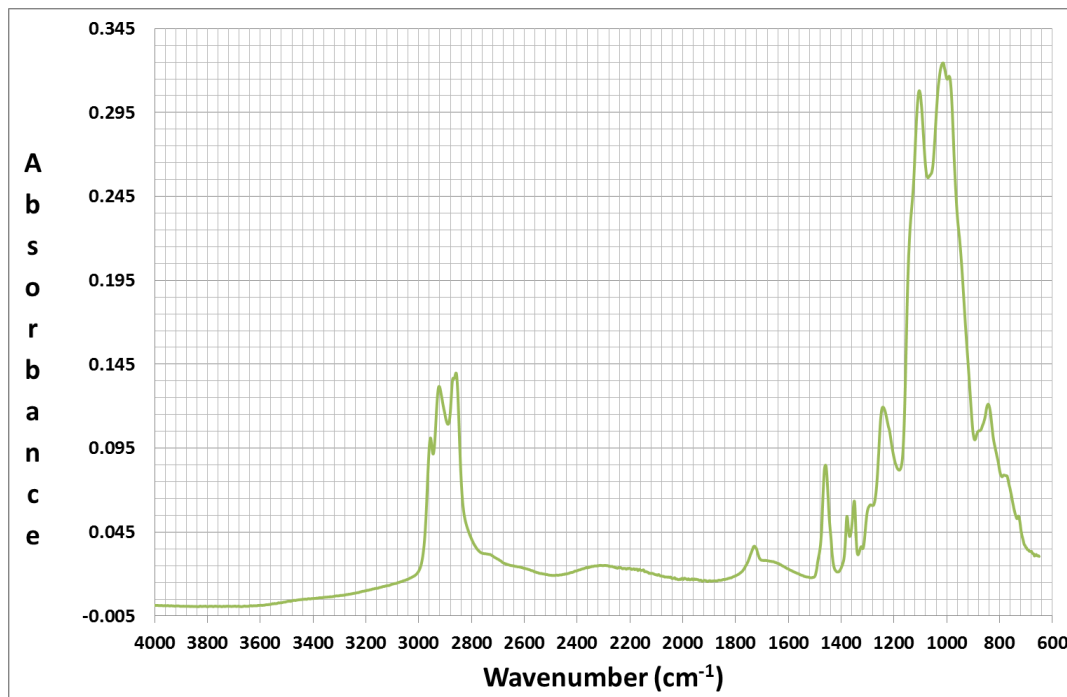


Figure A.0.1: Infrared spectrum for neat alcohol ethoxy phosphate ester

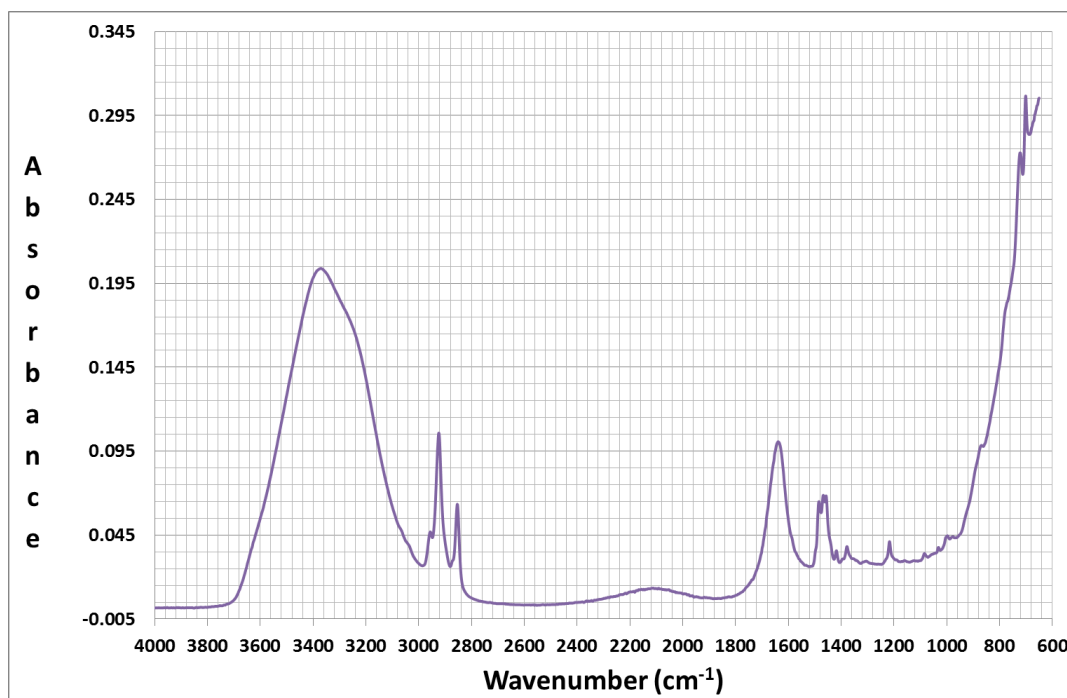


Figure A.0.2: Infrared spectrum for neat C12-C14 alkyl dimethyl benzyl-ammonium chloride

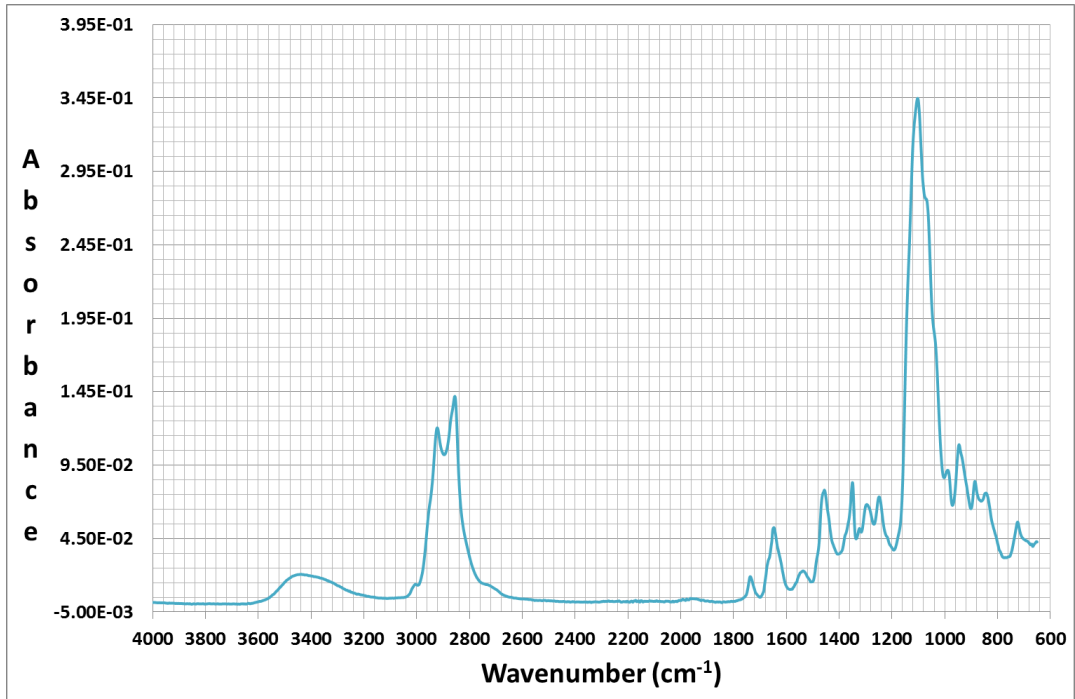


Figure A.0.3: Infrared spectrum for neat ethoxylated imidazolines

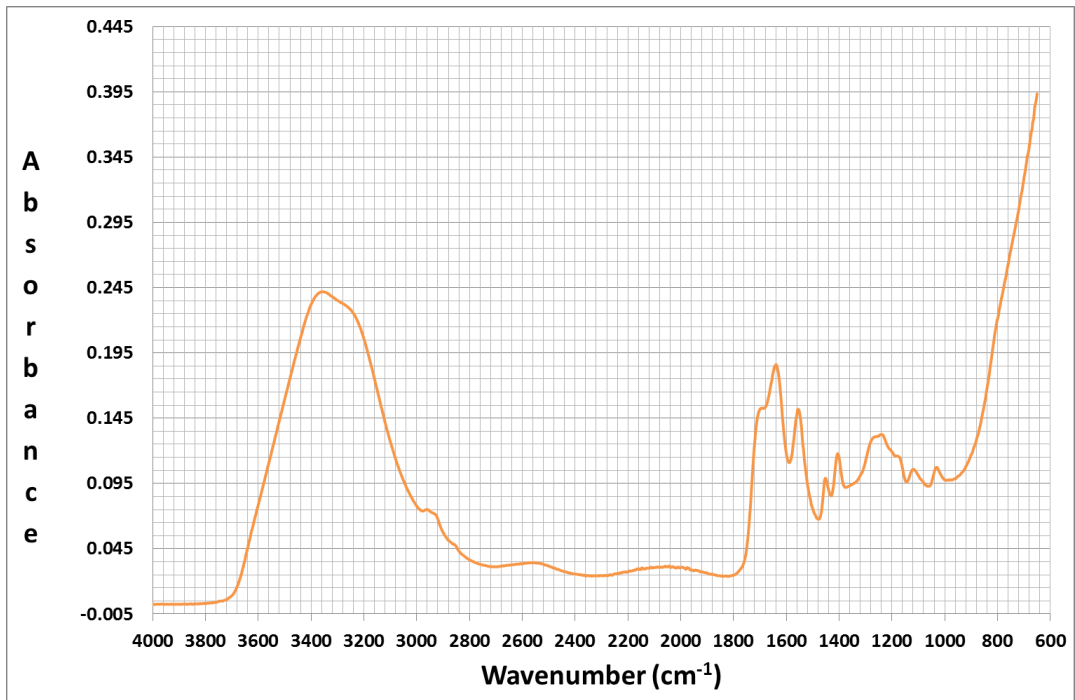


Figure A.0.4: Infrared spectrum for neat polyphosphinocarboxylic acid (PPCA)

Interaction between calcium carbonate and single components.

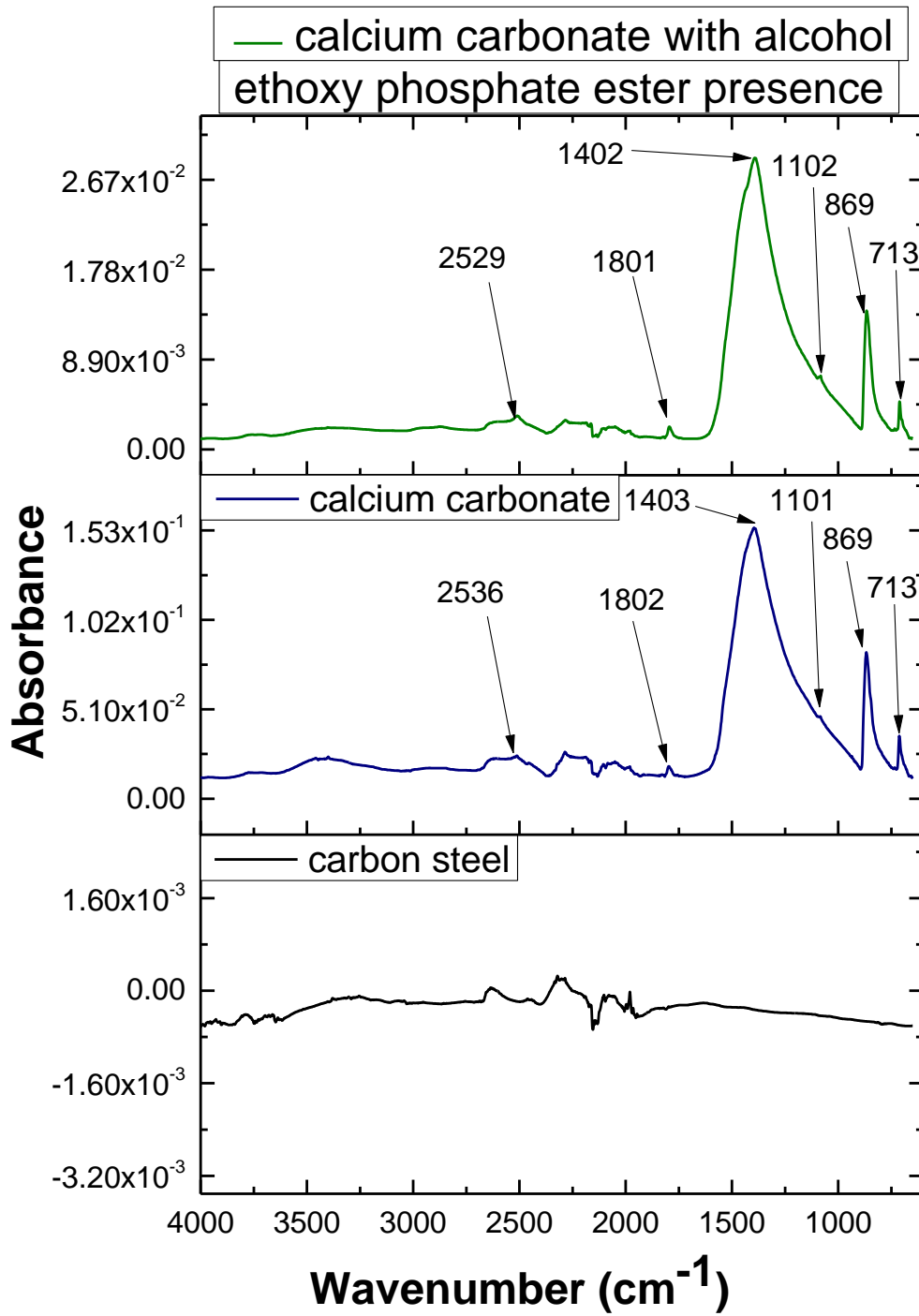


Figure A.0.5: Infrared spectrum for calcium carbonate formed with presence of alcohol ethoxy phosphate ester, calcium carbonate reference and carbon steel

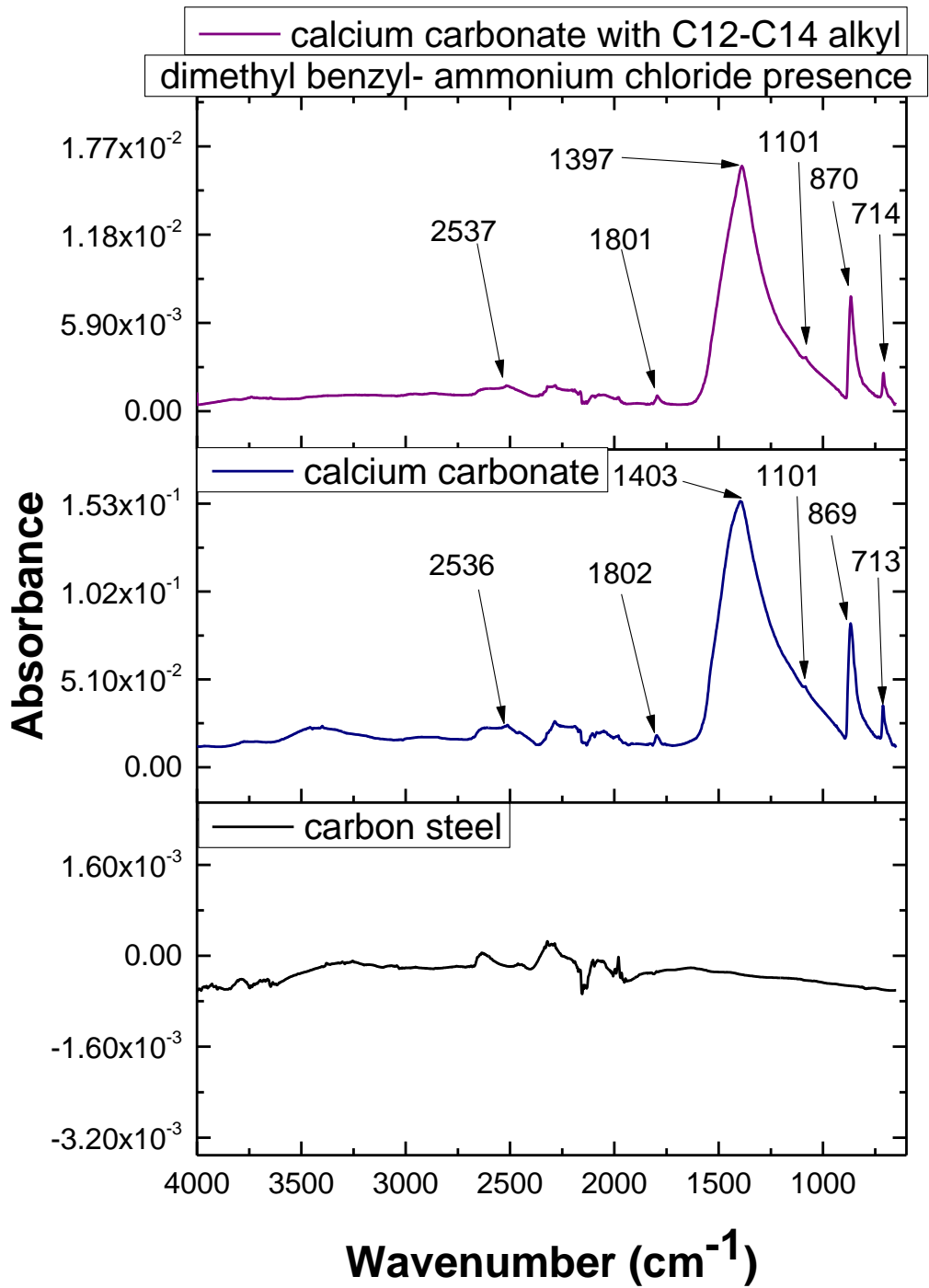


Figure A.0.6: : Infrared spectrum for calcium carbonate formed with presence of C12-C14 alkyl dimethyl benzyl- ammonium chloride, calcium carbonate reference and carbon steel

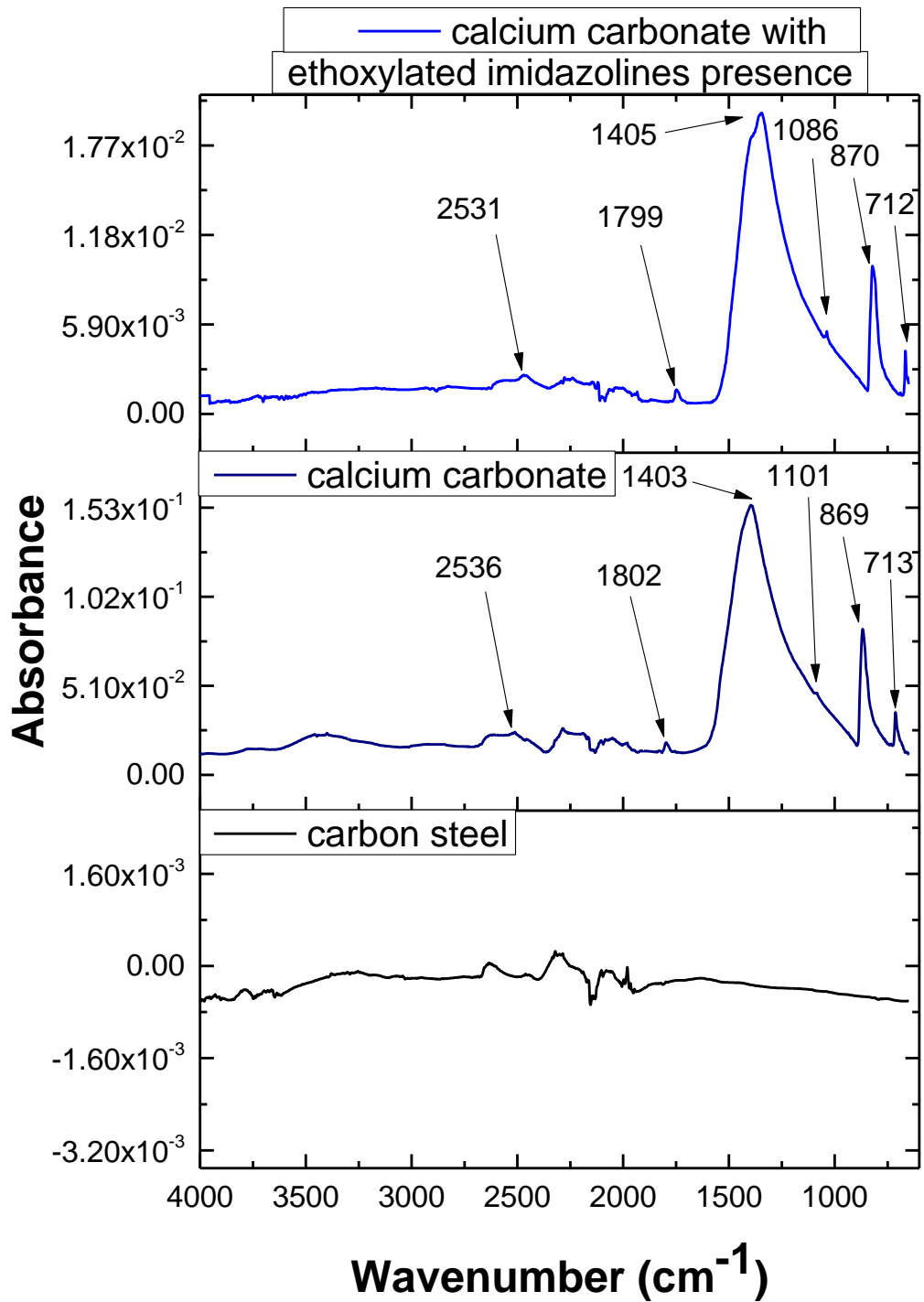


Figure A.0.7: Infrared spectrum for calcium carbonate formed with presence of ethoxylated imidazolines, calcium carbonate reference and carbon steel

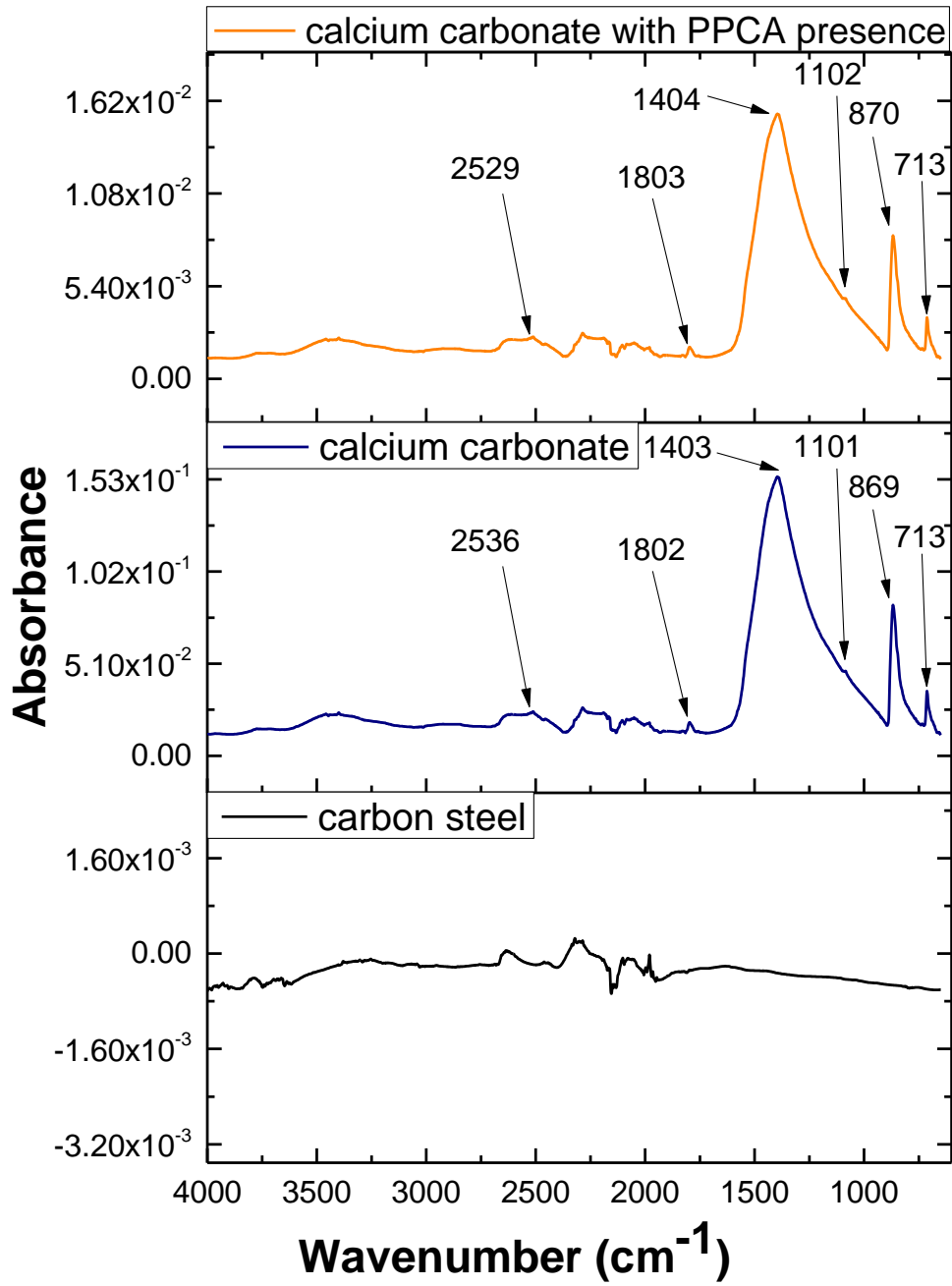


Figure A.0.8: Infrared spectrum for calcium carbonate formed with presence of polyphosphinocarboxylic acid (PPCA), calcium carbonate reference and carbon steel

Interaction between iron carbonate and single components.

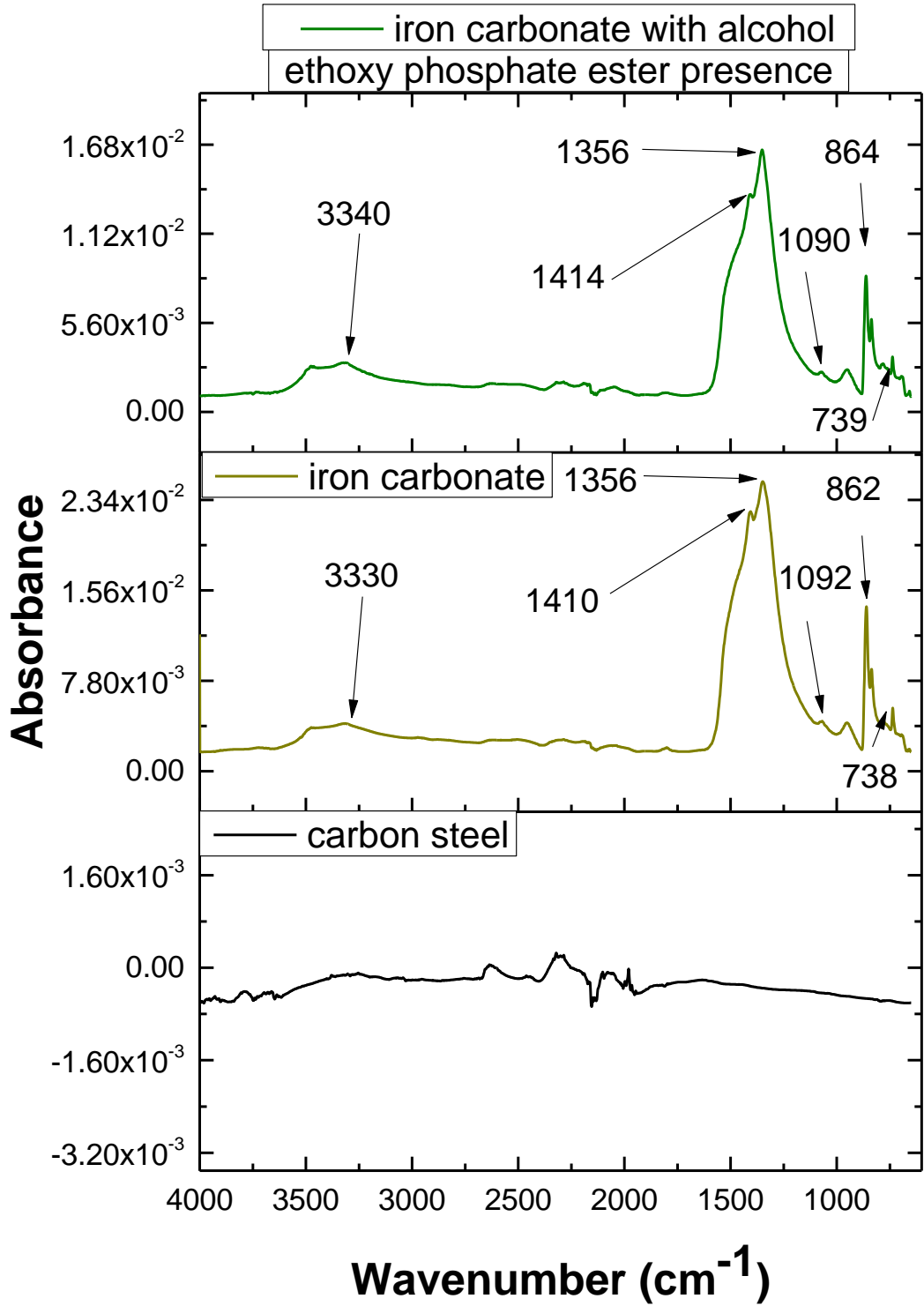


Figure A.0.9: Infrared spectrum for iron carbonate formed with presence of alcohol ethoxy phosphate ester, iron carbonate reference and carbon steel

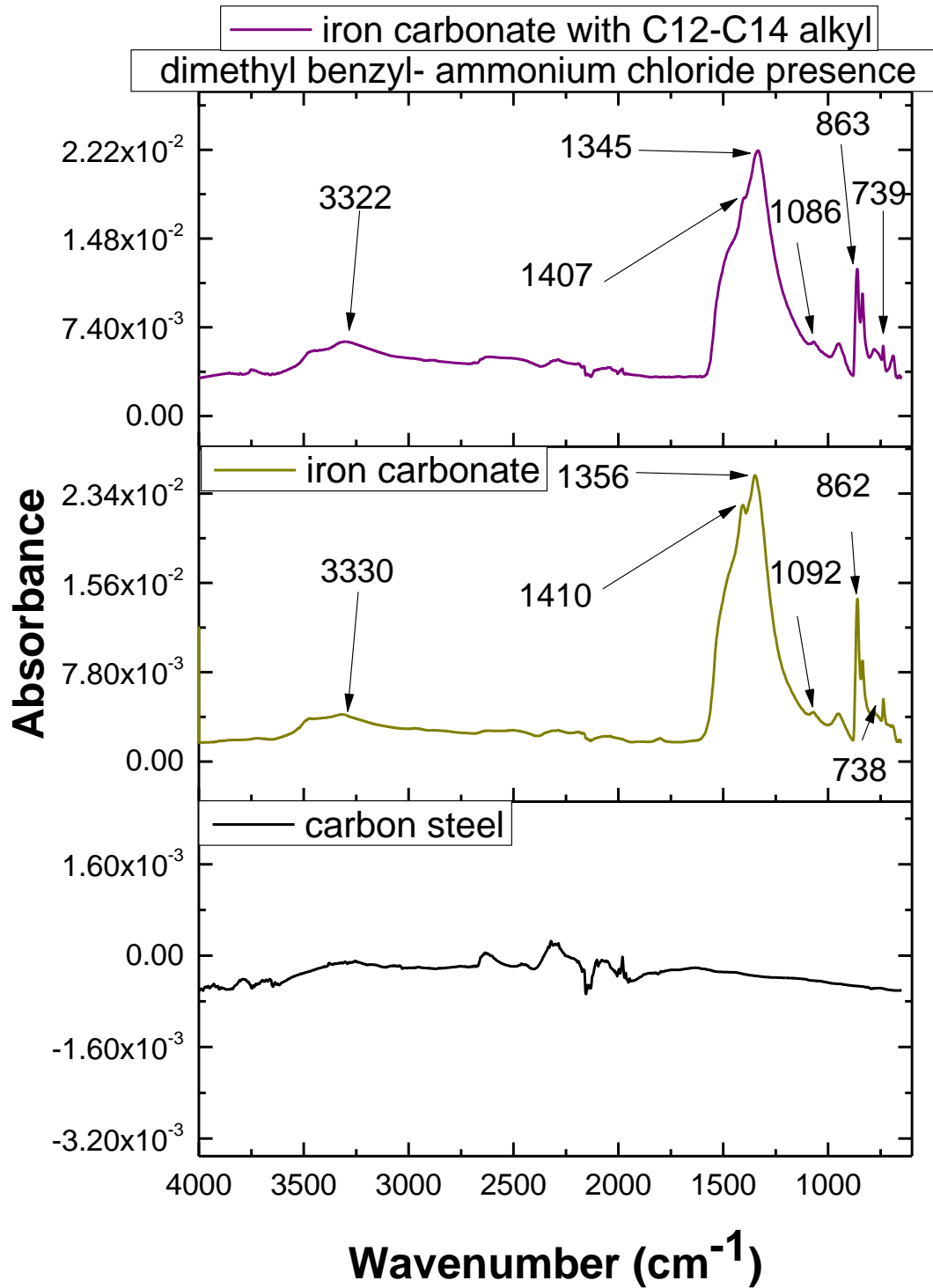


Figure A.0.10: Infrared spectrum for iron carbonate formed with presence of C12-C14 alkyl dimethyl benzyl- ammonium chloride, iron carbonate reference and carbon steel

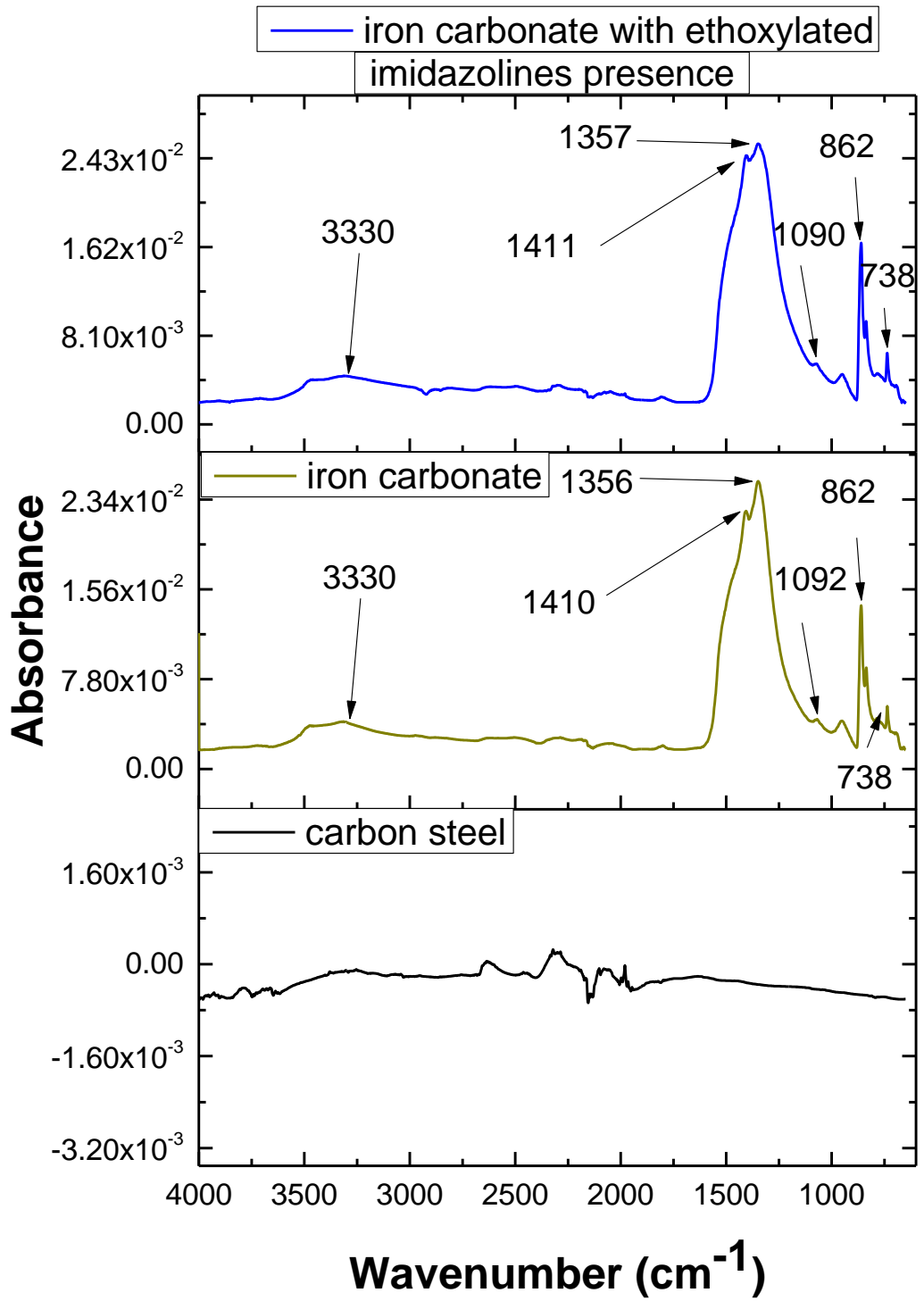


Figure A.0.11: Infrared spectrum for iron carbonate formed with presence of ethoxylated imidazolines, iron carbonate reference and carbon steel

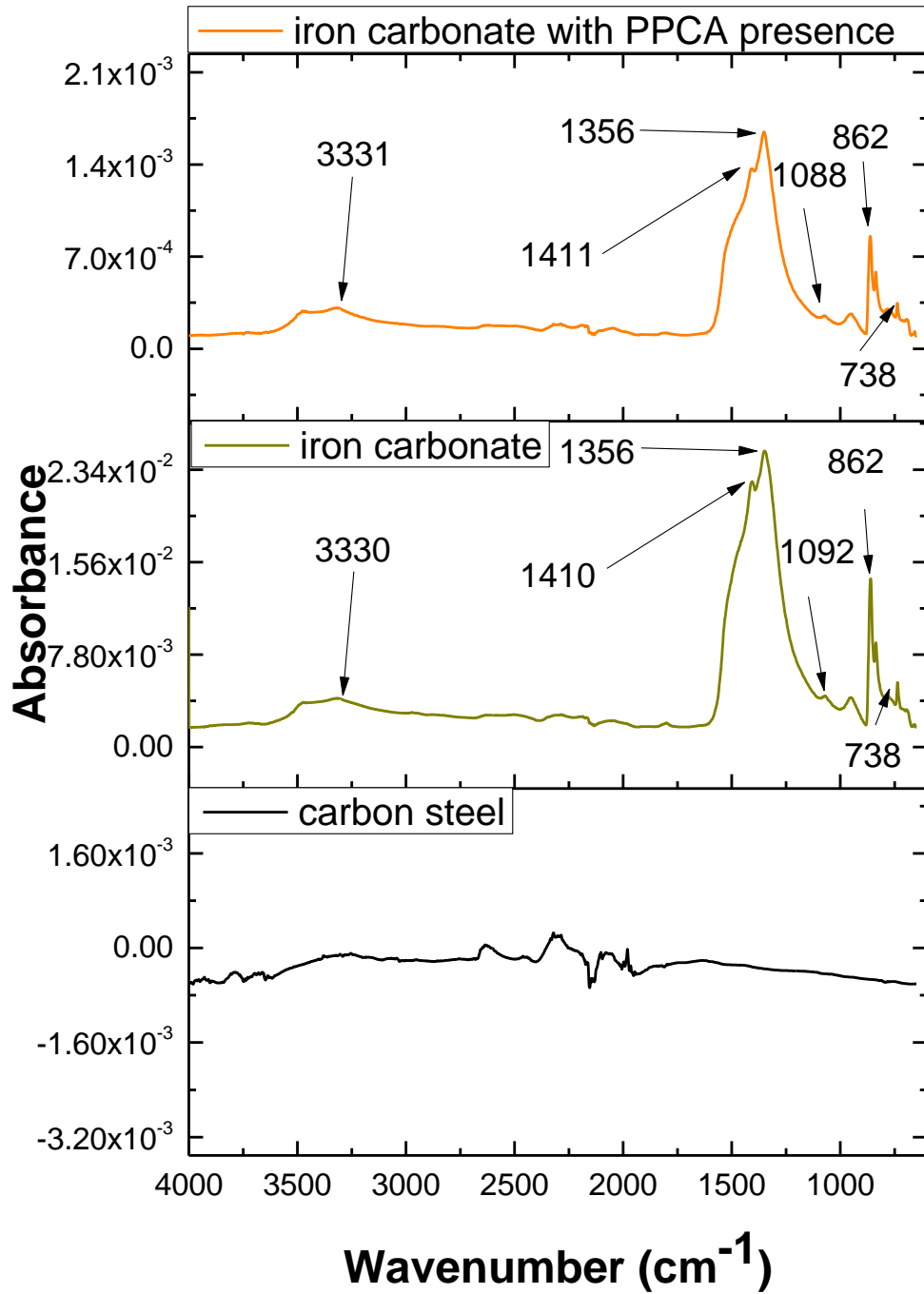


Figure A.0.12: Infrared spectrum for iron carbonate formed with presence of polyphosphinocarboxylic acid (PPCA, iron carbonate reference and carbon steel

Appendix B

Raman spectrum for neat single components.

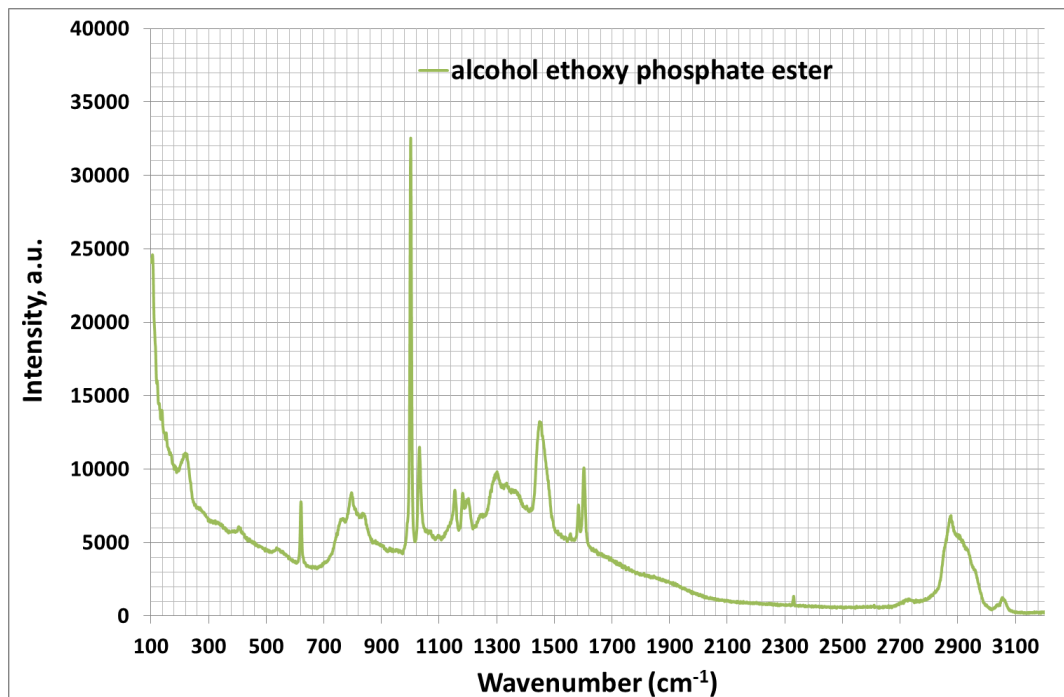


Figure B.0.1: Raman spectrum for neat alcohol ethoxy phosphate ester

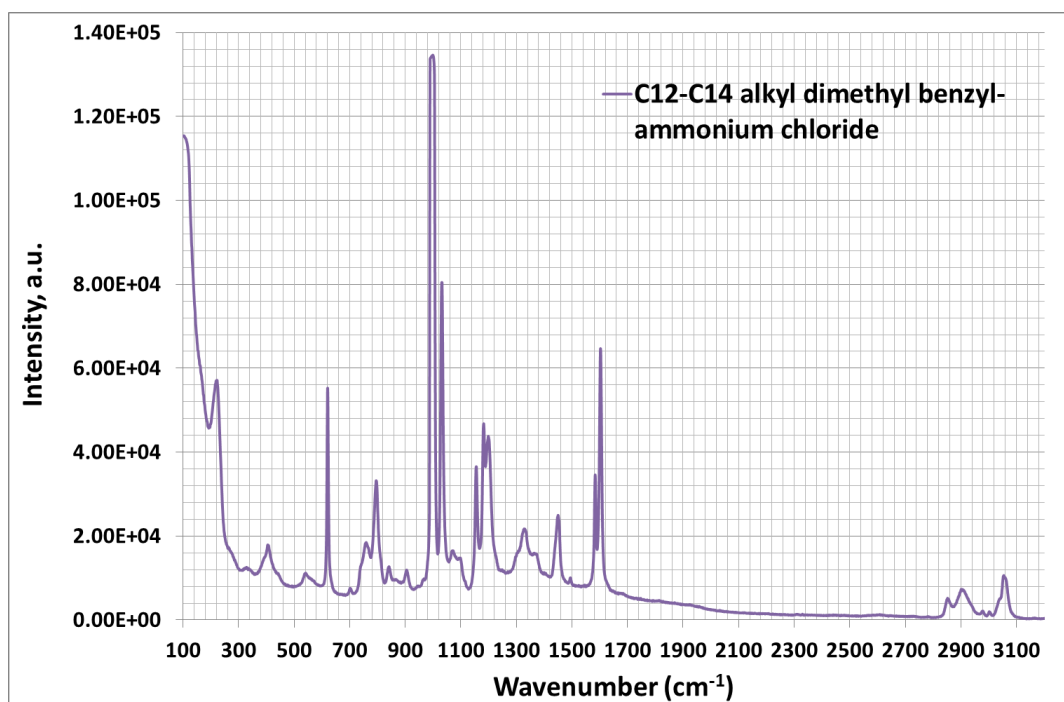


Figure B.0.2: Raman spectrum for neat C12-C14 alkyl dimethyl benzyl-ammonium chloride

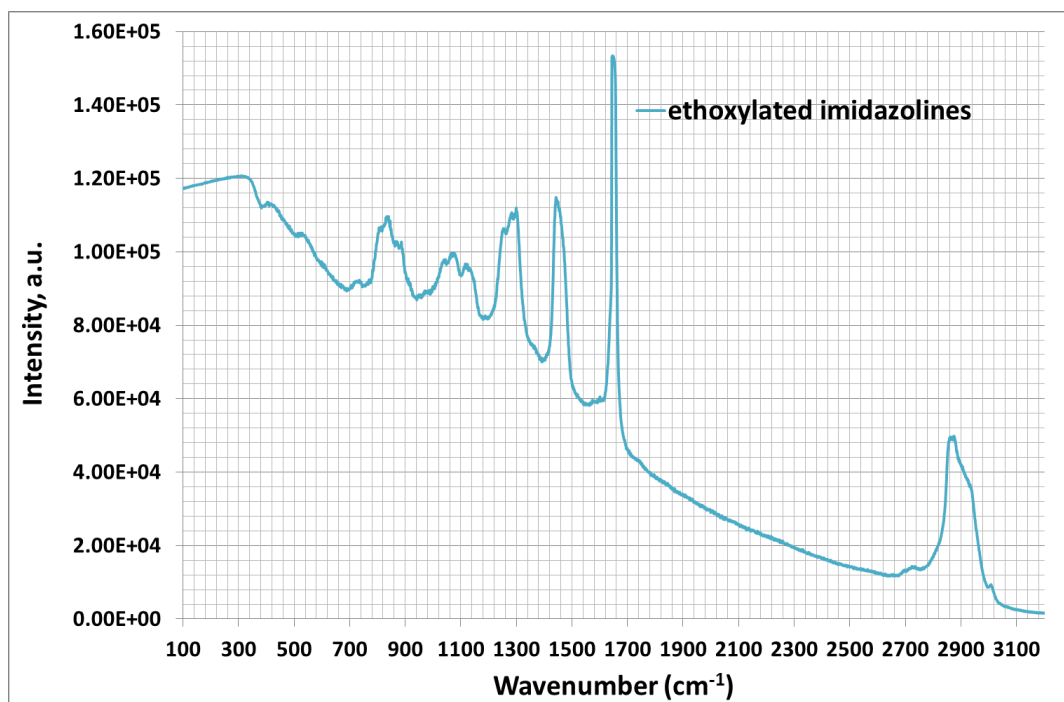


Figure B.0.3: Raman spectrum for neat ethoxylated imidazolines

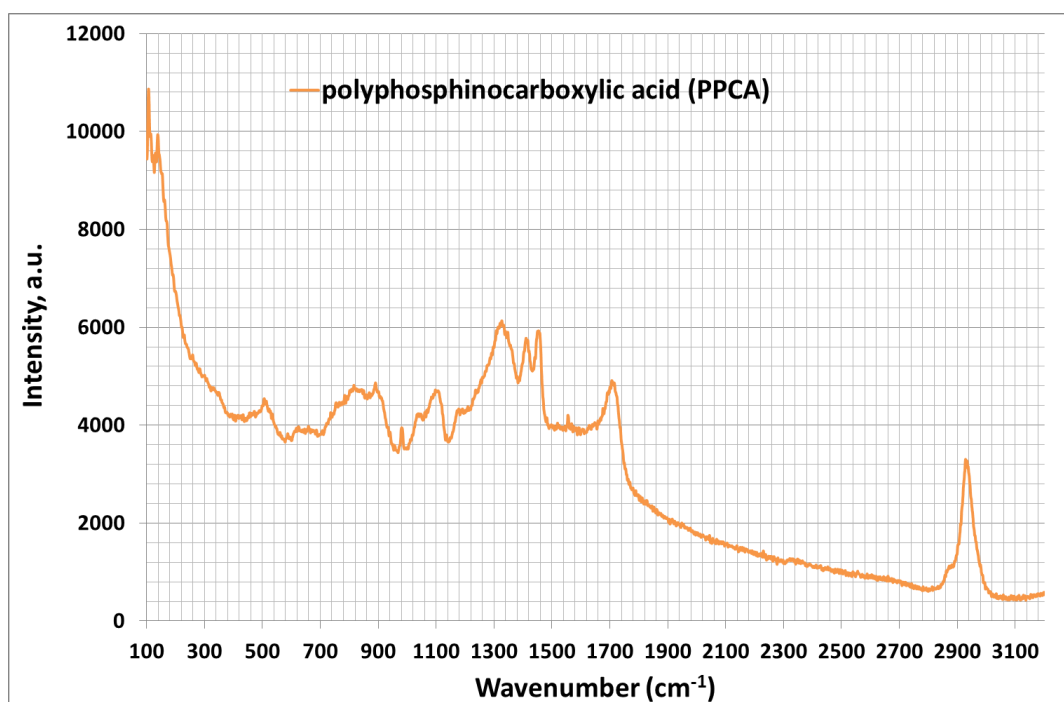


Figure B.0.4: Raman spectrum for neat polyphosphinocarboxylic acid (PPCA)

Interaction between calcium carbonate and single components.

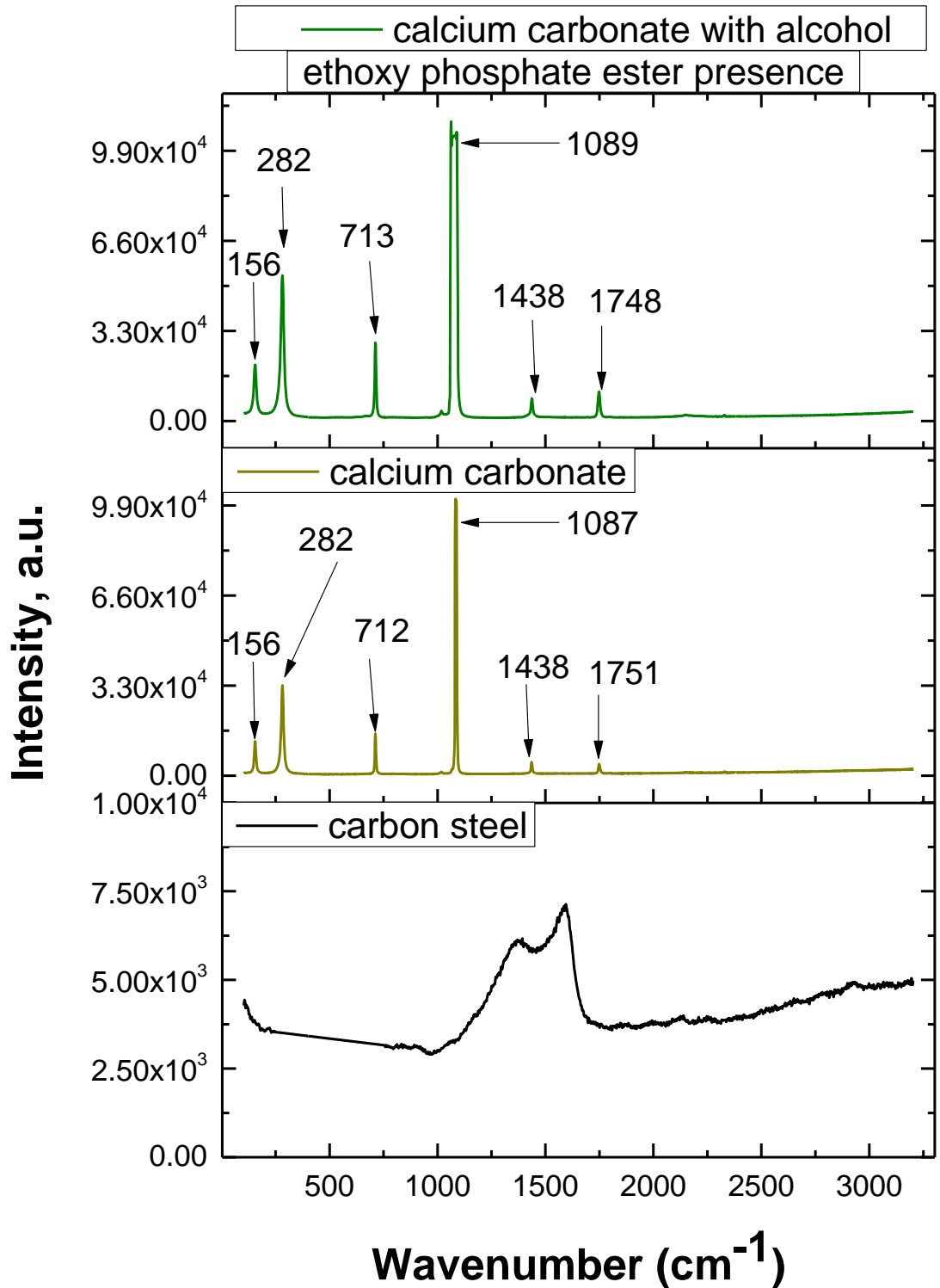


Figure 0.5: Raman spectrum for calcium carbonate formed with presence of alcohol ethoxy phosphate ester, calcium carbonate reference and carbon steel

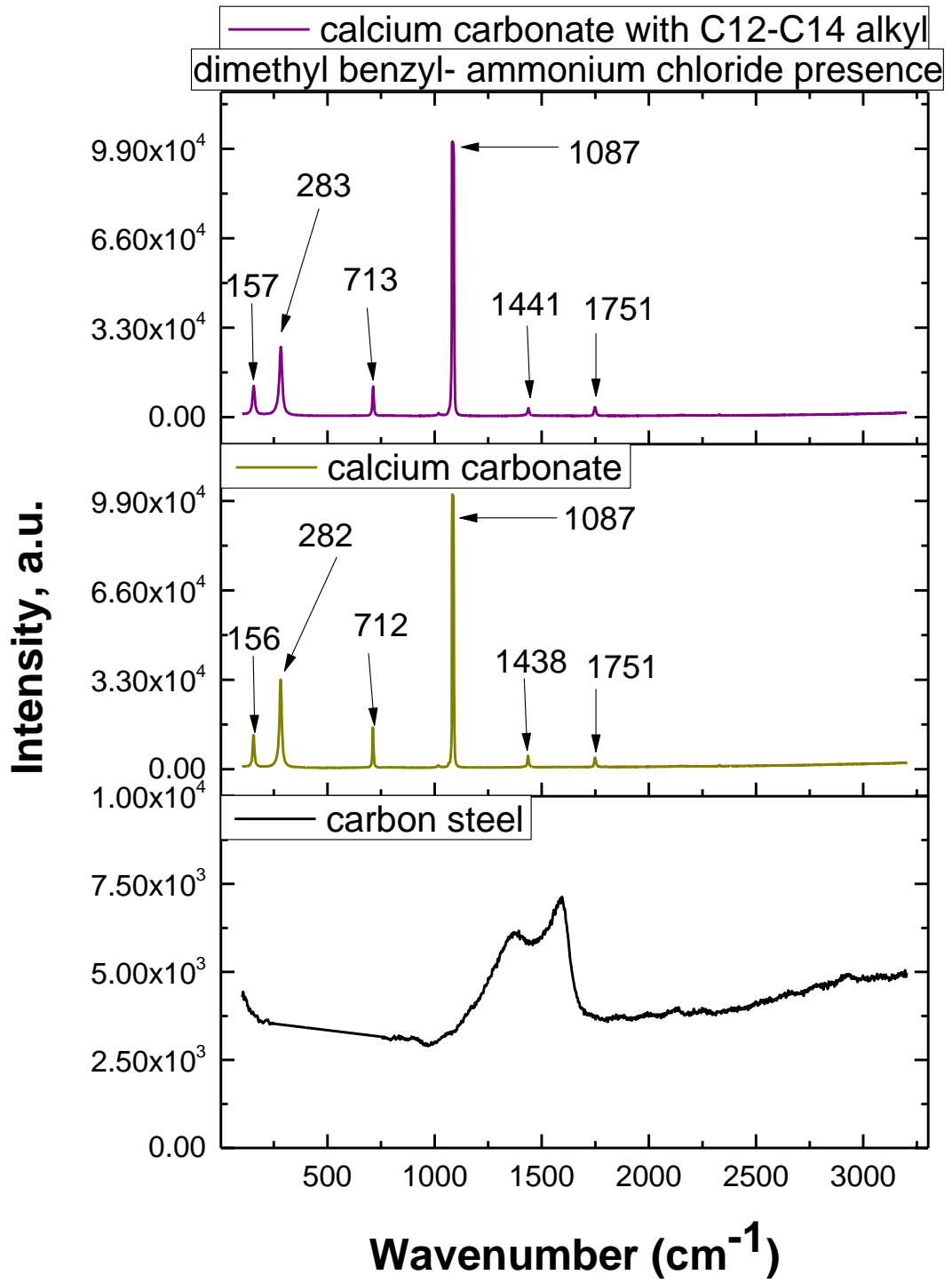


Figure 0.6: Raman spectrum for calcium carbonate formed with presence of C12-C14 alkyl dimethyl benzyl-amonium chloride, calcium carbonate reference and carbon steel

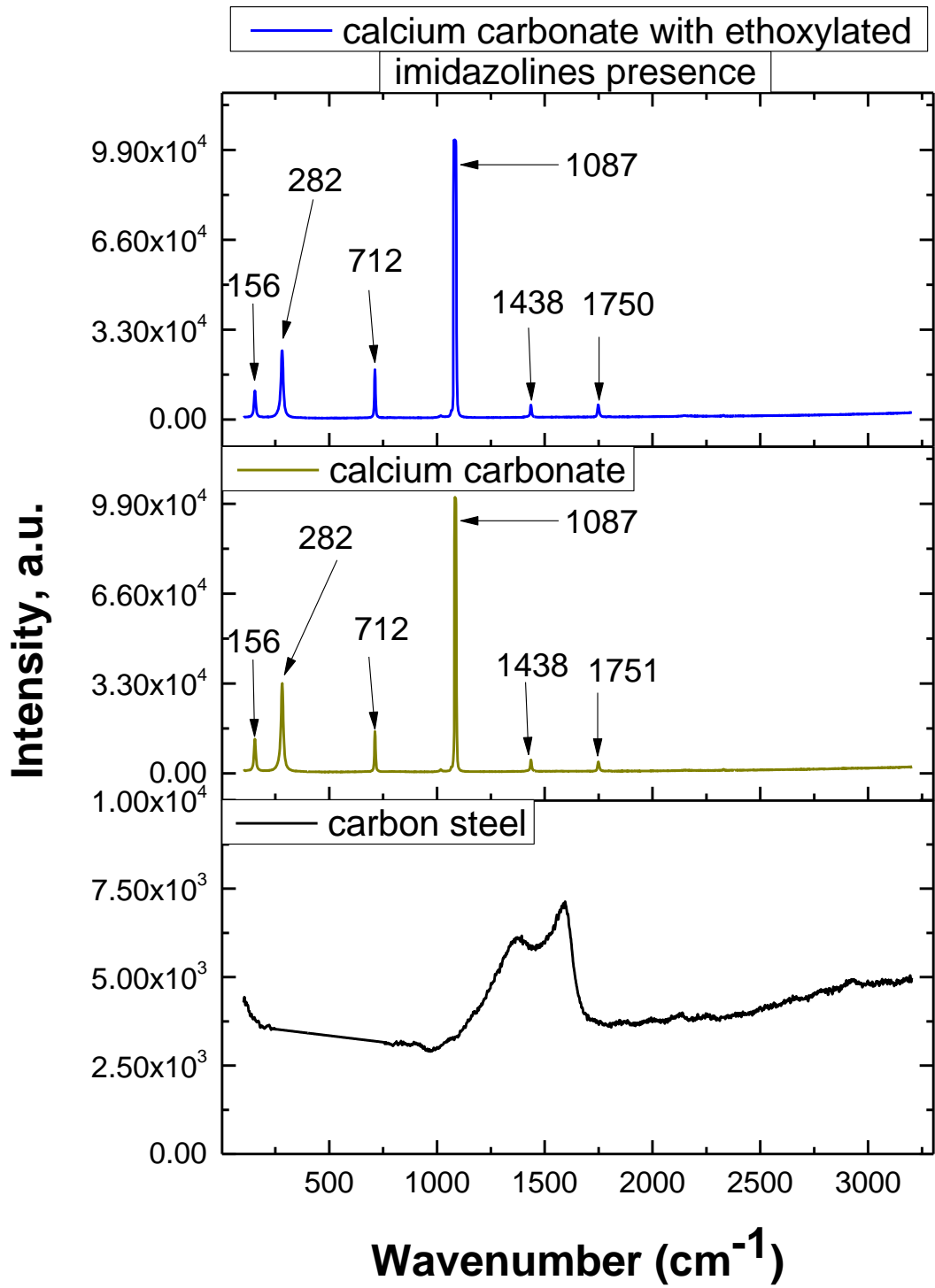


Figure 0.7: Raman spectrum for calcium carbonate formed with presence of ethoxylated imidazolines, calcium carbonate reference and carbon steel

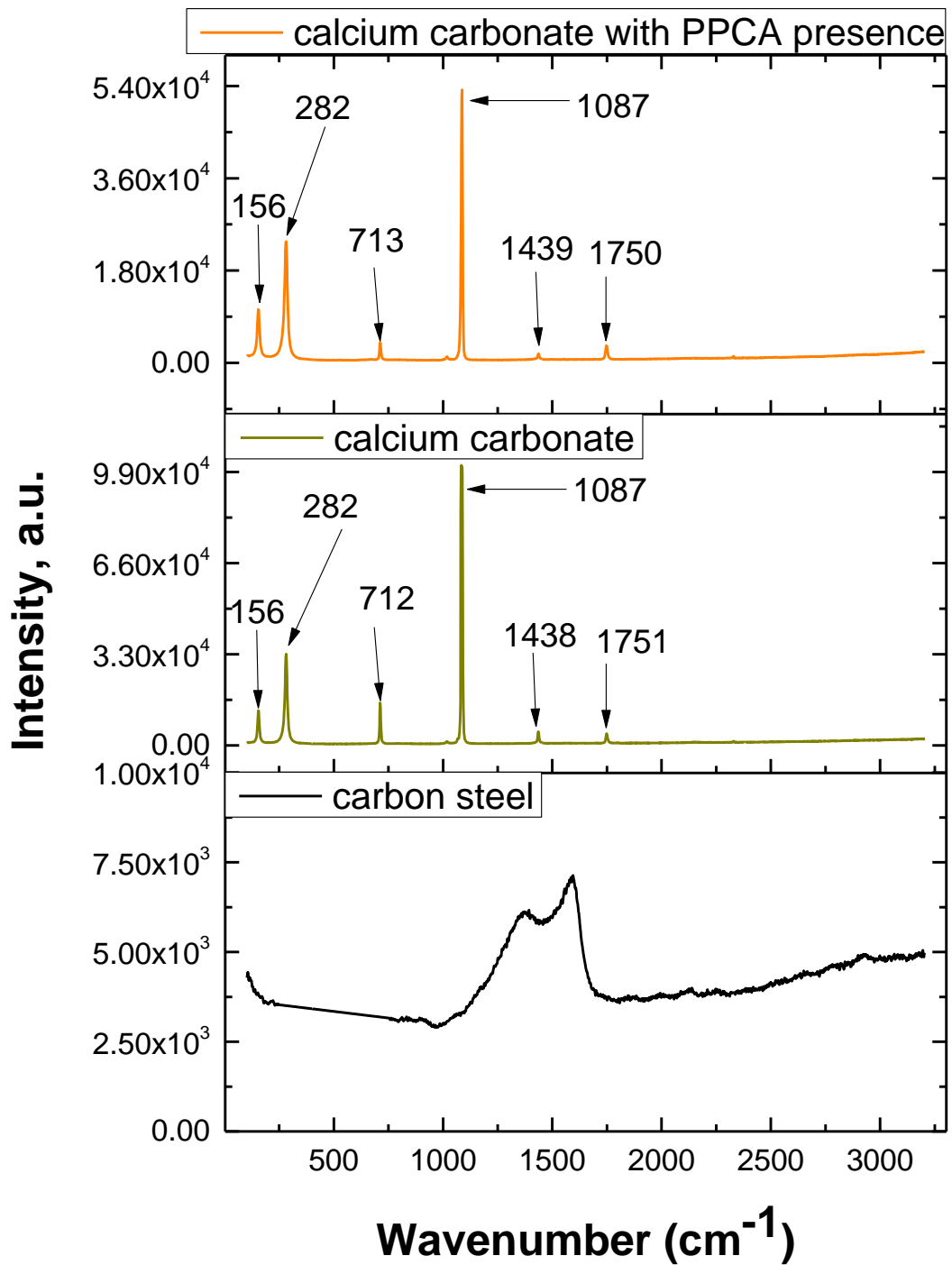


Figure 0.8: Raman spectrum for calcium carbonate formed with presence of polyphosphinocarboxylic acid (PPCA), calcium carbonate reference and carbon steel

Interaction between iron carbonate and single components.

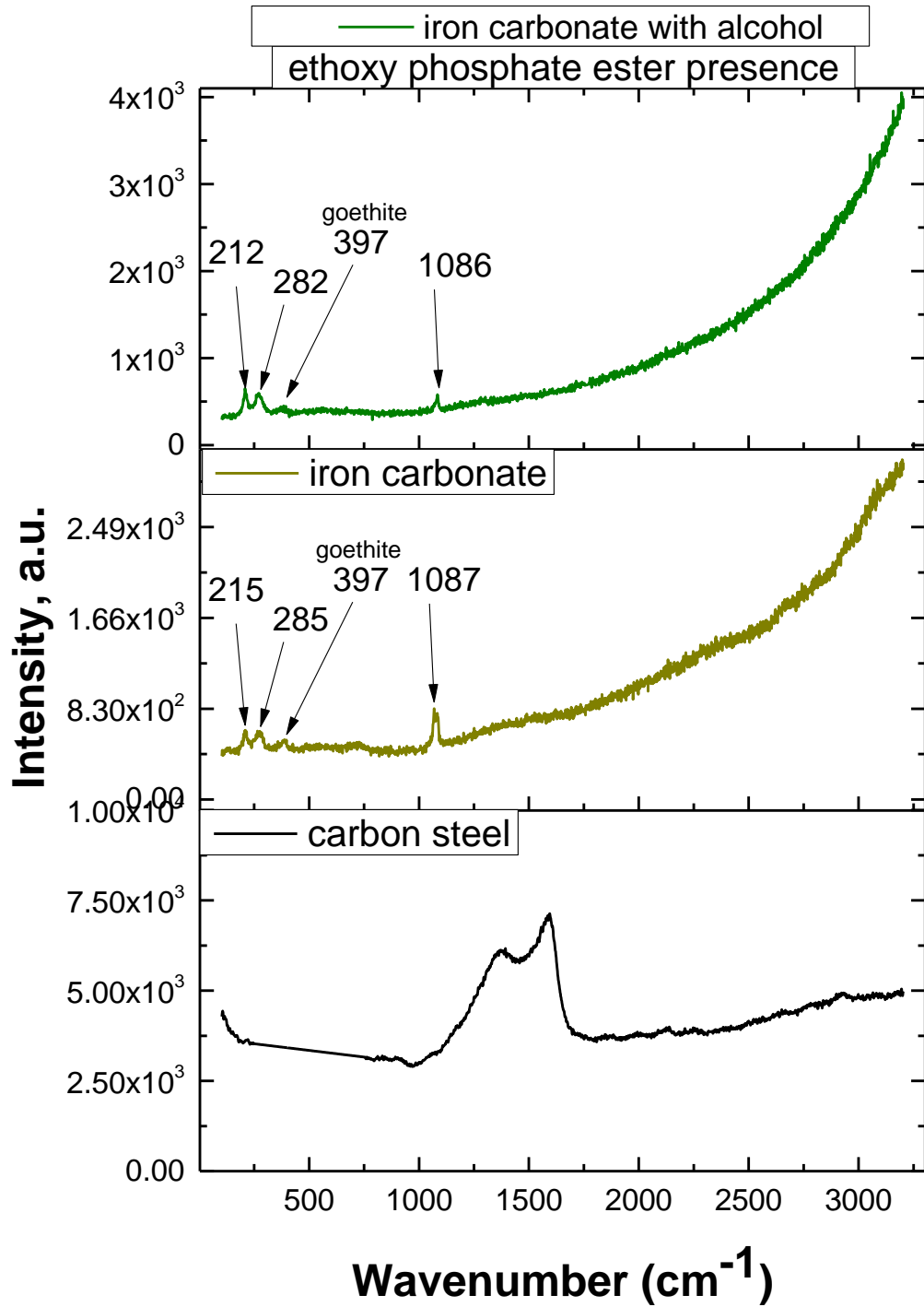


Figure 0.9: Raman spectrum for iron carbonate formed with presence of alcohol ethoxy phosphate ester, iron carbonate reference and carbon steel

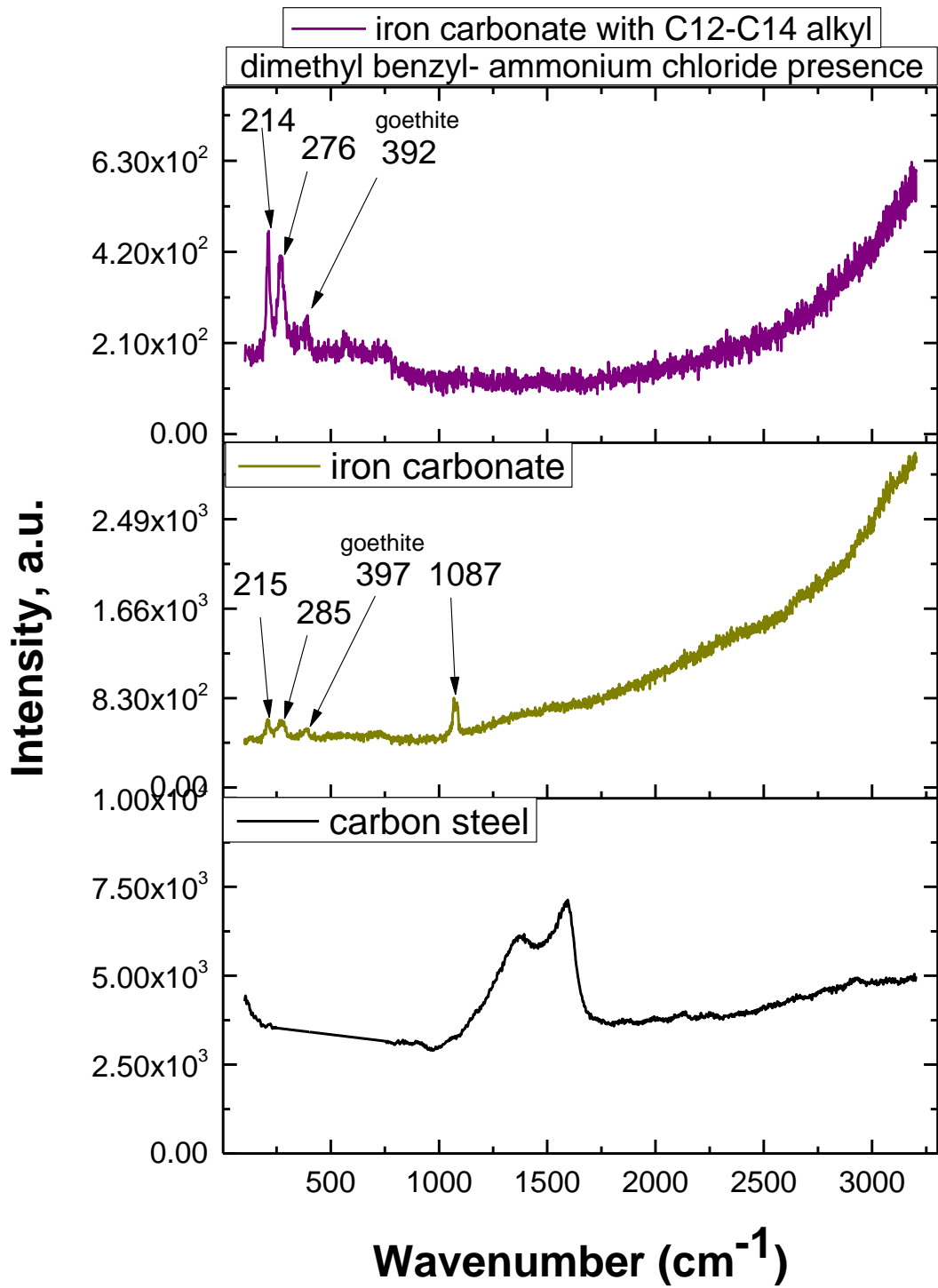


Figure 0.10: Raman spectrum for iron carbonate formed with presence of C12-C14 alkyl dimethyl benzyl-amonium chloride, iron carbonate reference and carbon steel

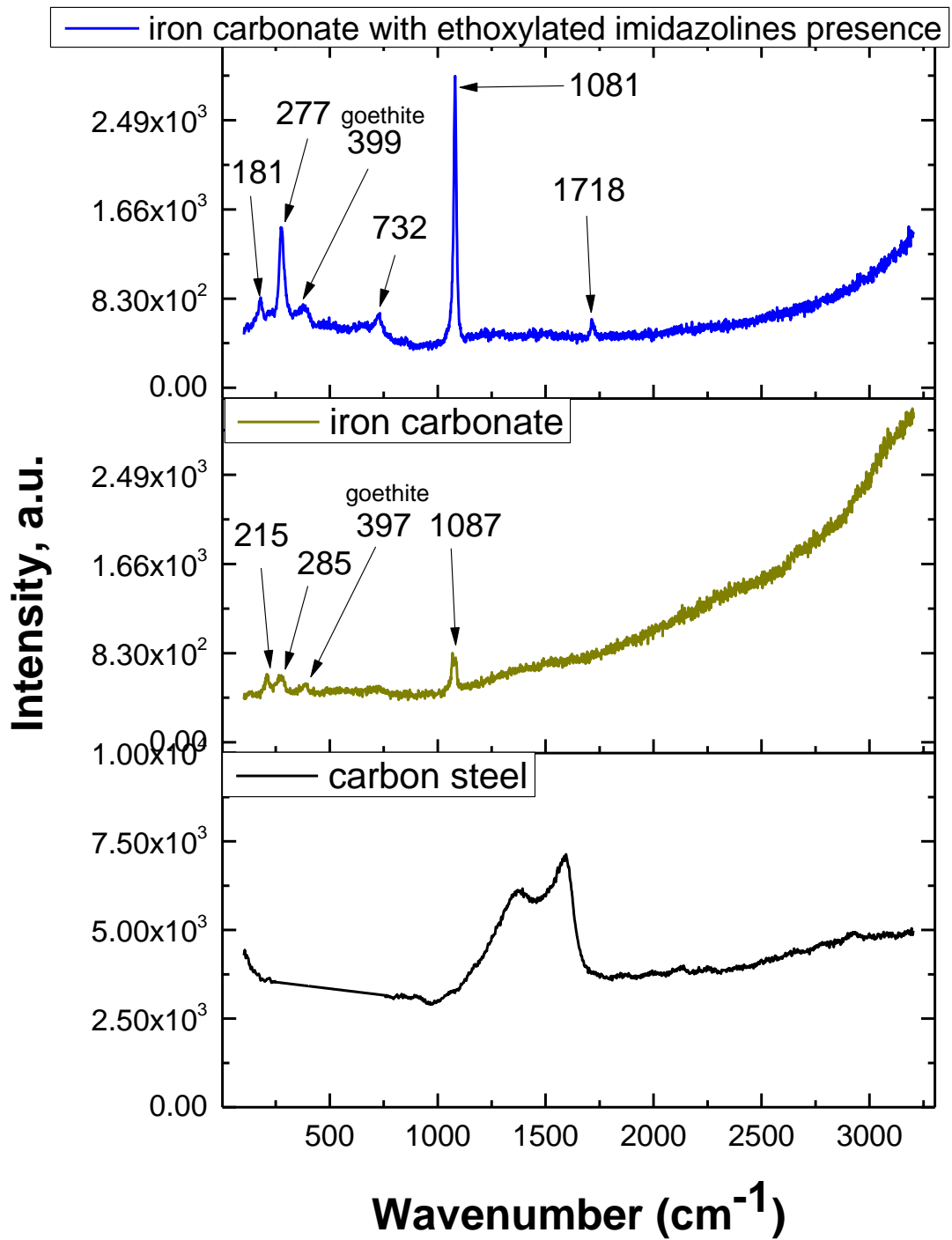


Figure 0.11: Raman spectrum for iron carbonate formed with presence of ethoxylated imidazolines, iron carbonate reference and carbon steel